

PREDICTION OF THE TRANSIENT FORCE SUBSEQUENT
TO A LIQUID MASS IMPACT ON AN ELBOW
OF AN INITIALLY VOIDED LINE

A THESIS SUBMITTED TO
THE GRADUTE SCHOOL OF NATURAL AND APPLIED SCIENCES
OF
MIDDLE EAST TECHNICAL UNIVERSITY

BY

BÜLENT ABBAS KAYHAN

IN PARTIAL FULFILLMENT OF THE REQUIREMENTS
FOR
THE DEGREE OF DOCTOR OF PHILOSOPHY
IN
CIVIL ENGINEERING

FEBRUARY 2009

Approval of the thesis:

**PREDICTION OF THE TRANSIENT FORCE SUBSEQUENT
TO A LIQUID MASS IMPACT ON AN ELBOW
OF AN INITIALLY VOIDED LINE**

submitted by **BÜLENT ABBAS KAYHAN** in partial fulfillment of the requirements
for the degree of **Doctor of Philosophy in Civil Engineering Department, Middle
East Technical University** by,

Prof. Dr. Canan Özgen
Dean, Graduate School of **Natural and Applied Sciences**

Prof. Dr. Güney Özcebe
Head of Department, **Civil Engineering**

Assoc. Prof. Dr. Zafer Bozkuş
Supervisor, **Civil Engineering Dept., METU**

Examining Committee Members:

Prof. Dr. Turgut Tokdemir
Engineering Sciences Dept., METU

Assoc. Prof. Dr. Zafer Bozkuş
Civil Engineering Dept., METU

Prof. Dr. Metin Ger
Civil Engineering Dept., METU

Assist. Prof. Dr. Şahnaz Tiğrek
Civil Engineering Dept., METU

Dr. Uğraş Baran
Havelsan A.Ş.

Date: February 27, 2009

I hereby declare that all information in this document has been obtained and presented in accordance with academic rules and ethical conduct. I also declare that, as required by these rules and conduct, I have fully cited and referenced all material and results that are not original to this work.

Name, Last Name: BÜLENT ABBAS KAYHAN

Signature :

ABSTRACT

PREDICTION OF THE TRANSIENT FORCE SUBSEQUENT TO A LIQUID MASS IMPACT ON AN ELBOW OF AN INITIALLY VOIDED LINE

Kayhan, Bülent Abbas

Ph. D., Department of Civil Engineering

Supervisor: Assoc. Prof. Dr. Zafer Bozkuş

February 2009, 263 pages

The aim of the thesis, is to find the transient force applied by an individual transient liquid slug on an elbow at the end of a horizontal line due to an impact. The liquid slug is driven by pressurized air in a tank located upstream of the pipeline.

The time dependent pressure distribution along the elbow and a vertical extension segment after the elbow was solved, with a 1-D numerical approach along a curved line mesh. For this purpose; firstly, a 3-D axial turbulent velocity profile function was assumed for the slug, with its shape allowed to sway towards the convex side of the elbow along the curved mesh with the aid of a calibration tool.

Then, the pressure values were calculated by using 1-D application of Reynolds Equations in cylindrical polar and cartesian coordinates for the elbow and the vertical extension segment, respectively. The transient force acting on the elbow

and the following vertical extension segment was found by using these calculated pressure values and applying conservation of momentum principle over the volume elements selected along the elbow and the vertical extension segment.

For the analysis of the slug motion from the pressurizer tank to the elbow, a previously written computer code BOZKUŞ-2 was utilized. Then, the elbow and the vertical extension segment calculations in this study were made with a new code KAYHAN, which is an improved version of BOZKUŞ-2.

The calculated transient force and impact pressures at the elbow were also compared with those from previous studies.

Keywords: Liquid Slug, Elbow, Turbulent Velocity Profile, BOZKUŞ-2, KAYHAN, Transient Force

ÖZ

BAŞLANGIÇTA BOŞ OLAN BİR BORU HATTININ DİRSEĞİNE BİR SIVI KÜTLESİNİN ÇARPMASI SONUCU OLUŞAN TRANSİT KUVVETİN TAHMİNİ

Kayhan, Bülent Abbas

Doktora, İnşaat Mühendisliği Bölümü

Tez Yöneticisi: Doç. Dr. Zafer Bozkuş

February 2009, 263 sayfa

Bu tez çalışmasının amacı yatay bir boru hattının sonundaki dirseğe çarpan tekil bir su kütesinin uyguladığı transit kuvvetin belirlenmesidir. Su kütlesi membada bulunan bir tanktaki basınçlı hava tarafından itilmektedir.

Dirsekte ve ona bağlı, borunun bir düşey uzantı kısmındaki basınç dağılımının zamana bağlı değişimi, eğrisel bir hat şeklindeki ağ üzerinde 1 boyutlu nümerik bir yaklaşım ile çözümlenmiştir. Bu amaçla, ilk olarak 3 boyutlu bir eksenel, türbülanslı akım hız profili fonksiyonu tahmin edilmiştir ve bu fonksiyonun şeklinin seçilen hat üzerindeki eğrisel ağ boyunca, kalibrasyon parametresi olarak kullanılan diğer bir fonksiyon yardımı ile dirseğin konveks tarafına doğru deforme olabilmesi sağlanmıştır.

Basınç değerleri silindirik kutupsal ve kartezyen koordinatlardaki Reynolds

Denklemleri'nin, dirsek ve borunun düşey uzantı kısımlarında 1 boyutlu olarak uygulanması ile hesaplanmıştır. Dirseğe ve ona bağlı, düşey uzantı kısmına etkiyen transit kuvvet; hesaplanan bu basınç değerleri kullanılarak ve momentumun korunumu prensibinin dirsek ve düşey uzantı kısmı boyunca seçilen hacimsel elemanlar üzerinde uygulanması ile bulunmuştur.

Su kütlesinin basınç tankından dirseğe kadar olan hareketinin analizi için daha önce yazılmış bir bilgisayar kodu olan BOZKUŞ-2 kullanılmıştır. Daha sonra bu çalışmadaki dirsek ve düşey uzantı kısmı için olan hesaplamalar, BOZKUŞ-2'nin geliştirilmiş bir versiyonu olan KAYHAN isimli yeni bir kod ile yapılmıştır.

Tezde, dirsekte hesaplanan darbesel basınçlar ve bulunan transit kuvvet değerlerinin daha önce yapılan çalışmalarda bulunan sonuçlarla karşılaştırılması da yer almaktadır.

Anahtar Kelimeler: Su kütlesi, Dirsek, Türbülanslı Akım Hız Profili, BOZKUŞ-2, KAYHAN, Transit Kuvvet

To My Parents

ACKNOWLEDGEMENTS

I would like to express my deepest gratitude to my supervisor Assoc. Prof. Dr. Zafer Bozkuş for his invaluable guidance and suggestions throughout this study. I would like to express my special thanks also to my doctoral committee members, Prof. Dr. Metin Ger, Prof. Dr. Turgut Tokdemir, Assist. Prof. Dr. Şahnaz Tiğrek and Dr. Uğraş Baran for their valuable suggestions and comments.

My very special thanks extend to Assist. Prof. Dr. Özgür Kurç for his help in providing the opportunity to use METU Central Server System as a source of compiler software. Special thanks also go to Assist. Burak Anıl, Assist. Kaan Özenç and Assist. İlker Küçüktepe for their assistance in the procedure of setting up the compiler software on computer and making it ready for use.

TABLE OF CONTENTS

ABSTRACT	iv
ÖZ	vi
ACKNOWLEDGEMENTS	ix
TABLE OF CONTENTS	x
LIST OF TABLES	xiii
LIST OF FIGURES	xiv
LIST OF SYMBOLS	xvii
CHAPTERS	
1. INTRODUCTION	1
1.1 Rationale for the Present Study	1
1.2 Specific Objectives of the Present Study	2
1.3 Scope of the Present Study	3
2. LITERATURE REVIEW	4
3. MATHEMATICAL DEVELOPMENT FOR THE HORIZONTAL	
PART	11
3.1 Introduction	11
3.2 Slug Dynamics Equations	12
3.2.1 Conservation of Mass Equation	14
3.2.2 Conservation of Momentum Equation	16
3.2.3 Slug Kinematics Equation	18
3.3 Gas Dynamics Equations	19
3.4 Coupling of Gas and Slug Dynamics Equations	21
3.5 Functional Hold Up Coefficient	25
3.6 Closure	26
4. MATHEMATICAL DEVELOPMENT FOR THE ELBOW PART ...	28
4.1 Introduction	28

4.2 Assumed Axial Velocity Profile Function	29
4.3. Calculation of the Impact Pressures at the Elbow	36
4.3.1 Simplifying Assumptions	38
4.3.2 Pressure Distribution Equations	44
4.3.2.1 Average Pressure Distribution along the Vertical Extension Segment	44
4.3.2.2 Average Pressure Distribution along the Elbow	47
4.3.2.3 Calculation of Impact Pressures at the Convex Side of the Elbow	49
4.3.3 Calculations for that Part of the Slug in the Horizontal Pipe	53
4.3.4 The Initial and the Boundary Conditions	55
4.4 Transient Force Calculations at the Elbow Part	61
4.4.1 Calculations at the Elbow	62
4.4.1.1 Horizontal Transient Force Distribution at the Elbow	63
4.4.1.2 Vertical Transient Force Distribution at the Elbow	66
4.4.2 Calculations at the Vertical Extension Segment	67
4.4.2.1 Horizontal Transient Force Distribution at the Vertical Extension Segment	67
4.4.2.2 Vertical Transient Force Distribution at the Vertical Extension Segment	69
4.4.3 Total Horizontal and the Vertical Transient Forces	70
4.5 Numerical Integrations	71
4.5.1 Double Integration in Polar Coordinates	71
4.5.2 Evaluation of Numerical Line Integrals	77
4.5.2.1 Generation of 1-D Clustered Mesh	77
4.5.2.2. Application of 3-Point Gauss Quadrature Method	79

4.6 Calibration Function for the Velocity Profile	81
4.7 Non-Dimensionalization of the Equations	86
4.8 Discretization of the Equations	95
4.9 Evaluation of Local Peak Pressures	99
4.9 Input Data, Mesh Sizes and Error Analyses	99
4.10 Neglecting of Some Terms	100
4.11 Input Data, Mesh Sizes and Error Analyses	104
4.11.1 Input Data for Program KAYHAN	104
4.11.2 Error Analysis and Mesh Size for Area Integrals	106
4.11.3 Error Analysis and Mesh Size for Line Integrals	110
4.11.4 Mesh Size and Error Analysis for the Line Mesh along s -Curve	112
4.11.5 Error Analysis and the Mesh Size for Impact Pressure Calculation	115
5. RESULTS AND DISCUSSION	117
5.1 Peak Pressures at the Elbow	118
5.2 Pressure-Time History Plots	120
5.3 Transient Forces at the Elbow	129
5.4 Impact Pressure Distribution at the Elbow	137
5.5 Discussion on the Existence of Waterhammer Event	140
6. CONCLUSIONS	142
6.1 Summary	142
6.2 Concluding Remarks	143
REFERENCES	145
APPENDICES	
A. MATHEMATICAL DERIVATION OF THE EQUATIONS	150
A.1 Functional Hold up Coefficient Determination	150
A.1.1 Formulation for the Average Slug Length	150
A.1.2 Correlation between the Hold up and the Instantaneous Slug Length	152

A.2 Derivations for the Assumed Velocity Profile Function	151
A.2.1 Derivation of Bottom Cone Equation	151
A.2.2 Derivation of Upper Cone Equation	158
A.2.3 Calculation of Unknown Parameters	160
A.3 Derivations for the Pressure Distribution Equations	165
A.3.1 Derivation of Average Pressure Distribution Equation at the Vertical Extension Segment	165
A.3.2 Derivation of Average Pressure Distribution Equation at the Elbow	170
A.3.3 Derivation of the Equation for the Pressure at the Convex Side of the Elbow	179
A.4 Derivations for the Transient Force Calculations at the Elbow Part	184
A.4.1 Derivations for the Horizontal Transient Force Distribution at the Elbow	184
A.4.2 Derivations for the Vertical Transient Force Distribution at the Elbow	188
A.4.3 Derivations for the Horizontal Transient Force Distribution at the Vertical Extension Segment ...	191
A.4.4 Derivations for the Vertical Transient Force Distribution at the Vertical Extension Segment ...	194
A.5 Derivations for Numerical Integration Formulas	196
A.5.1 Derivations for Double Integrals in Polar Coordinates	196
A.5.2 Derivations for the Line Integrals	200
A.5.2.1 Derivations for 1-D Clustered Mesh Generation	201
A.5.2.2 Derivations for 3-Point Gauss Quadrature Method	202
A.6 Derivations for the Calibration Function	205

B. CORRELATION FUNCTION FOR THE MAXIMUM	
CALIBRATION ANGLE	206
C. COMPUTER PROGRAMS	213
C.1 Explanations for the Functions of the Computer	
Programs	213
C.2 Flow-Chart for the Computer Code KAYHAN	218
C.3 Computer Code KAYHAN	224

LIST OF TABLES

TABLES

Table 4.1 Initial and the boundary conditions for the elbow and the vertical extension segment calculations.	58
Table 4.2 Values for the terms in Equation (4.81).	100
Table 4.3 Values for the terms in Equation (4.85).	101
Table 4.4 Radial and axial velocities with their time derivatives.	103
Table 4.5 Input data for program KAYHAN.	105
Table 5.1 Peak pressures at the elbow (psig).	101
Table A.1 Calculation steps for L_p / L_{ave} ($L_p = 9.4488\text{ m.}$).	154
Table B.1. Peak pressures used for correlating $\theta_{c\max}$ (all in psig).	207
Table B.2 $\theta_{c\max}$ values vs. L_p / L_{in} used for correlation procedure.	211

LIST OF FIGURES

FIGURES

Figure 2.1 Fenton’s experimental setup [22].	5
Figure 2.2 System setup used in Bozkuş’s study [2].	6
Figure 2.3 Experimental setup used by Baran [27].	9
Figure 3.1 Control volume for the liquid slug selected by Bozkuş [2] along the horizontal pipeline.	13
Figure 3.2 Computational domain used by Bozkuş [2] for the solution of gas dynamics equations.	21
Figure 3.3 Variation of pressure at the upstream pressure tank (Bozkuş [2]).	25
Figure 4.1 Velocity distribution in a curved pipe given by Prandtl [13], [14] (Schlichting [10]).	29
Figure 4.2 Parameters for the general oblique cone equation.	30
Figure 4.3 Cross-sectional shape of the assumed turbulent velocity profile function.	32
Figure 4.4 Parameters used for the assumed velocity profile in a single coordinate system.	33
Figure 4.5 (a) Complete physical set up for the system (Bozkuş [2]); Computational domain for (b) the elbow and the vertical extension part, (c) the cross-section of the elbow, (d) the cross-section of vertical extension part of the pipe.	34
Figure 4.6 Sample volumetric pipe element on the s-curve, in the vertical extension segment.	45
Figure 4.7 Sample volumetric pipe element along the s-curve, for the elbow part.	48
Figure 4.8 1-D radial mesh at a cross-section of the elbow.	50
Figure 4.9 1-D radial mesh selection at elbow cross-sections, with the line meshes located in the vertical, mid $x - y$ plane of the elbow.	52

Figure 4.10 Computational domain with the nodal numbering along the s -curve given.	56
Figure 4.11 Control volume for the transient force calculations at the elbow.	62
Figure 4.12 Selection for the location of the P values along the s -curve, for the procedure of interpolation at the faces of the volume elements.	65
Figure 4.13 Control volume for the transient force calculations at the vertical extension segment.	68
Figure 4.14 Circular mesh over the pipe cross-section.	72
Figure 4.15 9-point mesh element selected for double integration in polar coordinates.	74
Figure 4.16 9-point mesh element for 2-D Gauss Quadrature in cartesian coordinates.	75
Figure 4.17 Mesh element for the center point of the circular domain in polar coordinates.	76
Figure 4.18 Line mesh for a given point K' on the elbow cross-section.	78
Figure 4.19 Parameters used for the 3-point Gauss Quadrature Method.	80
Figure 4.20 Shape of the calibration function θ_c	82
Figure 4.21 General variation of the shape of the assumed axial velocity profile along the s -curve.	85
Figure 4.22 Percentage error vs. total mesh size, for $m_{rt} = 0.1$	107
Figure 4.23 Percentage error vs. total mesh size, for $m_{rt} = 0.25$	108
Figure 4.24 Percentage error vs. total mesh size, for $m_{rt} = 0.5$	108
Figure 4.25 Percentage error vs. total mesh size, for $m_{rt} = 0.75$	109
Figure 4.26 Percentage error vs. total mesh size, for $m_{rt} = 1.0$	109
Figure 4.27 Percentage error vs. total mesh size, for $m_{rt} = 1.5$	110
Figure 4.28 Variation of percentage error vs. node number, M_L	112
Figure 4.29 Variation of percentage error vs. node number, N_{slug}	115

Figure 5.1 Normalized peak pressures vs. L_p / L_{in}	119
Figure 5.2 Pressure-time history plots at the elbow for $L_{in} = 4$ ft and $P_0 = 20$ psig.	123
Figure 5.3 Pressure-time history plots at the elbow for $L_{in} = 4$ ft and $P_0 = 30$ psig.	123
Figure 5.4 Pressure-time history plots at the elbow for $L_{in} = 4$ ft and $P_0 = 40$ psig.	124
Figure 5.5 Pressure-time history plots at the elbow for $L_{in} = 5$ ft and $P_0 = 10$ psig.	124
Figure 5.6 Pressure-time history plots at the elbow for $L_{in} = 7$ ft and $P_0 = 10$ psig.	125
Figure 5.7 Pressure-time history plots at the elbow for $L_{in} = 7$ ft and $P_0 = 20$ psig.	125
Figure 5.8 Pressure-time history plots at the elbow for $L_{in} = 7$ ft and $P_0 = 40$ psig.	126
Figure 5.9 Pressure-time history plots at the elbow for $L_{in} = 9$ ft and $P_0 = 10$ psig.	126
Figure 5.10 Pressure-time history plots at the elbow for $L_{in} = 11$ ft and $P_0 = 10$ psig.	127
Figure 5.11 Pressure-time history plots at the elbow for $L_{in} = 11$ ft and $P_0 = 20$ psig.	127
Figure 5.12 Pressure-time history plots at the elbow for $L_{in} = 11$ ft and $P_0 = 30$ psig.	128
Figure 5.13 Pressure-time history plots at the elbow for $L_{in} = 11$ ft and $P_0 = 40$ psig.	128
Figure 5.14 Transient force components for $L_{in} = 4$ ft and $P_0 = 10$ psig.	130
Figure 5.15 Transient force components for $L_{in} = 4$ ft and $P_0 = 20$ psig.	130

Figure 5.16 Transient force components for $L_{in} = 7$ ft and $P_0 = 10$ psig.	131
Figure 5.17 Transient force components for $L_{in} = 7$ ft and $P_0 = 20$ psig.	131
Figure 5.18 Transient force components for $L_{in} = 11$ ft and $P_0 = 20$ psig.	132
Figure 5.19 Transient force components for $L_{in} = 11$ ft and $P_0 = 40$ psig.	132
Figure 5.20 Values of F^* vs. D^* (Bozkuş's [2] 1 st peaks were used for normalization).	134
Figure 5.21 Values of F^* vs. D^* (Bozkuş's [2] 2 nd peaks were used for normalization).	136
Figure 5.22 Dynamic pressure distribution for $L_{in} = 4$ ft, $P_0 = 20$ psi, $t = 0.539$ s and $NELBW = 115$	138
Figure 5.23 Dynamic pressure distribution for $L_{in} = 4$ ft, $P_0 = 40$ psi, $t = 0.375$ s and $NELBW = 115$	138
Figure 5.24 Dynamic pressure distribution for $L_{in} = 7$ ft, $P_0 = 10$ psi, $t = 0.942$ s and $NELBW = 90$	139
Figure A.1 Normalized peak pressures vs. L_p / L_{in} from program BOZKUŞ-2 and from the experimental data (Bozkuş [2]).	153
Figure A.2 Variation of hold up coefficient, α , as a function of L_p / L_s	155
Figure A.3 Two coordinate systems combined together for the general oblique and symmetric cone equations.	156
Figure A.4 Control volume at the elbow with the components of the forces and the velocities shown.	185
Figure B.1 Normalized peak pressures at the elbow for $\theta_{c\ max} = 89.60^\circ$	208
Figure B.2 Normalized peak pressures at the elbow for $\theta_{c\ max} = 89.70^\circ$	208
Figure B.3 Normalized peak pressures at the elbow for $\theta_{c\ max} = 89.75^\circ$	209
Figure B.4 Normalized peak pressures at the elbow for $\theta_{c\ max} = 89.77^\circ$	209
Figure B.5 Normalized peak pressures at the elbow for $\theta_{c\ max} = 89.80^\circ$	210

Figure B.6 Normalized peak pressures at the elbow for $\theta_{c\max} = 89.82^\circ$	210
Figure B.7 Correlation function for $\theta_{c\max}$ vs. L_p / L_{in}	212

LIST OF SYMBOLS

- a : wave speed,
- a' : coordinate axis used as the transformation parameter,
- A : cross-sectional area of the pipeline, elbow and the vertical extension segment,
- A_1, A_2 : areas of the parts of the pipe cross-section,
- A_3, A_4 : outer surface areas of the infinitesimal volume element perpendicular to pipe axis and the at the pipe wall; respectively,
- A' : lower boundary of the line integral,
- A_c, B_c : points on the coordinate system for the calibration function, θ_c ,
- A_t^*, A_β^* : differential expression,
- B_t^* : differential expression,
- C : wave speed,
- $C\forall$: control volume,
- CS : control surface,
- C_1, C_2 : parameters,
- c_r : mesh clustering ratio used for the line mesh,
- D : pipe diameter,
- D^* : dispersion distance,
- E : integral expression,
- E_1^*, E_2^*, E_3^* : parameters,
- f : integrand function,
- f_f : friction factor,
- f_{fw} : friction factor for water,

F : friction force per unit length of the pipe assuming no reverse flow,
 \vec{F} : force vector acting on the control volume,
 F_m : predicted force at the elbow with the numerical model,
 F_p : experimentally obtained peak force at the elbow,
 \vec{F}_{vec} : vectorial expression,
 $F_{x\forall}$: force acting on the volumetric element in x -direction,
 F_x , F_y : x and y components of the total transient force acting on the elbow and the vertical extension segment, respectively,
 $F_{y\forall}$: force acting on the volumetric element in y -direction,
 F^* : normalized force,
 g : gravitational acceleration,
 g_x , g_y , g_z : components of gravitational acceleration respectively in x , y and z directions,
 g_r , g_θ : components of gravitational acceleration respectively in r and θ directions,
 g' : functional parameter as integrand,
 g'_i , g'_{ci} : parameters having discrete values at points i ,
 h_1 , h_2 , h_3 : parameters for the geometry of the velocity profile function,
 h' : any integrand function for the line integral,
 h'_1 , h'_2 , h'_3 : values of the function h' over the nodes of the 1-D Gauss element,
 i , j , k : incremental grid location in r , β and z directions, respectively,
 ip : indice for the node number,
 I_A : area integral expression,
 $I_{A;m,n}$: expression for the area integral over the mesh element in the circular domain A , with the mesh element's center point at node m,n ;
 $I^c_{A;m,n}$: expression for the area integral over the central mesh element in the circular domain A , with the mesh element's center point at node m,n ;

I_L : line integral expression,
 I_{L1} : integral expression,
 $I_{L,q}$: expression for the line integral over the line mesh element with the mesh elements's center point located at node q ,
 I_u^* , I_β^* , I_{us}^* : integral expressions,
 K_m : minor loss coefficient at the elbow,
 K' : upper boundary of the line integral,
 l : mixing length,
 l_m : mixing length,
 L : slug length remaining within the horizontal part of the pipeline,
 L' : scaling factor for length,
 L_{ave} : average length of the slug that occurs during the motion of the slug along the horizontal part of the pipeline,
 L_{elb} : central arc length of the elbow,
 L_{ext} : length of the vertical extension segment after the elbow,
 L_{fin} : final slug length of the horizontal pipe calculations ,
 L_{final} : final length of the slug remaining in the horizontal part of the pipeline obtained from horizontal pipe calculations,
 L_{in} : initial slug length,
 L_p : length of the horizontal part of the pipeline,
 L_s : instantaneous slug length at any time during its travel along the horizontal part of the pipeline,
 L_{simp} : slug length at the instant that the slug front enters the elbow,
 L_t : travel distance of the slug,
 L_{tot} : total axial length of the elbow and the vertical extension segment,
 m : indice for the radial location of the mesh element in the circular domain,
 M and N : number of mesh elements in the radial and the circumferential directions of the pipe cross-section, respectively,

$MLPRSS$: number of nodes for the line mesh used for the impact pressure calculation,

M_L : total number of clustered line mesh elements in case the domain of line integral is the whole diameter of the cross-section of the elbow, in r direction,

m_{rt} : Ratio of the circumferential mesh size to the radial one, at any cross-section of the pipe,

$m_{\theta c1}$, $m_{\theta c2}$: slopes of the calibration function, θ_c , before and after its point of maximum, respectively,

n : indice for the circumferential location of the mesh element circular domain,

$NBOUND$: point on the s -curve at the boundary of the elbow and the vertical extension segment,

$NELBW$: number of nodes along the axis of the elbow,

$NLFF$: nodal number corresponding to the location of the slug front face along the s -curve,

N_{slug} : number of nodes selected over the slug length, L_{simp} .

$NSTOT$: total number of nodal points along the s -curve,

N_{tank} : number of tank pressure data points,

\vec{n} : outer unit normal vector,

O : center of curvature of the elbow,

O' : origin of the local coordinate system,

O'' : origin of the upper local coordinate system,

O_c : origin of the coordinate system for the calibration function, θ_c ,

p : ensemble average local pressure,

P : average pressure over the pipe cross-section,

P_{calc} : calculated average pressure value at the elbow cross-section,

P_D : driving air pressure acting on the slug upstream face,

$P_{D final}$: final driving air pressure value at the upstream face of the slug from horizontal pipe calculations at the instant that the slug front face reaches the entrance section of the elbow,

P_E : average liquid pressure retarding the motion of that part of the slug in the horizontal part of the pipeline, and acting at the entrance section of the elbow,

$P_{E\,calc}$: calculated average liquid pressure retarding the motion of that part of the slug in the horizontal part of the pipeline, and acting at the entrance section of the elbow,

P_0 : initial tank pressure at the pressurizer tank,

P_{atm} : atmospheric absolute pressure,

P_d : average pressure acting at the downstream face of the control volume,

P_{NLFF} : atmospheric pressure at the front face of the liquid slug,

P_{NBOUND} : average pressure at the connection boundary of the elbow and the vertical extension segment,

$p_{O'}$: local pressure at the center point O' of the elbow cross-section,

P_p , P_m and P_n : average pressures at the center points of respectively the previous, current and next volume elements on the s -curve,

p_{peak} : peak pressure from program KAYHAN at the location of transducer #2.

P_T : tank pressure,

$P_{T\,final}$: final tank pressure value from horizontal pipe calculations at the instant that the slug front face reaches the entrance section of the elbow,

P_u : average pressure acting at the upstream face of the control volume,

P_w : driving air absolute pressure acting at the upstream face of the slug,

P_{wet} : wetted perimeter,

PO : atmospheric pressure,

PO_{gage} : atmospheric gage pressure,

q : any node number of the line mesh, also coinciding with the center point of a 1-D Gauss element,

Q : discharge,

$Q_{K'}$: mesh size of the 1-D clustered line mesh,

r : radial axis of the cylindrical coordinate system,
 R : internal radius of the pipe,
 R' : radius of the bottom circle of the lower cone,
 R'' : radius of the bottom circle of the upper cone,
 Re : Reynolds number,
 RHS : right-hand side of equation,
 R_g : gas constant,
 R_0 : radius of curvature of the elbow,
 r_m : given radial coordinate in the cross-section of the elbow, with respect to the cylindrical coordinate system,
 R_m : distance of the point of maximum velocity from the origin of the local coordinate system, measured along the y' axis,
 r_q : radial location of the center point of the 1-D Gauss element over the clustered mesh, with respect to the cylindrical coordinate system,
 s : curvilinear coordinate,
 S : surface area of the control volume,
 S_d : downstream pipe cross-sectional area for the control volume,
 s_d, s_u : location of respectively the downstream and the upstream faces of the current volume element at node ip , on the s -curve,
 s_{elb} : location on s -curve for the exit section of the elbow,
 s_{ext} : location on s -curve for the exit section of the vertical extension segment,
 S_m : area of the mid-plane of the volume element perpendicular to pipe axis,
 s_{max} : location on s -curve where the maximum value of θ_c occurs,
 s_p, s_m, s_n : location of the center points of respectively the previous, current and next volume elements on the s -curve,
 S_u : upstream pipe cross-sectional area for the control volume,
 s_{frol}^n : slug front face location on the s -curve at ant time step n ,
 s', t' : cartesian axes as parameters for coordinate transformation,

t : time,
 T : temperature,
 t' : scaling factor for time,
 t_{in} : initial time of slug motion,
 t_{fin} : final time of slug motion,
 t_n : time value at any time step n ,
 U : average slug velocity,
 U' : scaling factor for velocity,
 U_{ave} : average velocity of the slug taken over the cross-section of the elbow,
 \vec{U}_b : velocity of the boundary of the control surface,
 U_B : velocity of the back face of the slug,
 U_{final} : final slug velocity obtained from horizontal pipe calculations,
 U_F : velocity of the front face of the slug,
 U_{in} : initial slug velocity,
 U_{ix} : fluid velocity relative to the global coordinate axis, on the surface i for the control volume, and in the x -direction,
 U_m : maximum velocity on the assumed velocity profile function,
 U_{pas} : slug passage velocity through the elbow,
 \vec{U}_r : liquid velocity relative to the control surface boundary,
 U_{ri} : fluid velocity relative to the control surface i ,
 u_s : velocity profile function defined along the s-curve,
 u_{su} , u_{sd} : axial velocity profile functions at the upstream and the downstream faces of the volume element,
 \bar{u}_s : average value of the assumed axial velocity profile function along the s - curve,
 U_x : liquid velocity relative to the fixed reference frame,
 u_β : axial velocity profile function in the elbow, in β direction,
 \bar{u}_β : average value of the velocity profile function in the elbow, in β

direction,

$u_{\beta u}, u_{\beta d}$: assumed and calibrated axial velocity profile functions evaluated at

respectively the upstream and downstream faces of the control volume,

V : velocity within the air volume, in the x -direction,

V_{axial} : axial velocity,

\vec{V} : velocity vector at any point of the flow,

V_r, V_θ : ensemble average local velocity components respectively in r and

θ directions,

V'_r, V'_θ : turbulence fluctuations of the velocity components respectively in r

and θ directions,

V_{rd} : local radial velocity at the downstream face of the control volume,

V_{ru} : local radial velocity at the upstream face of the control volume,

V_x, V_y, V_z : ensemble average local velocities respectively in x, y and z

directions,

V'_x, V'_y, V'_z : turbulence fluctuations of the velocity components respectively

in x, y and z directions,

V_{xd} : local velocity in x -direction at the downstream face of the control volume,

V_{xu} : local velocity in x -direction at the upstream face of the control volume,

\bar{V}_y : average velocity in y direction,

V_{yu}, V_{yd} : local velocities in y -direction at respectively the upstream and the

downstream faces of the control volume,

$V_{\beta d}$: local axial velocity at the downstream face of the control volume,

$V_{\beta u}$: local axial velocity at the upstream face of the control volume,

\bar{V}_θ : average axial velocity in θ -direction,

w_1, w_2, w_3 : weighting coefficients,

x, y : cartesian coordinate axes,

x', y', z' : coordinate axes for the local coordinate system,

x'' , y'' , z'' : coordinate axes for the upper local coordinate system,
 X_{in} : initial slug position,
 x'_0 , y'_0 , z'_0 : coordinates for the apex point of the general cone equation,
 x''_0 , y''_0 , z''_0 : coordinates for the apex point of the upper cone with respect to the upper local coordinate system,
 y_w : distance from the pipe wall,
 y'_1 , y'_2 : parameters for the geometry of the velocity profile function,
 z : axis of the cylindrical polar coordinate axes,
 z_n : given z coordinate in the cross-section of the elbow, with respect to the cylindrical coordinate system.

Greek symbols:

α : hold up coefficient,
 β : angular axis,
 β_d : reference angle for the downstream face of the control volume,
 β_u : reference angle for the upstream face of the control volume,
 β_p : circumferential coordinate for the given cross-section of the elbow , with respect to the cylindrical coordinate system,
 $\Delta F_x , \Delta F_y$: horizontal and the vertical components of the reaction force applied by the pipe on the control volume, respectively,
 ΔL_s : whole change in slug length during the travel of the slug from the pressurizer tank up to the elbow,
 ΔP_{WH} : pressure rise due to sudden valve closure,
 Δr_q : length of the clustered line mesh element at node q ,
 Δs : axial length of the volume element,
 $\Delta t , \Delta t_1 , \Delta t_2$: time increments for the horizontal pipe calculations,
 Δt_{pas} : slug passage time through the elbow,
 Δt_s : time increment at any time step of the elbow and the vertical extension

segment calculations,

Δt_{s1} : first time increment value used for the elbow and the vertical extension

segment calculations,

Δt_s^n : time increment at any time step, n ,

ΔU : change in slug velocity,

ΔW : weight of the control volume,

$\Delta \beta$: incremental angle of curvature over the infinitesimal element in the elbow,

$\Delta \eta$: incremental angle of the mesh in η direction (angular direction),

$\Delta \xi$: incremental length of the mesh in ξ direction (radial direction),

$\Delta \forall$: volume of the selected pipe element,

$\vec{\nabla}$: divergence operator,

ε : roughness height of the pipe wall,

ε_t : turbulent eddy viscosity of the liquid,

ξ : radial coordinate axis over the pipe cross-section,

ξ_m : radial distance of the central node of the 9-point mesh element from the center-point of the domain of the circular cross-section,

η : circumferential coordinate axis over the pipe cross-section,

η_n : angular distance between the line connecting the central node of the 9-point mesh element to the origin of the circular domain, and the x' axis,

μ : dynamic viscosity of water,

π : pi number,

ν : kinematic viscosity of the liquid,

ρ : density of the liquid (water),

ρ_a : density of air,

ρ_w : density of water,

θ : circumferential axis of the cylindrical polar coordinate system,

θ_c : calibration function for the angle at a selected point of the velocity profile function,

θ_{cent} : θ_c value at the entrance section of the elbow,
 θ_{ext} : θ_c value at the exit section of the vertical extension segment,
 θ_{cmax} : maximum value of θ_c along the s -curve,
 θ_f : angle for the gradient of the velocity profile at the pipe wall,
 τ : shear stress value at y_w distance away from the circular pipe wall,
 τ_0 : wall shear stress,
 ∇ : divergence operator,
 \forall : volume of the control volume,
 \forall_r : volume of the volumetric element,
 \forall_1 : volume of the bottom cone,
 \forall_2 : volume of the oblique upper cone,
 $\langle \rangle$: symbol indicating ensemble averaging.

Subscripts:

ip : variable at this node
 L : location of the left boundary of the gas volume,
 R : location of the right boundary of the gas volume,
 S : location of the right at the mid-time step.

Superscripts:

n : time level,
 $*$: dimensionless parameter.

CHAPTER I

INTRODUCTION

1.1 Rationale for the Present Study

Study of the impact pressures applied by high pressure air or steam driven liquid pockets, called slugs, formed in voided lines is an important phenomenon as far as the resulting potential damage on the pipelines is concerned. There are some different mechanisms that cause formation of speed motion of liquid slugs in nuclear power plants.

One of these mechanisms is the creation of a condensate in steam lines of a power plant during its operation, and following motion of this condensate in the form of a liquid slug along a voided line (Kim [17]; Merilo and et al. [18]; Bozkuş and Wiggert [20]). Inadequate draining is one of the factors that yields the formation of condensate in a steam line which afterwards under the pushing effect of high pressure steam may accelerate along the voided line, and turn into a slug as a whole liquid pocket filling all the pipe cross-section during its motion. Then, the liquid slug which attains very high speeds along the pipeline may hit elbows, partially or fully open valves or junctions applying very high impact pressures on these parts of the pipeline.

Another cause of slug creation in voided lines is the pushing effect of high pressure steam on water, collected in loop seal parts of the pipelines in power plants (Bozkuş [2]; Wheeler and Siegel [19]; Bozkuş and Wiggert [20]). A loop seal is that part of a pressurized water reactor which is located upstream the pressurizer safety and relief valves and it is used for preventing excessive gas leakage through these valves. When the upstream pressure in the reactor coolant system exceeds a previously defined limiting value, the safety or relief valves suddenly open to relieve

the excess pressure in the system. As soon as the valves open, the high pressure steam starts to push the water in the loop seal causing the formation of a liquid slug which attains very high velocities in the pipeline and applies high dynamic pressures on such pipe components as elbows, tees and valves as a source of potential damage.

The parameters to describe the hydraulic properties of the slug motion and the following impact event consist of initial mass and length of the slug, magnitude of the driving pressure acting on the upstream face of the slug, pipe material and pipe geometry. These hydraulic parameters are all effective in the value that the magnitude of the dynamic pressures on the pipe components will reach. Since the magnitude of the dynamic loads acting on the pipeline and its supports is a measure of the possible damage that the pipeline system will experience, a hydrodynamic analysis is essential to predict and mitigate any potential risk of damage to the pipeline system. This field of hydrodynamics that analyses the forces applied by propelled liquid slugs in voided lines is actually a subject on which a limited number of studies have been performed so far and this makes the subject an issue that requires more attention. Also considering that pipeline systems and pipe supports and restraints constitute quite a large amount of the total investments to be made for nuclear power plants, prediction of the forces acting on these support and restraint structures becomes an important subject of research (Bozkuş [2]; Smith and Van Laan [21]).

1.2 Specific Objectives of the Present Study

In previously performed numerical studies related with estimation of impact pressures and dynamic loads applied by liquid slugs on elbows of initially voided lines, different 1-D mathematical models were proposed for the simulation of slug motion along straight pipelines and following impact events at elbows located at the end of the pipelines. Although these 1-D mathematical models were adequate enough to describe the actual flow conditions for the slug motion along straight pipelines, they have not included a much detailed modeling of elbow part calculations up to now. Actually, differing from case for the motion of a liquid slug along a straight part of a pipeline, the asymmetric axial velocity profile of a slug in an elbow part requires special attention to consider that distorted profile in a numerical model.

The aim of the present study is to predict numerically the transient force acting on a 90° degree elbow with its axis extending in the vertical plane, and on a following vertical extension segment, subsequent to a liquid mass impact on those parts. In the study, both of the elbow and the following vertical extension segment were taken to be located at the end of a straight and initially voided pipeline extending in the horizontal plane. For the part of the calculations that accounts for the motion of the liquid slug in the horizontal pipeline, a previous 1-D study performed by Bozkuş and Wiggert [2, 20] that contains gas and slug dynamics equations were utilized. And for the elbow and the following vertical extension segment calculations, a new 1-D analysis was performed with the intention of making a more detailed consideration of the flow in those parts, and by taking into account the variation of 3-D shape of the asymmetric axial velocity profile along the elbow and the vertical extension segment.

1.3 Scope of the Present Study

In the present study, the transient force acting on a 90° elbow and the following vertical extension segment was calculated by making a 1-D numerical analysis. For the analysis, a calibration technique was adopted to determine the unknown parameters for the change in the shape of an assumed 3-D axial velocity profile along the elbow and the vertical extension segment. For the calibration purposes, some experimental data of peak pressures obtained previously by Bozkuş [2] were utilized as reference values. By using the calibration function obtained from correlated data, various computer runs were made with different initial slug lengths and initial tank pressures to get a set of plots for the peak pressure time histories at the elbow and the time histories for the transient forces acting on the elbow and the vertical extension segment. The obtained results for the pressure peaks, and impact pressure and transient force time history plots were also compared with those from previously made studies.

CHAPTER II

LITERATURE REVIEW

There are various studies performed by different researchers, related with the prediction of forces that arise due to impact of a liquid slug on an elbow of an initially voided pipeline, but the number of these works is not quite high. Those of them which are most relevant to the present study were carried out by Woo and Papadakis [23], Fenton [22], Bozkuş [2], Neumann and Griffith [24], Baran [27].

Woo and Papadakis [23] developed a mathematical model for the determination of hydrodynamic forces at pipe bends that arise while an initially voided pipeline system was being filled. In that study, a combination of rigid column theory and method of characteristics was utilized for the mathematical modeling. As a result of the analysis, discharges, and forces at the pipes and pipe bends calculated with that model were seemed to be smaller than those in a previous made model by Papadakis and Hollingshead [37]. The reason for this reduction was attributed to the fact that in the previously made model, minor head losses at pipe junctions and pipe bends had been neglected; and therefore, it was indicated that the inclusion of minor losses became important if the velocities in the system were high [2, 23].

Fenton [22] performed both an analytical and an experimental study with the purpose of predicting the forces at a pipe bend, induced by the impact of a liquid slug which was driven by air along a pipeline. The aim of the analytical study was to develop a simple method for the prediction of loads acting on the pipe supports. And, an experimental work was performed to check the validity of the analytical method developed in the same study. For this purpose, he used an experimental apparatus as shown in Figure 2.1.

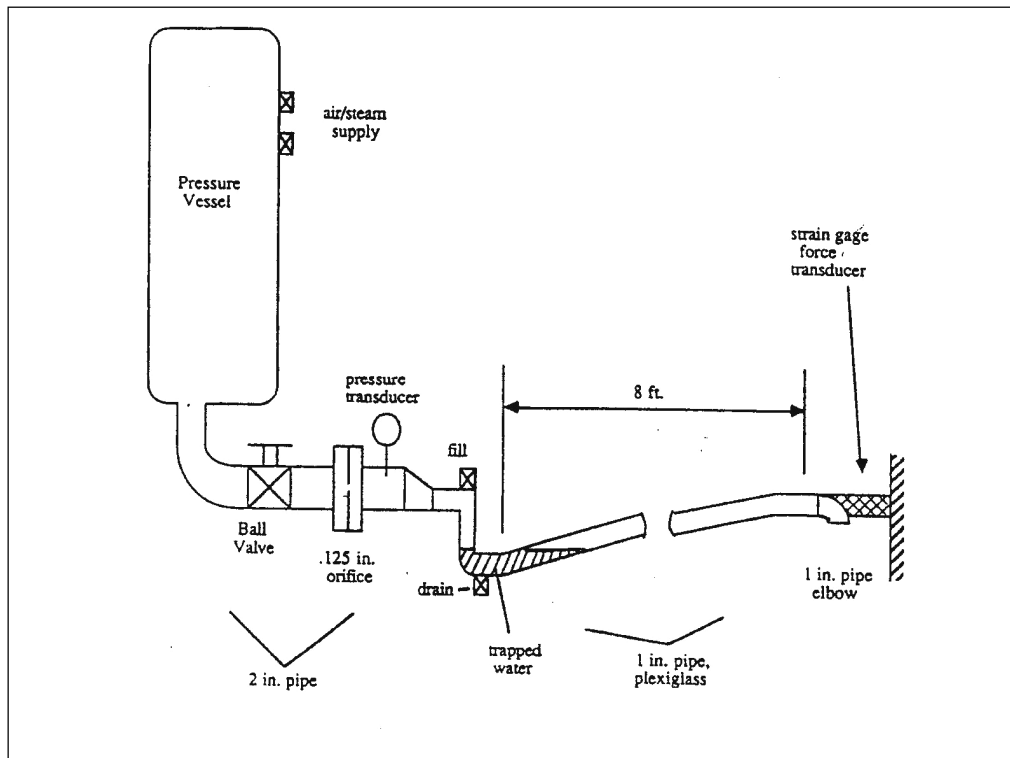


Figure 2.1 Fenton's experimental setup [22].

The experimental apparatus was composed of an air pressurizer vessel to supply high pressure air to the system and a 2-inch-diameter steel pipe was connected to this vessel. There was ball valve at the entrance of the steel pipe to control air flow to the system, and an orifice and a pressure transducer were also attached to the steel pipe. At the downstream side, a 1-inch-diameter plexiglass pipe which was inclined upwards was connected to the steel pipe. The connection here was made by means of a Tee section which was also utilized for the purpose of filling and draining water to the lower part of the plexiglass pipe. There was an elbow located at the downstream end of the plexiglass pipe, which was open to the atmosphere.

Fenton carried out his experiments with different initial slug lengths, initial tank pressures, and also by varying the distance between the slug front face and the elbow at the downstream side.

Fenton's analytical model included some assumptions, the most restrictive of which was that the slug as a coherent mass. Due to this coherent mass assumption,

amount of liquid that was left behind during the slug motion was neglected. As other assumptions, the gas from the pressure vessel, driving the liquid slug was taken to be compressed isothermally and as ideal, and the slug flow was considered as incompressible. During the flow of gas and the liquid slug, the shear resistance acting on the flow at the pipe wall was taken into consideration.

Fenton's analytical study overestimated the impact loads at the elbow especially when the normalized slug travel distance was equal to or greater than 7 [2, 22].

Bozkuş [2] performed an experimental study together with an analytical modeling to investigate the hydrodynamics of a transient liquid mass driven by high pressure air in a voided line. For this purpose, he used an experimental setup which consisted of a pressurizer and a horizontal pipeline connected to this pressurizer, and at the downstream end of the pipeline there was a 90° elbow attached together with a vertical extension segment, as shown in Figure 2.2. There was also a slug generator

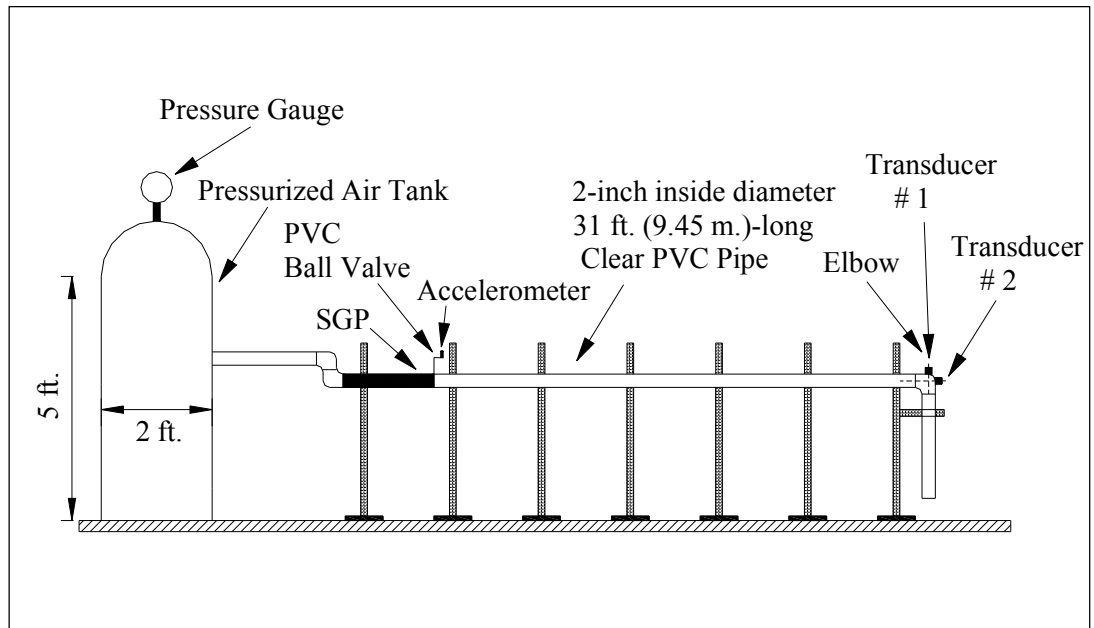


Figure 2.2 System setup used in Bozkuş's study [2].

pipe (SGP) located between the pressurizer and a PVC ball valve. By selecting a SGP of any desired length and filling it with water, it was possible to generate slugs with different initial lengths. With this system setup, liquid slugs with various initial

lengths and under the propelling effect of different initial tank pressures were driven along the horizontal and initially empty pipeline and the pressure time histories that form due to impact of the liquid slugs on the elbow were recorded by the transducers mounted on the elbow as shown in Figure 2.2. As a result of the analysis it was concluded that long slugs lost more amount of their initial masses than did the short slugs during their motion along the horizontal pipeline. In addition, for long and medium slugs, two different peak pressures were observed in the pressure recordings with respect to time at the elbow. The reason for the occurrence of this double peak phenomenon was attributed to the disintegration of the slug mass into two pieces following the sudden opening of the ball valve upstream. Another conclusion drawn in this study was that more air entrainment effect was observed in the cases of short slugs than compared to long slugs and this difference between the two cases was explained with the reason that short slugs had a longer normalized travel distance. It was also indicated in that study that large amounts of air entrainment was a factor that caused significant reduction in the densities of especially short liquid slugs.

Analytical study of Bozkuş [2] consisted of two different mathematical models. The first one of these models, called “Simple Model” [2], included two different control volume analyses; one for the determination of peak pressures at the elbow and another for obtaining pressure time history plots for the variation of impact pressures at the elbow. The second mathematical model was called the “Advanced Model” [2] and in this model, in addition to the slug dynamics equations that was used in the Simple Model, another set of equations that also takes into account the gas dynamics effects were included as a further improvement. The peak pressures at the elbow were also calculated with this advanced model. Both of the analytical models gave the peak pressures at the elbow induced by the short slugs as being higher than the experimentally obtained ones. This overestimation of the analytical models was indicated to be due to the fact that the air entrainment effect was neglected in these models, which was a phenomenon that caused the density of the liquid slug to reduce and thus, the experimentally obtained impact pressures to become smaller as compared to those from the analytical models. The analytically obtained peak pressures for long and medium slugs were stated to match closely with the experimental results. A detailed explanation for the Advanced Model of Bozkuş

[2] is given in Chapter III together with the analytical methods followed in writing the computer codes with both the Simple Model and the Advanced Model.

Bozkuş, et. al [20] published the findings of the study by comparing them to those from Fenton and Griffith [26] and it was stated that the normalized forces in Bozkuş's experimental study were nearly the same as those given by Fenton and Griffith except that the results from Bozkuş's study showed a variation of data over a relatively larger range of normalized force values. This discrepancy between the two results was indicated to be probably due to the differences in the experimental setups used. For example, it was pointed out that the pipe diameter in Bozkuş's study was twice as large as the one in the case of Fenton and Griffith's study. In addition, it was expressed that the pipe in Bozkuş's study was horizontal rather than the pipe inclined upwards pipe towards downstream that was used in the study of Fenton and Griffith. Furthermore, it was stated that in Bozkuş's study, a ball valve was used to control the motion of the slug; however, Fenton and Griffith utilized a ruptured disk for the same purpose. In conclusion, Bozkuş and Wiggert [20] suggested that these differences between the experimental setups were likely to be the reason for higher scatter of data in Bozkuş's study as compared to the values obtained by Fenton and Griffith.

Neumann and Griffith [24] studied how the forces acting on a 90° bend are affected if the bend is located downstream of a pipe expansion. As a result of an analysis by conducting a set of experiments it was concluded that the peak forces at a bend located after an expansion were very close to those that occurred in case of a pipe with a constant diameter. Another conclusion reached in that study was that for both types of the pipes considered, the slug traveling distances required for the force at the pipe bend to reduce to very small values were nearly the same.

Baran also [27] carried out an experimental and numerical study to investigate the hydrodynamics of an individual transient liquid mass in voided line. Baran's experimental setup consisted of an air tank and a pipeline which was inclined upward towards downstream, and this pipeline was connected to an air tank at its upstream end through a ball valve as shown in Figure 2.3. There was a

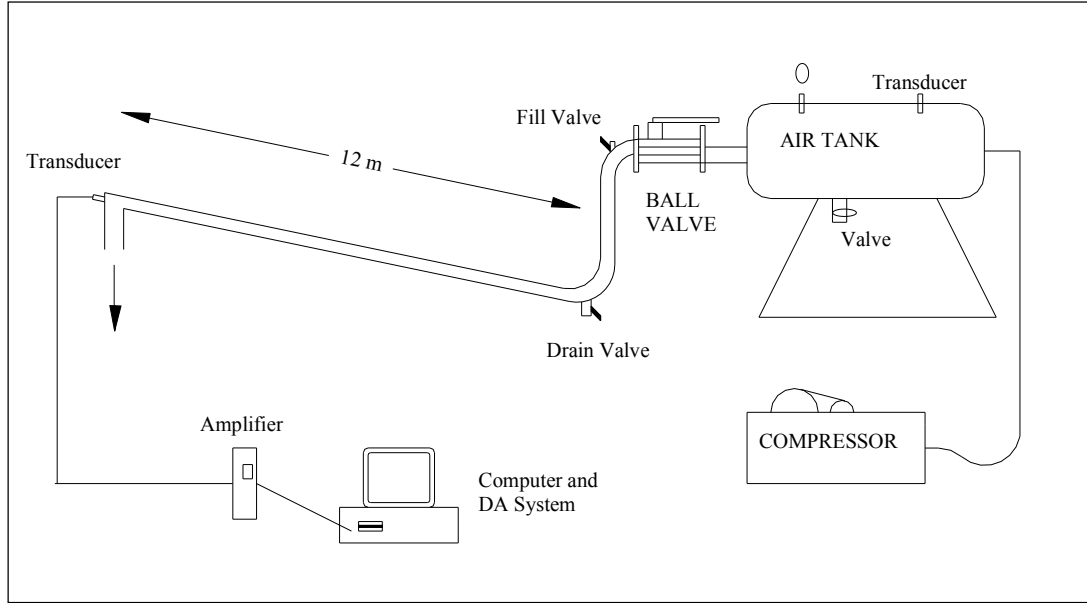


Figure 2.3 Experimental setup used by Baran [27].

sharp turn elbow connected to the downstream end of the inclined pipeline, which was extending downwards in the vertical plane. A transducer was located on the elbow to be used with the purpose of measuring slug impact pressures at that point of the elbow. It was possible with this system to create slugs with desired initial lengths by filling water from the fill valve into the pipeline, and then drive these slugs under the action of high pressure air from the air tank along the inclined pipeline upon sudden opening of the ball valve. With this experimental setup, Baran conducted a set of tests by propelling slugs with different initial lengths and tank pressures and by measuring the impact pressures at the elbow. The experimental results from these test cases were compared with those from Bozkuş's experimental study [2] and it was concluded that the results from both studies were in accordance with each other although there were some differences between the experimental setups used in these two studies as far as the sizes of the pipe diameters and the pipe inclinations selected were concerned.

Baran's numerical analysis was composed of the solution of Euler Equations with Godunov Method for the compressible gas part in the system shown in Figure 2.3 and of the calculation of impact pressures at the elbow by utilizing a method proposed by Daugherty and et. al. [30]. In the mathematical modeling, the mass loss

from the slug body during the motion of the slug was neglected in Baran's study. For the impact pressure calculation as suggested by Daugherty and et. al., a fictitious surge tank was assumed to exist at the elbow. Thus, the impact pressures were allowed to take values somewhere between those of sudden valve closure case, and of a stagnation pressure estimates that would have computed with the use energy equation for an elbow open to the atmospheric pressure at one end. The impact pressures at the elbow computed with this method underestimated the peak pressures at the elbow with respect to those from the experimental findings obtained in the same study. As a result of this numerical analysis, it was concluded that the modeling of the elbow so as to give results between the cases of existence of a surge tank and of a sudden valve closure would have provided the improvement of the results for the peak pressures obtained at the elbow.

Baran's results [27] for the variation of normalized peak force with respect to normalized dispersion distance was compared with the values in Bozkuş's [2] and Fenton's [22] studies in Bozkuş, et. al [28]. From this comparison, it was concluded that Baran's results complied with those of Bozkuş and Fenton although the normalized force values from Baran's study had some tendency to remain on the conservative side as Fenton's data. Making a comment on the obtained results from the three studies performed by Fenton [22], Bozkuş [2] and Baran [27], it was stated that there was a sharp drop in the normalized forces when the normalized slug travel distance with respect to initial slug length was greater than 6. Another conclusion drawn in this study was that the slanted configuration of the slug front shape with respect to the inclined pipeline had an increased effect in the occurrence of Taylor-Instability and thereby resulting in more air entrainment into the slug body to take place especially for short slugs during their motion.

CHAPTER III

MATHEMATICAL DEVELOPMENT FOR THE HORIZONTAL PART

3.1 Introduction

In the present study, the formulations for the calculation of impact pressures at the elbow of an initially voided horizontal pipeline applied by an air driven liquid slug are made in two stages. At first stage, the calculations required for the analysis of the motion of the liquid slug along the horizontal part of the pipeline is made by using a previously developed formulation by Bozkuş [2]. Then, in the second stage, final values for the hydrodynamics parameters obtained from the first part are used as initial conditions for the analysis of the motion of the slug in the elbow and the following vertical extension segment of the pipeline as the main purpose of the thesis

In this chapter, a numerical analysis for the hydrodynamics of the motion of an air driven liquid slug along an initially voided horizontal pipeline, performed previously by Bozkuş [2], is presented. The system setup used by Bozkuş for this purpose is as shown in Figure 2.2 and the description of this system was given in Chapter II. The mathematical formulation given in this chapter which was named as “Advanced Method” [2] in Bozkuş’s study covers the description of the accelerated motion of an individual liquid slug from zero initial velocity upon a sudden valve opening, under the action of the driving effect of high pressure air acting at the upstream side of the slug. The mass loss from the liquid slug due to its interaction with the pipe wall during the slug motion along the horizontal pipeline is also considered with the use of a calibration parameter. The flow of the high pressure gas upstream the liquid slug is analyzed by using 1-D gas dynamics equations and thus, the waterhammer effects within the region of slug driving gas volume is taken into

account. The solution of gas dynamics equations are made with method of characteristics and the mathematical expressions obtained from this part are coupled with a set of slug dynamics equations obtained from a control volume analysis, to close the system. During the solution, the upstream pressure boundary condition for the system is taken as the tank pressure at the pipe inlet and the downstream boundary condition is the zero atmospheric pressure at the slug front face. The calculations are performed until the computational procedure results in the case that the slug front face of the liquid slug reaches the elbow at the downstream end of the horizontal pipeline. The values for the slug driving pressure and the slug velocity corresponding to the arrival time of the slug front face at the entrance section of the elbow were then, taken to be utilized as initial conditions for a second stage of calculations that were made for the analysis of the slug motion within the elbow and the vertical extension segment of the same system shown in Figure 2.2.

In the following subsections, the derivation of slug dynamics equations with a control volume analysis, and the formulation for the flow of the gas driving the liquid slug by using 1-D gas dynamics equations and method of characteristics are presented. An algorithm that explains the use of the resulting equations from the above procedure is also given. In Section 3.5 of this chapter, a new formulation for the calculation of a functional hold up coefficient that was developed in the present study as an improvement of Bozkuş's [2] Advanced Method is also presented.

3.2 Slug Dynamics Equations

To analyze the motion of a liquid slug propelled by upstream high pressure air along a horizontal pipeline, Bozkuş [2] made a control volume analysis by selecting a control volume as shown in Figure 3.1. Then, he applied the conservation of mass and conservation of momentum principles over this control volume.

For the analysis of the slug motion, a set of simplifying assumptions were made. These assumptions are that:

- a) The slug flow is accepted as one-dimensional, incompressible and planar.
- b) Liquid density is constant.
- c) Pipe material is rigid and the pipe does not vibrate or move in any direction during the slug motion.

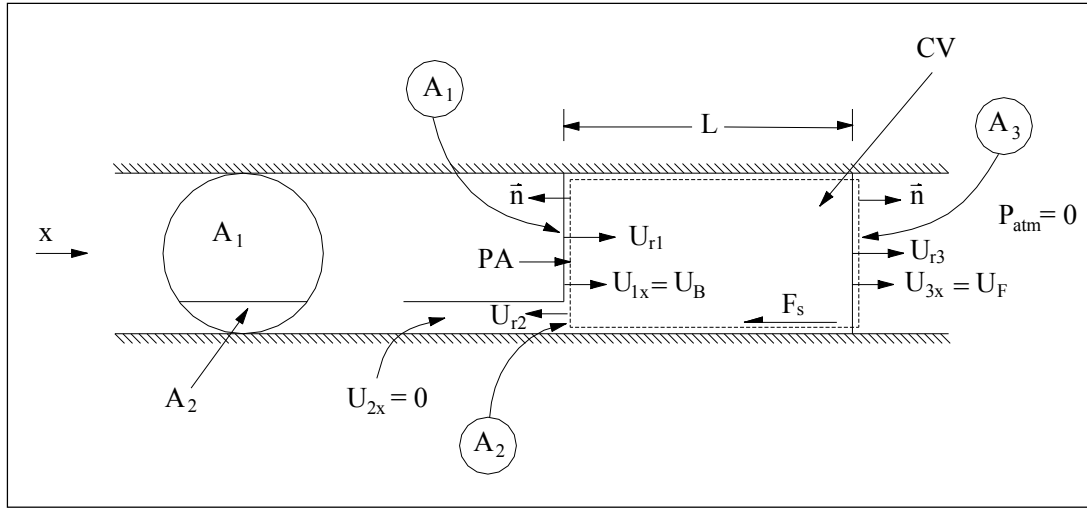


Figure 3.1 Control volume for the liquid slug selected by Bozkuş [2] along the horizontal pipeline.

- d) Gas (air) does not entrain into the liquid slug (water), in other words, one phase assumption is valid during the entire motion of the slug.
- e) A quasi-steady flow assumption is made to find the shear resistance to the slug flow.
- f) Some of the slug mass is lost during the motion.

The mass loss from the liquid slug during its motion due to interaction of the slug with the pipe wall by means of shearing effects was taken into account by using a hold up coefficient, α . An α value for the hold up coefficient means that the slug loses its mass through a percentage of $1-\alpha$ of pipe cross-sectional area, during its motion. For example, if α value is equal to 0.99, it means that slug losses its mass at a rate of 1% of the total pipe cross-sectional area. Thus, during the motion of the liquid slug by a distance of Δx along the horizontal pipeline, an amount of mass loss from the slug equal to the value of $\rho(1-\alpha)A\Delta x$ occurs. Here, the meanings of the symbols are as,

ρ : density of water

and

A : pipe cross-sectional area.

The hold up coefficient value, α , can only take values between 0 and 1. The

α value being equal to 1 indicates that there is no hold up or mass loss from the slug, while decreasing values of α indicates that more amount of mass loss from the slug is taking place.

In Bozkuş's study [2], during the motion of a liquid slug along the horizontal pipeline only single, selected fixed values of hold up coefficients were used in the calculations. However, in the present study, a function was developed which accounts for the variation of the value of the hold up coefficient, α , along the horizontal pipeline during the slug motion, in terms of the normalized travel distance of the liquid slug with respect to instantaneous slug length. The mathematical procedure for the development of this function is given in Section 3.5 of this chapter.

With the above indicated simplifying assumptions, the application of conservation of mass and conservation of momentum equations are given in the following subsections.

3.2.1 Conservation of Mass Equation

For the analysis of the slug motion, firstly the conservation of mass equation was written in its integral form for a control volume which is moving together with the liquid slug along the horizontal pipeline, as shown in Figure 3.1:

$$\int_{C.V.} \left(\frac{\partial \rho}{\partial t} \right) d\forall + \int_{C.S.} \rho (\vec{U}_b \cdot \vec{n}) dS + \int_{C.S.} \rho (\vec{U}_r \cdot \vec{n}) dS = 0 \quad (3.1)$$

In this equation \vec{U}_b and \vec{U}_r stand for the velocity of the boundary of the control surface, and the liquid velocity relative to the control surface boundary, respectively. Also, S is the surface area and \forall is the volume of the control volume selected.

Canceling first and second terms of Equation (3.1) and then, applying remaining part of Equation (3.1) and the relations

$$A_1 = \alpha A \quad (3.2)$$

$$A_2 = (1 - \alpha) A \quad (3.3)$$

$$A_3 = A \quad (3.4)$$

$$\vec{U}_{r1} = \vec{U}_B - \vec{U}_F \quad (3.5)$$

$$\vec{U}_{r2} = \vec{U}_F \quad (3.6)$$

and

$$\vec{U}_{r3} = 0 \quad (3.7)$$

to the control volume in Figure 3.1; Equation (3.8) below is obtained (Bozkuş [2]).

$$U_F = \alpha U_B \quad (3.8)$$

In above equations,

A : cross-sectional area of the pipe,

A_1, A_2, A_3 : areas of the parts of the pipe cross-section as shown in Figure 3.1,

U_{ri} : fluid velocity relative to the control surface i ,

U_B : velocity of the back face of the slug,

U_F : velocity of the front face of the slug,

\vec{n} : outer unit normal vector.

Now, apart from the above conservation of mass principle, a differential equation which relates the hold up coefficient, α , to the slug length, L , is utilized as given below.

$$\frac{dL}{dt} = U_F - U_B \quad (3.9)$$

Solving for U_B from (3.9) and substituting into (3.8), the following expression is obtained:

$$\frac{dL}{dt} = -\left(\frac{1}{\alpha} - 1\right) U_F \quad (3.10)$$

The resulting equation given in (3.10) is actually a form of continuity equation and given a value of hold up coefficient α , this equation can be used as a relation between the slug length L and the slug front velocity U_F .

3.2.2 Conservation of Momentum Equation

The general form of the conservation of momentum equation utilized is of the form

$$\sum F_x = \frac{d}{dt} \int_{C.V.} \rho U_x dV + \int_{C.S.} \rho U_x (\vec{U}_r \cdot \vec{n}) dS \quad (3.11)$$

Here,

U_x : liquid velocity relative to the fixed reference frame,

\vec{U}_r : liquid velocity relative to the control surface boundary,

F_x : net force acting on the selected control volume, in x -direction.

The left side of (3.11) can be written as:

$$\sum F_x = P A - \tau_0 (\pi D L) \quad (3.12)$$

where,

$$\tau_0 = \frac{1}{8} \rho f_f U_F^2 \quad (3.13)$$

and

D : pipe diameter,

P : air gage pressure driving the liquid slug acting at the slug upstream face,

π : pi number,

f_f : the Moody's friction factor,

τ_0 : wall shear stress.

In this formulation, the change in the direction of friction force with that of

fluid velocity was discarded with the assumption of no reverse flow.

In Bozkuş's study [2], a fixed average value of Moody's friction factor, f_f , was used in the calculations but in the present study, the friction factor value was calculated from Swamee-Jain formula (Walski [11]; Swamee and Jain [12]) given in (3.14) to improve the method.

$$f_f = \frac{1.325}{\left[\ln \left(\frac{\varepsilon}{3.7D} + \frac{5.74}{Re^{0.9}} \right) \right]^2} \quad (3.14)$$

In this expression,

ε : roughness height of the pipe wall,

Re : Reynolds number.

The Reynolds number can be calculated from

$$Re = \frac{\rho U_F D}{\mu} \quad (3.15)$$

where μ is the dynamic viscosity of water.

Next, substituting,

$$d\forall = A dL \quad (3.16)$$

$$U_{1x} = U_B \quad (3.17)$$

$$U_{2x} = 0 \quad (3.18)$$

$$U_{3x} = U_F \quad (3.19)$$

$$\vec{U}_{r1} = \vec{U}_B - \vec{U}_F \quad (3.20)$$

$$U_{r2} = U_F \quad (3.21)$$

$$U_{r3} = 0 \quad (3.22)$$

in Equation (3.11) according to the control volume selected in Figure 3.1, and also

using Equation (3.8) together with the final form of the conservation of mass expression given by (3.10), the following equation is obtained (Bozkuş [2]):

$$\frac{dU_F}{dt} + \left[\frac{f_f}{2D} - \frac{2}{L} \left(\frac{1-\alpha}{\alpha} \right) \right] U_F^2 = \frac{P}{\rho L} \quad (3.23)$$

In above derivation, U_{ix} stands for the fluid velocity relative to the global coordinate axis, on the surface i for the control volume, and in the x -direction

3.2.3 Slug Kinematics Equation

To complete the slug dynamics equations, in addition to above conservation equations, which are Equations (3.10) and (3.23), one more equation independent of these can be obtained from the slug kinematics. This last equation is simply an expression for the rate of change of the position of the front face of the slug with time, and can be given as:

$$\frac{dx}{dt} = U_F \quad (3.24)$$

In all of the expressions (3.10), (3.23) and (3.24), the slug front velocity U_F can be replaced with the mean slug velocity U and then, the final system of differential slug dynamics equations becomes

$$\frac{dU}{dt} + \left[\frac{f_f}{2D} - \frac{2}{L} \left(\frac{1-\alpha}{\alpha} \right) \right] U^2 = \frac{P}{\rho L} \quad (3.25)$$

$$\frac{dL}{dt} = -\left(\frac{1}{\alpha} - 1 \right) U \quad (3.26)$$

$$\frac{dx}{dt} = U \quad (3.27)$$

The average pressure value, P , in (3.25), is calculated from the analysis of the flow of the high pressure gas at the upstream side of the slug, and the formulations for this part of the calculation are given in the following section which includes the solution of gas dynamics equations.

3.3 Gas Dynamics Equations

For the analysis of the flow of the high pressure gas upstream the liquid slug, the conservation of mass, momentum and energy equations in differential form given by Equations (3.28), (3.29), (3.30) below were utilized by Bozkuş [2];

$$\frac{\partial P}{\partial t} + V \frac{\partial P}{\partial x} + \rho_a C^2 \frac{\partial V}{\partial x} = 0 \quad (3.28)$$

$$\frac{\partial V}{\partial t} + V \frac{\partial V}{\partial x} + \frac{1}{\rho_a} \frac{\partial P}{\partial x} = F_2 \quad (3.29)$$

$$\frac{\partial \rho_a}{\partial t} + V \frac{\partial \rho_a}{\partial x} - \frac{1}{C^2} \left(\frac{\partial P}{\partial t} + V \frac{\partial P}{\partial x} \right) = 0 \quad (3.30)$$

where

$$F_2 = - \frac{f_f P_{wet} V^2}{8 A} \quad (3.31)$$

and

$$C = \sqrt{\frac{\partial P}{\partial \rho_a}} = \sqrt{R_g T} . \quad (3.32)$$

Here, the meanings of the symbols are as follows:

ρ_a : density of air,

V : velocity within the air volume, in the x -direction,

P : average pressure at a cross-section of the pipeline,

t : time,

x : space coordinate along the axes of the horizontal pipe,

F : friction force per unit length of the pipe assuming no reverse flow,

P_{wet} : wetted perimeter of the cross-section,

C : wave speed,

R_g : gas constant,

T : temperature.

As the assumptions in using the above gas dynamics equations given by (3.28), (3.29), (3.30); one-dimensional, unsteady, nonuniform and a compressible gas flow was considered. In addition to these, the flow was also accepted as adiabatic, isothermal and turbulent.

The system of hyperbolic partial differential equations given by (3.28), (3.29), (3.30) were transformed to a set of total ordinary differential equations by using method characteristics. The transformation procedure followed for this purpose can be found in references from Moody [31], Chaudhry [32] or Streeter [33]. The resulting ordinary differential equations are given by expressions (3.33) and (3.34).

$$dP + \rho C V = F dt \quad \text{for} \quad \frac{dx}{dt} = V + C \quad (3.33)$$

$$dP - \rho C dV = -F dt \quad \text{for} \quad \frac{dx}{dt} = V - C \quad (3.34)$$

with

$$F = -\frac{\rho f_f CP_{wet} V^2}{8 A} \quad (3.35)$$

Equations (3.33) and (3.34) are valid over the computational domain starting from the upstream pressurizer up to the back face of the liquid slug shown in Figure 3.2. As the slug is moving downstream continuously in an accelerating pattern, the computational domain gets larger and larger by time as shown in this figure. Equation (3.33) here is a right travelling characteristic equation and is valid along the C^+ line in the computational domain, and Equation (3.34) is a left travelling characteristics equation which is valid along the C^- line.

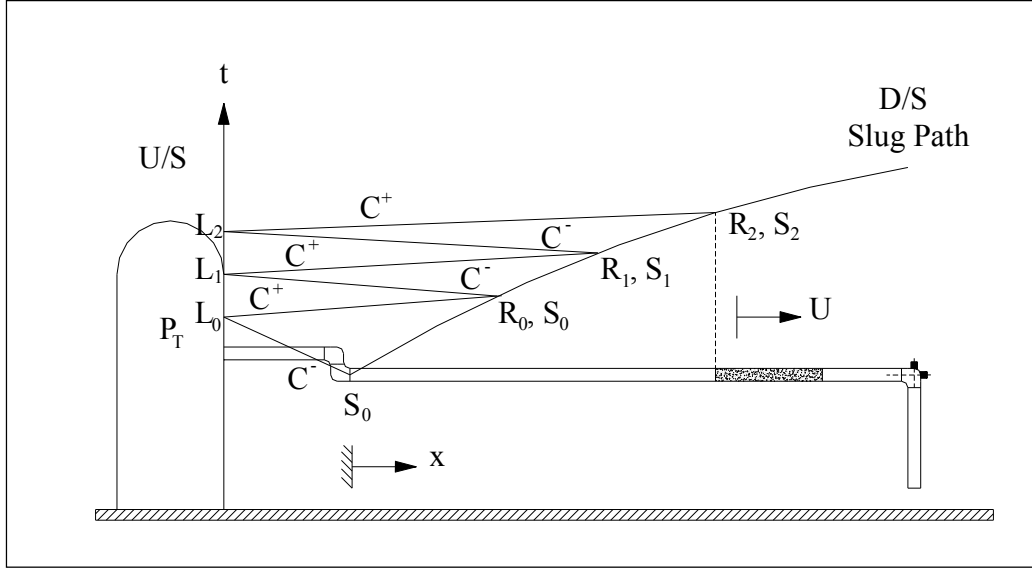


Figure 3.2 Computational domain used by Bozkuş [2] for the solution of gas dynamics equations.

3.4 Coupling of Gas and Slug Dynamics Equations

To solve the gas dynamics and slug dynamics equations in a closed form pattern, the first slug dynamics equation given by (3.25) can be rewritten as in the following form:

$$\frac{dU}{dt} + \left[\frac{f_{fw}}{2D} - \frac{2}{L} \left(\frac{1-\alpha}{\alpha} \right) \right] U^2 = \frac{P_w - P_{atm}}{\rho_w L} \quad (3.36)$$

The meanings of the symbols here are as:

f_{fw} : friction factor for water,

P_w : driving air absolute pressure acting at the upstream face of the slug,

P_{atm} : atmospheric absolute pressure,

ρ_w : density of water.

Then, by integrating the slug dynamics equations given in (3.26), (3.27) and (3.36) between the grid points along the slug path curve shown in Figure 3.2; and integrating the gas dynamics equations given by (3.33) and (3.34) along the

corresponding characteristic lines in the computational domain, a set of formulas for the upstream and the downstream boundary computations of the pressurized gas region in the horizontal pipeline is obtained. While making these calculations, the known boundary conditions of the system together with Equation (3.32) and the ideal gas equation given in (3.37) are also used (Bozkuş [2]).

$$\rho = \frac{P}{R_g T} \quad (3.37)$$

The formulas for the calculation of upstream boundary conditions are as follows as obtained by Bozkuş [2]:

$$P_L = P_T \quad (3.38)$$

$$\rho_L = \frac{P_L}{R_g T} \quad (3.39)$$

$$C_L = C = \sqrt{R_g T} \quad (3.40)$$

$$t_L = t_S + \frac{x_L - x_S}{(V - C)_S} \quad (3.41)$$

$$\Delta t = t_L - t_S \quad (3.42)$$

$$V_L = \frac{P_L - P_S + (\rho_a)_S C V_S}{(\rho_a)_S C \left[\left(\frac{f_a}{2D} \right) V_S \Delta t + 1 \right]} \quad (3.43)$$

The subscripts L and S of the variables in above equations indicate the location of left rights boundaries where the variables are being evaluated as shown in Figure 3.2.

The algorithm for the calculation of the values at the upstream boundary of the pressurized gas region in the system is presented below.

- 1) Calculate P_L from Equation (3.38) by using the boundary value for the

gas pressure P_T at the pressurizer tank.

- 2) Calculate gas density ρ_L by using (3.39).
- 3) Compute the wave speed C_L at the upstream boundary of the pressurized gas region from (3.40).
- 4) Calculate t_L from Equation (3.41) by taking $x_L = 0$, and using the known values of variables with the subscript S that were calculated at the previous time step (Figure 3.2).
- 5) Compute Δt from (3.42).
- 6) Calculate the gas velocity at the left boundary, V_L , using (3.43).

The set of equations obtained by Bozkuş [2] for the calculation of downstream boundary values of the computational domain of the pressurized gas volume are given below.

$$x_R = \frac{U_S (V + C)_L (t_L - t_S) - x_L U_S + x_S (V + C)_L}{(V + C)_L - U_S} \quad (3.44)$$

$$\Delta t_1 = \frac{(x_R - x_L)}{(V + C)_L} \quad (3.45)$$

$$t_R = t_L + \Delta t_1 \quad (3.46)$$

$$\Delta t_2 = \frac{(x_R - x_S)}{U_S} \quad (3.47)$$

$$L_R = L_S - \left(\frac{1 - \alpha}{\alpha} \right) U_S \Delta t_2 \quad (3.48)$$

$$C_R = C = \sqrt{R_g T} \quad (3.49)$$

$$C_1 = \left[f_a \frac{(\rho_a)_L C}{2D} V_L \Delta t_1 + (\rho_a)_L C \right] \quad (3.50)$$

$$C_2 = \left[1 + \frac{f_w}{2D} U_s \Delta t_2 - 2 \left(\frac{1-\alpha}{\alpha} \right) \frac{U_s}{L_s} \Delta t_2 \right] \quad (3.51)$$

$$P_R = P_L + (\rho_a)_L C V_L - \frac{C_1}{C_2} \left[\frac{1}{\rho_w} \left(\frac{P_w - P_{atm}}{L} \right)_s \Delta t_2 + U_s \right] \quad (3.52)$$

$$u_R = \frac{\frac{1}{\rho_w} \left[\frac{P_w - P_{atm}}{L} \right]_s \Delta t_2 + U_s}{\left[1 + \frac{f_w}{2D} U_s \Delta t_2 - 2 \left(\frac{1-\alpha}{\alpha} \right) \frac{U_s}{L_s} \Delta t_2 \right]} \quad (3.53)$$

The downstream boundary conditions indicated with the subscript R , for the domain of gas volume are calculated with the following algorithm:

- 1) Calculate the position of the upstream face of the slug from (3.44).
- 2) Compute the time increment, Δt_1 and Δt_2 , values from Equations (3.45) and (3.47).
- 3) Calculate t_R value by using (3.46).
- 4) Compute slug length, L_R , by using the expression given by (3.48).
- 5) Calculate the wave speed, C_R , from (3.49).
- 6) Compute the pressure acting at the upstream face of the slug, P_R , by using Equation (3.52).
- 7) Calculate the velocity of the upstream face of the slug, U_R , from Equation (3.53).

During the above calculations, the time dependent decrease of the tank pressure, P_T , is also taken into account according to the data given in Figure 3.3. In this figure;

P_0 : initial tank pressure at the pressurizer tank.

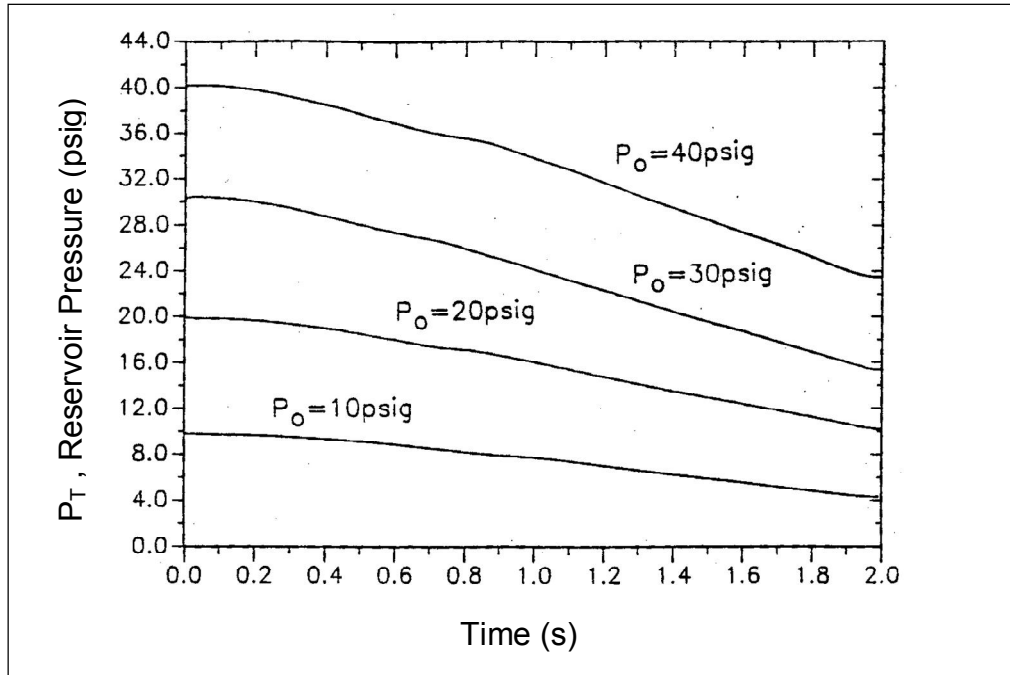


Figure 3.3 Variation of pressure at the upstream pressure tank (Bozkuş [2]).

The calculation procedure given above is continued until the front face of the slug reaches the entrance section of the elbow with a computer program BOZKUŞ-2 coded by Bozkuş [2]. Then, the final values for the slug velocity, slug length and the driving air pressure acting at the upstream face of the liquid slug obtained from these horizontal pipe calculations are used as initial conditions for the analysis of the slug motion in the elbow and the following vertical extension segment of the pipeline, given in the later chapters of the thesis.

3.5 Functional Hold Up Coefficient

To be able to better represent the actual hold up amount that occurs during the motion of the slug along the horizontal part of the pipeline, a new approach of using a functional hold up coefficient was made in the present study. The new hold up coefficient that was developed in this study is in the form a function of normalized slug travel distance with respect to the instantaneous slug length as given in Equation (3.54). The details for the development of this function are presented in Appendix

A.1.

$$\left. \begin{aligned} \alpha(L_p / L_s) &= 0.0385(L_p / L_s) + 0.7439 \quad \text{if} \quad 5.4940 \leq L_p / L_s \leq 6.6519 \\ \text{and} \\ \alpha(L_p / L_s) &= 1. \quad \text{if} \quad 6.6519 < L_p / L_s \end{aligned} \right\} \quad (3.54)$$

This method of calculating the hold up coefficient, α , is actually a more developed form of the previous one used in Bozkuş's [2] study in which the hold up coefficient was kept at a constant value during the whole motion of the slug along the horizontal part of the pipeline.

The expression in (3.54) is the functional hold up coefficient in terms of the travel distance normalized with respect to the instantaneous slug length. Thus, with the use of this formula, the hold up coefficient was allowed to change as a function of instantaneous slug length, L_s , during the motion of the slug along the pipeline, given a certain value for the length of the horizontal part of the pipeline, L_p .

With this new development of the functional hold up coefficient, the hold up value, α , is calculated by using the formula given by (3.54) at the beginning of each time step of the calculations made by executing the algorithm given in Section 3.4 for the motion of the liquid slug along the horizontal part of the pipeline

3.6 Closure

In this chapter, an analytical method for the analysis of an air driven liquid slug motion along a horizontal pipeline was given as proposed by Bozkuş [2]. For the improvement of the method, a mathematical development to obtain a functional hold up coefficient as a part of the present study was also presented in Section 3.5 of this chapter.

The same system setup given in Figure 2.2, which was used by Bozkuş [2] for the analysis of the slug motion along the horizontal part of the pipeline, was also utilized as the system in the present study for the modeling of the slug motion in the elbow and the following vertical extension segment of the pipeline. In the present

study, for the calculation of impact pressures applied by the slug at the elbow of the system; firstly, that motion of the slug along the horizontal pipeline was analyzed with Bozkuş's [2] method given in this chapter, and the final values of the hydrodynamic parameters for the case that the slug front face reached the elbow were calculated. Then, by using those final set of values as the initial values in the new mathematical model that was made in the present study, the analysis of the slug motion in the elbow and the following vertical extension segment was made. To perform these calculations, a computer program KAYHAN was coded in this study with the purpose of computing the impact pressure at the elbow by simulating the slug motion in the system. This code was written in FORTRAN, and it used a previously written code BOZKUŞ-2 by Bozkuş [2] for the simulation of the slug motion along the horizontal pipe in the system.

The formulation for the analysis of the slug motion in the elbow and the vertical extension segment as the aim of the present study, after the slug reaches the entrance section of the elbow, is given in the next chapter of the thesis, together with the discussion of the results and the comparison of them with those from the previous studies.

CHAPTER IV

MATHEMATICAL DEVELOPMENT FOR THE ELBOW PART

4.1 Introduction

In this chapter, a mathematical development for the analysis of the slug motion in the elbow and the following vertical extension segment of the pipeline system shown in Figure 2.2 is given. The elbow and the vertical extension segment calculations here are a continuation of the analysis of the slug motion along the horizontal pipeline presented in Chapter III. Therefore, the final values for the hydrodynamic parameters obtained from horizontal pipe calculations are used as the initial conditions for the elbow and the vertical extension segment calculations given in this chapter.

The aim for making the numerical analysis of the slug motion in the elbow and the vertical extension segment given in this chapter is to predict the time dependent impact pressures at the elbow and to find the transient hydrodynamic forces acting on the elbow and the vertical extension segment.

For this purpose, an axial velocity profile function with a 3-D shape was assumed in Section 4.2. Then, by utilizing this velocity profile function, the time dependent impact pressures at the elbow, and the transient forces applied by the liquid slug on the elbow and the vertical extension segment of the pipeline were formulated in Sections 4.3 and 4.4, respectively. In Section 4.5, some numerical integration methods are presented to be used for the evaluation of some integral terms of the equations given in Sections 4.3 and 4.4. A calibration function was proposed in Section 4.6 for the variation of the skewed shape of the axial velocity profile function in the elbow and the vertical extension segment. The non-

dimensionalization and the discretization of the equations are given in Sections 4.7 and 4.8, respectively. In section 4.9, the mesh sizes and the input data used are presented.

4.2 Assumed Axial Velocity Profile Function

In this section, an axial velocity profile function with a 3-D shape is assumed in the elbow and the vertical extension segment of the system shown in Figure 2.2, which can change in shape along these parts of the pipeline with the help of a calibration function. This assumed velocity profile function was used later on, in reducing the number of unknown dependent variables in momentum equations given in Section 4.3. The transient force calculations in Section 4.4 were also made by using this velocity profile function.

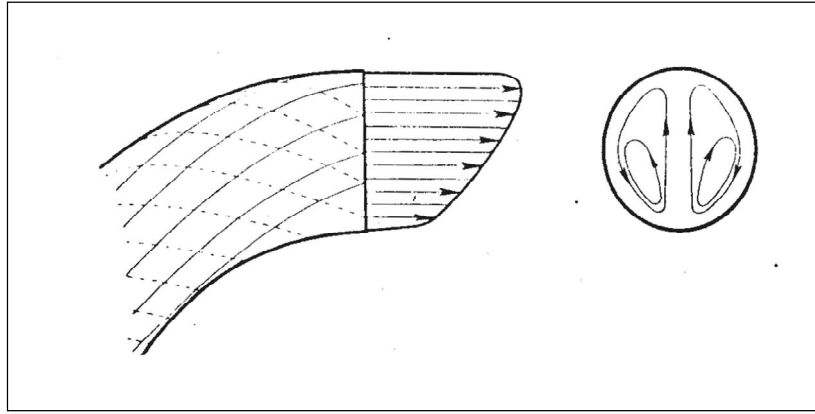


Figure 4.1 Velocity distribution in a curved pipe given by Prandtl [13], [14] (Schlichting [10]).

The general pattern of the cross-sectional view of the axial velocity profile and the velocity distribution over the pipe cross-section, for steady uniform turbulent pipe flow in curved pipes is given in Figure 4.1 as investigated firstly by Prandtl [13], [14] (Schlichting [10]). The flow of the liquid slug in the elbow and vertical extension segment of the pipeline in the present study is actually of type unsteady and non-uniform; however, as a simplification, the shape of the axial velocity profile in the current study was selected in such a way that the cross-section of the assumed

profile is of the form depicted in Figure 4.1 as suggested by Prandtl.

For this purpose two cone equations were utilized one being an oblique cone and the other having a symmetric and truncated shape and the plot of these two cones were mounted on each other to get an assumed turbulent velocity profile with its point of maximum shifted towards the convex side of the elbow by some amount.

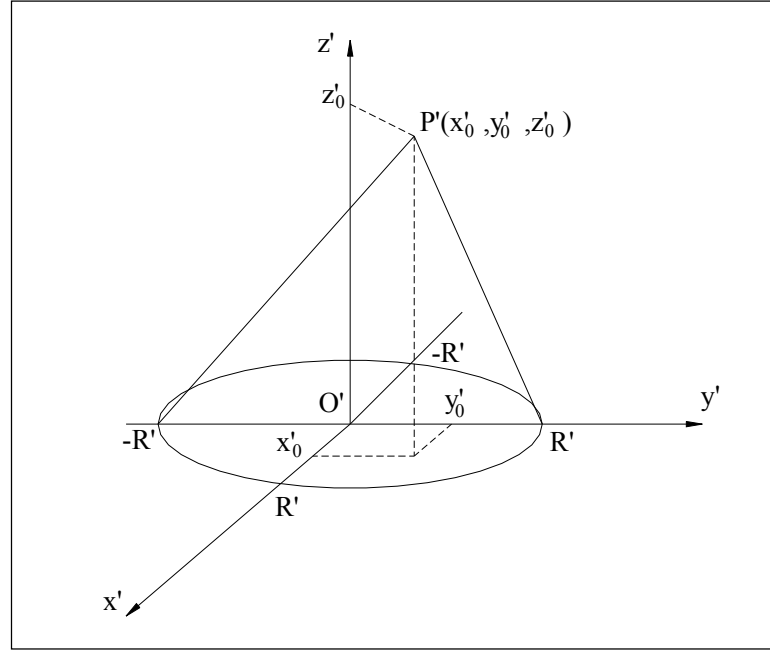


Figure 4.2 Parameters for the general oblique cone equation.

The most general equation for an oblique cone is given in cartesian coordinates in Equation 4.1. (Young [9])

$$(x'_0 z' - x' z'_0)^2 + (y'_0 z' - y' z'_0)^2 = R'^2 (z' - z'_0)^2 \quad (4.1)$$

The parameters for this general oblique cone equation in (4.1) are as given in Figure 4.2.

According to this figure,

x', y', z' : coordinate axes,

x'_0, y'_0, z'_0 : coordinates of the apex of the cone,

R' : radius of the bottom circle of the cone,

O' : origin of the cartesian coordinate system.

By using the general cone equation given in (4.1), an equation in the form of a non-differentiable function for the assumed turbulent axial velocity profile with 3-D shape was obtained, the cross-sectional view of the plot of which is shown in Figure 4.3. In this figure, the cross-sectional shape of the assumed velocity profile function is given over the vertical mid-plane of the elbow and the vertical extension segment.

While selecting the velocity profile equation, it was accepted that the maximum velocity occurs in the vertical mid-plane of the elbow and at a distance R_m away from the origin of the local coordinate system as measured in the positive y' - direction as shown in Figure 4.3. This general pattern for the shape of the velocity profile was suggested by making an analogy with that of a steady uniform turbulent pipe flow in curved pipes as investigated firstly by Prandtl [13], [14]. (Schlichting [10])

For the symmetrical bottom cone part of the axial velocity profile equation, with 3-D shape, the following function was used.

$$u_s = (R - \xi) \tan \theta_f \quad (4.2)$$

Equation given in (4.2) is valid for the domain of the bottom cone which is defined by

$$y'_1 < \xi \leq R \quad (4.3)$$

according to the polar coordinate system given for the cross-sectional view of the elbow in Figure 4.5, and considering the placement pattern of the bottom cone in the cartesian coordinate system shown in Figure 4.4.

And, for the upper oblique cone part of the axial velocity profile function, the expression given by (4.4) was utilized.

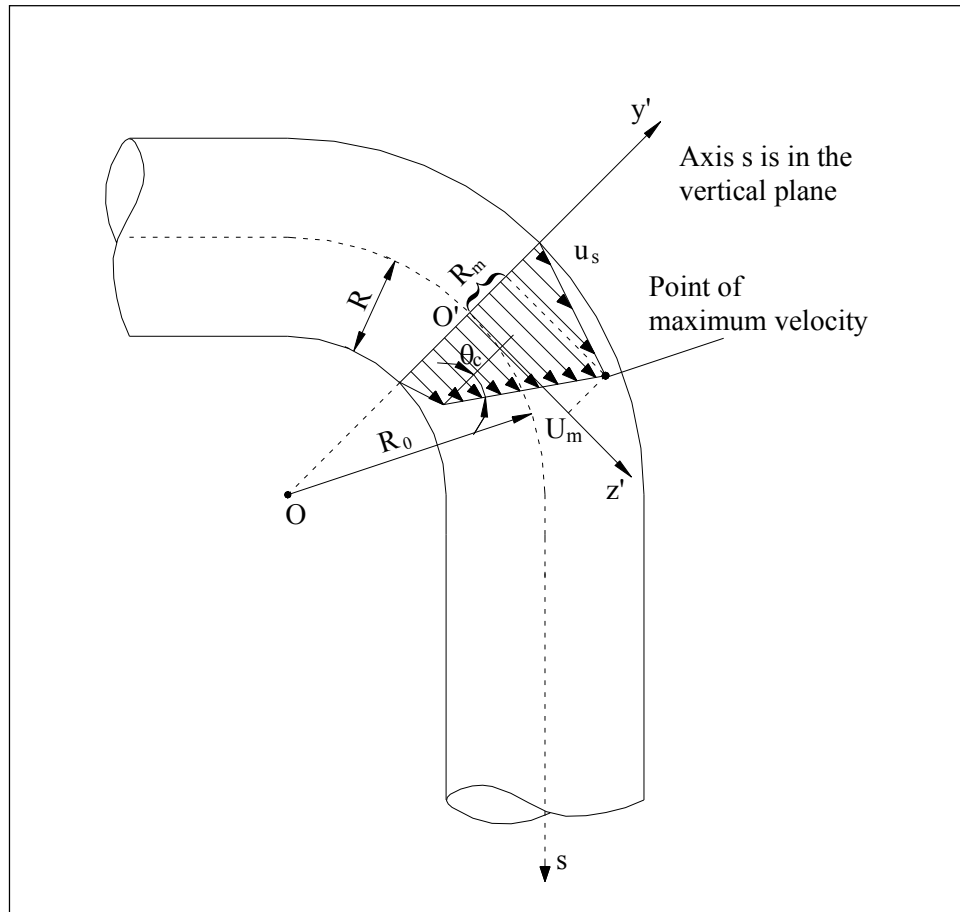


Figure 4.3 Cross-sectional shape of the assumed turbulent velocity profile function.

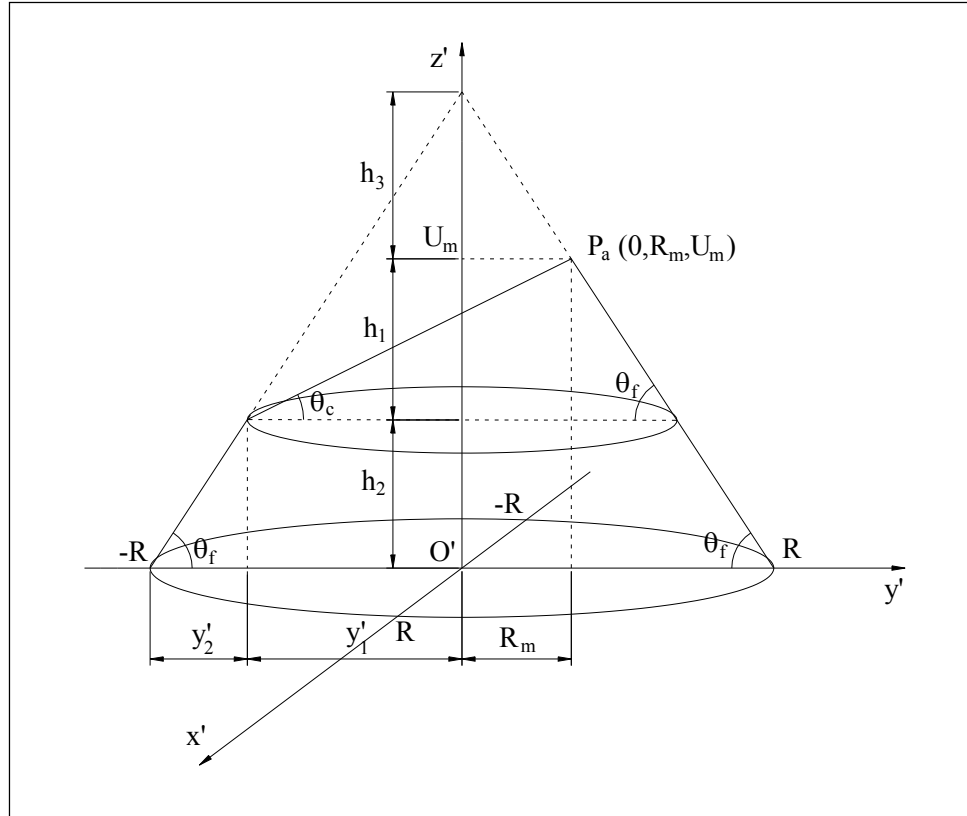


Figure 4.4 Parameters used for the assumed velocity profile in a single coordinate system.

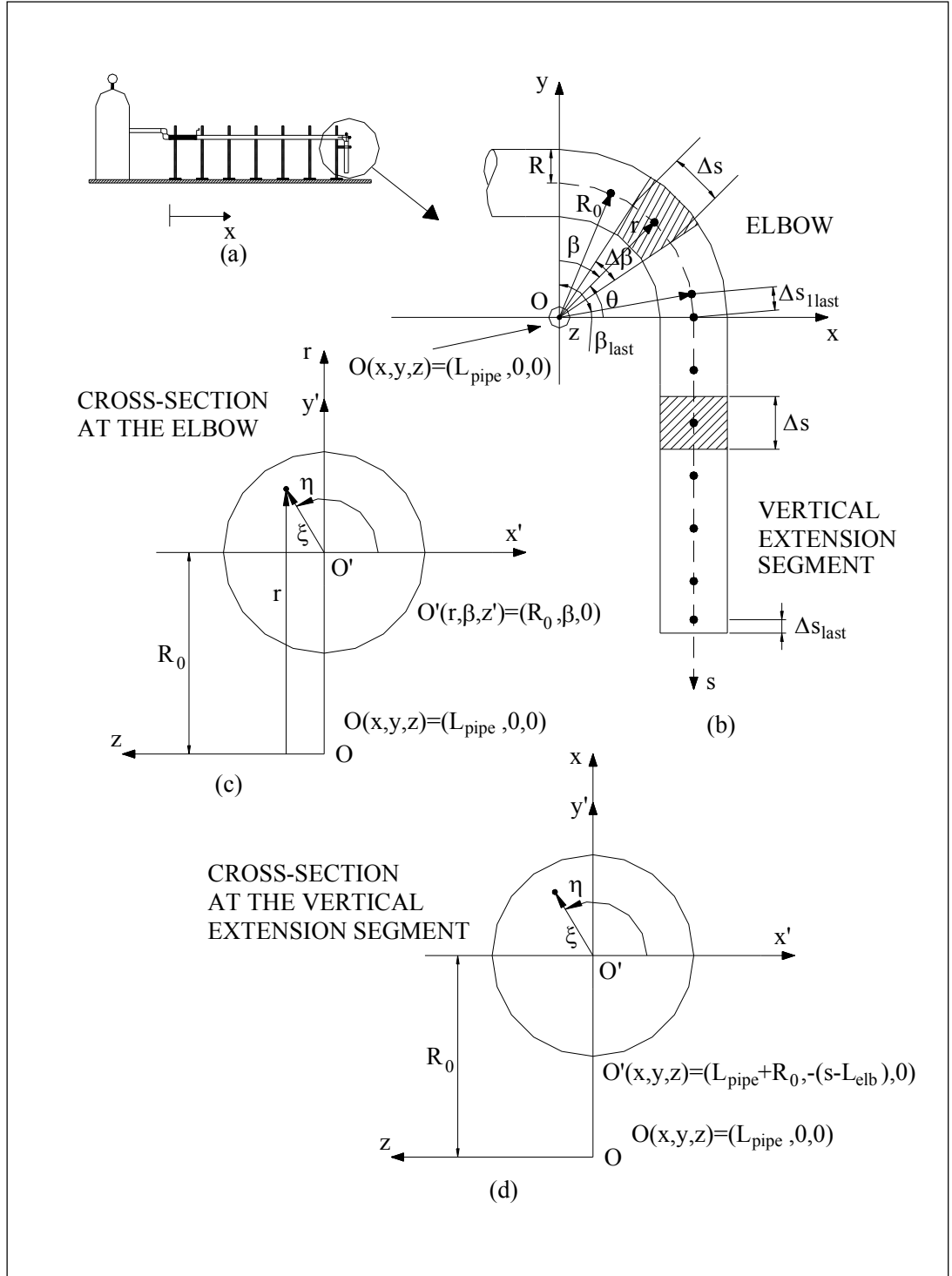


Figure 4.5 (a) Complete physical setup for the system (Bozkuş [2]);
 Computational domain for (b) the elbow and the vertical extension segment,
 (c) the cross-section of the elbow,
 (d) the cross-section of vertical extension segment of the pipe.

$$u_s = \frac{1}{(y_1'^2 - R_m^2)} \left[y_1'^2 h_1 - R_m h_1 \xi \sin \eta - R_m^2 h_2 + y_1'^2 h_2 - \left[-2y_1'^2 h_1^2 R_m \xi \sin \eta - R_m^2 h_1^2 (\xi \cos \eta)^2 + R_m^2 y_1'^2 h_1^2 + y_1'^2 h_1^2 (\xi \cos \eta)^2 + y_1'^2 h_1^2 (\xi \sin \eta)^2 \right]^{\frac{1}{2}} \right] \quad (4.4)$$

The expression in (4.4) for the upper oblique cone part of the velocity profile function shown in Figure 4.4 is valid over that region of the pipe cross-section defined by

$$0 \leq \xi \leq y_1' \quad (4.5)$$

according to the polar coordinate system for the cross-section of the elbow given in Figure 4.5.

The procedure for the mathematical development of the expressions given by (4.2) and (4.4) above are given in Appendices A.2.1 and A.2.2, respectively.

The meanings of the symbols in equations (4.2) to (4.5) are as:

ξ : radial coordinate axis over the pipe cross-section,

η : circumferential coordinate axis over the pipe cross-section,

R : pipe radius,

R_m : distance of the point of maximum velocity from the origin of the local coordinate system, measured along the y' axis, according to Figure 4.4,

θ_f : angle for the gradient of the velocity profile at the pipe wall,

with other parameters being as shown in Figure 4.4.

By combining two cone equations, the assumed velocity profile was intended to be given a shape similar to the actual turbulent velocity profile. The shape of this assumed profile was also allowed to change along the elbow and the extension segment with the aid of a calibration function for the angle θ_c shown in Figure 4.4. With this calibration function in the form of

$$\theta_c = \theta_c(s), \quad (4.6)$$

θ_c value was changed along the s -curve in the elbow and the extension segment of the pipe at the desired rate for the calibration purposes.

The values for the parameters R_m , y'_1 , h_1 , h_2 can be calculated by using geometry, from Figure 4.4 as

$$R_m = R - \frac{U_m}{\tan \theta_f} \quad (4.7)$$

$$y'_1 = \frac{(U_m - R \tan \theta_f)(\tan \theta_c + \tan \theta_f)}{\tan \theta_f (\tan \theta_c - \tan \theta_f)} \quad (4.8)$$

$$h_1 = 2 \tan \theta_c \left(\frac{U_m - R \tan \theta_f}{\tan \theta_c - \tan \theta_f} \right) \quad (4.9)$$

$$h_2 = \frac{2R \tan \theta_c \tan \theta_f - U_m (\tan \theta_c + \tan \theta_f)}{\tan \theta_c - \tan \theta_f} \quad (4.10)$$

where

U_m : maximum velocity on the assumed velocity profile function.

The parameters U_m and θ_f in expressions (4.7) to (4.10) are calculated as given in Appendix A.2.3.

By knowing the values of the parameters given in (4.7), (4.8), (4.9) and (4.10), the piece-wise smooth velocity profile function given by Equations (4.2) and (4.4) can be defined.

4.3 Calculation of the Impact Pressures at the Elbow

In the present study, the time dependent impact pressure distribution on an elbow of an initially voided pipeline, applied a by a propelled liquid slug under the driving effect of high pressure air from upstream, were obtained by solving 1-D Reynolds Equations numerically. The reason for choosing the Reynolds Equations was the highly turbulent character of the slug flow due to very high velocities

attained in the system. The solution was made over a computational domain selected within the elbow and the following vertical extension segment of Bozkuş's [2] system setup shown in Figure 2.2. The elbow and the vertical extension segment calculations given here are a continuation of those made for the analysis of the slug motion along the horizontal part of the pipeline, performed previously by Bozkuş [2] as presented in Chapter III. In the analysis, the final values for the hydraulic parameters obtained from the horizontal pipe calculations that corresponds to the arrival time of the slug front face at the entrance section of the elbow, were utilized as the initial values of the elbow and the vertical extension segment calculations given in this chapter.

As the domain over which the Reynolds Equations were solved, that portion of the elbow and the vertical extension segment of the system occupied by the liquid slug at any instant during its motion was selected. With this selection of the solution domain, the downstream boundary condition for the pressure value was taken as the atmospheric pressure that occurs at the slug front face. By using this downstream boundary condition, the average pressure values were calculated starting from the exit of the vertical extension segment towards upstream up to the entrance section of the elbow. While calculating the average pressure distribution along the elbow, the local impact pressures that occur at the top point of each cross-section of the elbow were also calculated with another application of 1-D Reynolds Equations applied in the direction of radius of curvature of the elbow this time, starting from the center point up to the top point of the same cross-section. During these radial calculations, the local pressure boundary condition at center point of the each cross-section was accepted to be equal to the average pressure that occurs at the same cross-section as an assumption. While calculating the pressure values, 1-D Reynolds Equations in cartesian coordinates were used in the calculations that were made for the vertical extension segment, whereas 1-D cylindrical polar Reynolds Equations were utilized for the elbow part calculations. The pressure values were solved from these Reynolds Equations by using an assumed axial velocity profile function having a skewed 3-D shape, and the shape of this velocity profile was allowed to change along the elbow and the vertical extension segment by means of a calibration process.

The actual pressure distribution along the elbow and the vertical extension

segment has a time dependent pattern due to the transient nature of the liquid slug motion in the system and; therefore, the above mentioned pressure distribution calculations were repeated for each time step of the slug motion along the elbow and the following vertical extension segment. During these calculations, the time dependent average velocity of the liquid slug was found from a set of slug dynamics equations applied on that part of the slug remaining in the horizontal part of the pipeline as proposed by Bozkuş [2]. The value for the average velocity calculated from the slug dynamics equations were then, taken to be same along that length of the slug remaining horizontal pipeline, elbow and the vertical extension segment due to incompressibility assumption made for the flow of the liquid slug.

4.3.1 Simplifying Assumptions

A set of assumptions were made to simplify the numerical procedure for the solution of Reynolds Equations in the domain of the elbow and the vertical extension segment of the system. These assumptions are;

- a) Slug front is planar but the shape of the axial velocity profile of the liquid slug is three-dimensional:

Accepting that the slug front face is always a plane surface permitted the application of 1-D Reynolds Equations to solve for the pressure distribution along the elbow and the vertical extension segment. While making these 1-D solutions, the 3-D skewed shape of the axial velocity profile of the liquid slug was also considered with the aid of an assumed and calibrated 3-D axial velocity profile function.

- b) Flow is incompressible:

Although during the motion of the liquid slug along the horizontal pipeline the compressibility effects of high pressure gas from the pressurizer was taken into account; in the part of the calculations for the motion of the slug along the elbow and the vertical extension segment, the gas which drives the slug was accepted as incompressible by neglecting gas dynamics effects in the calculations. The flow of the liquid slug was also accepted as incompressible during its whole motion in the system. As a result of this incompressible flow assumption for the liquid slug, and the continuity principle; the discharge of the slug flow was taken as constant in all parts of the pipeline it occupies at given time step of the slug motion. However, the

3-D skewed shape of an assumed and the calibrated axial velocity profile function was allowed to change for the slug flow in the elbow and the vertical extension segment with the aid of a calibration function.

- c) The liquid slug was accepted as having a constant density during its motion.
- d) The pipe material was accepted to be rigid, and the pipe was taken to fixed at its place so that it does not move in any direction and does not vibrate.
- e) One phase flow assumption was made for the liquid slug (water) and therefore, gas (air) entrainment into the slug was neglected.
- f) Shear resistance to the gas and liquid slug flow was considered by assuming that the flow is steady, fully developed and incompressible.
- g) No hold up was considered to occur during the motion of the slug in the elbow and the vertical extension segment of the pipeline.
- h) Reduction of the air pressure between the exit of the pressurizer tank and the slug upstream face was taken to be a constant value and is equal to that which occurs at instant of arrival time of the slug front face at the entrance section of the elbow, during the elbow and the vertical extension segment calculations.
- i) Frictional resistance and dynamics of the air downstream the slug front face was neglected.
- j) The axial velocity profile function with a 3-D skewed shape was assumed to be composed two cone equations as given previously in Chapter IV.
- k) Average pressure at any section of the elbow was assumed to be equal to the local pressure value at the center point of the same cross-section.

The planar slug front face assumption given in item (a) above was made in order to avoid the difficulties in the solution that would have arisen due to consideration of the deformation of the slug front shape during its motion through the elbow and the vertical extension segment of the pipeline. Neglecting the deformation of the slug front face and accepting the front face as planar brought adopting of a 1-D numerical solution technique for the elbow and the vertical extension segment calculations as was the case also for the horizontal part calculations of the pipeline.

Selection of a 1-D solution procedure for Reynolds Equations in the elbow and the vertical extension segment of the present study can be considered as a continuation of 1-D approach used for the horizontal pipe calculations performed by Bozkuş [2]. Also, adopting a 1-D solution technique can be thought to be a suitable choice since the experimental data for the peak pressures at the elbow are available only at single points for the locations of transducer #1 and #2 from Bozkuş's study.

As a part of the simplification process, some dependent variables in the cartesian and cylindrical polar Reynolds Equations were eliminated while obtaining the formulas given in this section. The incompressible Reynolds Equations in cartesian coordinates are given below as presented by Bird and et. al. [8]:

In x -direction:

$$\begin{aligned} \rho \left(\frac{\partial V_x}{\partial t} + V_x \frac{\partial V_x}{\partial x} + V_y \frac{\partial V_x}{\partial y} + V_z \frac{\partial V_x}{\partial z} \right) &= -\frac{\partial p}{\partial x} \\ -\rho \left(\frac{\partial}{\partial x} \langle V'_x V'_x \rangle + \frac{\partial}{\partial y} \langle V'_y V'_x \rangle + \frac{\partial}{\partial z} \langle V'_z V'_x \rangle \right) &+ \mu \left(\frac{\partial^2 V_x}{\partial x^2} + \frac{\partial^2 V_x}{\partial y^2} + \frac{\partial^2 V_x}{\partial z^2} \right) + \rho g_x \end{aligned} \quad (4.11)$$

In y -direction:

$$\begin{aligned} \rho \left(\frac{\partial V_y}{\partial t} + V_x \frac{\partial V_y}{\partial x} + V_y \frac{\partial V_y}{\partial y} + V_z \frac{\partial V_y}{\partial z} \right) &= -\frac{\partial p}{\partial y} \\ -\rho \left(\frac{\partial}{\partial x} \langle V'_x V'_y \rangle + \frac{\partial}{\partial y} \langle V'_y V'_y \rangle + \frac{\partial}{\partial z} \langle V'_z V'_y \rangle \right) &+ \mu \left(\frac{\partial^2 V_y}{\partial x^2} + \frac{\partial^2 V_y}{\partial y^2} + \frac{\partial^2 V_y}{\partial z^2} \right) + \rho g_y \end{aligned} \quad (4.12)$$

In z -direction:

$$\begin{aligned} \rho \left(\frac{\partial V_z}{\partial t} + V_x \frac{\partial V_z}{\partial x} + V_y \frac{\partial V_z}{\partial y} + V_z \frac{\partial V_z}{\partial z} \right) &= -\frac{\partial p}{\partial z} \\ -\rho \left(\frac{\partial}{\partial x} \langle V'_x V'_z \rangle + \frac{\partial}{\partial y} \langle V'_y V'_z \rangle + \frac{\partial}{\partial z} \langle V'_z V'_z \rangle \right) &+ \mu \left(\frac{\partial^2 V_z}{\partial x^2} + \frac{\partial^2 V_z}{\partial y^2} + \frac{\partial^2 V_z}{\partial z^2} \right) + \rho g_z \end{aligned} \quad (4.13)$$

The Reynolds Equations in cartesian coordinates given by (4.11), (4.12) and (4.13) were used for the analysis of the flow of the slug in the vertical extension

segment of the pipeline in Bozkuş's setup given in Figure 2.2, with the selection pattern of the coordinate axes x , y and z shown in Figure 4.5. In these equations, the meanings of the symbols are as;

V_x, V_y, V_z : ensemble average local velocities respectively in x, y and z directions,

V'_x, V'_y, V'_z : turbulent fluctuations of the velocity components respectively in x, y and z directions,

p : ensemble average local pressure,

$\langle \rangle$: symbol indicating ensemble averaging,

g_x, g_y, g_z : components of gravitational acceleration respectively in x, y and z directions.

The calculation of the average pressure distribution along the vertical extension segment was made by solving the Reynolds Equation which was written in y -direction given in (4.12). For this purpose; firstly, the Reynolds Equation in (4.12) was taken and three of the unknown velocity components V_x, V_y, V_z in this equation were reduced to one by eliminating V_x and V_z making use of Gauss' Divergence Theorem and continuity condition (Ger and Holley [5]; Quarteroni and Valli [6]). Also replacing the term including the Reynolds Stresses and the term for the laminar shear stresses, which are respectively the second and the third terms on the right-hand side of Equation (4.12), with the Darcy-Weishbach friction force formula (Munson [3]); an expression in terms of the dependent variables of the pressure and the axial velocity, V_y , was obtained. For the axial velocity component V_y , an assumed and calibrated axial velocity profile function with a skewed 3-D shape was utilized. Thus, by using this 1-D Reynolds Equation written in only y -direction, it became possible to calculate the pressure values in that direction as the only unknowns, by using the known values of the axial velocity profile function, the necessary initial and boundary conditions and also the value of the average slug velocity through the pipeline at any given time. The average velocity value was used for the determination of some parameters of the assumed and calibrated axial velocity profile function, for finding the value of the friction factor in the Darcy-

Weishbach Equation and also for the calculation of the unsteady term in Reynolds Equation. The average velocity value at any time step was calculated from slug dynamics equations of Bozkuş [2] applied on that length of the slug remaining in the horizontal part of the pipeline, which were coupled with the Reynolds Equations.

In the present study, the incompressible Reynolds Equations in cylindrical polar coordinates were used for those part of the calculations that account for the motion of the slug flow in the elbow part of the Bozkuş's [2] system setup given by Figure 2.2. The incompressible cylindrical polar Reynolds Equations are as given below as stated by Bird and et. al. [8] and Davidson [15]:

In r -direction:

$$\begin{aligned} \rho \left(\frac{\partial V_r}{\partial t} + V_r \frac{\partial V_r}{\partial r} + \frac{V_\theta}{r} \frac{\partial V_r}{\partial \theta} - \frac{V_\theta^2}{r} + V_z \frac{\partial V_r}{\partial z} \right) = - \frac{\partial p}{\partial r} \\ - \rho \left[\frac{1}{r} \frac{\partial}{\partial r} (r \langle V_r' V_r' \rangle) + \frac{1}{r} \frac{\partial}{\partial \theta} \langle V_r' V_\theta' \rangle + \frac{\partial}{\partial z} \langle V_r' V_z' \rangle - \frac{\langle V_\theta' V_\theta' \rangle}{r} \right] \\ + \mu \left[\frac{\partial}{\partial r} \left(\frac{1}{r} \frac{\partial}{\partial r} (r V_r) \right) + \frac{1}{r^2} \frac{\partial^2 V_r}{\partial \theta^2} - \frac{2}{r^2} \frac{\partial V_\theta}{\partial \theta} + \frac{\partial^2 V_r}{\partial z^2} \right] + \rho g_r \end{aligned} \quad (4.14)$$

In θ -direction:

$$\begin{aligned} \rho \left(\frac{\partial V_\theta}{\partial t} + V_r \frac{\partial V_\theta}{\partial r} + \frac{V_\theta}{r} \frac{\partial V_\theta}{\partial \theta} + \frac{V_r V_\theta}{r} + V_z \frac{\partial V_\theta}{\partial z} \right) = - \frac{1}{r} \frac{\partial p}{\partial \theta} \\ - \rho \left[\frac{1}{r^2} \frac{\partial}{\partial r} (r^2 \langle V_\theta' V_r' \rangle) + \frac{1}{r} \frac{\partial}{\partial \theta} \langle V_\theta' V_\theta' \rangle + \frac{\partial}{\partial z} \langle V_\theta' V_z' \rangle \right] \\ + \mu \left[\frac{\partial}{\partial r} \left(\frac{1}{r} \frac{\partial}{\partial r} (r V_\theta) \right) + \frac{1}{r^2} \frac{\partial^2 V_\theta}{\partial \theta^2} + \frac{2}{r^2} \frac{\partial V_r}{\partial \theta} + \frac{\partial^2 V_\theta}{\partial z^2} \right] + \rho g_\theta \end{aligned} \quad (4.15)$$

In z -direction:

$$\begin{aligned} \rho \left(\frac{\partial V_z}{\partial t} + V_r \frac{\partial V_z}{\partial r} + \frac{V_\theta}{r} \frac{\partial V_z}{\partial \theta} + V_z \frac{\partial V_z}{\partial z} \right) = - \frac{\partial p}{\partial z} \\ - \rho \left[\frac{1}{r} \frac{\partial}{\partial r} (r \langle V_z' V_r' \rangle) + \frac{1}{r} \frac{\partial}{\partial \theta} \langle V_z' V_\theta' \rangle + \frac{\partial}{\partial z} \langle V_z' V_z' \rangle \right] \\ + \mu \left[\frac{1}{r} \frac{\partial}{\partial r} \left(r \frac{\partial V_z}{\partial r} \right) + \frac{1}{r^2} \frac{\partial^2 V_z}{\partial \theta^2} + \frac{\partial^2 V_z}{\partial z^2} \right] + \rho g_z \end{aligned} \quad (4.16)$$

The cylindrical polar coordinate system used for the incompressible cylindrical polar Reynolds Equations given by (4.14), (4.15) and (4.16) is shown in Figure 4.5 together with the placement pattern of r , θ and z axes of this coordinate system over the elbow. In Equations (4.14), (4.15) and (4.16); the symbols are as:

V_r , V_θ : ensemble average local velocities respectively in r and θ directions,

V'_r , V'_θ : turbulent fluctuations of the velocity components respectively in r and θ directions,

g_r , g_θ : components of gravitational acceleration respectively in r and θ directions.

For the average pressure distribution along the axis of the elbow, the Reynolds Equation in θ -direction given by (4.15) was taken and the terms including the dependent variable V_r were eliminated from this equation by proper use of Gauss' Divergence Theorem and the continuity equation. During the elimination process, an integral expression derived from continuity equation for the variation of V_r in terms of the dependent variable, V_θ , and the independent variable, r , was also utilized. In addition, the variable V_z was removed from (4.15) by making use of the symmetry of the domain for the elbow, with respect to a vertical plane of $z = 0$ as the plane of symmetry. By replacing the friction terms on the right-hand side of (4.15) with the Darcy-Weishbach friction formula, an expression for the pressure in terms of the axial velocity V_θ was obtained and the average pressure values along the axis of the elbow were solved from a 1-D application of this equation as was done in the case of the vertical extension segment given above.

The local pressure at the top point of each cross-section of the elbow was also calculated with again a 1-D application of the Reynolds Equation but in the r -direction this time as given in (4.14), by eliminating V_r and V_z respectively with the use of continuity expression and using the symmetry of the domain of the elbow with respect to the plane of $z = 0$.

4.3.2 Pressure Distribution Equations

As the physical domain over which the pressure distribution calculations were made in the present study, the elbow and the following vertical extension segment of the system developed by Bozkuş [2] was taken as shown in Figure 2.2. Selection of the computational domain over this elbow and the vertical extension segment is given in Figure 4.5. In this computational domain, a cartesian coordinate system was chosen for the analysis of the slug flow in the vertical extension segment and a cylindrical polar coordinate system was taken for the analysis of that part of the flow of the slug in the elbow. The computational solution domain at a given time consisted of the volume occupied by the slug in the elbow and the vertical extension segment, and the solution for the pressure distributions were made with the Reynolds Equations starting from the front face of the slug towards upstream up to the entrance section of the elbow. After the front face of the liquid slug exited past the end section of the vertical extension segment to the atmosphere from the pipeline, the solution domain for the Reynolds Equations was taken as the whole region inside the elbow and the vertical extension segment. The calculations were stopped when the upstream face of the liquid slug came to very close locations of the entrance section of the elbow to avoid some unstable oscillations that would have appeared due to the liquid slug being unstable. Here, the instability of the liquid slug was caused by the driving and retarding forces acting of the slug having very close values to each other.

The formulas for the calculation of average pressure distributions along the axes of the vertical extension segment and the elbow, and the expresion for finding the local impact pressures at the top point of each cross-section of the elbow are given in the following subsections.

4.3.2.1 Average Pressure Distribution along the Vertical Extension Segment

The calculation of average pressures along the vertical extension segment was made along that part of the s -curve extending in the vertical extension segment and remaining inside the volume occupied by the liquid slug at any given time. The solution for this purpose was made by using incompressible cartesian Reynolds Equations written in the vertical direction along the y axis given in Equation (4.12)

above (Bird and et. al. [8]).

By integrating the Reynolds Equation given by (4.12) over the volume element shown in Figure 4.6 and simplifying some of the terms in the equation, the following average pressure distribution equation was obtained:

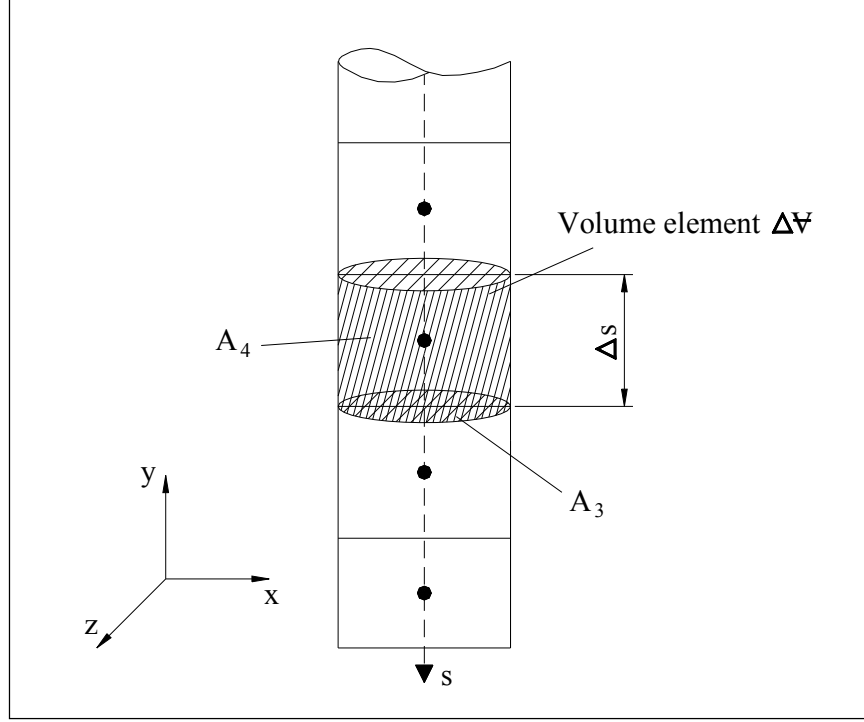


Figure 4.6 Sample volumetric pipe element on the s-curve, in the vertical extension segment.

$$\frac{\partial P}{\partial s} = -\rho \left[\left[\frac{\partial \bar{u}_s}{\partial t} \right]_{t=t_n} + \frac{1}{A} \frac{\partial}{\partial s} \int_A u_s^2 dA + \frac{f_f P_{wet} \bar{u}_s^2}{8A} - g \right] \quad (4.17)$$

The procedure for obtaining (4.17) is presented in Appendix A.3.1.

In this equation;

u_s : assumed and calibrated axial velocity profile function given in Section 4.2, at any cross-section of the vertical extension segment of the pipe,

\bar{u}_s : average value of the assumed and calibrated axial velocity profile

function at any cross-section of the vertical extension segment of the pipe,

s : curvilinear coordinate shown in Figure 4.5,

g : gravitational acceleration.

According to Equation (4.17), it can be said that for a given constant value of $\frac{\partial \bar{u}_s}{\partial t}$ at any given time t_n , one can get a differential relation that is valid over that portion of the curve s remaining in the vertical extension segment, in the form of an ordinary differential equation because in that case the only independent variable will be the s .

The derivative expression in the first term in parenthesis on the right-hand side of Equation (4.17) was discretized by using first order backward finite differences as;

$$\left[\frac{\partial \bar{u}_s}{\partial t} \right]_{t=t_n} = \frac{(\bar{u}_s)^n - (\bar{u}_s)^{n-1}}{\Delta t_s} \quad (4.18)$$

where

Δt_s : time increment at any time step of the elbow and the vertical extension segment calculations,

And, superscripts n and $n-1$ in indicates the time levels for the finite difference approximation.

$(\bar{u}_s)^n$ and $(\bar{u}_s)^{n-1}$ terms in (4.18) were taken from another part of the computer program coded by Bozkuş [2], which used slug dynamics equations, to be able to utilize Equation (4.17) as a closed form expression. Bozkuş's formulations here are related with the motion of the slug remaining within that part of the pipe at the upstream side of the elbow, and the velocity values obtained from that part are also valid for that continued length of the liquid slug in the elbow and the vertical extension segment of the pipe. The set of slug dynamics equations for that upstream part of the liquid slug from Bozkuş's study are given in Section 4.3.3.

In the second term in parenthesis on the right-hand side of Equation (4.17), u_s is the velocity profile function in the direction of s -curve, which is actually the

assumed and then calibrated velocity profile given in Section 4.2. Since that velocity profile function introduces difficulty in taking the integral in the expression given by (4.17), that term was numerically integrated with a numerical integration process over the pipe cross-section. Velocity profile function u_s in the integral expression here, changes depending on location on curve s and on time t , according to where and when the calculation is being made in the computational domain. Variation of the velocity profile along the curve s at any time t , was allowed by the change in value of the calibration function, $\theta(s)$, with s since the discharge of the slug was taken to be constant along the pipe at any time t .

4.3.2.2 Average Pressure Distribution along the Elbow

To calculate the average pressure distribution along the axis of the elbow, the incompressible Reynolds Equation in cylindrical polar coordinates written in θ -direction was utilized as given in Equation (4.15) (Bird and et. al. [8]; and Davidson [15]). As the computational domain of average pressure calculations with Equation (4.15) at the elbow, that part of the s -curve shown in Figure 4.5, extending in the elbow and remaining within the volume occupied by the liquid slug at any time step was taken.

The Reynolds Equation in θ -direction given by (4.15) was integrated over the volume element in the elbow shown in Figure 4.7, and after some simplifications, the following average pressure distribution equation along the axis of the elbow was obtained.

$$\begin{aligned} \frac{\partial P}{\partial s} = & -\rho \left[\left[\frac{\partial \bar{u}_\beta}{\partial t} \right]_{t=t_n} - \frac{1}{R_0 A} \int_A \frac{1}{r} \left(\int_{R_0 - \sqrt{R^2 - z^2}}^r \frac{\partial u_\beta}{\partial \beta} dr \right) u_\beta dA + \frac{1}{R_0 A} \frac{1}{\partial \beta} \int_A u_\beta^2 dA \right. \\ & \left. + \frac{f_f P_{wet} \bar{u}_\beta^2}{8A} + \frac{K_m \bar{u}_\beta^2}{2L_{elb}} - g \sin \beta \right] \end{aligned} \quad (4.19)$$

The details of obtaining (4.19) are given in Appendix A.3.2.

In Equation (4.19);

\bar{u}_β : average value of the velocity profile function in the elbow, in β direction,

\bar{u}_β : average value of the velocity profile function in the elbow, in β direction,

R_0 : radius of curvature of the elbow,

$\Delta\beta$: incremental angle of curvature over the infinitesimal element in the elbow as shown in Figure 4.6,

K_m : minor loss coefficient at the elbow,

L_{elb} : the central arc length of the elbow.

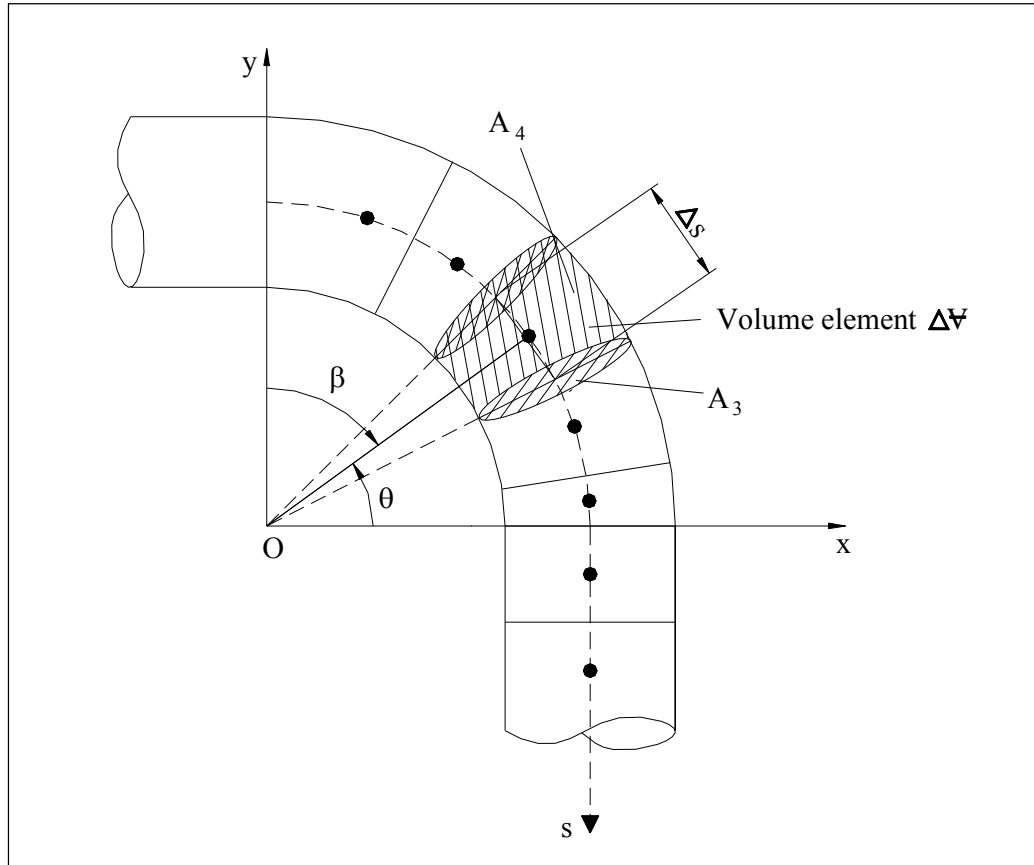


Figure 4.7 Sample volumetric pipe element along the s-curve, for the elbow part.

The first term in parenthesis on the right-hand side of the equation above can be calculated as was done for Equation (4.17) for the vertical extension segment of the pipe in Section 4.3.2.1. The equation to be used for this purpose for the current case of elbow calculations is given below.

$$\left[\frac{\partial \bar{u}_\beta}{\partial t} \right]_{t=t_n} = \frac{(\bar{u}_\beta)^n - (\bar{u}_\beta)^{n-1}}{\Delta t_s} \quad (4.20)$$

The cross-sectional-average velocity values $(\bar{u}_\beta)^n$ and $(\bar{u}_\beta)^{n-1}$ at time levels n and $n-1$ for the elbow part here are to be determined in the same manner as was done for the vertical extension segment of the pipeline in Section 4.3.2.1.

4.3.2.3 Calculation of Impact Pressures at the Convex Side of the Elbow

For the impact pressure calculations at the elbow, the r -component of incompressible Reynolds Equations in cylindrical polar coordinates was used as given in (4.14).

For the calculation of impact pressure distribution at the convex side of the elbow, the computational domain was selected as the line mesh starting from the center point O' of each cross-section at the elbow up to the top point C' on the convex side of the cross-section as shown in Figure 4.8. Here, the location of coordinate axes over the elbow is the same as shown in Figure 4.5. In Figure 4.8,

$MLPRSS$: number of nodes for the line mesh used for the impact pressure calculation.

Making some simplifications on the r -component of the Reynolds Equation given by (4.14), the following equation for the local pressure calculation at the convex side of the elbow was obtained:

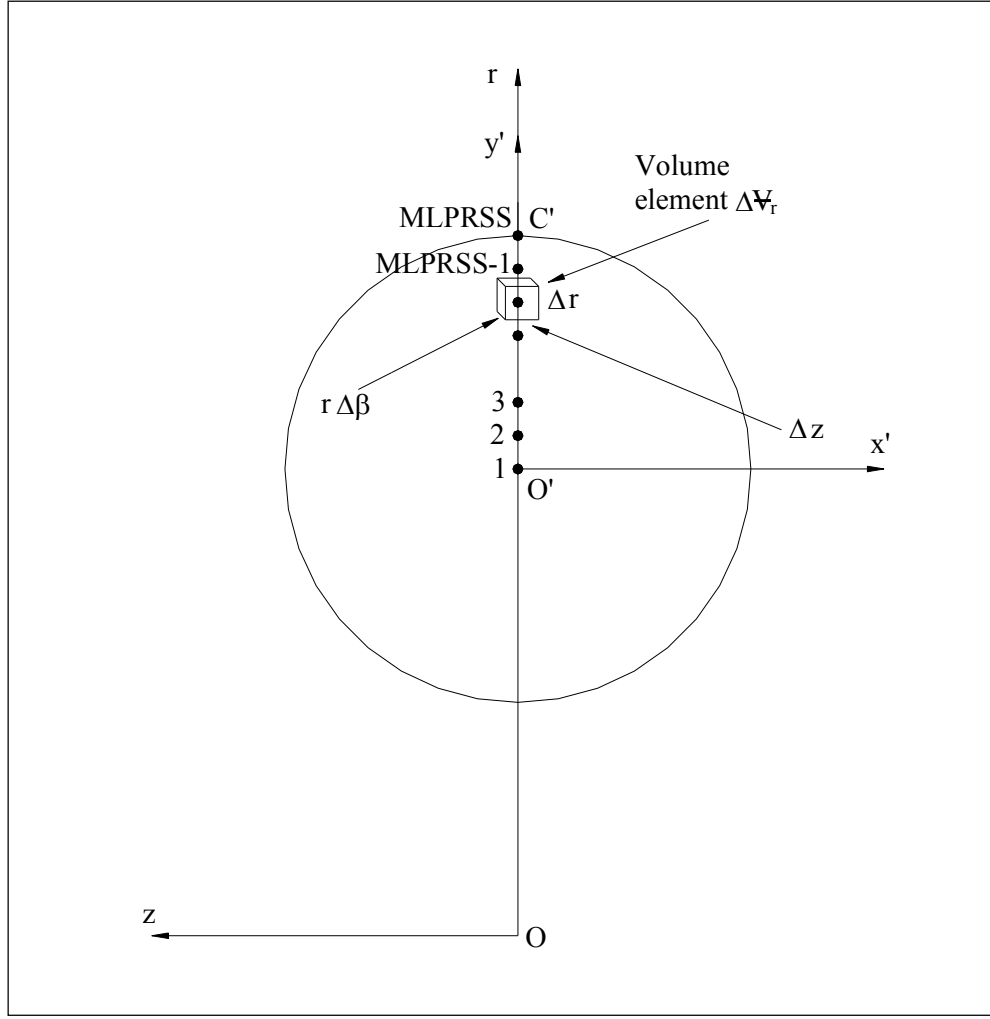


Figure 4.8 1-D radial mesh at a cross-section of the elbow.

$$\begin{aligned}
 \frac{\partial p}{\partial r} = & \rho \left\{ \frac{1}{r} \frac{\partial}{\partial t} \int_{R_0-R}^r \frac{\partial u_\beta}{\partial \beta} dr + \frac{1}{2} \frac{\partial}{\partial r} \left(\frac{1}{r} \int_{R_0-R}^r \frac{\partial u_\beta}{\partial \beta} dr \right)^2 + \frac{u_\beta}{r} \frac{\partial}{\partial \beta} \left(\frac{1}{r} \int_{R_0-R}^r \frac{\partial u_\beta}{\partial \beta} dr \right) + \frac{u_\beta^2}{r} \right. \\
 & - \frac{1}{r} \frac{\partial}{\partial r} \left[r \varepsilon_t \frac{\partial}{\partial r} \left(\frac{1}{r} \int_{R_0-R}^r \frac{\partial u_\beta}{\partial \beta} dr \right) \right] - \frac{1}{r^2} \frac{\partial}{\partial \beta} \left[\varepsilon_t \frac{\partial}{\partial \beta} \left(\frac{1}{r} \int_{R_0-R}^r \frac{\partial u_\beta}{\partial \beta} dr \right) \right] \\
 & \left. - \frac{\partial}{\partial z} \left[\varepsilon_t \frac{\partial}{\partial z} \left(\frac{1}{r} \int_{R_0-\sqrt{R^2-z^2}}^r \frac{\partial u_\beta}{\partial \beta} dr \right) \right] + \frac{\varepsilon_t}{r^3} \int_{R_0-R}^r \frac{\partial u_\beta}{\partial \beta} dr - \frac{2\varepsilon_t}{r^2} \frac{\partial u_\beta}{\partial \beta} \right\} - \rho g \cos \beta \quad (4.21)
 \end{aligned}$$

The procedure for finding the expression in (4.21) is given in Appendix A.3.3.

In Equation (4.21),

ε_t : turbulent eddy viscosity of the fluid.

For the determination of the turbulent eddy viscosity, ε_t , in Equation (4.21); the mixing length theory as a zero-equation turbulence model was utilized as suggested in Chen and Jaw [36]. The resulting expressions from this theory are given below from (4.22) to (4.24) and the mathematical procedure for reaching those form of the equations is given in Appendix A.3.3.

$$g_m = \frac{\xi}{R} \quad (4.22)$$

$$\frac{l_m}{R} = 0.14 - 0.08g_m^2 - 0.06g_m^4 \quad (4.23)$$

$$\varepsilon_t = l_m^2 \left| \frac{\partial u_\beta}{\partial y_w} \right| \quad (4.24)$$

In above equations,

l_m : mixing length,

g_m : a parameter.

The turbulent eddy viscosity, ε_t , here can be calculated by using (4.22), (4.23) and (4.24) at any point in the elbow, given the radial distance from the pipe centerline, ξ , of that point, while the local pressure distribution is being solved from the pressure distribution equation (4.21).

The impact pressures at the convex side of the elbow were calculated for each cross-section of the elbow selected and for each time step of the calculations, by solving the differential equation (4.21) along the radial line $O'C'$ shown in Figures 4.8 and 4.9, as an ordinary differential equation by using the assumed axial velocity profile function for u_β given in Section 4.2. During these calculations, the only

independent variable was taken as r , with other variables t , β and z being constants at that time step and along the line of integration at a cross-section shown in Figure 4.8. The seventh term in parenthesis on the right-hand side of (4.21) was calculated with the finite difference method, as was done for the other terms including derivatives; with central differences along lines of constant $z = 0$, with a certain incremental length used for z in the finite difference formula. For the boundary values needed for the solution of the differential equation in (4.21), the local pressure at the center point of each cross-section was taken as an equal value to the average pressure for that cross-section calculated in Section 4.3.2.2.

4.3.3 Calculations for that Part of the Slug in the Horizontal Pipe

To solve for the velocity of the slug during its motion along the elbow and the vertical extension segment, a set of slug dynamics equations were used, which were developed by Bozkuş [2] previously for a writing a computer code BOZKUŞ-1. These slug dynamics equations govern the motion of that part of the liquid slug remaining in the horizontal part of the pipeline, and the average velocity value, U , calculated from this part is also valid all along the whole length of the slug extending into the elbow and the vertical extension segment due to the continuity principle and the incompressible flow assumption. The slug dynamics equations utilized for this part of the calculations are as follows:

$$\frac{dU}{dt} = -\frac{f_f}{2D}U^2 + \frac{P_D - P_E}{\rho L} \quad (4.25)$$

$$\frac{dL}{dt} = -U \quad (4.26)$$

In above equations,

P_D : driving air pressure acting on the slug upstream face,

P_E : average liquid pressure retarding the motion of that part of the slug in the horizontal part of the pipeline, and acting at the entrance section of the elbow,

L : slug length remaining within the horizontal part of the elbow.

The difference between Bozkuş's equations and the ones given above is that, in Bozkuş's study, the retarding pressure effect at the elbow was not considered by taking the pressure as atmospheric there. However, in the current study the retardation of the motion of the slug in the horizontal part of the pipe was also taken into account by subtracting the P_E value from the air pressure driving the liquid slug, P_D , as in Equation (4.25).

For the elbow and the vertical extension segment calculations, no hold up was assumed to exist for the whole volume of the liquid slug during its motion in these parts of the pipeline. As another assumption, the difference between the timely decreasing instantaneous value of the tank pressure and the driving air pressure, P_Δ , at the upstream face of the liquid slug was taken to be constant and equal to the value that occurred when the slug front face reached at the entrance section of the elbow. This constant value was calculated from the final pressure values obtained from the horizontal pipe calculations given in Chapter III, as

$$P_\Delta = P_{T\ final} - P_{D\ final} . \quad (4.27)$$

Here,

$P_{T\ final}$: final tank pressure value from horizontal pipe calculations at the instant that the slug front face reaches the entrance section of the elbow,

$P_{D\ final}$: final driving air pressure value at the upstream face of the slug from horizontal pipe calculations at the instant that the slug front face reaches the entrance section of the elbow.

Then, the driving pressure, P_D , at the upstream face of the slug at any time step during the elbow and the vertical extension segment calculations was obtained with the formula;

$$P_D = P_T - P_\Delta . \quad (4.28)$$

The U value computed from the system given by (4.25) and (4.26) was equated to

\bar{u}_s ($\bar{u}_s = \bar{u}_\beta = U_{ave} = U$) to be used in the pressure distribution calculations in the elbow and the vertical extension segment performed in Section 4.3.2, due to the continuity principle and the incompressible flow assumption all along the liquid slug in the pipe. The calculated average velocity values, U_{ave} , which were constant along the slug in the horizontal part of the pipeline, and in the elbow and the vertical extension segment of the pipe at any given time step, were also utilized in the determination of the assumed and calibrated axial velocity profile function for the slug flow at any cross-section of the elbow and vertical extension segment along the s -curve given in Section 4.2.

Since U is always positive, in other words, slug is always moving towards the downstream end of the pipeline, it can be deduced from (4.26) that $\frac{dL}{dt}$ is always negative. Therefore, the length of the slug remaining within the horizontal part of the pipeline, L , continuously decreases from its initial value to 0, and the computation is stopped when the back face of the slug reaches at very close locations of the entrance section of the elbow which means that L becomes very close to 0.

4.3.4 The Initial and the Boundary Conditions

For the solution of average pressure distribution equations given by (4.17) and (4.19), the computational domain for the elbow and the vertical extension segment was taken as that length of the s -curve shown in Figure 4.10, which remains within the volume occupied by the liquid slug at a given time step during the numerical solution of the equations. In this figure,

$NLFF$: nodal number corresponding to the location of the slug front face along the s -curve,

$NELBW$: number of nodes along the axis of the elbow,

$NBOUND$: point on the s -curve at the boundary of the elbow and the vertical extension segment,

$NSTOT$: total number of nodal points along the s -curve.

The solution of the equations was made by using a FORTRAN subroutine with the name DVERK written by Hull and et. al. [25], and Jackson and et. al. [35], which was utilized as a part of the main program KAYHAN developed in the present

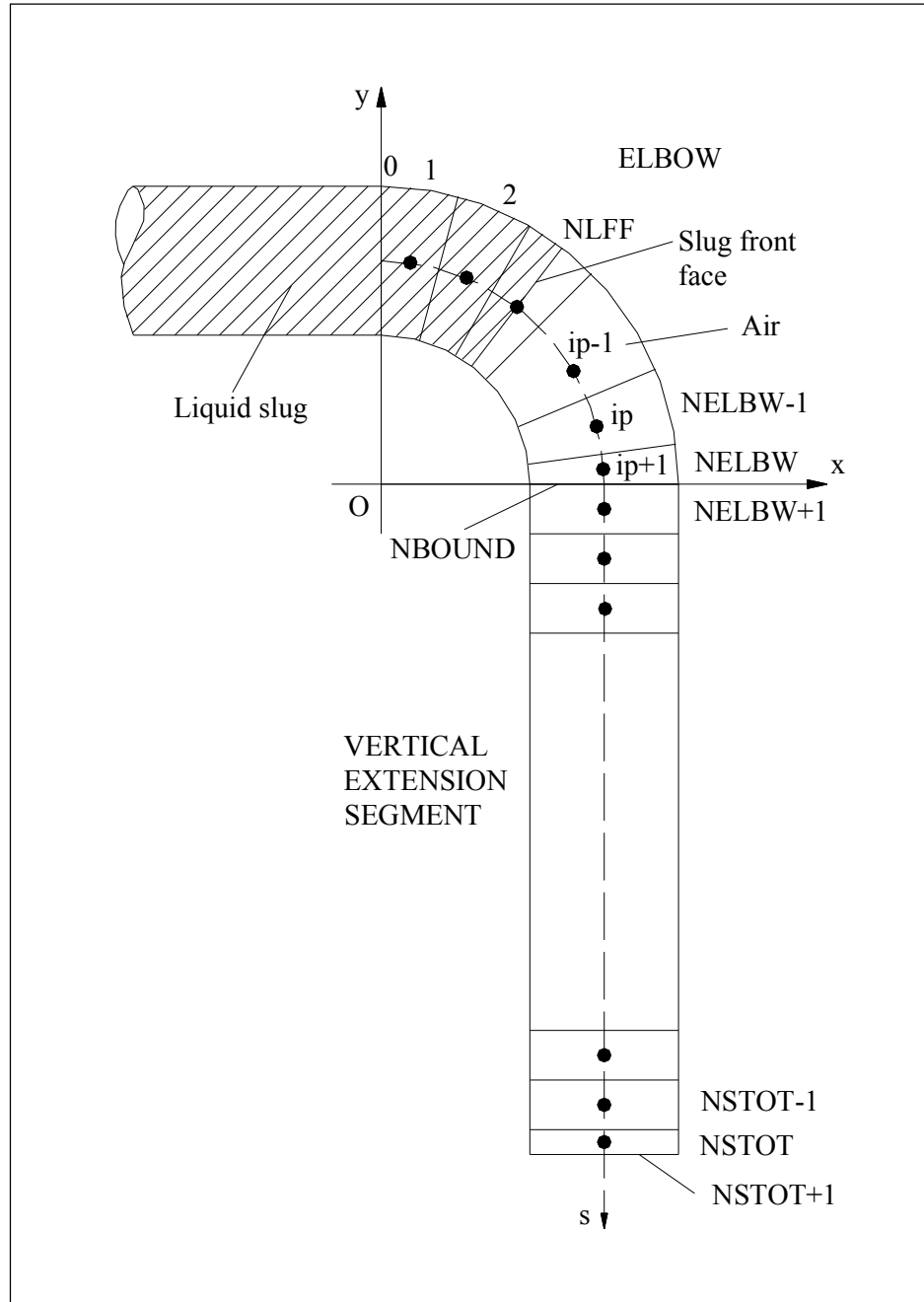


Figure 4.10 Computational domain with the nodal numbering along the s -curve given.

study. The subroutine DVERK is an ordinary differential equation solver which utilizes Runge-Kutta-Verner fifth and the sixth order method. Equations (4.17) and (4.19) were solved with the subroutine DVERK by using the necessary initial and boundary conditions for the elbow and the vertical extension segment calculations in the present study. Since these equations are in the form of ordinary differential equations of the first order at a given time step, only one boundary condition together with the initial conditions were required for the solution of each equation. The initial and the boundary conditions for Equations (4.17) and (4.19) are given in Table 4.1. Here,

U_{final} : final slug velocity obtained from horizontal pipe calculations,

P_{NLFF} : atmospheric pressure at the front face of the liquid slug,

P_{NBOUND} : average pressure at the connection boundary of the elbow and the vertical extension segment.

In Table 4.1, the boundary conditions for the elbow and the vertical extension segment calculations are given for two main cases. The first one is the case that the slug front face is within the elbow which means that

$$0 < NLFF \leq NBOUND .$$

The other case is that the slug front face is in the vertical extension segment of the pipeline or exited from the that part which means that

$$NBOUND < NLFF \leq NSTOT + 1 .$$

For both of these cases, the position of the front face of the liquid slug on the s -curve at any time step was determined from the equations given by (4.29) and (4.30) below:

$$s_{frol}^n = s_{frol}^{n-1} + U_{ave} \Delta t_s \quad \text{if} \quad s_{frol}^{n-1} + U_{ave} \Delta t_s < L_{tot} \quad (4.29)$$

$$s_{frol}^n = L_{tot} \quad \text{if} \quad s_{frol}^{n-1} + U_{ave} \Delta t_s \geq L_{tot} \quad (4.30)$$

Table 4.1 Initial and the boundary conditions for the elbow and the vertical extension segment calculations.

		Equation (4.17)	Equation (4.19)	Equation (4.21)	Equations (4.25) and (4.26)
Initial Conditions		$\bar{u}_s = U_{final}$	$\bar{u}_\beta = U_{final}$	$\bar{u}_\beta = U_{final}$	$U = U_{final}$ $P_D = P_{D_{final}}$ $P_E = 0$ $L = L_{final}$
Boundary Conditions	$0 < NLFF \leq NBOUND$	—	$P = P_{NLFF} = 0$	$p = p_{O'} = P_{calc}$	$P_D = P_T - P_\Delta$ $P_E = P_{E_{calc}}$
	$NBOUND < NLFF \leq NSTOT + 1$	$P = P_{NLFF} = 0$	$P = P_{NBOUND}$	$p = p_{O'} = P_{calc}$	$P_D = P_T - P_\Delta$ $P_E = P_{E_{calc}}$

In these equations;

s_{frol}^n : slug front face location on the s -curve at ant time step n ,

L_{tot} : total axial length of the elbow and the vertical extension segment.

Then, the node number $NLFF$ corresponding to the location of the front face of the slug, s_{frol}^n , on the s -curve was taken as the largest node number the location of which remained just upstream the slug front face location at any given time step.

The average pressure equation in cartesian coordinates given by (4.17) was solved along s -curve in the vertical extension segment if the slug front face was at a stage of progressing in this part of the pipeline or the slug front exited to the atmosphere from this part. If the first case was valid that the slug front face was moving in the vertical extension segment, the boundary condition for (4.17) was used as the atmospheric zero gage pressure at the node for the current slug front face location, $NLFF$, according to Table 4.1 and the general slug front face location pattern shown in Figure 4.10. Then, the average pressure values along the vertical extension segment were calculated stating from this point towards upstream until calculating the average pressure value at the boundary section of the elbow and the vertical extension segment, $NBOUND$. If on the other hand the second case was valid that the slug front has exited from the end section of the vertical extension segment, the same calculations were made but starting from the section $NSTOT + 1$ this time and by using the zero atmospheric pressure at this section as the boundary condition.

Equation (4.19), which is the average pressure distribution equation in cylindrical polar coordinates, was solved along that part of the s -curve remaining in the elbow. In case the slug front face was moving in the elbow towards downstream, the boundary condition was selected as the zero atmospheric pressure at the node for the slug front face location, $NLFF$, as given in Table 4.1 and according to the general form for the location of the slug front face depicted in Figure 4.10. However, if the slug front passed the connection boundary of the elbow and the vertical extension segment, $NBOUND$; Equation (4.19) was solved starting from the connection section, $NBOUND$, towards upstream up the entrance section of the elbow. In this case, the boundary value for the average pressure at section,

$NBOUND$, was taken from the final average pressure value obtained from the vertical extension segment calculations.

The above procedure of finding the average pressures was repeated for every time step of slug motion during the calculations.

For Equation (4.21), which was used for the impact pressure calculation at the top point of each cross-section of the elbow, the computational domain is as given in Figure 4.8. The initial and the boundary conditions for this equation is presented in Table 4.1, where

$p_{O'}$: local pressure at the center point O' of the elbow cross-section,

P_{calc} : calculated average pressure value at the elbow cross-section.

The boundary condition given here for Equation (4.21) was taken as the local pressure, $p_{O'}$, at the center point of the each cross-section of the elbow, and the local pressure at this point was taken as equal to the calculated average pressure value for that cross-section as an assumption. The solution of (4.21) here was also made with the subroutine DVERK by using the indicated boundary condition.

By using the boundary condition at point O' and the initial conditions, Equation (4.21) was solved at every time step of the calculations along the radius of the each cross-section of the elbow upstream the liquid slug front face, starting from point O' up to the top point of the cross-section at the convex side of the elbow, C' , shown in Figure 4.8 with aim of calculating the local impact pressure value p at point C' .

The solution for the system of slug dynamics equations given by (4.25) and (4.26) were again made with the subroutine DVERK by utilizing the initial and the boundary conditions stated in Table 4.1. In the table the meanings of the symbols are as:

L_{final} : final length of the slug remaining in the horizontal part of the pipeline obtained from horizontal pipe calculations,

P_{Ecalc} : calculated average liquid pressure retarding the motion of that part of the slug in the horizontal part of the pipeline, and acting at the entrance section of the elbow.

The system of slug dynamics equations given by (4.25) and (4.26) were

solved at each time step of the calculations to find U and L values at the current time step. The calculated average slug velocity, U , values were then utilized in determining the unsteady terms in (4.17) and (4.19), and also in finding the unknown parameters of the assumed and calibrated axial velocity profile function used in equations (4.17), (4.19) and (4.21). The length of the slug remaining in the horizontal part of the pipeline, L , values were used in determining final stage at which the calculations were stopped, when L approached 0.

4.4 Transient Force Calculations at the Elbow Part

In the present study, the transient forces acting on the elbow and the following vertical extension segment of Bozkuş's [2] system setup given in Figure 2.2 were calculated with a set of control volume analyses by applying conservation momentum principle over the elbow and the vertical extension segment. For this purpose, two types of control volumes were selected as small elements in the elbow and the vertical extension segment. The volume elements in the elbow had a shape in the form of a segment of a torus while the elements in the vertical extension segment were in the shape of a slice of a cylinder. Applying the conservation of momentum principle over these volume elements, the horizontal and the vertical components of the reaction forces acting on each of the elements were calculated. Then, by adding up these force components, the total horizontal and the vertical forces acting on the elbow and the vertical extension segment were calculated.

During the transient force calculations at the elbow and the vertical extension segment of the system, the values for forces acting on the volume elements in the direction of the pipe axis were found by using the calculated average pressure values along the s -curve, given in Section 4.3.2.1 and 4.3.2.2. And, the momentum fluxes over the surfaces of the volume elements perpendicular to the flow direction were calculated with the aid of the assumed and calibrated axial velocity profile function given in Section 4.2.

The formulas for the calculation of the transient forces acting on the elbow and the vertical extension segment are given in the following sections.

4.4.1 Calculations at the Elbow

The computational domain for the calculation of transient forces applied by the liquid slug on the elbow while the slug is passing through the elbow and the vertical extension segment is given in Figure 4.11. The control volumes at the elbow were selected during the calculations within the volume occupied by the liquid slug at the elbow at any instant while the slug front is at a stage of advancing in the elbow. If the slug front passed into the vertical extension segment; then, the control volumes were selected all along the axis of the elbow. By applying the conservation of momentum principle in integral form over these control volumes, the horizontal and the vertical transient force distributions along the axis of the elbow were obtained for every time step of the liquid slug motion in the elbow and the vertical extension segment.

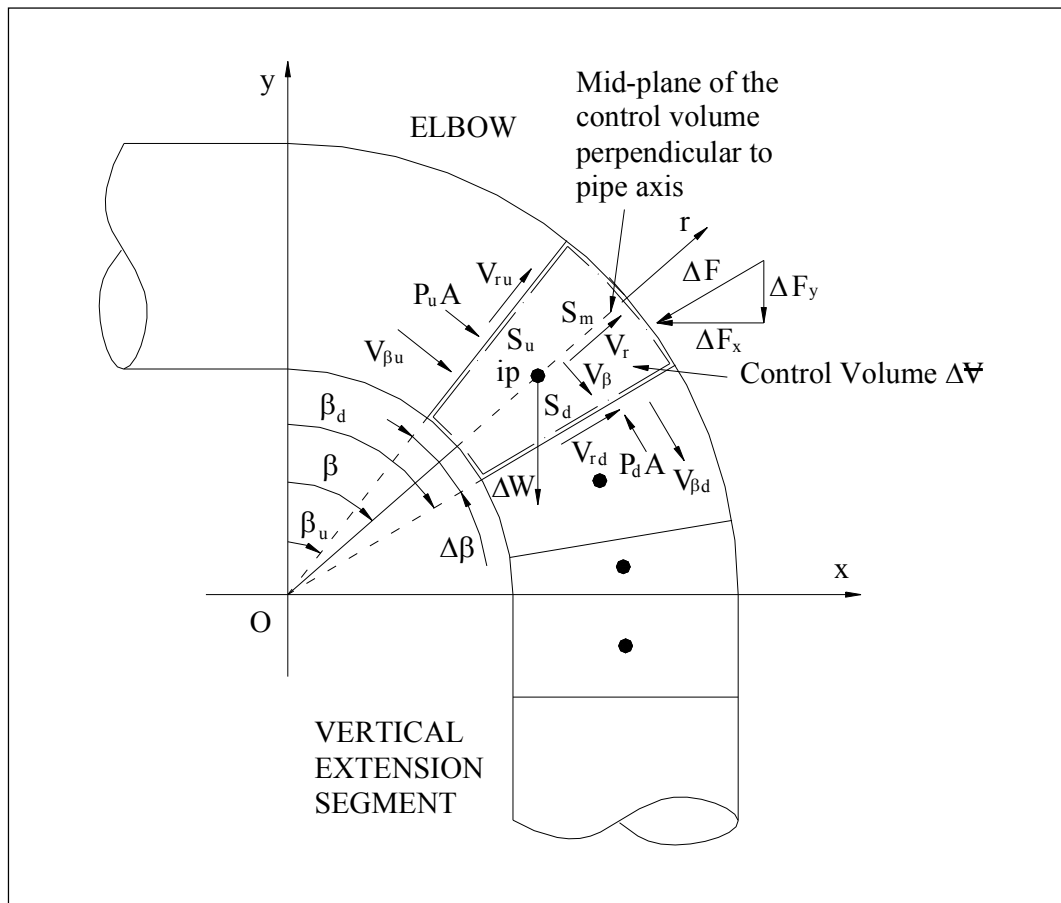


Figure 4.11 Control volume for the transient force calculations at the elbow.

The derivation of the formulas for calculation of the horizontal and the vertical components of the transient forces acting of the volume elements along the elbow are presented in the following subsections.

4.4.1.1 Horizontal Transient Force Distribution at the Elbow

For the purpose of finding the distribution of horizontal transient forces acting on the volume elements along the axis of the elbow, the conservation of momentum principle in its integral form as given below was taken as the starting point.

$$\frac{\partial}{\partial t} \int_{C\forall} \vec{V} \rho d\forall + \int_{CS} \vec{V} \rho (\vec{V} \cdot \vec{n}) dA = \sum \vec{F} \quad (4.31)$$

In Equation (4.31);

\vec{V} : velocity vector at any point of the flow,

\vec{F} : force vector acting on the control volume,

$C\forall$: control volume,

CS : control surface.

By applying the conservation of momentum equation over the control volume selected in the elbow as shown in Figure 4.11, the horizontal transient force acting on the volume element was calculated as the following:

$$\begin{aligned} \Delta F_x = & \rho R_0 \Delta \beta \frac{\partial}{\partial t} \int_{S_m} \left[\left(\frac{1}{r} \int_{R_0 - \sqrt{R^2 - z^2}}^r \frac{\partial u_\beta}{\partial \beta} dr \right) \sin \beta - u_\beta \cos \beta \right] dA \\ & - \rho \int_{S_u} \left[\left(\frac{1}{r} \int_{R_0 - \sqrt{R^2 - z^2}}^r \frac{\partial u_{\beta u}}{\partial \beta} dr \right) \sin \beta_u - u_{\beta u} \cos \beta_u \right] u_{\beta u} dA \\ & + \rho \int_{S_d} \left[\left(\frac{1}{r} \int_{R_0 - \sqrt{R^2 - z^2}}^r \frac{\partial u_{\beta d}}{\partial \beta} dr \right) \sin \beta_d - u_{\beta d} \cos \beta_d \right] u_{\beta d} dA \end{aligned} \quad (4.32)$$

$$+ P_u \cos \beta_u A - P_d \cos \beta_d A$$

The details of the mathematical procedure for deriving Equation (4.32) above are presented in Appendix A.4.1.

In Equation (4.32),

S_m : area of the mid-plane of the volume element perpendicular to pipe axis.

S_u : upstream pipe cross-sectional area for the control volume,

S_d : downstream pipe cross-sectional area for the control volume,

ΔF_x : horizontal reaction force applied by the pipe on the control volume,

P_u : average pressure acting at the upstream face of the control volume,

P_d : average pressure acting at the downstream face of the control volume,

β_u : reference angle for the upstream face of the control volume,

β_d : reference angle for the downstream face of the control volume.

$u_{\beta u}$ and $u_{\beta d}$: assumed and calibrated axial velocity profile functions evaluated at respectively the upstream and downstream faces of the control volume.

Having known the values for the average pressures at the center points ip of the control volume elements, which were calculated with the formula (4.19) given in Section 4.3.2.2, the P_u and P_d values at the upstream and the downstream faces of the volume elements were calculated with the linear interpolation formulas as given below in Equations (4.33) and (4.34).

$$P_u = P_m + \left(\frac{P_m - P_n}{s_m - s_n} \right) (s_u - s_m) \quad (4.33)$$

$$P_d = P_p + \left(\frac{P_p - P_m}{s_p - s_m} \right) (s_d - s_p) \quad (4.34)$$

In Equations (4.33) and (4.34), the symbols are as;

s_d , s_u : location of respectively the downstream and the upstream faces of the current volume element at node ip , on the s -curve,

s_p , s_m and s_n : location of the center points of respectively the previous, current and next volume elements on the s -curve,

P_p , P_m and P_n : average pressures at the center points of respectively the previous, current and next volume elements on the s -curve,

The location of the average pressure, P , values and the coordinates, s , on the s -curve, which were used in (4.33) and (4.34) are also shown in Figure 4.12.

To find the horizontal transient force distribution along the axis of the elbow, ΔF_x values were calculated at each time step with the expression given by (4.32) over the same computational domain as was used for the average pressure distribution calculations at the elbow given in Section 4.3.2.2. During the calculations, in case the slug front face is at a stage of advancing along the elbow axis; that contribution to the transient force by the volume element at the downstream boundary $NLFF$, which is half filled with the liquid slug as shown in Figure 4.10, was neglected.

4.4.1.2 Vertical Transient Force Distribution at the Elbow

The vertical transient force distribution acting on the volume elements in the elbow was found by applying the conservation of momentum equation over the volume element selected in the elbow shown in Figure 4.11.

The resulting expression for the transient force acting on the volume element is as given below:

$$\begin{aligned}
 \Delta F_y = & \rho R_0 \Delta \beta \frac{\partial}{\partial t} \int_{S_m} \left[\left(\frac{1}{r} \int_{R_0 - \sqrt{R^2 - z^2}}^r \frac{\partial u_\beta}{\partial \beta} dr \right) \cos \beta + u_\beta \sin \beta \right] dA \\
 & - \rho \int_{S_u} \left[\left(\frac{1}{r} \int_{R_0 - \sqrt{R^2 - z^2}}^r \frac{\partial u_{\beta u}}{\partial \beta} dr \right) \cos \beta_u + u_{\beta u} \sin \beta_u \right] u_{\beta u} dA \\
 & + \rho \int_{S_d} \left[\left(\frac{1}{r} \int_{R_0 - \sqrt{R^2 - z^2}}^r \frac{\partial u_{\beta d}}{\partial \beta} dr \right) \cos \beta_d + u_{\beta d} \sin \beta_d \right] u_{\beta d} dA \\
 & - P_u \sin \beta_u A + P_d \sin \beta_d A - \rho g R_0 \Delta \beta A
 \end{aligned} \tag{4.35}$$

Here,

ΔF_y : vertical reaction force applied by the pipe on the control volume,

Equation (4.35) can be solved over the same computational domain in which (4.32) was applied, at each time step of the calculations. While using (4.35), the same simplifying assumption is also valid that in case the slug front is inside the elbow, the vertical transient force contribution from the volume element at the downstream slug front face boundary, which was half filled with the liquid slug, is neglected.

4.4.2 Calculations at the Vertical Extension segment

The computational domain used for the calculating the distribution of transient force applied by the liquid slug, along the axis of the vertical extension segment of the pipeline is given in Figure 4.13. If the slug front is at a stage of propagating in the vertical extension segment, the computational domain was selected as that volume of the vertical extension segment occupied by the liquid slug at that time step of the calculations. However, if the slug front reached or passed the downstream end section of the vertical extension segment; then, the whole volume of the vertical extension segment was used as the computational domain. The horizontal and the vertical transient force distributions along the vertical extension segment were calculated by applying the conservation of momentum equation over the volume elements selected in the vertical extension segment, for every time step of the calculations during the motion of the liquid slug in this part of the pipeline.

4.4.2.1 Horizontal Transient Force Distribution at the Vertical Extension Segment

For calculating the distribution of horizontal transient forces acting on the volume elements selected along the axis of the vertical extension segment, the conservation of momentum equation given by (4.31) was applied in x -direction over the control volume selected in the vertical extension segment as shown in Figure 4.13. The resulting expression for the transient force obtained is as given in (4.36).

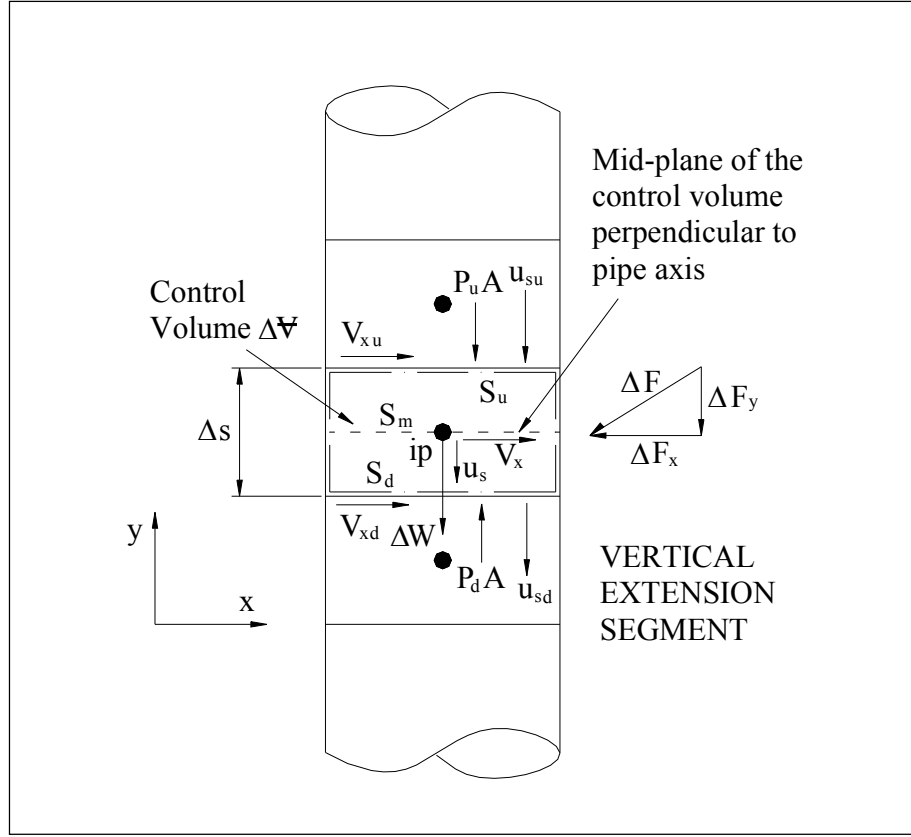


Figure 4.13 Control volume for the transient force calculations at the vertical extension segment.

$$\begin{aligned} \Delta F_x = & \frac{\partial}{\partial t} \int_{S_m} \left(\int_{R_0 - \sqrt{R^2 - z^2}}^x \frac{\partial u_s}{\partial s} dx \right) \rho \Delta s dA - \int_{S_u} \left(\int_{R_0 - \sqrt{R^2 - z^2}}^x \frac{\partial u_{su}}{\partial s} dx \right) \rho u_{su} dA \\ & + \int_{S_d} \left(\int_{R_0 - \sqrt{R^2 - z^2}}^x \frac{\partial u_{sd}}{\partial s} dx \right) \rho u_{sd} dA \end{aligned} \quad (4.36)$$

Here,

u_{su} and u_{sd} : axial velocity profile functions at the upstream and the downstream faces of the volume element.

The mathematical procedure for obtaining Equation (4.36) is given Appendix A.4.3.

Equation (4.36) can be solved over the same computational domain as was used for the average pressure distribution calculations at the vertical extension segment of the pipeline given in Section 4.3.2.1, at each time step of the slug motion. During the calculations, the horizontal transient force contribution by the volume element which is half filled by the liquid slug at the downstream boundary location of the slug front face in the vertical extension segment was neglected as in the case of elbow part calculations given in Sections 4.4.1.1 and 4.4.1.2.

4.4.2.2 Vertical Transient Force Distribution at the Vertical Extension Segment

For the calculation of vertical transient force distribution along the axis of the vertical extension segment, the conservation of momentum equation given by (4.31) was written in y -direction over the control volume selected in the vertical extension segment, which is shown in Figure 4.13. This application of the conservation of momentum principle results in the expression for the vertical component of the transient force acting on the volume element as given by Equation (4.37).

$$\Delta F_y = \rho \Delta s \frac{\partial Q}{\partial t} - \rho \int_{S_u} u_{su}^2 dA + \rho \int_{S_d} u_{sd}^2 dA - P_u A + P_d A - \rho g \Delta s A \quad (4.37)$$

The details for obtaining the expression given by (4.37) are presented in Appendix A.4.4.

Equation (4.37) can be solved over the same computational domain that was indicated for the average pressure distribution calculations at the vertical extension segment given in Section 4.3.2.1, at each time step of the calculations. The P_u and P_d values in (4.37) were calculated from the interpolation equations (4.33) and (4.34). And, the calculated average pressure values from Equation (4.17) at the center points of the volume elements shown in Figure 4.13 were utilized in interpolating these P_u and P_d values at the upstream and downstream faces of the volume elements.

The vertical transient force ΔF_y acting on the volume element at the

downstream solution boundary at the slug front face location inside the vertical extension segment, which is half filled by the liquid slug, was again neglected as in the case of other transient force calculations given in previous sections.

4.4.3 Total Horizontal and the Vertical Transient Forces

By using the distribution of the horizontal and the vertical transient forces acting on the volume elements along the axes of elbow and the vertical extension segment of the pipeline calculated at each time step, the time dependent variation of the horizontal and the vertical components of the total transient force acting on the elbow and the vertical extension segment was found with a summation procedure as indicated below:

$$F_x = \sum_{ip=1}^{NLFF-1} \Delta F_x \quad (4.38)$$

$$F_y = \sum_{ip=1}^{NLFF-1} \Delta F_y \quad (4.39)$$

In Equations (4.38) and (4.39);

F_x and F_y : x and y components of the total transient force acting on the elbow and the vertical extension segment, respectively,

ip : indice for the node number.

The summations in (4.38) and (4.39) are to be made starting from the first volume element at the entrance of the elbow up to the element previous to the one at the downstream boundary at the slug front face location if the slug front is at a stage of advancing in the elbow and the vertical extension segment according to Figure 4.10. If the slug front reached the exit section of the vertical extension segment or in case the liquid slug started to exit to the atmosphere from that exit section; then, the summations in (4.38) and (4.39) were carried out starting from the first volume element at the entrance of the elbow up to the final element at the exit of the vertical extension segment.

The calculations for the transient forces acting on the elbow and the vertical extension segment were stopped when the slug upstream face in the horizontal

pipeline reached at very close locations upstream the entrance section of the elbow.

4.5 Numerical Integrations

In order to calculate the area integrals of the form given in Equations (4.17), (4.19), (4.32), (4.35), (4.36) and (4.37); a numerical method for taking double integrals in polar coordinates was developed. And, for taking the line integrals that appear (4.19), (4.21), (4.32), (4.35) and (4.36); a numerical line integration procedure was also utilized. In the following subsections, the formulas used for these integration processes, both for area and line integrals, are given.

4.5.1 Double Integration in Polar Coordinates

The second term in parenthesis on the right-hand side of Equation (4.17); the second and the third terms in parenthesis on the right-hand side of (4.19); the first, second and third terms on the right-hand side of (4.32), (4.35) and (4.36); and the second and third terms on the right-hand side of (4.37) involve area integrals over the pipe cross-section that are not possible to be integrated analytically. Therefore, a numerical double integration method was needed to utilize to calculate those terms.

The general form of the area integral to be taken can be stated as

$$I_A = \int_A f(\xi, \eta) dA \quad (4.40)$$

or

$$I_A = \int_A f(\xi, \eta) r d\xi d\eta \quad (4.41)$$

according to the polar coordinate system for the pipe cross-section given in Figure 4.14. In these equations, $f(\xi, \eta)$ stands for any function that is to be integrated over the circular domain of integration.

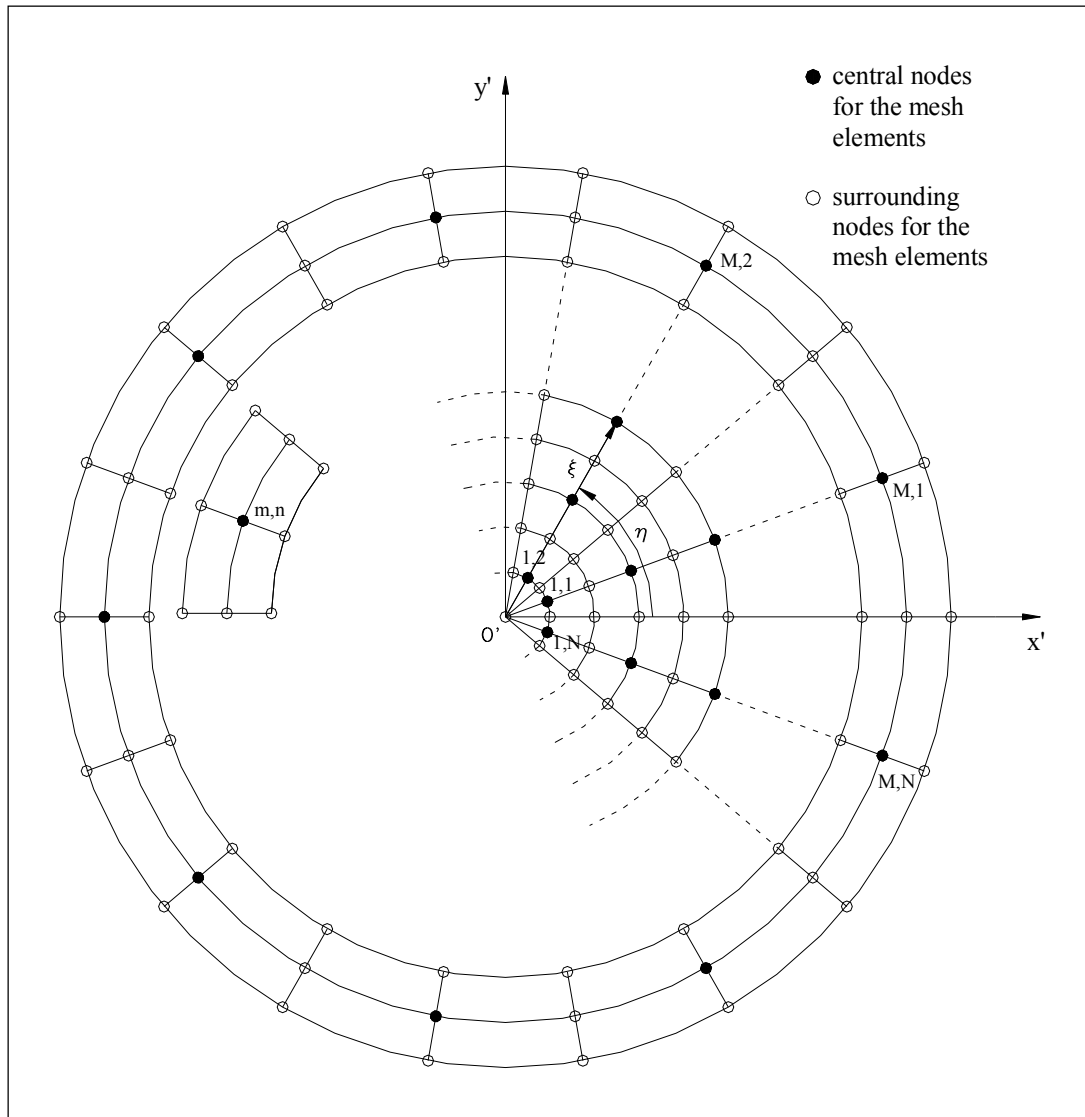


Figure 4.14 Circular mesh over the pipe cross-section.

In the present study, the integrals of the form given by (4.41) were taken by 2-D Gauss Quadrature in cartesian coordinates, by using a transformation procedure of the integral from polar to cartesian coordinates.

For the part of the area integral over the mesh elements except central region of the circular domain, the formulas resulting from the transformation process are as follows:

$$g'(\xi, \eta) = f(\xi, \eta) \left(\xi_m + \frac{\Delta \xi}{2} s' \right) \quad (4.42)$$

$$I_{A;m,n} = \frac{\Delta \xi \Delta \eta}{4} [w_1 (g'_1 + g'_3 + g'_7 + g'_9) + w_2 (g'_2 + g'_4 + g'_6 + g'_8) + w_3 g'_5] \quad (4.43)$$

The details of the mathematical procedure for deriving these equations are given in Appendix A.5.1.

In these equations;

ξ_m : value of ξ at the center point of 9-point mesh element as in Figure 4.15,

$I_{A;m,n}$: value of area integration over the mesh element with the center point at node m, n ; and with the mesh element being selected inside the region of circular area A as shown in Figure 4.15.

In these equations,

s', t' : cartesian coordinates used for coordinate transformation,

$\Delta \xi, \Delta \eta$: incremental mesh spacings that are taken in the polar coordinate system respectively in the radial and the circumferential directions as shown in Figure 4.15.

In Equation (4.43),

w_1, w_2 and w_3 are the weighting coefficients as $w_1 = \frac{25}{81}$, $w_2 = \frac{40}{81}$, $w_3 = \frac{64}{81}$; and the parameters g'_i with the subscript i ranging from 1 to 9 stand for the values of the function given in (4.42) evaluated at the corresponding locations of the grid points shown in Figure 4.16.

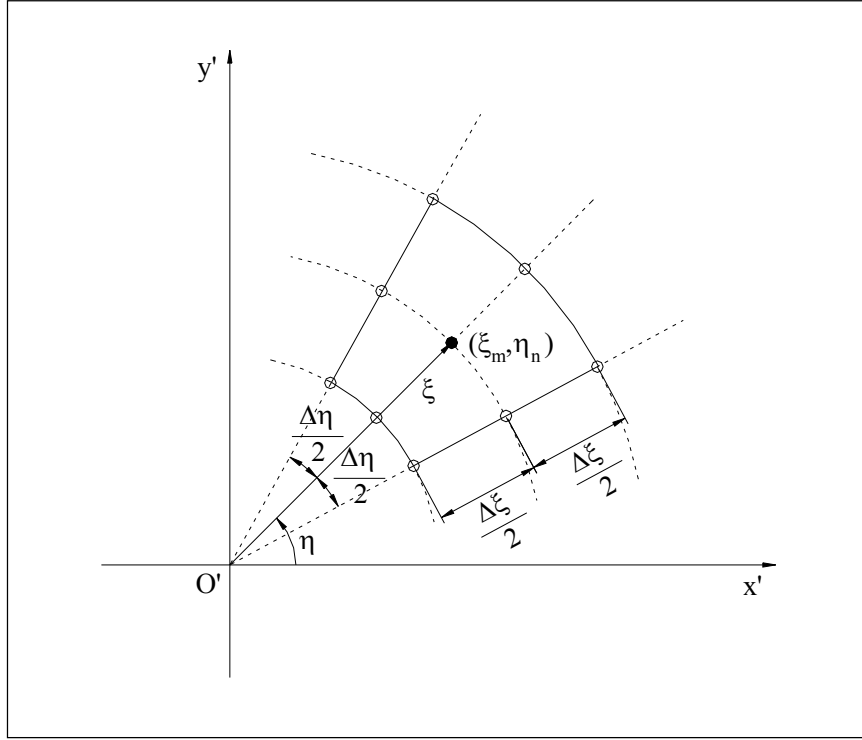


Figure 4.15 9-point mesh element selected for double integration in polar coordinates.

For that part of the area integral over the mesh elements at the central region of the circular domain, the transformation procedure gives the following equations:

$$g'_c(\xi, \eta) = f(\xi, \eta) \left(\frac{\Delta \xi}{2} + \frac{\Delta \xi}{2} s' \right) \quad (4.44)$$

$$I^c_{A;m,n} = \frac{\Delta \xi \Delta \eta}{4} [w_1 (g'_{c1} + g'_{c3} + g'_{c7} + g'_{c9}) + w_2 (g'_{c2} + g'_{c4} + g'_{c6} + g'_{c8}) + w_3 g'_{c5}] \quad (4.45)$$

The details for the derivation of the formulas in (4.44) and (4.45) are given in Appendix A.5.1.

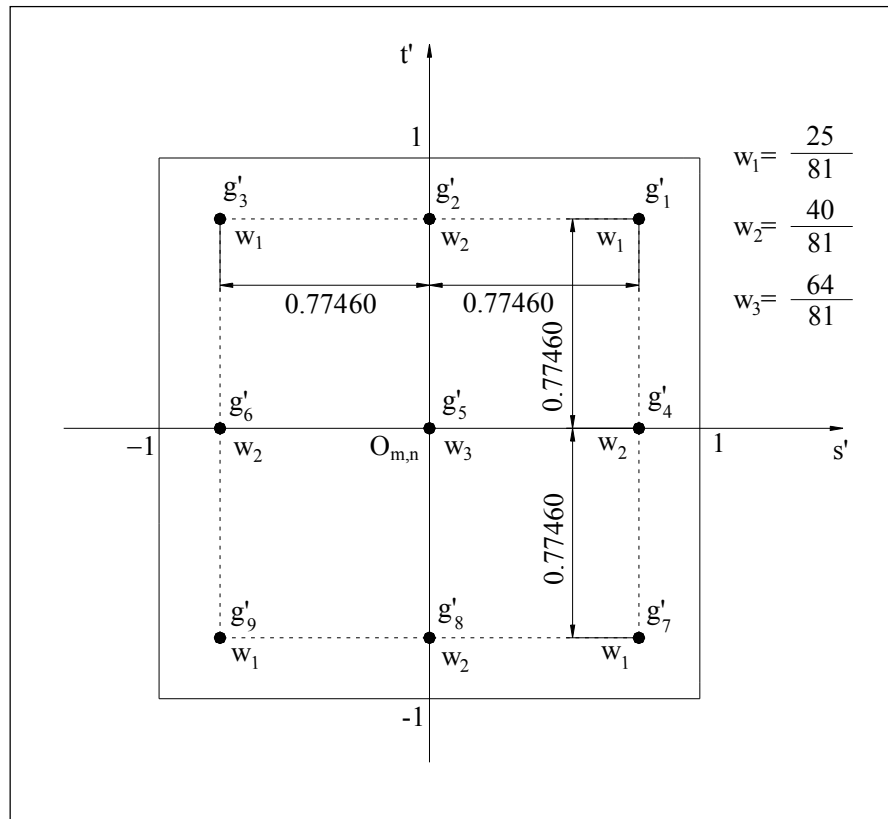


Figure 4.16 9-point mesh element for 2-D Gauss Quadrature in cartesian coordinates.

Here,

$I_{A;m,n}^c$: integral over the mesh element at the central part of the circular domain of area A shown in Figure 4.17, with center point of the mesh element located at the node m,n .

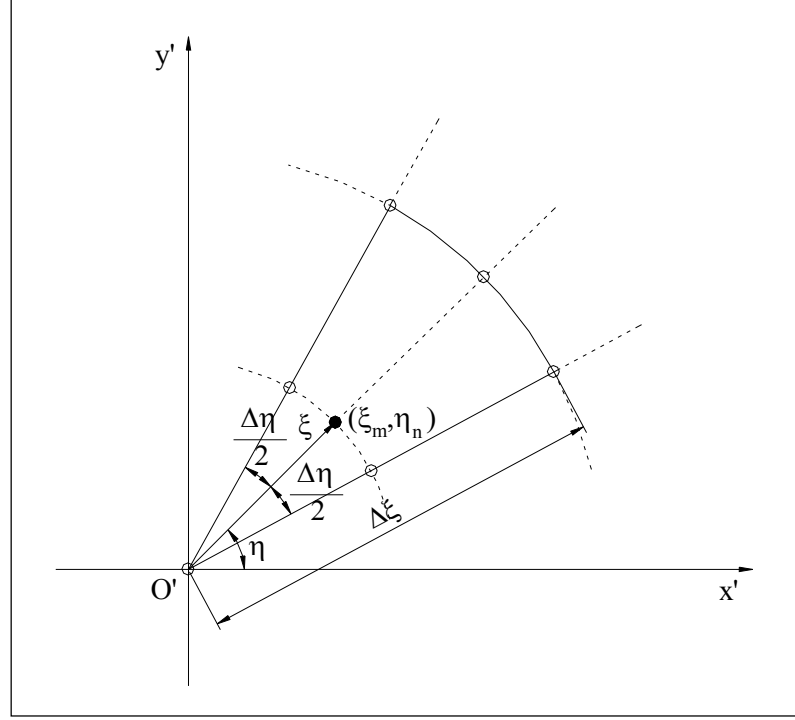


Figure 4.17 Mesh element for the center point of the circular domain in polar coordinates.

In (4.45), parameter g'_{ci} with the subscript i ranging between values of 1 to 9 represents the values of the expression $g'_c(\xi, \eta)$ evaluated at the location of the nodal points depicted in Figure 4.18.

Now, by using the circular mesh taken over the pipe cross-section, which is shown in Figure 4.14, the area integral in (4.40) can be expressed numerically as

$$I_A = \sum_{n=1}^N \sum_{m=2}^M I_{A;m,n} + \sum_{n=1}^N I_{A;1,n}^c \quad (4.46)$$

In Equation (4.46);

M and N : number of mesh elements in the radial and the circumferential directions of the pipe cross-section, respectively.

4.5.2 Evaluation of Numerical Line Integrals

The evaluation of the second term in parenthesis on the right-hand side of the momentum equation given by (4.19); and of the first, second and third terms on the right-hand side of (4.32), (4.35) and (4.36) includes the process of taking an area integral over the area A with the integrand itself including a line integral in the radial direction r of the cylindrical coordinate system given in Figure 4.5. There are also some other line integrals on the right-hand side of Equation (4.21) which are to be evaluated during the pressure distribution calculations at the convex side of the elbow. The evaluation of these line integrals were performed numerically by using 1-D Gauss Quadrature in the present study.

A clustered mesh generation was also made for the application of the 1-D Gauss Quadrature to take the line integrals. In Section 4.5.2.1 below; firstly, the formulas for the generation of the clustered mesh are given; then, in Section 4.5.2.2, application of 1-D Gauss Quadrature over the clustered mesh is presented.

4.5.2.1 Generation of 1-D Clustered Mesh

The general pattern of selected 1-D meshes for 1-D numerical line integrations is given in Figure 4.18. In this figure, the coordinate axes z and r were rotated clockwise by 90° with respect to those shown in Figure 4.5 (c) and (d).

In this general case, the line integral is taken from point A' to K' over the selected clustered mesh elements. The purpose of using clustered mesh in Figure 4.18 is to have mesh spacing small enough to be able to evaluate line integrals in case the point K' is very close to the concave side of the computational domain of the elbow cross-section, but at the same time reduce the simulation time with the advantage of using larger line mesh elements in the direction of r axis, with increasing r values.

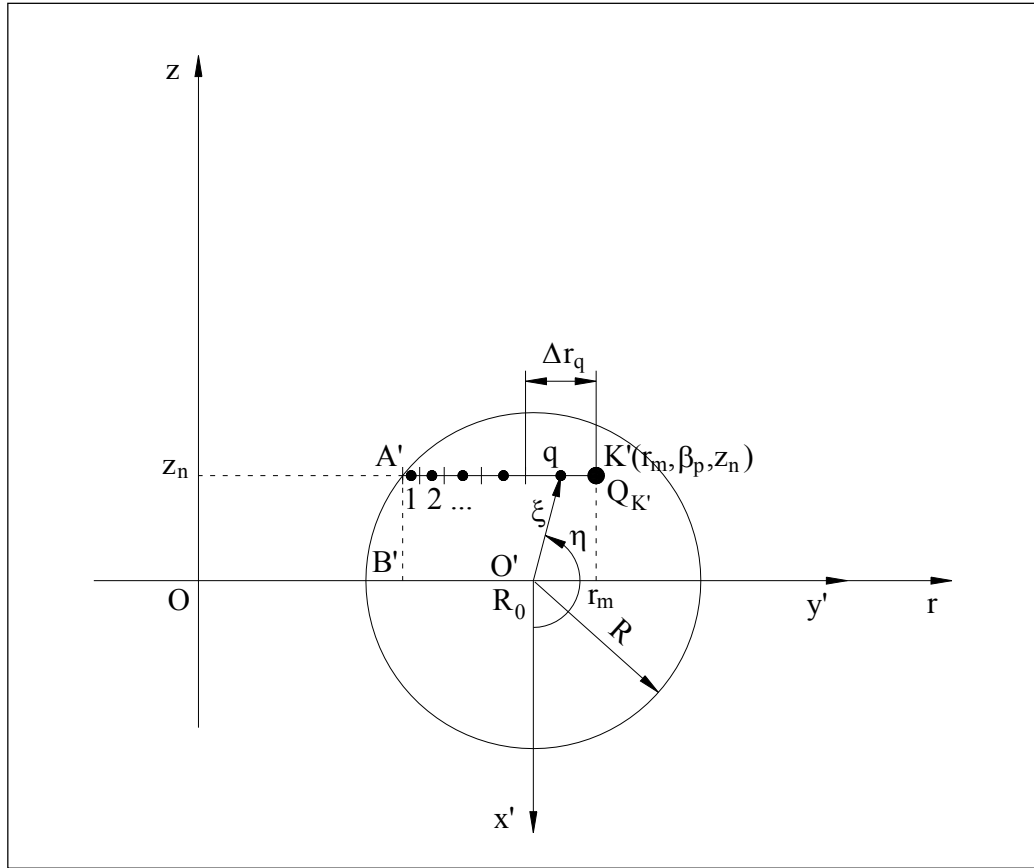


Figure 4.18 Line mesh for a given point K' on the elbow cross-section.

If the line integrals are to be taken on the cross-section of the vertical extension segment of the pipeline and in the direction of x - axis as in the case of Equation (4.36); then, the only change in Figure 4.18 must be that r -axis is replaced with the axis x .

The generation of the clustered 1-D mesh was made by using the formulation given in this section, over the diameter of the elbow cross-section in the direction of r axis, which is actually the largest span length for a line integral. Then, in case the point K' was somewhere inside the circular domain during a line integration, the part of this generated clustered line mesh was used in a left justified way such that the left end of the line mesh matched point A' , and that length of the line mesh extending up to point K' was utilized. During this left justification of the clustered mesh, the rightmost mesh element was selected having a smaller length so as to complete the span length without exceeding past the point K' on the right end of the

domain.

The sizes of the mesh elements on the line mesh were calculated with the formula given below in (4.47), and the derivation of this formula is given in Appendix A.5.2.1.

$$\Delta r_q = \frac{D(c_r - 1)}{c_r^{M_L} - 1} c_r^{q-1} \quad (4.47)$$

In Equation (4.47), subscript q is the indicial variable used for the nodes of the clustered line mesh elements, and

Δr_q : length of the clustered line mesh element at node q ,

M_L : total number of clustered line mesh elements in case the domain of line integral is the whole diameter of the cross-section of the elbow, in r direction,

c_r : mesh clustering ratio.

4.5.2.2 Application of 3-Point Gauss Quadrature Method

The general form of the 1-D numerical integrals that are taken in the present study is as given below:

$$I_L = \int_{A'}^{K'} h'(\xi, \eta) dr, \quad (4.48)$$

where I_L indicates the line integral, being taken over the line mesh between points A' and K' shown in Figure 4.18. The integrand h' in (4.48) is any function in terms of the independent variables ξ and η as defined before.

In Equation (4.48), K' is any point in the circular computational domain of the elbow cross-section, and is located at the points of upper boundaries of the line integrals that are taken in Equations (4.19), (4.21), (4.32), (4.35) and (4.36). And, point A' is the projected location of point K' on the concave side of the elbow cross-section which is a sample point of lower boundary of the line integrals.

The point $K'(r_m, \beta_p, z_n)$ shown in Figure 4.18 is actually a given point

(r_m, z_n) in the circular domain of the elbow cross-section such that the elbow cross-section is taken at an angle β_p according to the cylindrical coordinate system given in Figure 4.5.

To evaluate the line integral given in (4.48), 3-point Gauss Quadrature Method was utilized with the required parameters for the method given in Figure 4.19 (Mathews, [16]). The sample Gauss element given in Figure 4.19, is actually located on the clustered 1-D mesh in Figure 4.18 with the center point O_q of the Gauss element matching the center point q of any element in the clustered mesh.

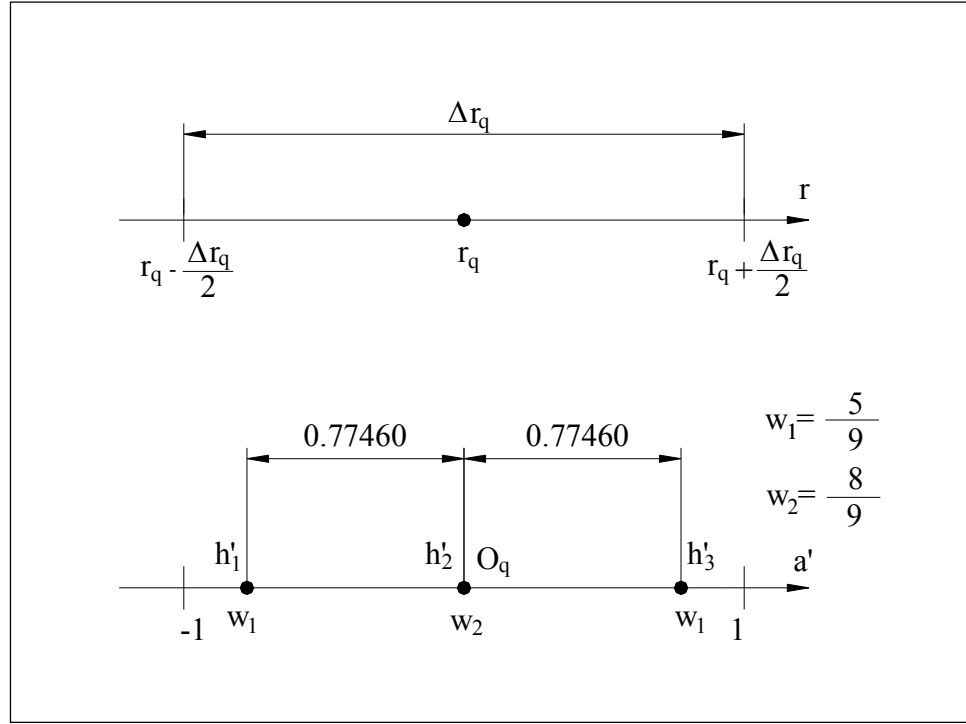


Figure 4.19 Parameters used for the 3-point Gauss Quadrature Method.

The line integral over any Gauss element was calculated by using the formula given in (4.51) below, with the function h' evaluated at the nodal points of the Gauss element having coordinates (ξ, η) as calculated with Equations (4.49) and (4.50).

$$\xi = \sqrt{z^2 + (r - R_0)^2} \quad (4.49)$$

$$\eta = \tan^{-1} \left(\frac{R_0 - r}{z} \right) \quad (4.50)$$

$$I_{L,q} = \frac{\Delta r_q}{2} (w_1 h'_1 + w_2 h'_2 + w_3 h'_3) , \quad (4.51)$$

where

$I_{L,q}$: expression for the line integral over the line mesh element with the mesh element's center point located at node q .

The mathematical derivation for obtaining Equation (4.51) is presented in Appendix A.5.2.2.

Then, the line integral given in (4.48) can be calculated with the summation given by

$$I_L = \sum_{q=1}^{Q_{K'}} I_{L,q} , \quad (4.52)$$

where

$Q_{K'}$: mesh size of the 1-D clustered line mesh shown in Figure 4.18.

4.6 Calibration Function for the Velocity Profile

A calibration function for the change of skew of the assumed axial velocity profile function with 3-D shape in the elbow and the vertical extension segment was proposed in the present study. The calibration function is of the form $\theta_c = \theta_c(s)$ as indicated previously by Equation (4.6). The functional parameter θ_c of the assumed velocity profile function was also shown previously in Figures 4.3 and 4.4.

In the present study, a linear variation of the calibration function, θ_c , was assumed, and the general shape of the calibration function is given in Figure 4.20.

In this figure;

$\theta_{c_{ent}}$: θ_c value at the entrance section of the elbow,

$\theta_{c_{ext}}$: θ_c value at the exit section of the vertical extension segment,

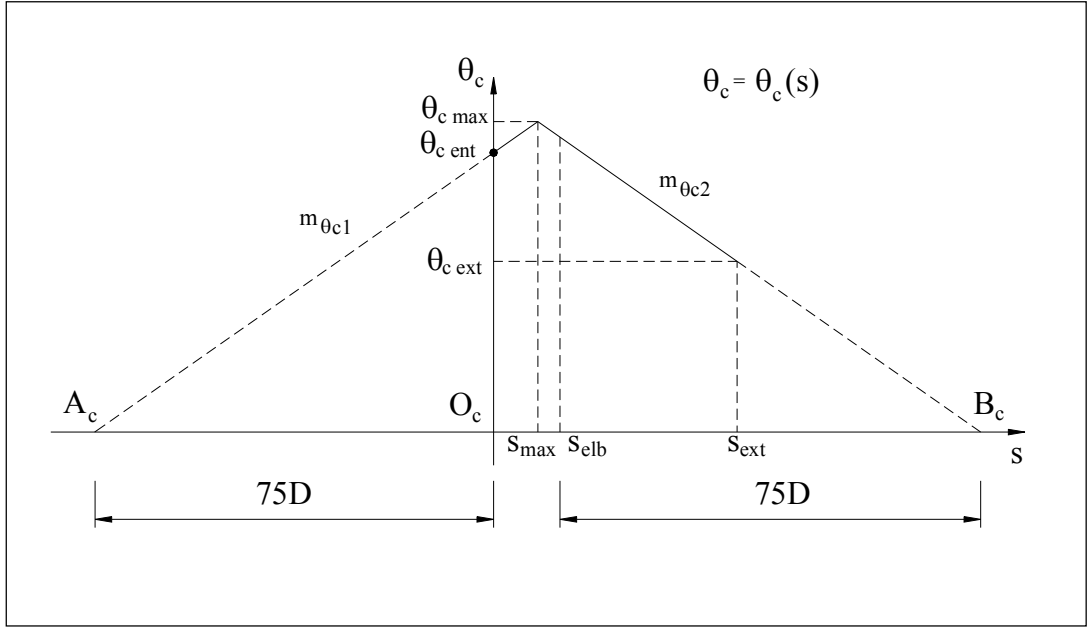


Figure 4.20 Shape of the calibration function θ_c .

$\theta_{c\max}$: maximum value of θ_c along the s -curve,

s_{\max} : location on s -curve where the maximum value of θ_c occurs,

s_{elb} : location on s -curve for the exit section of the elbow,

s_{ext} : location on s -curve for the exit section of the vertical extension segment,

O_c : origin of the coordinate system for the calibration function, θ_c ,

$m_{\theta c1}$, $m_{\theta c2}$: slopes of the calibration function, θ_c , before and after its point of maximum, respectively.

According to Figure 4.20, the value of the calibration function, θ_c , increases linearly starting from the entrance section of the elbow and then, after a maximum value is attained at a location s_{\max} in the elbow, a linear reduction in θ_c values occur up to the exit location s_{ext} of the vertical extension segment.

The s_{\max} value shown in Figure 4.20 was selected in the present study, as the point on s -curve where the transducer #2 was located in Bozkuş's [2] setup shown in Figure 2.2. Thus, it was supposed that the maximum skew of the assumed axial

velocity profile function occurred at this point on the s -curve within the elbow.

Then, given a $\theta_{c\max}$ value, which was actually determined by correlation of peak pressures at the elbow with experimental data later on, the only unknowns for the calibration function, θ_c , left are the slopes $m_{\theta c1}$ and $m_{\theta c2}$. The slopes $m_{\theta c1}$ and $m_{\theta c2}$ were determined from the formulas

$$m_{\theta c1} = \frac{\theta_{c\max}}{s_{\max} + 75D} \quad \text{if} \quad s < s_{\max} \quad (4.53)$$

$$m_{\theta c2} = -\frac{\theta_{c\max}}{s_{elb} + 75D - s_{\max}} \quad \text{if} \quad s > s_{\max} \quad (4.54)$$

according to Figure 4.20.

The distances which are equal to $75D$ in Figure 4.20 as measured along the axis s from the entrance and the exit sections of the elbow up to the points A_c and B_c , where the function θ_c cuts the s -axis were determined according to some experimental data given by Laribi, et. al. [38].

In that study performed by Laribi, et. al. [38]; it is indicated that the swirl, asymmetries and the turbulence distortions after a pipe bend continues up to 80 to 100 pipe diameters downstream the pipe bend. Also, according to the results of an experiment conducted in the same study, it was stated that the swirl in a pipe flow after a double 90° elbows extending in perpendicular planes, the fully developed flow profile was reached after about 90 pipe diameters downstream the elbow.

In Laribi, et. al.'s study, the swirl in the pipe flow is actually an indication of unsymmetrical properties of the axial velocity profile. And, the attaining of the fully developed flow conditions here can be considered as the state that the flow profile becomes symmetrical. Therefore, in the present study, it was assumed that the axial velocity profile function becomes completely symmetrical at $75D$ upstream the entrance section of the elbow, and $75D$ downstream of the cross-section for the exit of the elbow as an approximation. Since $\theta_c = 0$ for the symmetric case of the

assumed velocity profile function according to the general shape shown in Figure 4.4, the θ_c values at these locations $75D$ upstream and downstream of the entrance and the exit sections of the elbow, respectively, were taken as zero as shown in Figure 4.20.

The θ_c values for the cases that $0 \leq s < s_{max}$ and $s_{max} \leq s \leq s_{ext}$ were calculated with the expressions:

$$\theta_c = \theta_{cmax} + \frac{\theta_{cmax}}{s_{max} + 75D}(s - s_{max}) \quad \text{if} \quad 0 \leq s < s_{max} \quad (4.55)$$

$$\theta_c = \theta_{cmax} - \frac{\theta_{cmax}}{s_{elb} + 75D - s_{max}}(s - s_{max}) \quad \text{if} \quad s_{max} \leq s \leq s_{ext} \quad (4.56)$$

the derivations of which are given in Appendix A.6.

By knowing the values of s_{elb} and s_{max} from pipe geometry, and for a given value of θ_{cmax} , which was correlated later on in the present study as given in Appendix B; θ_c values can be calculated along the s -curve as a function of s utilizing the expressions given by (4.55) and (4.56). By using the calculated values for the calibration angle, θ_c , along the s -curve, such a variation of the shape of the axial velocity profile function, u_s , along the curve s , as depicted in Figure 4.21, is possible to obtain.

In Figure 4.21, the change in shape of the axial velocity profile function along the s -curve over the vertical, mid symmetry plane of the elbow and the vertical extension segment is given. This variation of the assumed axial velocity profile function along the s -curve is an instantaneously given one, and the variation of the shape here itself is also supposed to change with time as the value of the discharge, Q , changes; due to continuity condition.

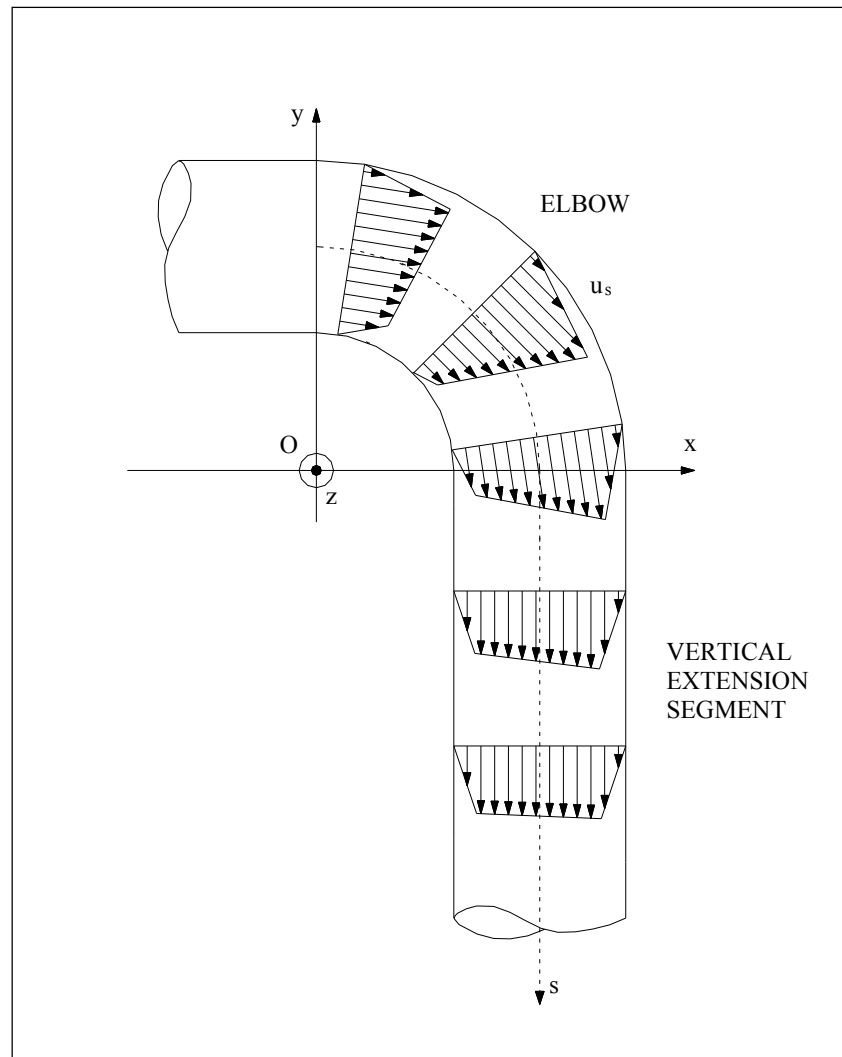


Figure 4.21 General variation of the shape of the assumed axial velocity profile along the s -curve.

4.7 Non-Dimensionalization of the Equations

The equations derived in the in the present study were non-dimensionalized by using the scaling factors given below:

$$t' = \Delta t_{s1} \quad (4.57)$$

$$L' = \frac{2L_{elb}}{K_m} \quad (4.58)$$

$$U' = \frac{L'}{t'} \quad (4.59)$$

In above equations,

t' , L' and U' : scaling factors for time, length and velocity, respectively,

Δt_{s1} : first time increment value used for the elbow and the vertical extension segment calculations.

The formula for the calculation of Δt_{s1} is given later in Section 4.9.

By using the scaling factors given by (4.57) to (4.59), the dimensionless variables to used can be given as the following:

$$\begin{aligned} U^* &= \frac{U}{U'} , \quad L^* = \frac{L}{L'} , \quad t^* = \frac{t}{t'} , \quad P^* = \frac{P}{\rho U'^2} , \quad \Delta s^* = \frac{\Delta s}{L'} , \\ U_{ave}^* &= \frac{U_{ave}}{U'} , \quad s_{frol}^* = \frac{s_{frol}}{L'} , \quad \tau_0^* = \frac{\tau_0}{\rho U'^2} , \quad y_w^* = \frac{y_w}{L'} , \\ \tau^* &= \frac{\tau}{\rho U'^2} , \quad l^* = \frac{l}{L'} , \quad u^* = \frac{u}{U'} , \quad s^* = \frac{s}{L'} , \quad Q^* = \frac{Q}{U' L'^2} , \\ U_m^* &= \frac{U_m}{U'} , \quad R_m^* = \frac{R_m}{L'} , \quad y_1'^* = \frac{y_1'}{L'} , \quad h_1^* = \frac{h_1}{L'} , \quad h_2^* = \frac{h_2}{L'} , \\ u_s^* &= \frac{u_s}{U'} , \quad u_\beta^* = \frac{u_\beta}{U'} , \quad \bar{u}_s^* = \frac{\bar{u}_s}{U'} , \quad \bar{u}_\beta^* = \frac{\bar{u}_\beta}{U'} , \quad l_m^* = \frac{l_m}{L'} , \\ \varepsilon_t^* &= \frac{\varepsilon_t}{U' L'} , \quad p^* = \frac{p}{\rho U'^2} , \quad P_D^* = \frac{P_D}{\rho U'^2} , \quad P_E^* = \frac{P_E}{\rho U'^2} \end{aligned}$$

$$\begin{aligned}
P_u^* &= \frac{P_u}{\rho U'^2} \quad , \quad P_m^* = \frac{P_m}{\rho U'^2} \quad , \quad P_d^* = \frac{P_d}{\rho U'^2} \quad , \quad P_p^* = \frac{P_p}{\rho U'^2} \\
P_n^* &= \frac{P_n}{\rho U'^2} \quad , \quad s_u^* = \frac{s_u}{L'} \quad , \quad s_m^* = \frac{s_m}{L'} \quad , \quad s_d^* = \frac{s_d}{L'} \quad , \quad s_p^* = \frac{s_p}{L'} \\
s_n^* &= \frac{s_n}{L'} \quad , \quad \Delta F_x^* = \frac{\Delta F_x}{\rho U'^2 L'^2} \quad , \quad \Delta F_y^* = \frac{\Delta F_y}{\rho U'^2 L'^2} \quad , \\
F_x^* &= \frac{F_x}{\rho U'^2 L'^2} \quad , \quad F_y^* = \frac{F_y}{\rho U'^2 L'^2}
\end{aligned} \tag{4.60}$$

In above expressions, the superscript * indicates non-dimensional variable.

Using the non-dimensional parameters given by (4.60), the equations used in the present study were non-dimensionalized as given below:

Calculation of the location of the slug front face:

Equation (4.29):

$$s_{frol}^{*n} = s_{frol}^{*(n-1)} + U_{ave}^* \Delta t_s^{*n} \quad \text{if} \quad s_{frol}^{*n} + U_{ave}^* \Delta t_s^* \leq L_{tot} / L' \tag{4.61}$$

Equation (4.30):

$$s_{frol}^{*n} = L_{tot} / L' \quad \text{if} \quad s_{frol}^{*(n-1)} + U_{ave}^* \Delta t_s^* > L_{tot} / L' \tag{4.62}$$

Formulas for the calculation of the angle for the friction slope at a point very close (R / 250 distance) to the pipe wall:

Equation (A.36):

$$\tau_0^* = \frac{1}{8} f_f U_{ave}^{*2} \tag{4.63}$$

Equation (A.39):

$$\tau^* = \tau_0^* \left(1 - \frac{y_w^* L'}{R} \right) \quad (4.64)$$

Equation (A.40):

$$l^* = 0.4 y_w^* \quad (4.65)$$

Equation (A.41):

$$\frac{du^*}{dy_w^*} = \frac{1}{l^*} \sqrt{\tau^*} \quad (4.66)$$

Equation (A.42):

$$y_w^* = \frac{R}{L'} - \xi^* \quad (4.67)$$

Equation (A.43):

$$\theta_f = \tan^{-1} \left(\frac{1}{t'} \frac{du^*}{dy_w^*} \right) \quad (4.68)$$

Formulas for the calibration angle for the velocity profile that occurs along the s -curve:

Equation (4.55):

$$\theta_c = \theta_{cmax} + \frac{\theta_{cmax}}{s_{max} + 75D} (s^* L' - s_{max}) \quad \text{if } s^* < \frac{s_{max}}{L'} \quad (4.69)$$

Equation (4.56):

$$\theta_c = \theta_{cmax} - \frac{\theta_{cmax}}{s_{elb} + 75D - s_{max}} (s^* L' - s_{max}) \quad \text{if } s^* > \frac{s_{max}}{L'} \quad (4.70)$$

Calculation of the parameters for the axial velocity profile that has a skewed 3-D shape along the s -curve:

Equation (A.34):

$$Q^* = \frac{U_{ave}^* A}{L'^2} \quad (4.71)$$

Equation (A.33):

$$U_m^* = \frac{1}{U'} \sqrt[3]{\frac{\left(\frac{3Q^* U' L'^2}{\pi} - R^3 \tan \theta_f \right) \tan^2 \theta_f (\tan \theta_c - \tan \theta_f)^2}{(\tan \theta_c + \tan \theta_f)^2}} + \frac{R \tan \theta_f}{U'} \quad (4.72)$$

Equation (4.7):

$$R_m^* = \frac{R}{L'} - \frac{U_m^*}{t' \tan \theta_f} \quad (4.73)$$

Equation (4.8):

$$y_1'^* = \frac{(U_m^* U' - R \tan \theta_f) (\tan \theta_c + \tan \theta_f)}{L' \tan \theta_f (\tan \theta_c - \tan \theta_f)} \quad (4.74)$$

Equation (4.9):

$$h_1^* = \left(\frac{U_m^* U' - R \tan \theta_f}{\tan \theta_c - \tan \theta_f} \right) \frac{2 \tan \theta_c}{L'} \quad (4.75)$$

Equation (4.10):

$$h_2^* = \frac{2R \tan \theta_c \tan \theta_f - U_m U' (\tan \theta_c + \tan \theta_f)}{L' (\tan \theta_c - \tan \theta_f)} \quad (4.76)$$

Axial velocity profile equation along the s -curve that has 3-D skewed shape:

Equation (4.2):

$$u_s^* = \frac{L'}{U'} \left(\frac{R}{L'} - \xi^* \right) \tan \theta_f \quad \text{if} \quad y_1'^* < \xi^* < \frac{R}{L'} \quad (4.77)$$

Equation (4.4):

$$u_s^* = \frac{t'}{y_1'^{*2} - R_m^{*2}} \left\{ y_1'^{*2} h_1^* + y_1'^{*2} h_2^* - R_m^{*2} h_2^* - R_m^* h_1^* \xi^* \sin \eta \right. \\ \left. - \left[-2 y_1'^{*2} h_1^{*2} R_m^* \xi^* \sin \eta + R_m^{*2} y_1'^{*2} h_1^{*2} - (R_m^{*2} h_1^{*2} - y_1'^{*2} h_1^{*2}) \cos^2 \eta \xi^{*2} \right. \right. \\ \left. \left. + y_1'^{*2} h_1^{*2} \sin^2 \eta \xi^{*2} \right]^{1/2} \right\} \quad \text{if} \quad 0 < \xi^* < y_1'^* \quad (4.78)$$

Calculation of the time derivative terms:

Equation (4.18):

$$\left[\frac{\partial \bar{u}_s^*}{\partial t^*} \right]_{t^* = t^{*n}} = \frac{\bar{u}_s^{*n} - \bar{u}_s^{*(n-1)}}{\Delta t_s^{*n}} \quad (4.79)$$

Equation (4.20):

$$\left[\frac{\partial \bar{u}_\beta^*}{\partial t^*} \right]_{t^*=t^{*n}} = \frac{\bar{u}_s^{*n} - \bar{u}_s^{*(n-1)}}{\Delta t_s^{*n}} \quad (4.80)$$

Differential equation for the average pressure variation along the elbow part of the s -curve:

Equation (4.19):

$$\begin{aligned} \frac{\partial P^*}{\partial s^*} = & - \left[\frac{\partial \bar{u}_\beta^*}{\partial t^*} \right]_{t^*=t^{*n}} + \frac{L'^3}{R_0 A} \int_A \left[\frac{1}{r^*} \int_{R_0/L' - \sqrt{R^2/L'^2 - z^{*2}}}^{r^*} \frac{\partial u_\beta^*}{\partial \beta} dr^* \right] u_{\beta^*} dA^* - \frac{L'^3}{R_0 A} \frac{\partial}{\partial \beta} \int_A u_{\beta^*}^2 dA^* \\ & - L' \left(\frac{f_f P_{wet}}{8A} \right) \bar{u}_{\beta^*}^2 - \bar{u}_{\beta^*}^2 + \frac{L' g}{U'^2} \sin \beta \end{aligned} \quad (4.81)$$

Equations for the turbulent Eddy Viscosity calculation at the elbow:

Equation (4.22):

$$g_m = \frac{\xi^* L'}{R} \quad (4.82)$$

Equation (4.23):

$$l_m^* = \frac{R}{L'} (0.14 - 0.08 g_m^2 - 0.06 g_m^4) \quad (4.83)$$

Equation (4.24):

$$\varepsilon_t^* = l_m^{*2} \left| \frac{\partial u_\beta^*}{\partial \xi^*} \right| \quad (4.84)$$

Differential equation in radial direction of the cylindrical coordinate system,
for the impact pressure calculation at the convex side of the elbow:

Equation (4.21):

$$\begin{aligned}
 \frac{\partial p^*}{\partial r^*} = & \frac{1}{r^*} \left[\frac{\partial}{\partial t^*} \int_{\frac{R_0-R}{L'}}^{\frac{r^*}{L'}} \frac{\partial u_{\beta}^*}{\partial \beta} dr^* \right]_{t^*=t^{*n}} + \frac{1}{2} \frac{\partial}{\partial r^*} \left(\frac{1}{r^*} \int_{\frac{R_0-R}{L'}}^{\frac{r^*}{L'}} \frac{\partial u_{\beta}^*}{\partial \beta} dr^* \right)^2 \\
 & + \frac{u_{\beta}^*}{r^{*2}} \frac{\partial}{\partial \beta} \left(\int_{\frac{R_0-R}{L'}}^{\frac{r^*}{L'}} \frac{\partial u_{\beta}^*}{\partial \beta} dr^* \right) + \frac{u_{\beta}^{*2}}{r^*} - \frac{1}{r^*} \frac{\partial}{\partial r^*} \left[r^* \varepsilon_t^* \frac{\partial}{\partial r^*} \left(\frac{1}{r^*} \int_{\frac{R_0-R}{L'}}^{\frac{r^*}{L'}} \frac{\partial u_{\beta}^*}{\partial \beta} dr^* \right) \right] \\
 & - \frac{1}{r^{*3}} \frac{\partial}{\partial \beta} \left[\varepsilon_t^* \frac{\partial}{\partial \beta} \left(\int_{\frac{R_0-R}{L'}}^{\frac{r^*}{L'}} \frac{\partial u_{\beta}^*}{\partial \beta} dr^* \right) \right] - \frac{1}{r^*} \frac{\partial}{\partial z^*} \left[\varepsilon_t^* \frac{\partial}{\partial z^*} \left(\int_{\frac{R_0}{L'} - \sqrt{R^2/L'^2 - z^{*2}}}^{\frac{r^*}{L'}} \frac{\partial u_{\beta}^*}{\partial \beta} dr^* \right) \right] \\
 & + \frac{\varepsilon_t^*}{r^{*3}} \int_{\frac{R_0-R}{L'}}^{\frac{r^*}{L'}} \frac{\partial u_{\beta}^*}{\partial \beta} dr^* - \frac{2\varepsilon_t^*}{r^{*2}} \frac{\partial u_{\beta}^*}{\partial \beta} - \frac{L'}{U'^2} g \cos \beta
 \end{aligned} \tag{4.85}$$

Linear interpolation equations for the calculation of the average pressure at
the upstream and downstream call faces:

Equation (4.33):

$$P_u^* = P_m^* + \left(\frac{P_m^* - P_n^*}{s_m^* - s_n^*} \right) (s_u^* - s_m^*) \tag{4.86}$$

Equation (4.34):

$$P_d^* = P_p^* + \left(\frac{P_p^* - P_m^*}{s_p^* - s_m^*} \right) (s_d^* - s_p^*) \tag{4.87}$$

Expression for the calculation of the horizontal components of the transient forces acting on the cell elements in the elbow part (Equation (4.32)):

$$\begin{aligned}
\Delta F_x^* &= \frac{1}{L'} R_0 \Delta \beta \frac{\partial}{\partial t^*} \int_{S_m} \left[\left(\frac{1}{r^*} \int_{R_0/L' - \sqrt{R^2/L'^2 - z^{*2}}}^{r^*} \frac{\partial u_{\beta}^*}{\partial \beta} dr^* \right) \sin \beta - u_{\beta}^* \cos \beta \right] dA^* \\
&- \int_{S_u} \left[\left(\frac{1}{r^*} \int_{R_0/L' - \sqrt{R^2/L'^2 - z^{*2}}}^{r^*} \frac{\partial u_{\beta u}^*}{\partial \beta} dr^* \right) \sin \beta - u_{\beta u}^* \cos \beta \right] u_{\beta u}^* dA^* \\
&+ \int_{S_d} \left[\left(\frac{1}{r^*} \int_{R_0/L' - \sqrt{R^2/L'^2 - z^{*2}}}^{r^*} \frac{\partial u_{\beta d}^*}{\partial \beta} dr^* \right) \sin \beta - u_{\beta d}^* \cos \beta \right] u_{\beta d}^* dA^* \\
&+ \frac{1}{L'^2} P_u^* \cos \beta_u A - \frac{1}{L'^2} P_d^* \cos \beta_d A
\end{aligned} \tag{4.88}$$

Expression for the calculation of the vertical components of the transient forces acting on the cell elements in the elbow part (Equation (4.35)):

$$\begin{aligned}
\Delta F_y^* &= \frac{1}{L'} R_0 \Delta \beta \frac{\partial}{\partial t^*} \int_{S_m} \left[\left(\frac{1}{r^*} \int_{R_0/L' - \sqrt{R^2/L'^2 - z^{*2}}}^{r^*} \frac{\partial u_{\beta}^*}{\partial \beta} dr^* \right) \cos \beta + u_{\beta}^* \sin \beta \right] dA^* \\
&- \int_{S_u} \left[\left(\frac{1}{r^*} \int_{R_0/L' - \sqrt{R^2/L'^2 - z^{*2}}}^{r^*} \frac{\partial u_{\beta u}^*}{\partial \beta} dr^* \right) \cos \beta + u_{\beta u}^* \sin \beta \right] u_{\beta u}^* dA^* \\
&+ \int_{S_d} \left[\left(\frac{1}{r^*} \int_{R_0/L' - \sqrt{R^2/L'^2 - z^{*2}}}^{r^*} \frac{\partial u_{\beta d}^*}{\partial \beta} dr^* \right) \cos \beta + u_{\beta d}^* \sin \beta \right] u_{\beta d}^* dA^* \\
&- \frac{1}{L'^2} P_u^* \sin \beta_u A + \frac{1}{L'^2} P_d^* \sin \beta_d A - \frac{1}{L'^2 U'^2} g R_0 \Delta \beta_{\nabla} A
\end{aligned} \tag{4.89}$$

Differential equation for the average pressure variation along the vertical extension segment of the s -curve:

Equation (4.17):

$$\frac{\partial P^*}{\partial s^*} = - \left[\frac{\partial \bar{u}_s^*}{\partial t^*} \right]_{t^*=t^{*n}} - \frac{L'^2}{A} \frac{\partial}{\partial s^*} \int_A u_s^{*2} dA^* - L' \left(\frac{f_f P_{wet}}{8A} \right) \bar{u}_s^{*2} + \frac{L'g}{U'^2} \quad (4.90)$$

Expression for the calculation of the horizontal component of the transient forces acting on the volume elements in the vertical extension segment:

Equation (4.36):

$$\begin{aligned} \Delta F_x^* &= \frac{1}{L'} \Delta s \frac{\partial}{\partial t^*} \int_{S_m} \left[\int_{R_0/L' - \sqrt{R^2/L'^2 - z^{*2}}}^{x^*} \frac{\partial u_s^*}{\partial s^*} dx^* \right] dA^* \\ &- \int_{S_u} \left[\int_{R_0/L' - \sqrt{R^2/L'^2 - z^{*2}}}^{x^*} \frac{\partial u_{su}^*}{\partial s^*} dx^* \right] u_{su}^* dA^* + \int_{S_d} \left[\int_{R_0/L' - \sqrt{R^2/L'^2 - z^{*2}}}^{x^*} \frac{\partial u_{sd}^*}{\partial s^*} dx^* \right] u_{sd}^* dA^* \end{aligned} \quad (4.91)$$

Expression for the calculation of the vertical component of the transient forces acting on the volume elements in the vertical extension segment:

Equation (4.37):

$$\Delta F_y^* = \Delta s^* \frac{\partial Q^*}{\partial t^*} - \int_{S_u} u_{su}^{*2} dA^* + \int_{S_d} u_{sd}^{*2} dA^* - \frac{1}{L'^2} P_u^* A + \frac{1}{L'^2} P_d^* A - \frac{g \Delta s^* A}{L' U'^2} \quad (4.92)$$

Formulas for the calculation of the horizontal and the vertical components of the total transient force acting on the elbow and the vertical extension segment:

Equation (4.38):

$$F_x^* = \sum_{ip=1}^{NLFF} \Delta F_x^* \quad (4.93)$$

Equation (4.39):

$$F_y^* = \sum_{ip=1}^{NLFF} \Delta F_y^* \quad (4.94)$$

Criteria to stop the simulation procedure:

Equation (4.):

$$R_s = \left| \frac{\frac{-f_f L^* L' U_{ave}^{*2}}{2D} + P_D^* - P_E^*}{P_D^*} \right| < 0.15 \quad (4.95)$$

4.8 Discretization of the Equations

The differential expressions in some of the above equations were discretized by using finite differences. The discretization procedure at any time step n of the calculations is as follows:

$$A_t^* = \frac{\partial \bar{u}_\beta^*}{\partial t_s^*} = \frac{(\bar{u}_\beta^*)^n - (\bar{u}_\beta^*)^{n-1}}{\Delta t_s^*} \quad (4.96)$$

$$A_{\beta}^* = \frac{\partial u_{\beta}^*}{\partial \beta} = \frac{u_{\beta;i,j+1,0}^{*n} - u_{\beta;i,j,0}^{*n}}{\Delta \beta} \quad (4.97)$$

$$I_u^* = \int_A u_{\beta}^{*2} dA^* \quad (4.98)$$

$$\frac{\partial}{\partial \beta} \int_A u_{\beta}^{*2} dA^* = \frac{I_{u;i,j+1,0}^{*n} - I_{u;i,j,0}^{*n}}{\Delta \beta} \quad (4.99)$$

Here, the indices are

i, j, k : incremental grid location in r, β and z directions, respectively; according to Figure 4.5.

The derivative expressions in the first, second and the third terms on the right-hand side of (4.81) were discretized by using (4.96), (4.97) and (4.99).

And the derivatives in the first and the second terms on the right-hand side of Equation (4.90) were discretized by (4.100) and (4.102) below, respectively.

$$B_t^* = \frac{\partial \bar{u}_s^*}{\partial t_s^*} = \frac{(\bar{u}_s^*)^n - (\bar{u}_s^*)^{n-1}}{\Delta t_s^*} \quad (4.100)$$

$$I_{us}^* = \int_A u_s^{*2} dA^* \quad (4.101)$$

$$B_s^* = \frac{\partial}{\partial s} \int_A u_s^{*2} dA^* = \frac{I_{us;i,j+1,0}^{*n} - I_{us;i,j,0}^{*n}}{\Delta s} \quad (4.102)$$

In Equations (4.101), the subscript j stands for the incremental grid location in s -direction in the vertical extension segment shown in Figure 4.5 .

The first up to sixth terms on the right-hand side of (4.85) can be calculated by using the expressions given by (4.103) to (4.118).

$$I_{\beta}^* = \int_{\frac{R_0}{L'} - \sqrt{R^2/L'^2 - z^{*2}}}^{r^*} \frac{\partial u_{\beta}^*}{\partial \beta} dr^* \quad (4.103)$$

$$\frac{\partial}{\partial t^*} \int_{\frac{R_0-R}{L'}}^{r^*} \frac{\partial u_{\beta}^*}{\partial \beta} dr^* = \frac{I_{\beta;i,j,0}^{*n} - I_{\beta;i,j,0}^{*n-1}}{\Delta t_s} \quad (4.104)$$

$$\frac{\partial}{\partial r^*} \left(\frac{1}{r^*} \int_{\frac{R_0-R}{L'}}^{r^*} \frac{\partial u_{\beta}^*}{\partial \beta} dr^* \right)^2 = \frac{\left(\frac{1}{r_{i+1}^*} I_{\beta;i+1,j,0}^{*n} \right)^2 - \left(\frac{1}{r_i^*} I_{\beta;i,j,0}^{*n} \right)^2}{\Delta r^*} \quad (4.105)$$

$$\frac{\partial}{\partial \beta} \left(\int_{\frac{R_0-R}{L'}}^{r^*} \frac{\partial u_{\beta}^*}{\partial \beta} dr^* \right) = \frac{I_{\beta;i,j+1,0}^{*n} - I_{\beta;i,j,0}^{*n}}{\Delta \beta} \quad (4.106)$$

$$E_1^* = r^* \varepsilon_t^* \frac{\partial}{\partial r^*} \left(\frac{1}{r^*} \int_{\frac{R_0-R}{L}}^{r^*} \frac{\partial u_{\beta}^*}{\partial \beta} dr^* \right) \quad (4.107)$$

$$\frac{\partial}{\partial r^*} \left[r^* \varepsilon_t^* \frac{\partial}{\partial r^*} \left(\frac{1}{r^*} \int_{\frac{R_0-R}{L'}}^{r^*} \frac{\partial u_{\beta}^*}{\partial \beta} dr^* \right) \right] = \frac{E_{1;i,j,\partial}^{*n} - E_{1;i-1,j,0}^{*n}}{\Delta r^*} \quad (4.108)$$

$$E_{1;i,j,0}^{*n} = r_i^* \varepsilon_{t;i,j,0}^{*n} \frac{\frac{1}{r_{i+1}^*} I_{\beta;i+1,j,0}^{*n} - \frac{1}{r_i^*} I_{\beta;i,j,0}^{*n}}{\Delta r^*} \quad (4.109)$$

$$E_{1;i-1,j,0}^{*n} = r_{i-1}^* \varepsilon_{t;i-1,j,0}^{*n} \frac{\frac{1}{r_i^*} I_{\beta;i,j,0}^{*n} - \frac{1}{r_{i-1}^*} I_{\beta;i-1,j,0}^{*n}}{\Delta r^*} \quad (4.110)$$

$$E_2^* = \varepsilon_t^* \frac{\partial}{\partial \beta} \left(\int_{\frac{R_0-R}{L}}^{r^*} \frac{\partial u_\beta^*}{\partial \beta} dr^* \right) \quad (4.111)$$

$$\frac{\partial}{\partial \beta} \left[\varepsilon_t^* \frac{\partial}{\partial \beta} \left(\int_{\frac{R_0-R}{L'}}^{r^*} \frac{\partial u_\beta^*}{\partial \beta} dr^* \right) \right] = \frac{E_{2;i,j,0}^* - E_{2;i,j-1,0}^*}{\Delta \beta} \quad (4.112)$$

$$E_{2;i,j,0}^{*n} = \varepsilon_{t;i,j,0}^{*n} \frac{I_{\beta;i,j+1,0}^{*n} - I_{\beta;i,j,0}^{*n}}{\Delta \beta} \quad (4.113)$$

$$E_{2;i,j-1,0}^{*n} = \varepsilon_{t,i,j-1,0}^{*n} \frac{I_{\beta;i,j,0}^{*n} - I_{\beta;i,j-1,0}^{*n}}{\Delta \beta} \quad (4.114)$$

$$E_3^* = \varepsilon_t^* \frac{\partial}{\partial z^*} \left(\int_{R_0/L' - \sqrt{R^2/L'^2 - z^{*2}}}^{r^*} \frac{\partial u_\beta^*}{\partial \beta} dr^* \right) \quad (4.115)$$

$$\frac{\partial}{\partial z^*} \left[\varepsilon_t^* \frac{\partial}{\partial z^*} \left(\int_{R_0/L' - \sqrt{R^2/L'^2 - z^{*2}}}^{r^*} \frac{\partial u_\beta^*}{\partial \beta} dr^* \right) \right] = \frac{E_{3;i,j,0}^{*n} - E_{3;i,j,-1}^{*n}}{\Delta z^*} \quad (4.116)$$

$$E_{3;i,j,0}^{*n} = \varepsilon_{t,i,j,0}^{*n} \frac{I_{\beta;i,j,1}^{*n} - I_{\beta;i,j,0}^{*n}}{\Delta z} \quad (4.117)$$

$$E_{3;i,j,-1}^{*n} = \varepsilon_{t;i,j,-1}^{*n} \frac{I_{\beta;i,j,0}^{*n} - I_{\beta;i,j,-1}^{*n}}{\Delta z} \quad (4.118)$$

The derivative expressions in the seventh and the eight terms on the right-hand side of (4.85) can be calculated with Equation (4.97).

The derivative term in Equation (4.84) was discretized as follows:

$$\frac{\partial u_{\beta}^{*}}{\partial \xi^{*}} = \frac{u_{\beta;i+1,j,0}^{*n} - u_{\beta;i,j,0}^{*n}}{\Delta \xi^{*}} \quad (4.119)$$

4.9 Evaluation of Local Peak Pressures

As a result of the proper selection of the calibration function given in Section 4.6, the calculated local peak value of the impact pressure distribution along the convex side of the elbow came out to be at a point where the transducer #2 was located in Bozkuş's [2] setup. The impact pressure distribution at this point had a high gradient and a discontinuous shape as discussed in Section 5.5. To predict the value of the peak pressure at this discontinuous region, the impact pressures were extrapolated by using the following second order forward finite difference expression

$$p_{ip} = p_{ip+1} + \left(\frac{-3p_{ip+1} + 4p_{ip+2} - p_{ip+3}}{2\Delta s} \right) (s_{ip} - s_{ip+1}) \quad (4.120)$$

Here,

p_{ip} : maximum impact pressure on the convex side of the elbow corresponding to node ip shown in Figure 4.10,

s_{ip} : location on s -curve at node ip .

The variable s_{ip} in Equation (4.120) was taken as

$$s_{ip} = s_{max} \quad (4.121)$$

4.10 Neglecting of Some Terms

To fasten the simulation speed of program KAYHAN, some terms in pressure distribution and transient force distribution equations developed in the present study were neglected.

Considering the average pressure distribution equation given in (4.81), the values of the six terms on the right-hand side of the equation are given in Table 4.2, for initial slug length, $L_{in} = 1.22$ m (4 ft); initial tank pressure, $P_0 = 68.91$ kPa (10 psi); and time, $t = 0.75860$ s.

Table 4.2 Values for the terms in Equation (4.81).

s (m)	TERM 1	TERM 2	TERM 3	TERM 4&5	TERM 6	TOTAL	$100 \frac{TERM 2}{TOTAL}$
0.0379	4.946E-8	-1.831E-7	-1.041E-7	-1.401E-6	1.800E-8	-1.621E-06	11.30
0.0386	4.946E-8	-1.913E-7	-1.102E-7	-1.401E-6	1.825E-8	-1.635E-06	11.70
0.0394	4.946E-8	-2.000E-7	-1.168E-7	-1.401E-6	1.851E-8	-1.650E-06	12.12
0.0400	4.946E-8	-2.094E-7	-1.239E-7	-1.401E-6	1.876E-8	-1.666E-06	12.57
0.0407	4.946E-8	-2.194E-7	-1.317E-7	-1.401E-6	1.900E-8	-1.684E-06	13.03

From this table, it can be seen that the ratio of the 2nd term on the right-hand side of Equation (4.81) to the total value of the terms is around 13 % and therefore, this term was neglected in the calculations.

Then Equation (4.81) becomes

$$\frac{\partial P^*}{\partial s^*} = - \left[\frac{\partial \bar{u}_\beta^*}{\partial t^*} \right]_{t^*=t^{*n}} - \frac{L^3}{R_0 A} \frac{\partial}{\partial \beta} \int_A u_\beta^{*2} dA^* - L' \left(\frac{f_f P_{wet}}{8A} \right) \bar{u}_\beta^{*2} - \bar{u}_\beta^{*2} + \frac{L' g}{U'^2} \sin \beta \quad (4.122)$$

Another equation in which some terms were neglected is the impact pressure distribution equation given by Equation (4.85). The values of the terms on the right-hand side of this equation is given in Table 4.3 for initial slug length , $L_{in} = 1.22$ m

Table 4.3 Values for the terms in Equation (4.85).

<i>r</i>	<i>TERM 1</i>	<i>TERM 2</i>	<i>TERM 3</i>	<i>TERM 4</i>	<i>TERM 5</i>	<i>TERM 6</i>	<i>TERM 7</i>	<i>TERM 8</i>	<i>TERM 9</i>	<i>TERM 10</i>	<i>TOTAL</i>
0.0508	1.152E-12	-5.195E-10	-6.013E-08	1.734E-05	-4.229E-10	7.403E-11	2.442E-10	-1.974E-11	4.550E-12	-2.609E-08	1.725E-05
0.0531	1.205E-12	-4.027E-10	-4.317E-08	1.672E-05	-3.494E-10	5.007E-11	3.384E-10	-1.340E-11	3.222E-12	-2.609E-08	1.665E-05
0.0554	1.255E-12	-2.284E-10	-2.592E-08	1.616E-05	-2.619E-10	2.776E-11	4.552E-10	-7.488E-12	1.871E-12	-2.609E-08	1.611E-05
0.0577	1.300E-12	-1.491E-12	-8.589E-09	1.565E-05	-1.602E-10	8.198E-12	5.262E-10	-2.303E-12	5.855E-13	-2.609E-08	1.562E-05
0.0600	1.342E-12	2.735E-10	-8.687E-09	1.517E-05	-4.383E-11	7.699E-12	5.682E-10	-1.916E-12	-5.435E-13	-2.609E-08	1.515E-05

(4 ft); initial tank pressure, $P_0 = 68.91$ kPa (10 psi); time, $t = 0.75642$ s. and for location on the s -curve of $s = 0.000348$ m.

By considering that the 5th, 6th and 7th terms require high simulation time and are smaller with respect to the total value of the terms, these three terms were neglected in the computations. Then, Equation (4.85) becomes

$$\begin{aligned} \frac{\partial p^*}{\partial r^*} = & \frac{1}{r^*} \left[\frac{\partial}{\partial t^*} \int_{\frac{R_0-R}{L'}}^{r^*} \frac{\partial u_\beta^*}{\partial \beta} dr^* \right]_{t^*=t^{*n}} + \frac{1}{2} \frac{\partial}{\partial r^*} \left(\frac{1}{r^*} \int_{\frac{R_0-R}{L'}}^{r^*} \frac{\partial u_\beta^*}{\partial \beta} dr^* \right)^2 \\ & + \frac{u_\beta^*}{r^{*2}} \frac{\partial}{\partial \beta} \left(\int_{\frac{R_0-R}{L'}}^{r^*} \frac{\partial u_\beta^*}{\partial \beta} dr^* \right) + \frac{u_\beta^{*2}}{r^*} + \frac{\varepsilon_t^*}{r^{*3}} \int_{\frac{R_0-R}{L'}}^{r^*} \frac{\partial u_\beta^*}{\partial \beta} dr^* \\ & - \frac{2\varepsilon_t^*}{r^{*2}} \frac{\partial u_\beta^*}{\partial \beta} - \frac{L'}{U'^2} g \cos \beta \end{aligned} \quad (4.123)$$

Some terms in transient force equations given by (4.88), (4.89) and (4.91) were also neglected to speed up the simulation time of program KAYHAN. In Table 4.4; V_r , V_β , $\frac{\partial V_r}{\partial t}$, $\frac{\partial V_\beta}{\partial t}$ values are given at time $t = 0.75666$ s and location on s -curve, $s = 0.00522$ m for different ξ and η values on the pipe cross-section. From this table, it can be seen that radial velocities in the pipeline are much smaller than axial velocities, and the time derivatives of radial velocities are also negligibly smaller than the time derivatives of axial velocities. Therefore, the terms in Equations (4.88), (4.89) and (4.91) which include those smaller quantities were neglected and the resulting expressions are as given in Equations (4.124), (4.125) and (4.126), respectively.

Table 4.4 Radial and axial velocities with their time derivatives.

ξ (m)	η	V_r (m/s)	V_β (m/s)	$\frac{\partial V_r}{\partial t}$ (m/s ²)	$\frac{\partial V_\beta}{\partial t}$ (m/s ²)
0.008128	28.8°	0.049830	18.255616	-0.000223	-3.856782
0.008128	57.6°	0.024373	18.410964	-0.000229	-3.856828
0.008128	86.4°	0.009614	18.493808	-0.000230	-3.856869
0.008128	115.2°	0.018855	18.442121	-0.000230	-3.856842
0.012192	28.8°	0.056203	18.193887	-0.000246	-3.856620
0.012192	57.6°	0.009903	18.464135	-0.000249	-3.856730
0.012192	86.4°	-0.021103	18.637800	-0.000242	-3.856867
0.012192	115.2°	-0.001349	18.526661	-0.000246	-3.856775
0.016256	28.8°	0.071275	18.046456	-0.000284	-3.856276
0.016256	57.6°	0.001630	18.440740	-0.000277	-3.856431
0.016256	86.4°	-0.054438	18.780079	-0.000252	-3.856861
0.016256	115.2°	-0.017482	18.553305	-0.000269	-3.856554

At the elbow:

$$\begin{aligned} \Delta F_x^* = & -\frac{1}{L'} R_0 \Delta \beta \frac{\partial}{\partial t^*} \int_{S_m} u_\beta^* \cos \beta dA^* + \int_{S_u} u_{\beta u}^{*2} \cos \beta dA^* - \int_{S_d} u_{\beta d}^{*2} \cos \beta dA^* \\ & + \frac{1}{L'^2} P_u^* \cos \beta_u A - \frac{1}{L'^2} P_d^* \cos \beta_d A \end{aligned} \quad (4.124)$$

At the elbow:

$$\begin{aligned} \Delta F_y^* = & \frac{1}{L'} R_0 \Delta \beta \frac{\partial}{\partial t^*} \int_{S_m} u_\beta^* \sin \beta dA^* - \int_{S_u} u_{\beta u}^{*2} \sin \beta dA^* + \int_{S_d} u_{\beta d}^{*2} \sin \beta dA^* \\ & - \frac{1}{L'^2} P_u^* \sin \beta_u A + \frac{1}{L'^2} P_d^* \sin \beta_d A - \frac{1}{L'^2 U'^2} g R_0 \Delta \beta_v A \end{aligned} \quad (4.125)$$

At the vertical extension segment:

$$\Delta F_x^* = 0 \quad (4.126)$$

4.11 Input Data, Mesh Sizes and Error Analyses

By using the formulations given in Chapters III and IV, a computer code with the name KAYHAN was written in FORTRAN Language in the present study for the calculation of impact pressures and the transient forces acting on the elbow and the vertical extension segment, by improving the code BOZKUŞ-2 previously written by Bozkuş [2]. The input data for program KAYHAN used in the current study is given in Section 4.11.1. In addition, the error analysis and the mesh size for numerical area integrals, for numerical line integrals with clustered mesh; error analysis for the determination of optimum mesh size along the s -curve, and for uniform mesh size for impact pressure calculation are given in subsections 4.11.2 to 4.11.5.

4.11.1 Input Data for Program KAYHAN

The input data used for program KAYHAN in the present study are given in Table 4.5.

The meanings of the symbols in Table 4.5 are as;

N_{tank} : number of tank pressure data points,

PO : atmospheric pressure,

U_{in} : initial slug velocity,

X_{in} : initial slug position,

L_{ext} : length of the vertical extension segment after the elbow,

PO_{gage} : atmospheric gage pressure,

m_{rt} : Ratio of the circumferential mesh size to the radial one, at any cross-section of the pipe,

M_L : Number of nodes for the line integrals, for the case of integrating along the pipe diameter as the largest span length.

Table 4.5 Input data for program KAYHAN

Explanation for the Parameter	Symbol	Value
Number of tank pressure data points	N_{tank}	10001
Roughness height of the pipe wall (m)	ε	0.00001
Pipe diameter (m)	D	0.0508
Density of air (kg/m ³)	ρ_a	1.23
Density of water (kg/m ³)	ρ_w	1000
Dynamic viscosity of air (Ns/m ²)	f_a	0.0000179
Dynamic viscosity of water (Ns/m ²)	f_{fw}	0.00112
Length of the horizontal pipe (m)	L_p	9.4488
Temperature (C°)	T	18
Atmospheric pressure (Pa)	PO	101300
Initial slug velocity (m/s)	U_{in}	0
Initial slug position (m)	X_{in}	0.05
Initial slug length (m)	L_{in}	1.22, 1.52, 2.13, 2.74, 3.35 (4 ft, 5 ft, 7 ft, 9 ft, 11 ft)
Initial tank pressure (kPa)	P_0	68.91, 137.82, 206.73, 275.64 (10psi, 20 psi, 30 psi, 40 psi)
Radius of curvature of the elbow (m)	R_0	0.0508
Gravitational acceleration (m/s ²)	g	9.81
Length of the vertical extension segment after the elbow (m)	L_{ext}	0.4
Minor loss coefficient at the elbow	K_m	0.26
Atmospheric gage pressure (Pa)	PO_{gage}	0
Radial mesh size of the pipe cross-section, the circumferential one being automatically generated	M	25
Ratio of the circumferential mesh size to the radial one, at any cross-section of the pipe	m_{rt}	1.0
Number of nodes for the line integrals, for the case of integrating along the pipe diameter as the largest span length	M_L	16
Mesh clustering ratio for the line integrals	c_r	1.4
Number of nodes for the uniform line mesh, along the pipe radius, to be used for impact pressure calculation at the pipe wall	$MLPRSS$	12
Number of volume elements corresponding to the slug length at the beginning of impact, mesh along s-curve being automatically generated	N_{slug}	1750
Coordinate on curve-s, where the maximum shift of the velocity profile occurs (m)	s_{max}	0.0532

The computer code KAYHAN was run for different initial slug lengths of 1.22 m, 1.52 m, 2.13 m, 2.74 m and 3.35 m (or 4 ft, 5 ft, 7 ft, 9 ft, 11 ft); and different initial tank pressures of 68.91 kPa, 137.82 kPa, 206.73 kPa and 275.64 kPa (or 10 psi, 20 psi, 30 psi, 40 psi) for the determination of peak pressures and the transient forces acting on the elbow and the vertical extension segment in the present study.

The mesh sizes M , M_L , $MLPRSS$ and N_{slug} in Table 4.5 were determined with error analyses conducted as given in the following sections.

4.11.2 Error Analysis and Mesh Size for Area Integrals

For the error analyses of the area integrals of the form (4.40) as given below

$$I_A = \int_A f(\xi, \eta) dA$$

and the function $f(\xi, \eta)$ was chosen as

$$f(\xi, \eta) = u_s(\xi, \eta) \quad (4.127)$$

where u_s is the assumed axial velocity profile function with 3-D shape. Then, the numerically calculated value of the discharge Q_{cal} can be expressed as

$$I_A = Q_{cal} = \int_A u_s(\xi, \eta) dA = \int_A u_s(\xi, \eta) \xi d\xi d\eta \quad (4.128)$$

By taking $\theta_c = 89.84^\circ$, $\theta_f = 89.9971^\circ$ and $U_m = 32.32059$ m/s as the parameters of the assumed velocity profile function u_s , the numerically calculated discharge, Q_{cal} , values were obtained for different mesh sizes $M \times N$ over the pipe cross-section. And the percentage error corresponding to each mesh size was

calculated with the formula

$$\% \text{ error} = 100 \frac{|Q - Q_{cal}|}{Q} \quad (4.129)$$

where Q is the analytically calculated discharge value found as the volume under the assumed axial velocity profile function, u_s .

Plots for the percentage error calculated by Equation (4.129), vs. total mesh size, $M \times N$, for different m_{rt} values defined as

$$m_{rt} = \frac{N}{M} \quad (4.130)$$

are given from Figures 4.22 to 4.27.

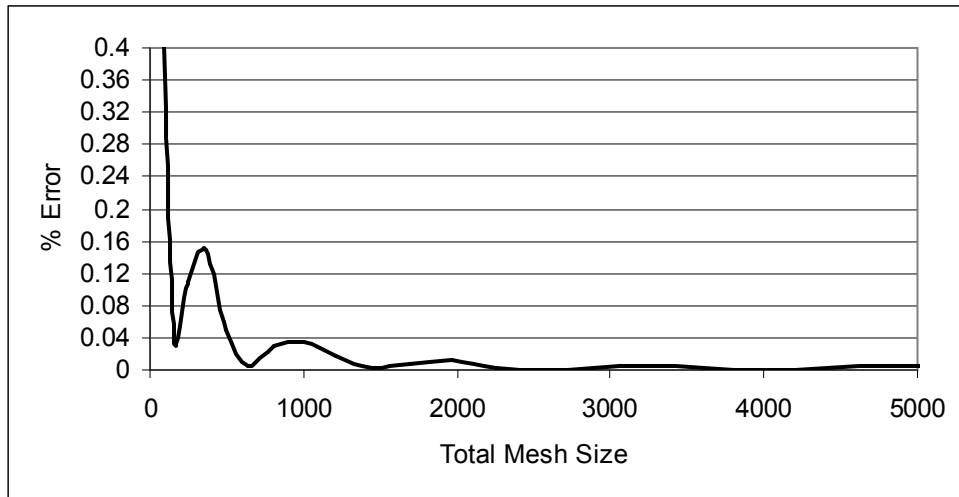


Figure 4.22 Percentage error vs. total mesh size, for $m_{rt} = 0.1$

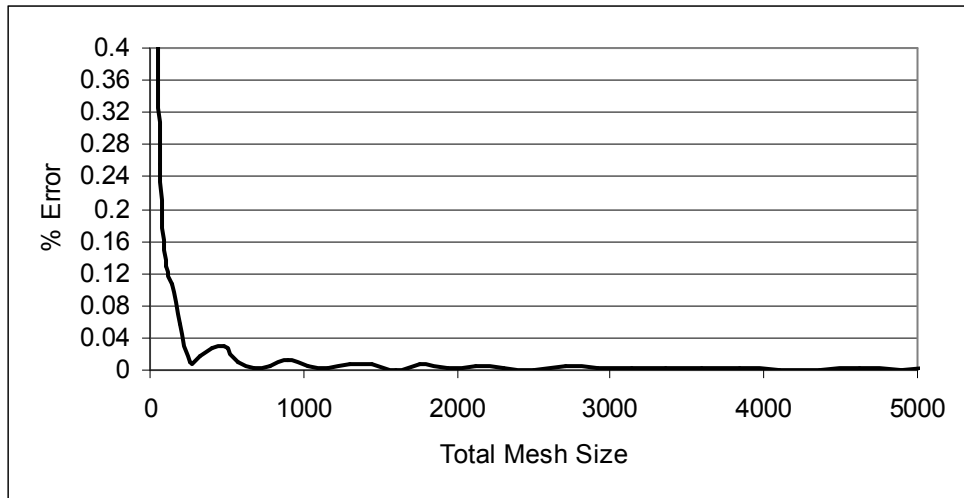


Figure 4.23 Percentage error vs. total mesh size, for $m_{rt} = 0.25$

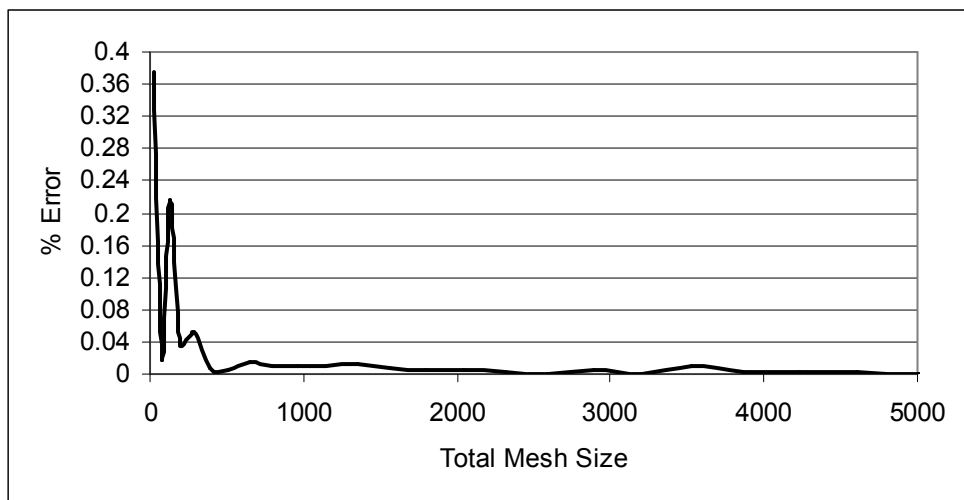


Figure 4.24 Percentage error vs. total mesh size, for $m_{rt} = 0.5$

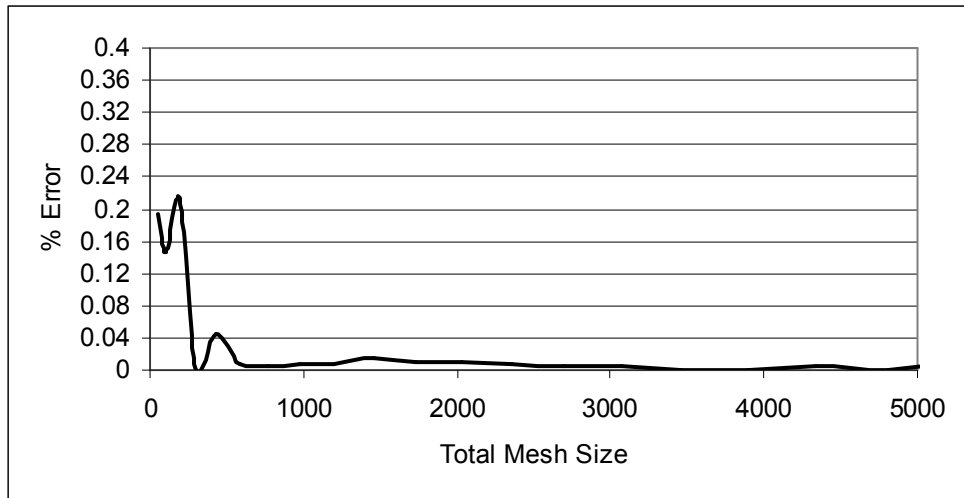


Figure 4.25 Percentage error vs. total mesh size, for $m_{rt} = 0.75$

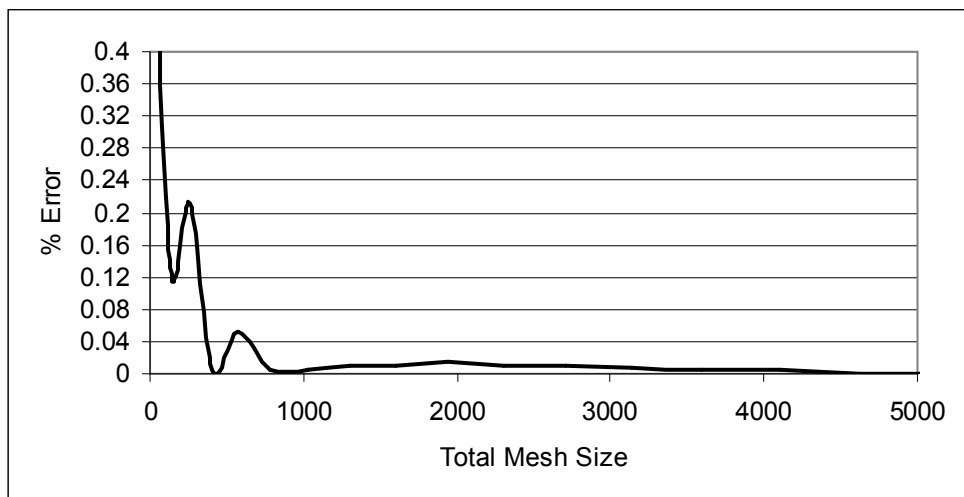


Figure 4.26 Percentage error vs. total mesh size, for $m_{rt} = 1.0$

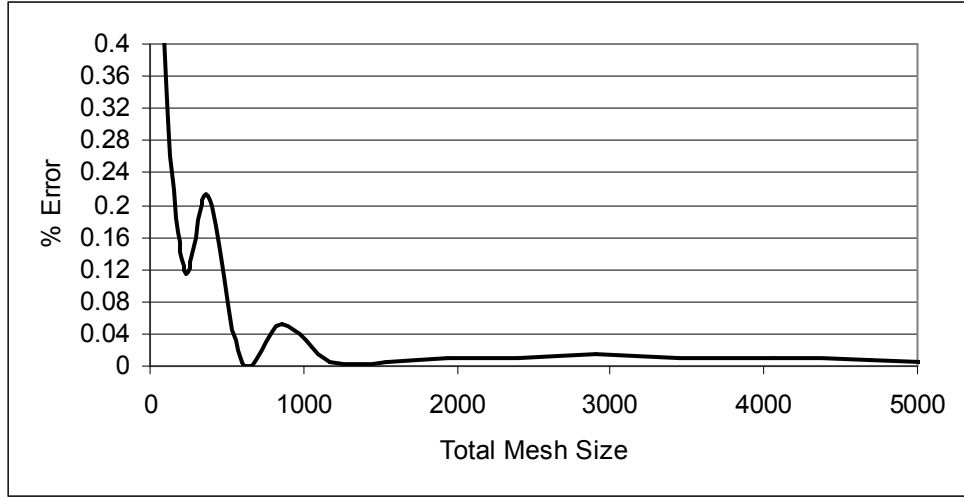


Figure 4.27 Percentage error vs. total mesh size, for $m_{rt} = 1.5$

From these figures, it can be concluded that for a total mesh size of $M \times N = 625$ and $m_{rt} = 1.0$, the percentage error remains below 0.06 % as given in Figure 4.26. Therefore, $M = 25$ and $N = 25$ was chosen for the mesh size over the pipe cross-section, which was accepted to give enough accuracy.

Although mesh sizes with $m_{rt} < 1.0$ requires smaller mesh size for the same accuracy as seen in Figures 4.23 to 4.25, they were not chosen since in that case the N values would be smaller which requires finer clustered line meshes for line integrals to be taken later on, causing larger simulation times as mentioned in Section 4.5.2.1.

4.11.3 Error Analysis and Mesh Size for Line Integrals

The size of the clustered line meshes used for the evaluation of numerical line integrals of the type given by Equation (4.48) as given below

$$I_L = \int_{A'}^{K'} h'(\xi, \eta) dr$$

were determined by an error analysis presented in this section.

The integrand $h'(\xi, \eta)$ in Equation (4.48) given above was selected as

$$h'(\xi, \eta) = \frac{\partial u_\beta}{\partial \beta} \quad (4.131)$$

as commonly encountered in pressure distribution equations and transient force calculations in Sections 4.3.2 and 4.4 of the present study, respectively.

Then, the integral to be used in the error analysis in (4.48) can be given as

$$I_{L1} = \int_{A'}^{K'} \frac{\partial u_\beta}{\partial \beta} dr \quad (4.132)$$

where

I_{L1} : integral expression.

For the error analysis, the location of point K' was selected on the pipe cross-section shown in Figure 4.18 as

$$K'(\xi, \eta) = K' \left(0.01847, \frac{\pi}{2} \right) \quad (4.133)$$

with ξ in meters, and the pipe cross-section on the s -curve shown in Figure 4.5 was chosen at location $s = 0.01637 \text{ m}$.

During the computer runs for the analysis, initial slug length, L_{in} , was taken as 1.21 m (4 ft) and initial tank pressure, P_0 , was used as 68.91 kPa (10 psi), together with other data given in Table 4.5. The I_{L1} values at time $t = 0.75723 \text{ s}$ were used for the analysis.

In the error analysis, the calculated values of I_{L1} for $M_L > 30$ gives $I_{L1} = 0.01384 \text{ m}^2/\text{s}$ as a constant value with 5 digits accuracy after the decimal point.

Then the percentage error for the line integral I_{L1} was calculated by the formula

$$\% \text{ error} = 100 \frac{|0.01384 - I_{L1}|}{0.01384} \quad (4.134)$$

The variation of percentage error calculated by (4.134), with the size of the clustered line mesh, M_L , is given in Figure 4.28.

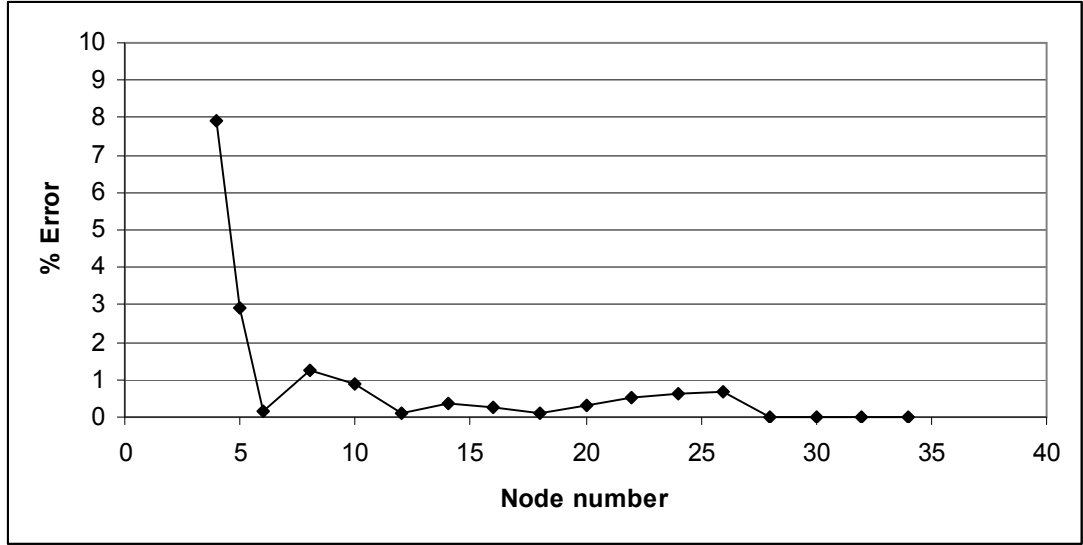


Figure 4.28 Variation of percentage error vs. node number, M_L .

According to Figure 4.28, the size of the clustered line mesh was chosen as $M_L = 16$ for which the percentage error remains below 1 %.

4.11.4 Mesh Size and Error Analysis for the Line Mesh along s -Curve

For the elbow and the vertical extension part calculations, the mesh spacing along the s -curve shown in Figure 4.5 was calculated by using the formula given by

$$\Delta s = \frac{L_{s \text{ imp}}}{N_{\text{slug}}} \quad (4.135)$$

Here,

$L_{s \text{ imp}}$: slug length at the instant that the slug front enters the elbow,

N_{slug} : number of nodes selected over the slug length, L_{simp} .

And, the time increment at each time step of the slug motion in the elbow and the vertical extension segment was calculated from the formula

$$Cr = \frac{\Delta t_s U_{ave}}{\Delta s} \leq 1 \quad (4.136)$$

given by Tannehill et. al. [39].

In Equation (4.136),

Δt_s^n : time increment at any time step, n ,

U_{ave}^n : average slug velocity at any time step, n ,

Cr : Courant number.

Equation (4.136) is called as the Courant number condition, which is used as the stability requirement of hyperbolic partial differential equations.

Since the pressure distribution equations given by (4.17), (4.19) and (4.21) to be solved in the elbow and the vertical extension segment of the pipeline are of integral type equations, which are unconditionally stable, the Courant number in (4.136) can be taken as

$$Cr = 1 \quad (4.137)$$

as being equal to the upper limit.

Then, the time increment, Δt_s , can be calculated from Equation (4.136) as follows:

$$\Delta t_s^n = \frac{\Delta s}{U_{ave}^n} \quad (4.138)$$

In non-dimensional form, the equations (4.135) and (4.138) can be expressed as

$$\Delta s^* = \frac{L_{simp}}{L'N_{slug}} \quad (4.139)$$

$$\Delta t_s^{*n} = \frac{\Delta s^*}{U_{ave}^{*n}} \quad (4.140)$$

Then, time value at any time step of elbow and the vertical extension segment calculations, can be calculated with the expression

$$t^{*n} = t^{*n-1} + \Delta t_s^{*n} \quad (4.141)$$

by using the final value for time t^* for the horizontal pipe calculations as the initial condition for the elbow and the vertical extension segment calculations.

The number of nodes, N_{slug} in Equation (4.139), selected on that length of the slug at the instant that the slug front reaches the entrance section of the elbow was found by an error analysis.

Since the peak pressure at the point on the convex side of the elbow at the location of transducer #2 in Bozkuş's [2] setup, is the parameter which is mostly affected by the mesh size N_{slug} in the present study, the error analysis was made by considering the variation of this peak pressure with mesh size.

The error analysis was made for slug lengths of $L_{in} = 1.21$ m (4 ft) and initial tank pressures of $P_0 = 69.91$ kPa (10 psi). In the analysis, it was seen that the peak pressures attained a constant value of 82. psi (or 565 kPa in SI units) with two decimal places of accuracy. Therefore, the percentage error was calculated with the expression

$$\%error = 100 \frac{|82 - p_{peak}|}{82} \quad (4.142)$$

Here,

p_{peak} : peak pressure from program KAYHAN at the location of transducer

#2.

The variation of percentage error given by Equation (4.142), with respect to mesh size, N_{slug} , is given in Figure 4.29.

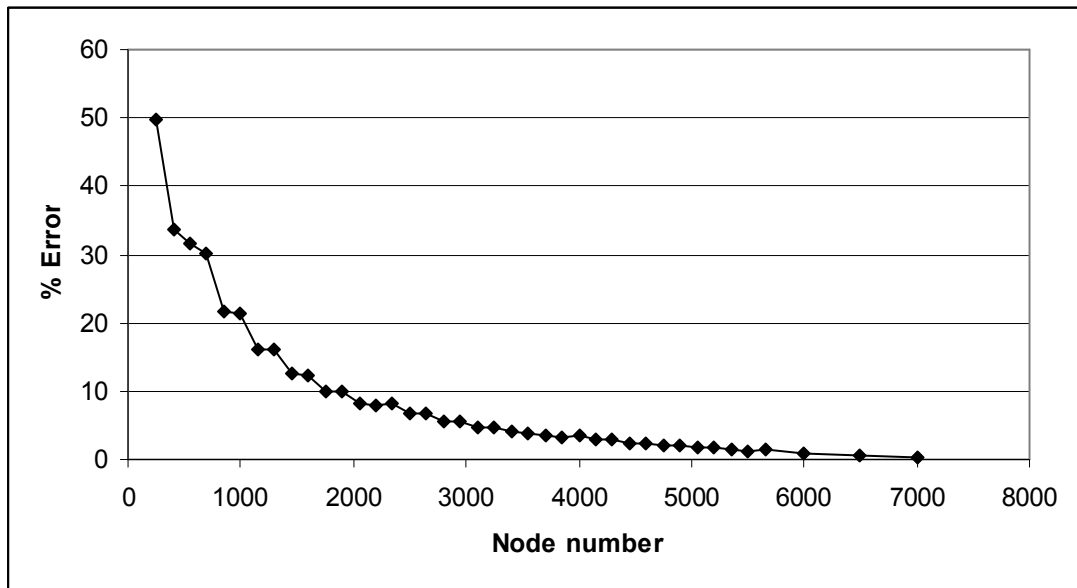


Figure 4.29 Variation of percentage error vs. node number, N_{slug} .

According to the variation of error in Figure 4.29, the mesh size N_{slug} was chosen as 1750, which gives percentage error for p_{peak} as less than 10 %. Larger N_{slug} values were not selected in order not to slow down the simulation speed.

4.11.5 Error Analysis and the Mesh Size for Impact Pressure Calculation

The size of the line mesh $MLPRSS$ along the radius of the pipe cross-section at the elbow shown in Figure 4.8, used for the calculation of impact pressures at the convex side of the elbow, was determined with an error analysis given in this section.

For the analysis, the impact pressure, p , values were calculated for initial

slug lengths, $L_{in} = 2.13$ m (7 ft), initial tank pressures, $P_0 = 68.91$ kPa (10 psi), at time, $t = 0.92277$ s and with other input parameters being as in Table 4.5.

It was seen that the impact pressure, p , values remain constant up to 3 digits of accuracy at a value of 20.2 psi (or 139 kPa in SI units) for node number values of $MLPRSS > 30$, and therefore, the percentage error was calculated with the expression given below:

$$\% \text{ error} = 100 \frac{|20.2 - p|}{20.2} \quad (4.143)$$

The variation of percentage error calculated by (4.143), with respect to node number $MLPRSS$ is given in Figure 4.30.

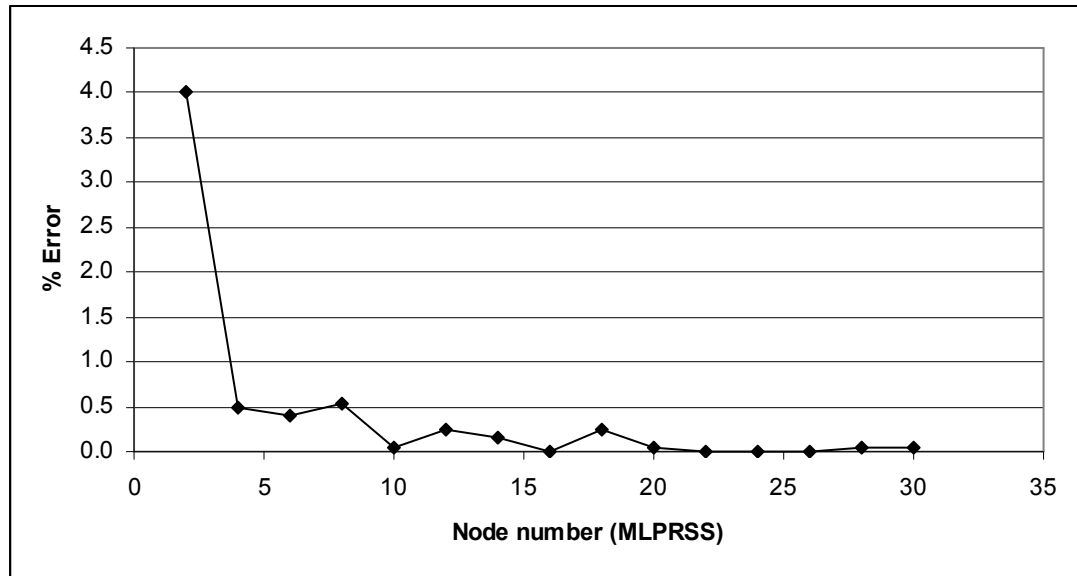


Figure 4.30 Variation of percentage error vs. node number $MLPRSS$.

According to the variation of the percentage error in Figure 4.30, the node number, $MLPRSS$, for impact pressure calculation at the convex side of the elbow was taken as $MLPRSS = 12$. For this mesh size selection it can be seen from Figure 4.30 that the percentage error remains below 0.3 %.

CHAPTER V

RESULTS AND DISCUSSION

5.1 Introduction

In this chapter, the results obtained from the computer simulations with program KAYHAN, which was developed in the present study, are presented and discussed. Comparisons of the obtained results from program KAYHAN with the previous studies are also given.

The computer simulations with KAYHAN were made with 4 different initial tank pressures of 68.91 kPa, 137.82 kPa, 206.73 kPa, 275.64 kPa (10, 20, 30 and 40 psi.) For each of these initial tank pressures, simulations with 5 different initial slug lengths of 1.22 m, 1.52 m, 2.13 m, 2.74 m and 3.35 m (4, 5, 7, 9 and 11 ft) were performed. Other data as input parameters are as given in Table 4.5.

The input data used for the computer programs and the data used in the experiments both in the present study and of previous studies are presented in units of International System (SI) together with their equivalents in British Gravitational System (BG) given in parenthesis. The results of the computer programs and the experiments for the pressure values are tabulated and plotted in BG System.

In Section 5.2, the normalized peak pressures at the elbow vs. the normalized slug travel distances as obtained from program KAYHAN are given and comparisons with some experimental and numerical results from Bozkuş's [2] study are made. In Section 5.3, the pressure-time history plots from program KAYHAN of the present study are compared with Bozkuş's [2] experimental results. The transient force-time history plots obtained from program KAYHAN are given in Section 5.4, and a comparison of the normalized peak horizontal transient force values vs. the dispersion distances at the elbow and the vertical extension segment are made with those from previous studies performed by Fenton [26], Bozkuş [2] and Baran [27]. A

set of plots for the impact pressure distribution at the convex side of the elbow at projected nodal points from the axial s -curve of the elbow are also given in Section 5.5.

5.2 Peak Pressures at the Elbow

The time dependent impact pressure distribution at the convex side of the elbow was calculated with program KAYHAN by using the formulation given in Section 4.3.2.3 in the present study. From this pressure distribution, the impact pressure value at nodal point C' on the convex side of the elbow shown in Figure 4.10 at a location $2/3$ of the total axial length of the elbow distance away from the entrance of the elbow was taken, as also being the maximum impact pressure value at the elbow. This location at the elbow actually corresponds approximately to the same point where the transducer #2 was located in Bozkuş's [2] setup shown in Figure 2.2. In the present study, the maximum impact pressure value was at this location of the transducer #2 because the maximum shift of the assumed and calibrated axial velocity profile function with 3-D shape was also here as a result of a proper selection of the related calibration parameter of the calibration function for the velocity profile.

By taking the time-peak of the maximum impact pressure values calculated with program KAYHAN in the present study, which corresponds to the location of transducer #2 on the elbow in Figure 2.2, the plot given in Figure 5.1 were prepared.

In Figure 5.1, the variation of the peak pressures at the elbow normalized with respect to the initial tank pressure vs. the slug travel distances as normalized with respect to the initial slug lengths are plotted. In this plot, the results from the computer programs KAYHAN, BOZKUŞ-2 [2], and Bozkuş's [2] experimentally obtained findings are given together. Totally 6 different hold up coefficients for BOZKUŞ-2 are involved in this plot ranging from no hold up to 5% hold up.

As can be deduced from Figure 5.1, it can be said the normalized pressures from program KAYHAN has a sinusoidal variation which provides a better approximation to Bozkuş's experimentally obtained values than the values from the program BOZKUŞ-2. This superiority of the program KAYHAN can be attributed mainly to two different correlation functions used for obtaining the functional hold

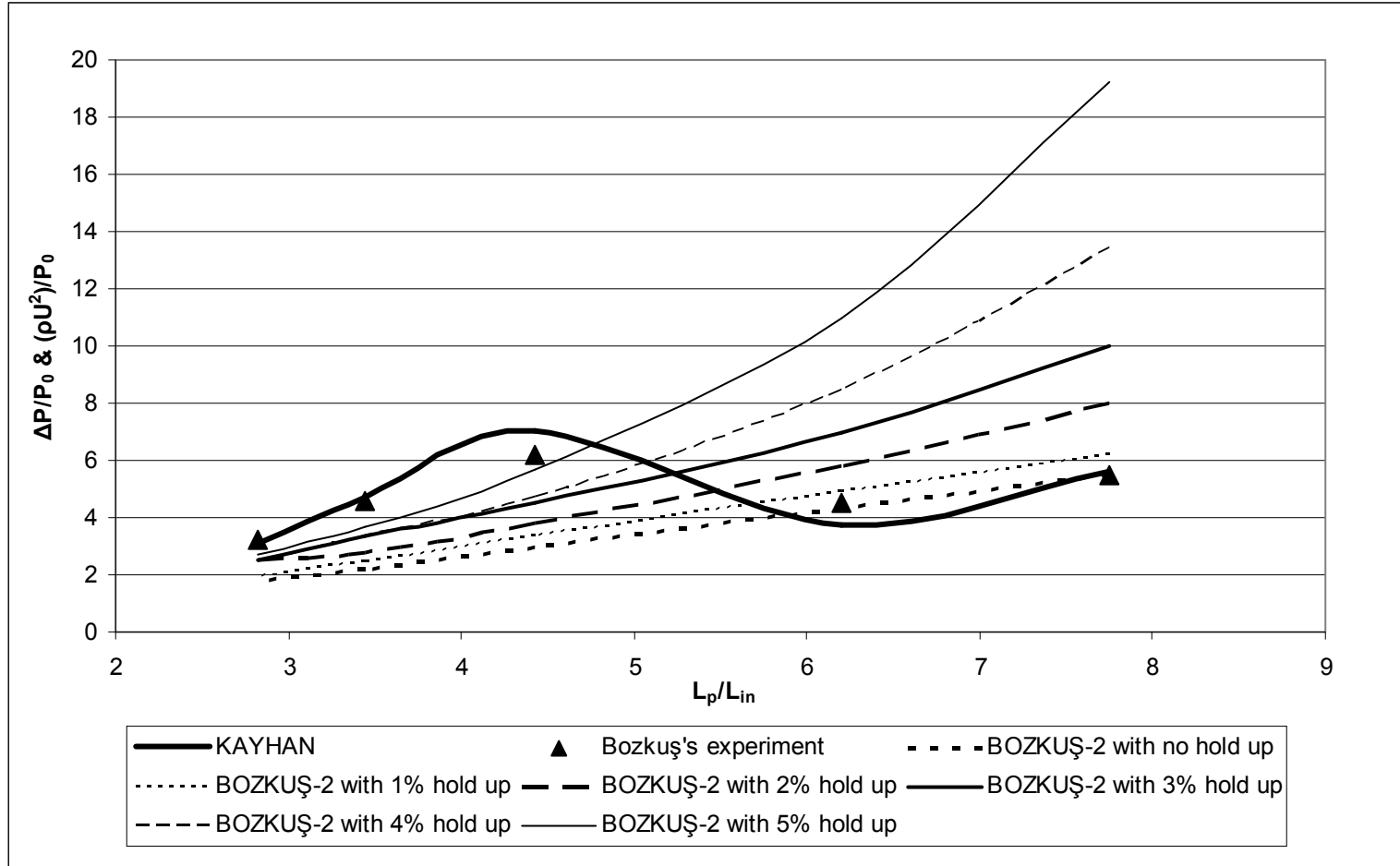


Figure 5.1 Normalized peak pressures vs. L_p / L_{in} .

up coefficient and the for calculating a parameter of the calibration function for the assumed velocity profile in the present study.

For 1.22 m (4 ft) slugs, which are at the right end of the data range of the plots, it can be seen from Figure 5.1 that the normalized peak pressures from program KAYHAN, and from program BOZKUŞ-2 with no hold up are in excellent agreement with the experimental findings of Bozkuş. For 2.13 m (7 ft) slugs, which are shown at the mid region of the data range, it can be said that the normalized peak pressure values are overestimated with program KAYHAN but for these slugs, the values from program BOZKUŞ-2 for all hold up values remain below the experimental data. For 3.35 m (11 ft) slugs, which are located at the left end of the data range in the plots, it can be concluded that the normalized peak pressures from program KAYHAN match with Bozkuş's experimental data well and the normalized peak pressures from program BOZKUŞ-2 remain slightly below the experimental data. For 1.52 m (5 ft) slugs, the results from program BOZKUŞ-2 with no hold up are closer to experimental data than the results are from program KAYHAN. However, for 2.74 m (9 ft) slugs, program KAYHAN gives better approximation to the experimental data than program BOZKUŞ-2 for all hold up values.

A tabulated output for the peak pressures at the location of transducer #2 on the elbow shown in Figure 2.2 is also given in Table 5.1. In this table the peak pressures obtained from programs BOZKUŞ-1, BOZKUŞ-2 and KAYHAN are presented together with the experimental data for different initial slug lengths and initial tank pressures. Explanations for the functions of these programs, and a flowchart and the computer code written in FORTRAN Language for program KAYHAN are given in Appendix C. In the last column of Table 5.1, the Joukowsky pressure rise values for a fictitious case of sudden valve closure at the elbow location are presented, and these values are referred later on in Section 5.6.

5.3 Pressure-Time History Plots

The variation of the impact pressures with time from program KAYHAN at the point on the convex side of the elbow where the transducer #2 in Bozkuş's [2] setup was located, was plotted to obtain pressure –time history plots at the elbow.

Table 5.1 Peak pressures at the elbow (psig).

Slug Length	Tank Pressure	BOZKUŞ-1						BOZKUŞ-2						KAYHAN	Bozkuş's Experiment		Joukowsky Pressure Rise
		A						α							1 st	2 nd	
		1.00	0.99	0.98	0.97	0.96	0.95	1.00	0.99	0.98	0.97	0.96	0.95		peak	peak	
1.22 m (4 ft)	68.91 kPa (10 psi)	48.95	57.98	70.54	88.84	117.11	164.27	48.88	57.84	70.36	89.08	119.32	174.43	73.82	49±14	-	-
	137.82 kPa (20 psi)	105.36	124.37	150.77	189.17	248.40	347.05	104.86	123.23	149.68	187.98	249.70	365.33	112.55	137±62	-	1106.85
	206.73 kPa (30 psi)	161.38	190.32	230.48	288.89	398.75	528.88	159.82	188.01	226.95	284.89	377.12	557.67	148.80	142±31	-	730.94
	275.64 kPa (40 psi)	220.22	259.44	313.87	392.98	514.90	717.77	218.22	254.50	307.13	384.67	509.85	718.71	183.37	217±119	-	1291.32
1.52 m (5 ft)	68.91 kPa (10 psi)	38.25	43.76	50.93	60.53	73.84	93.10	38.25	43.72	50.98	60.87	74.98	96.52	46.28	28±6	-	537.64
	137.82 kPa (20 psi)	83.20	94.90	110.08	130.38	158.47	199.07	83.02	94.43	109.77	130.24	159.73	204.70	72.16	131±48	-	992.78
	206.73 kPa (30 psi)	127.80	145.64	168.79	199.72	242.52	304.36	126.99	144.74	167.33	198.45	242.72	310.55	104.98	-	-	-
	275.64 kPa (40 psi)	174.93	199.16	230.60	272.59	330.66	414.53	173.65	196.85	227.30	269.82	328.44	419.83	133.50	-	-	-
2.13 m (7 ft)	68.91 kPa (10 psi)	26.16	28.11	32.00	35.92	40.81	47.03	26.23	28.88	32.11	36.15	41.37	48.17	99.71	96±17	79±9	1556.22
	137.82 kPa (20 psi)	58.08	63.75	70.60	78.99	89.45	102.75	58.06	63.79	70.64	79.38	90.35	104.89	138.34	135±35	151±18	2067.02
	206.73 kPa (30 psi)	89.66	98.35	108.83	121.67	137.66	157.99	89.52	98.06	108.72	121.87	138.47	160.57	168.29	139±27	222±41	990.26
	275.64 kPa (40 psi)	123.40	135.25	149.54	167.03	188.42	216.50	122.76	134.69	148.94	166.45	189.20	219.03	220.62	173±32	264±31	1098.88
2.74 m (9 ft)	68.91 kPa (10 psi)	19.56	21.09	22.87	24.96	27.43	30.39	19.64	21.18	22.96	25.13	27.93	30.96	59.26	56±11	71±6	1495.37
	137.82 kPa (20 psi)	44.25	47.57	51.43	55.95	61.30	67.72	44.34	47.66	51.58	56.33	61.96	68.96	89.17	78±16	131±5	1039.14
	206.73 kPa (30 psi)	68.64	73.74	79.66	86.60	94.81	104.65	68.68	73.82	79.76	86.94	95.76	106.29	129.59	-	-	-
	275.64 kPa (40 psi)	94.93	101.91	110.01	119.50	130.72	144.16	94.83	101.78	109.87	119.63	131.60	146.10	164.57	-	-	-
3.35 m (11 ft)	68.91 kPa (10 psi)	14.53	15.42	16.42	17.56	18.86	20.35	15.51	16.48	17.61	18.92	20.47	22.30	32.49	38±4	65±7	692.80
	137.82 kPa (20 psi)	33.64	35.60	37.80	40.30	43.15	46.40	33.76	35.71	37.96	40.59	43.62	47.18	62.34	63±14	124±8	775.83
	206.73 kPa (30 psi)	52.48	55.49	58.89	62.73	67.12	72.17	52.62	55.63	59.08	63.09	67.83	73.30	90.82	104±42	171±12	687.15
	275.64 kPa (40 psi)	73.00	77.14	81.00	87.08	93.11	100.03	73.06	77.17	81.91	87.43	93.91	101.51	120.78	126±40	207±16	725.70

The pressure-time history plots as obtained from program KAYHAN in the present study together with Bozkuş's [2] experimental results are shown in Figures 5.2 to 5.13.

In pressure – time history plots in Figures 5.2 to 5.13, the times for the starting point of the pressure peaks from program KAYHAN and from Bozkuş's experimental results show some differences. For example, in Figure 5.2, the peak pressure from program KAYHAN occurs earlier than the pressure peak from Bozkuş's experimental result by some amount. As another example, in Figure 5.3, program KAYHAN gives the peak pressure at a later time point than the experimental time value. The time value for the start of the pressure peak here is actually a very close value to the slug arrival time at the elbow and this time value was calculated in program KAYHAN by utilizing a modified version of computer code BOZKUŞ-2 developed by Bozkuş. The slug arrival time at the elbow here was calculated in program KAYHAN as a final result of the calculations at the horizontal section of the pipeline in the present study, and the mathematical development for this part was given in Chapter III.

The peak pressure values from program KAYHAN for shorts slugs as 1.22 m (4 ft) and 1.52 m (5 ft) initial length, are sometimes approximately half the experimental peak pressure value or twice the experimental peak as can be seen in Figures 5.2 to 5.5, which can be considered as a high deviation from the experimental pressure peaks. However, for medium and long slugs having initial lengths of 2.13 m, 2.74 m and 3.35 m (7, 9 and 11 ft); the pressure peaks from program KAYHAN are very close to the first peaks obtained experimentally by Bozkuş as in Figures 5.6 to 5.13. The higher deviation of the pressure peaks here obtained from program KAYHAN in the case of short slugs can be explained by the existence of more air entrainment effect that occurs for short slugs than the case of medium and long slugs.

As explained in Section 4.3.3, after the slug front face has entered the elbow, the driving air pressure acting at the upstream face of the slug was taken to be decreasing at the same rate as the tank pressure in program KAYHAN. Thus, the compressibility effect of the air column and therefore, the waterhammer effects that take place in the pipeline were neglected during the motion of the slug in the elbow

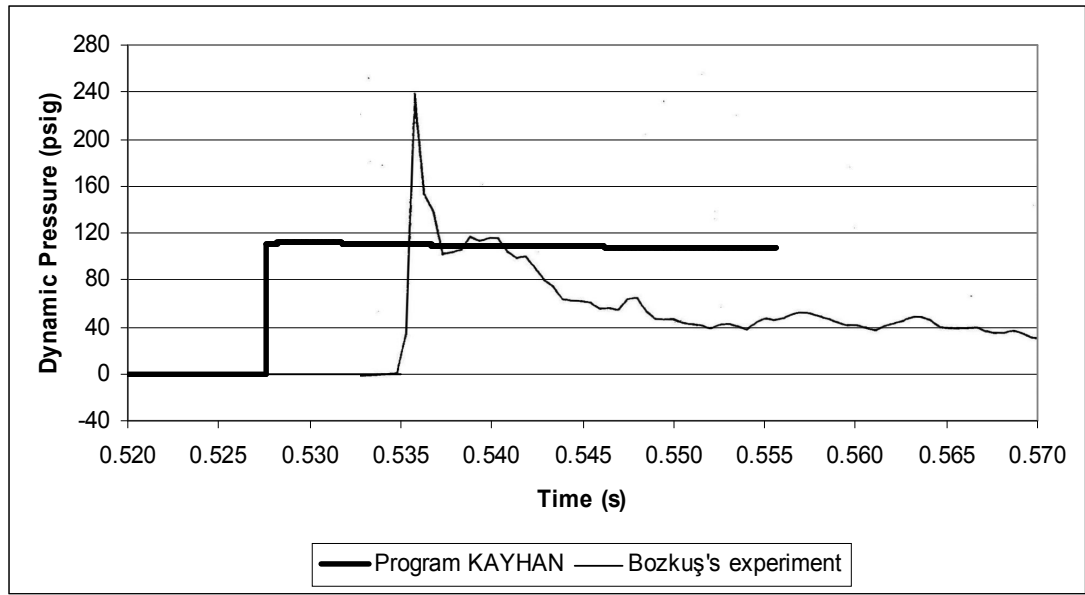


Figure 5.2 Pressure-time history plots at the elbow for $L_{in} = 1.22$ m (4 ft) and $P_0 = 137.82$ kPa (20 psig).

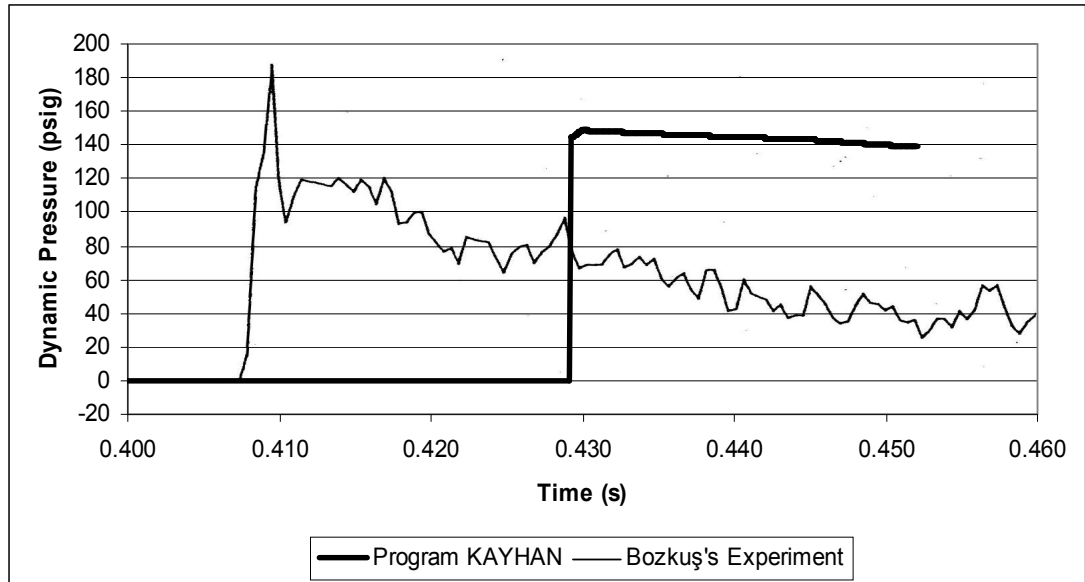


Figure 5.3 Pressure-time history plots at the elbow for $L_{in} = 1.22$ m (4 ft) and $P_0 = 206.73$ kPa (30 psig).

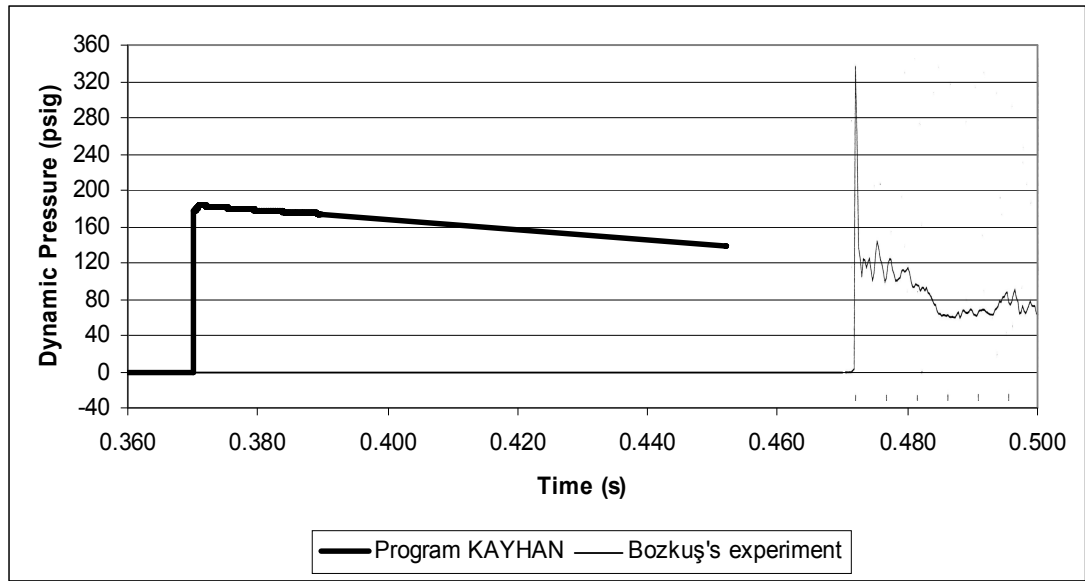


Figure 5.4 Pressure-time history plots at the elbow for $L_{in} = 1.22$ m (4 ft) and $P_0 = 275.64$ kPa (40psig).

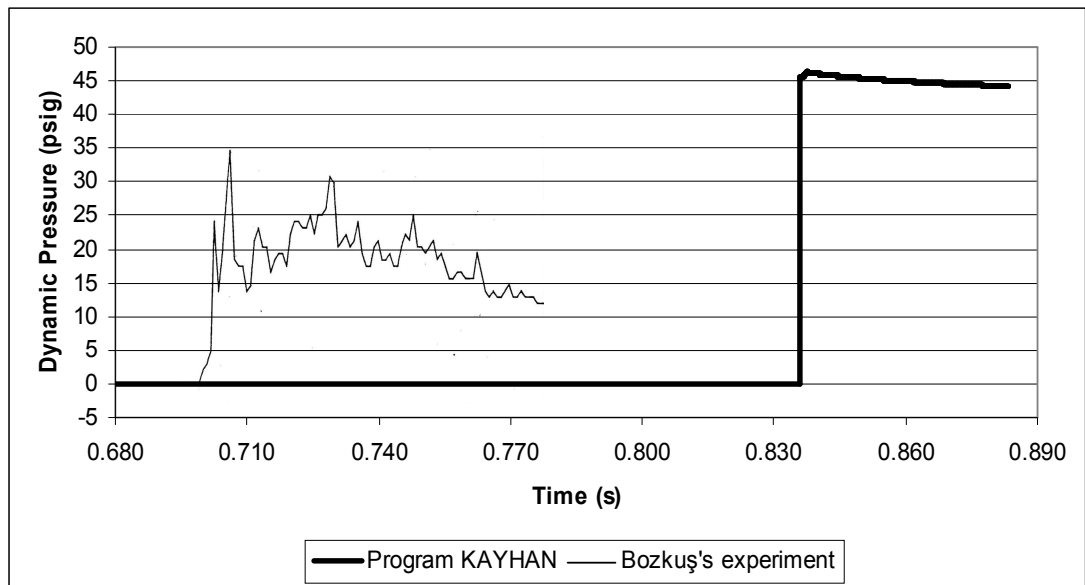


Figure 5.5 Pressure-time history plots at the elbow for $L_{in} = 1.52$ m (5 ft) and $P_0 = 68.91$ kPa (10 psig).

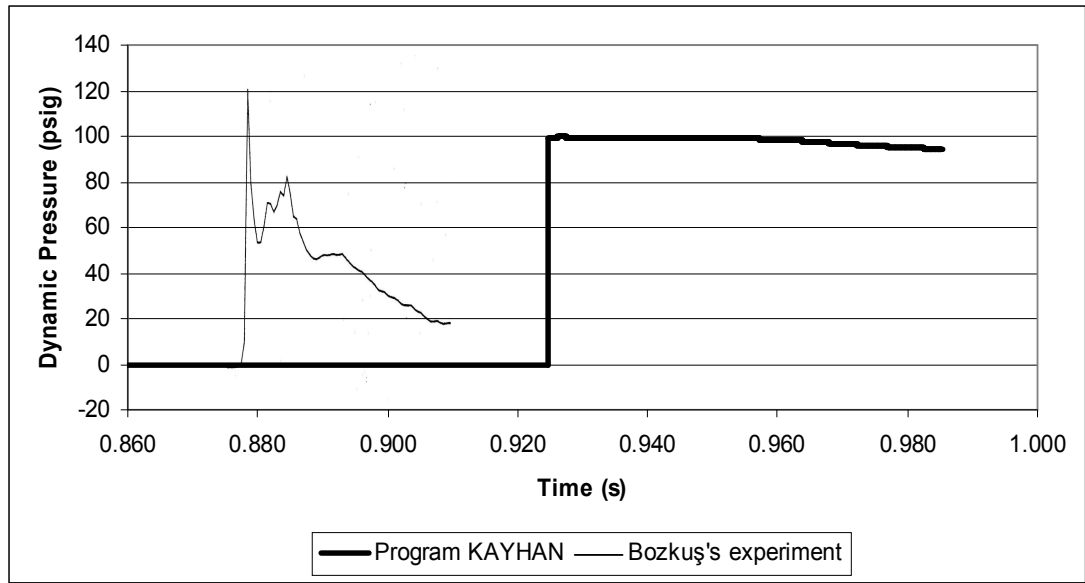


Figure 5.6 Pressure-time history plots at the elbow for $L_{in} = 2.13$ m (7 ft) and $P_0 = 68.91$ kPa (10 psig).

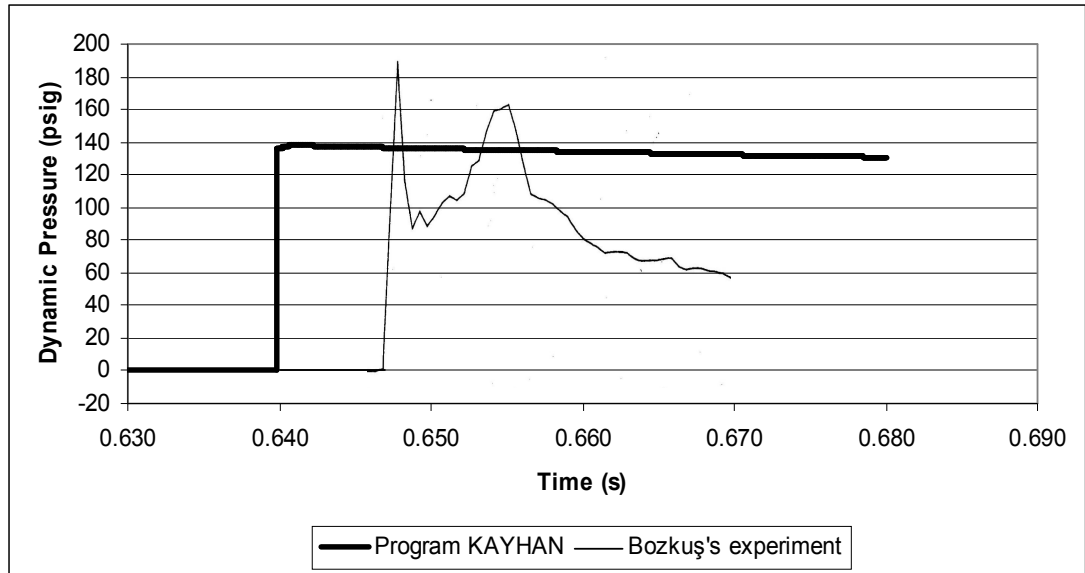


Figure 5.7 Pressure-time history plots at the elbow for $L_{in} = 2.13$ m (7 ft) and $P_0 = 137.82$ kPa (20 psig).

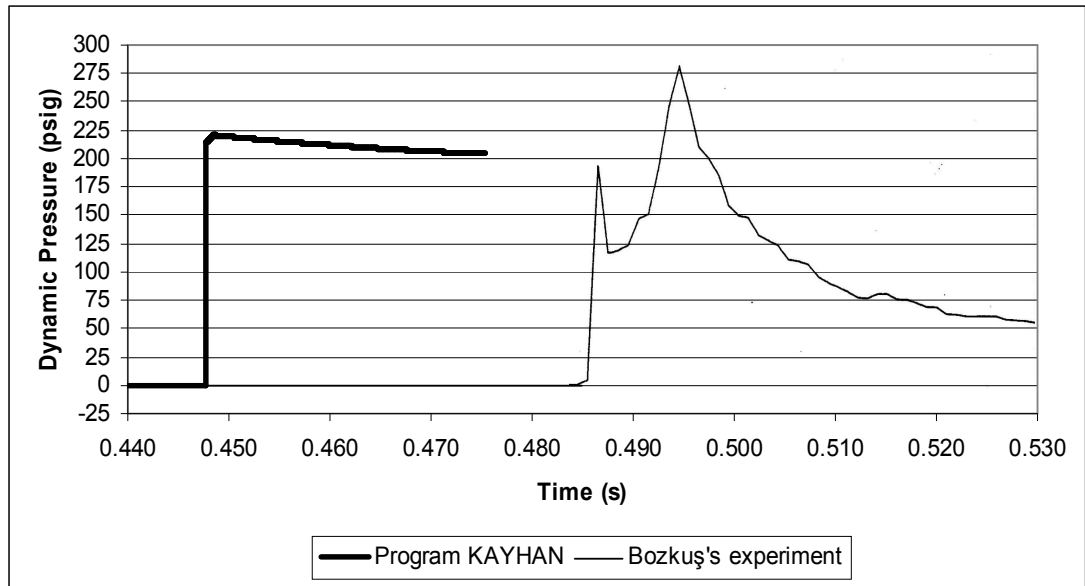


Figure 5.8 Pressure-time history plots at the elbow for $L_{in} = 2.13$ m (7 ft) and $P_0 = 275.64$ kPa (40 psig).

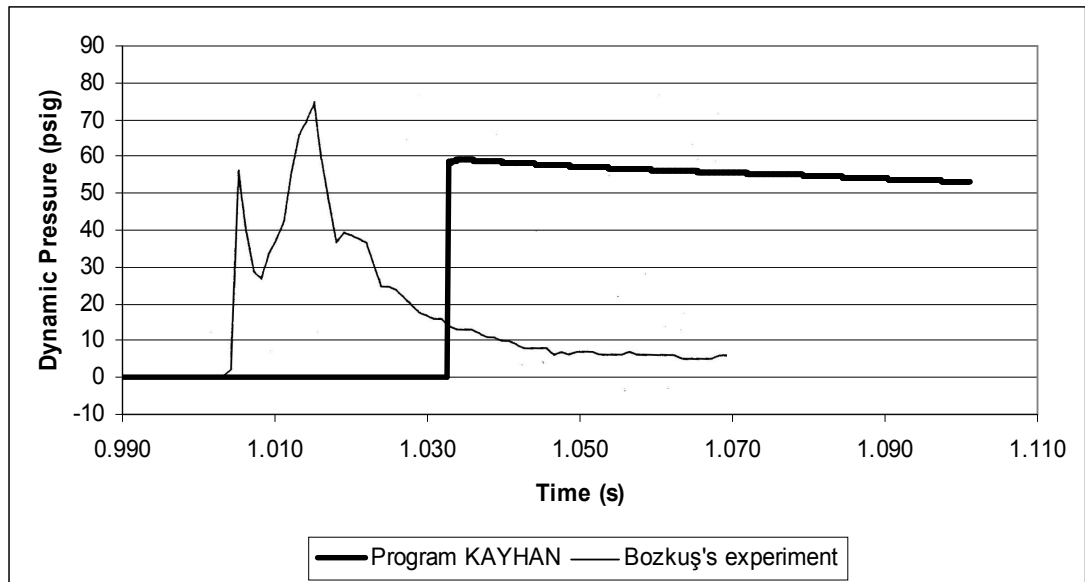


Figure 5.9 Pressure-time history plots at the elbow for $L_{in} = 2.74$ m (9 ft) and $P_0 = 68.91$ kPa (10 psig).

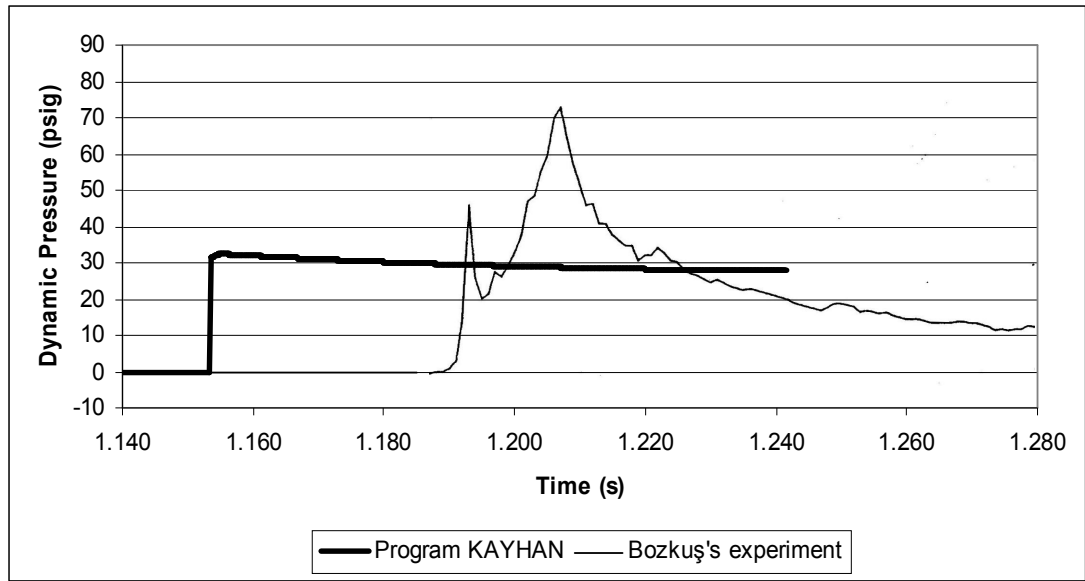


Figure 5.10 Pressure-time history plots at the elbow for $L_{in} = 3.35$ m (11 ft) and $P_0 = 68.91$ kPa (10 psig).

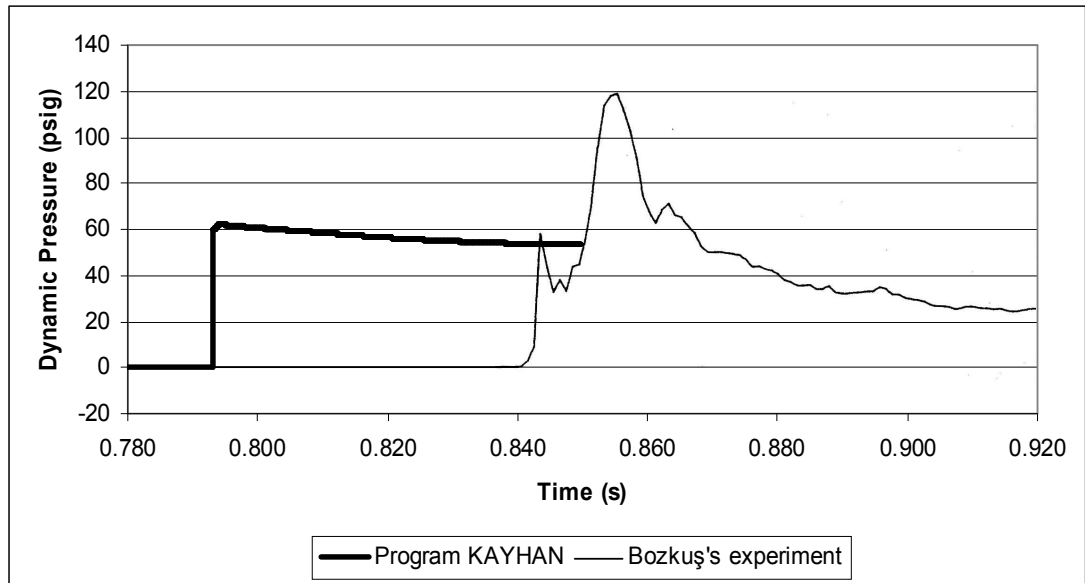


Figure 5.11 Pressure-time history plots at the elbow for $L_{in} = 3.35$ m (11 ft) and $P_0 = 137.82$ kPa (20 psig).

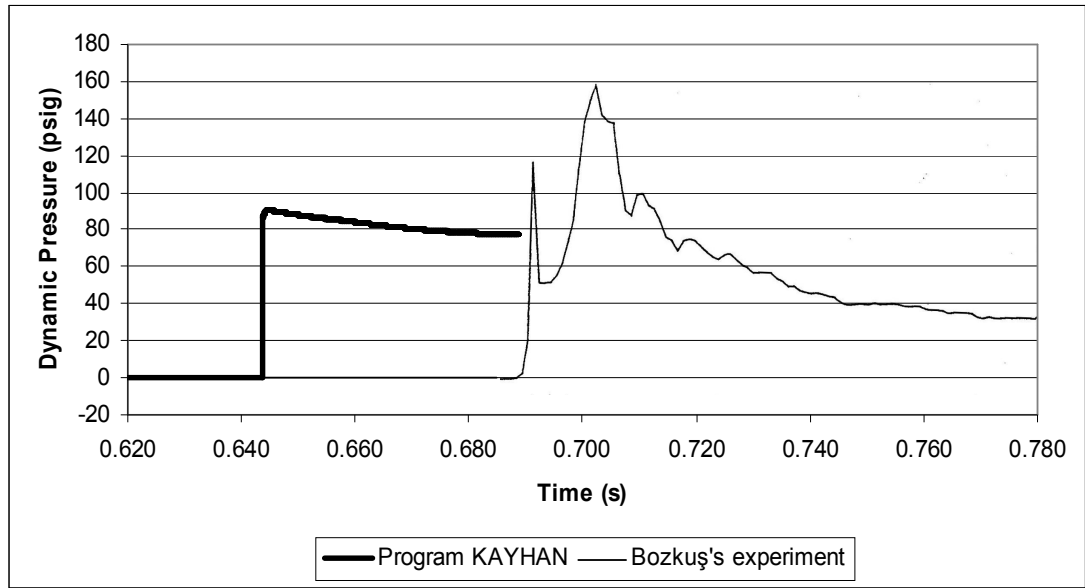


Figure 5.12 Pressure-time history plots at the elbow for $L_{in} = 3.35$ m (11 ft) and $P_0 = 206.73$ kPa (30 psig).

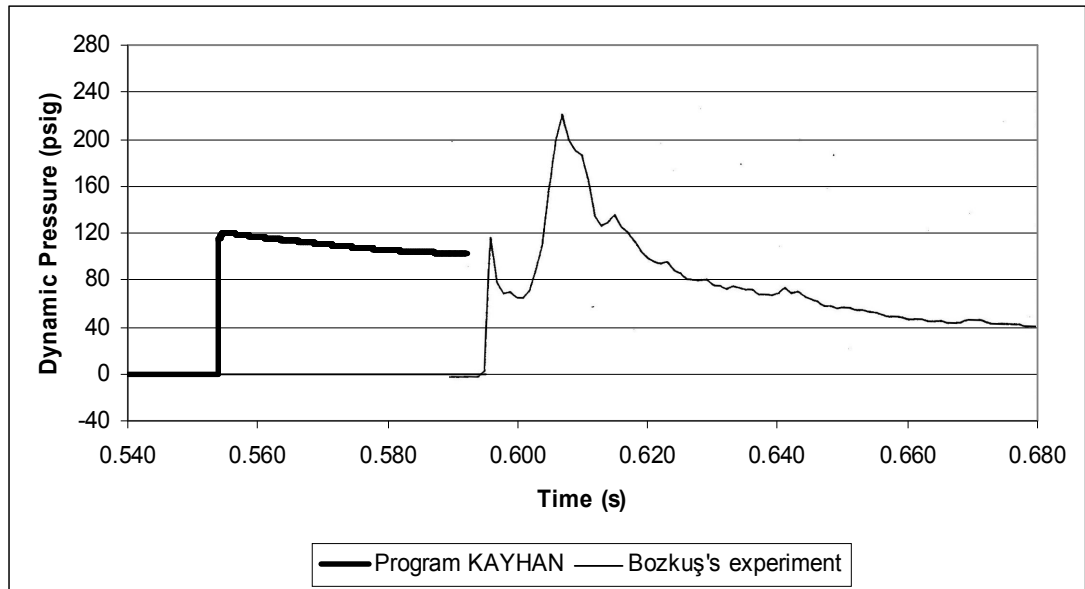


Figure 5.13 Pressure-time history plots at the elbow for $L_{in} = 3.35$ m (11 ft) and $P_0 = 275.64$ kPa (40 psig).

and the vertical extension segment. Neglecting the waterhammer effects here together with discarding the effect of air entrainment as a simplification, can be said to be the reasons that the pressure-time history diagrams from program KAYHAN does not reflect the wavy pattern seen in Bozkuş's experimental plots. However, the general shape of the tail regions of the pressure – time history plots are still in close agreement with the experimental data especially for 3.35 m (11 ft) slugs as shown in Figures 5.10 to 5.13.

The tail region of pressure-time history plots for 3.35 m (11 ft) slugs from program KAYHAN, shown in Figures 5.10 to 5.13 are in well agreement with Bozkuş's experimental findings. However, for slugs with initial length of 1.22 m, 1.52 m, 2.13 m and 2.74 m (4, 5, 7 and 9 ft); the tail region of the plots from the present study has a general tendency to remain above the experimental values of Bozkuş. This discrepancy of the values in the tail region of the pressure – time history plots in the cases of shorter slug lengths can be attributed to the existence of more air entrainment for shorter slugs.

5.4 Transient Forces at the Elbow

The horizontal and the vertical components of the transient forces acting on the elbow and the vertical extension segment were calculated by program KAYHAN in the present study according to the formulation derived in Section 4.4.

The variation of the horizontal and the vertical transient force components, F_x and F_y , acting on the elbow and the vertical extension segment are given from Figures 5.14 to 5.19 for different initial slug lengths and the initial tank pressures. As a general characteristic property, it can be said the there is an initial and sharp increasing part of the transient force components in all the plots which corresponds to the period that the slug front is at a stage of advancing within the elbow and the vertical extension segment. Then, after a peak value is attained for both force components, the transient force values start to decline with a relatively milder slope. This declining region of the plots can be said to be due to the reduction in slug speed under the effect of retarding forces applied by the elbow and the vertical extension segment on the liquid slug.

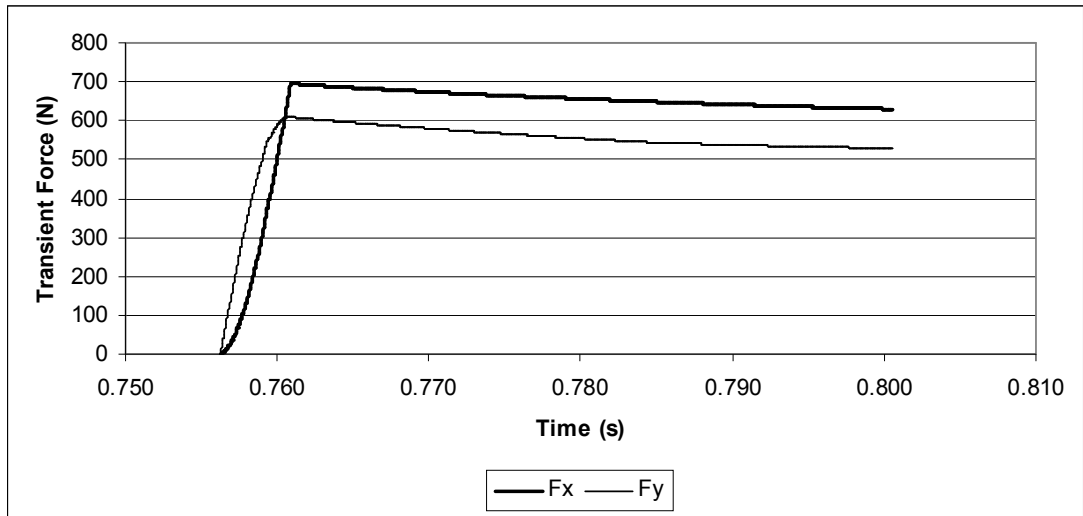


Figure 5.14 Transient force components for $L_{in} = 1.22$ m (4 ft) and $P_0 = 68.91$ kPa (10 psig).

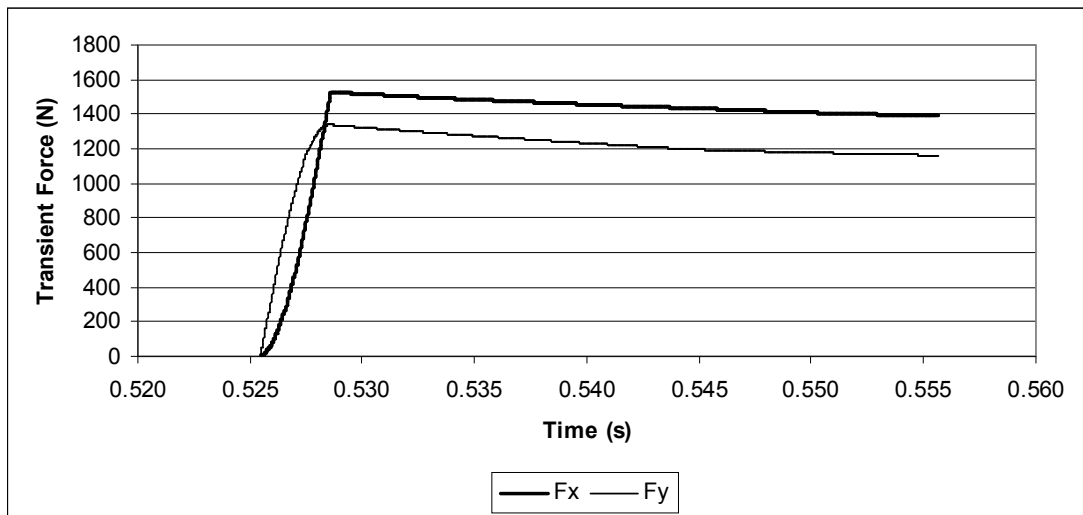


Figure 5.15 Transient force components for $L_{in} = 1.22$ m (4 ft) and $P_0 = 137.82$ kPa (20 psig).

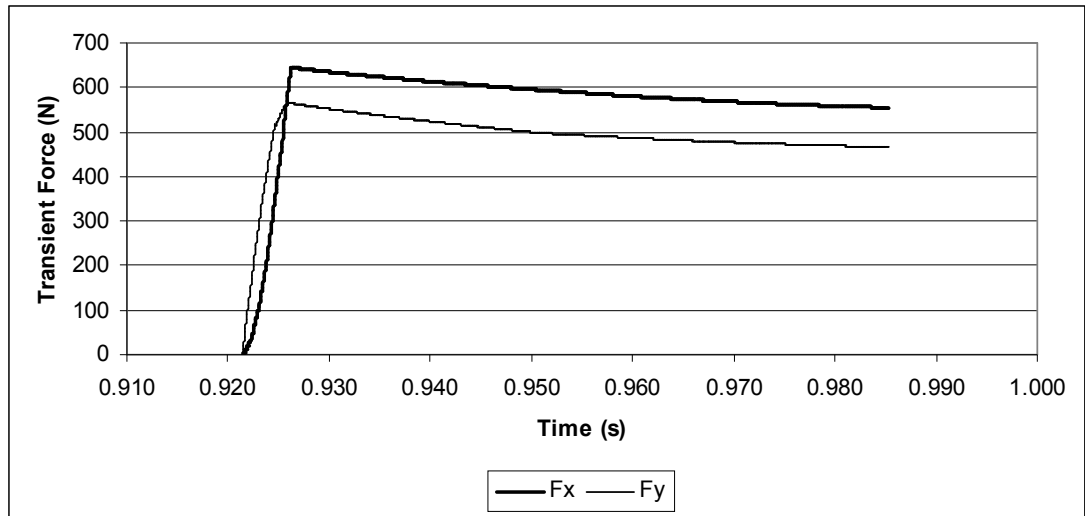


Figure 5.16 Transient force components for $L_{in} = 2.13$ m (7 ft) and $P_0 = 68.91$ kPa (10 psig).

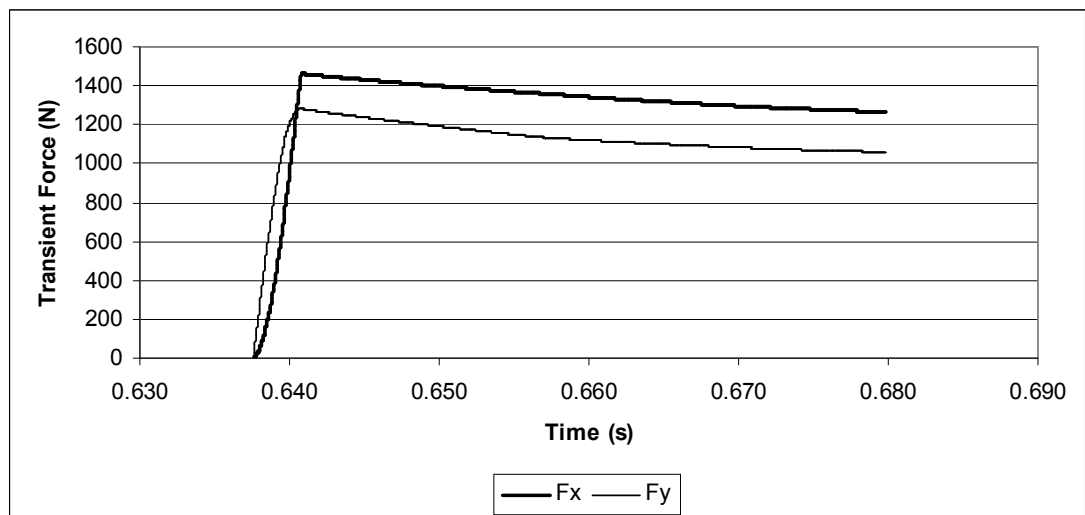


Figure 5.17 Transient force components for $L_{in} = 2.13$ m (7 ft) and $P_0 = 137.82$ kPa (20 psig).

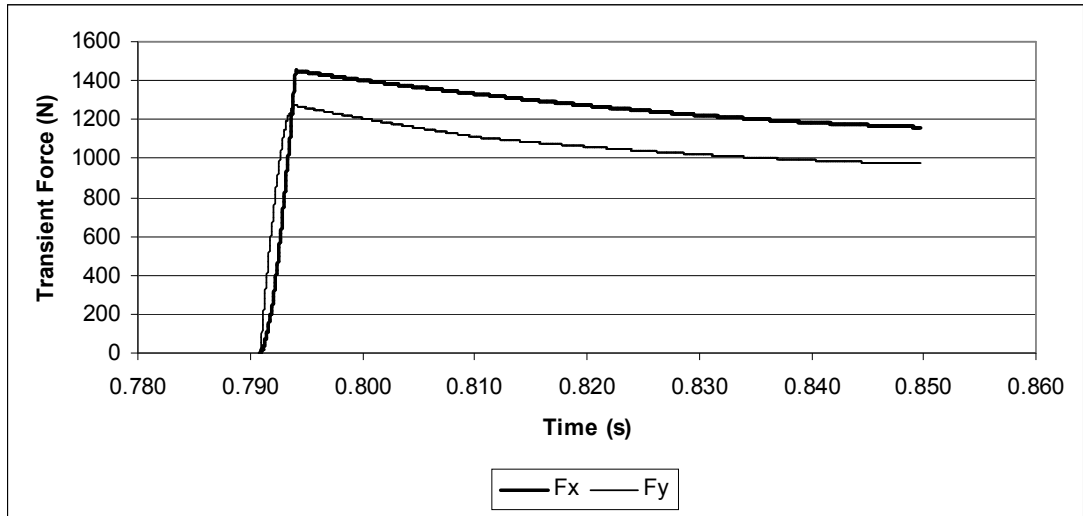


Figure 5.18 Transient force components for $L_{in} = 3.35$ m (11 ft) and $P_0 = 137.82$ kPa (20 psig).

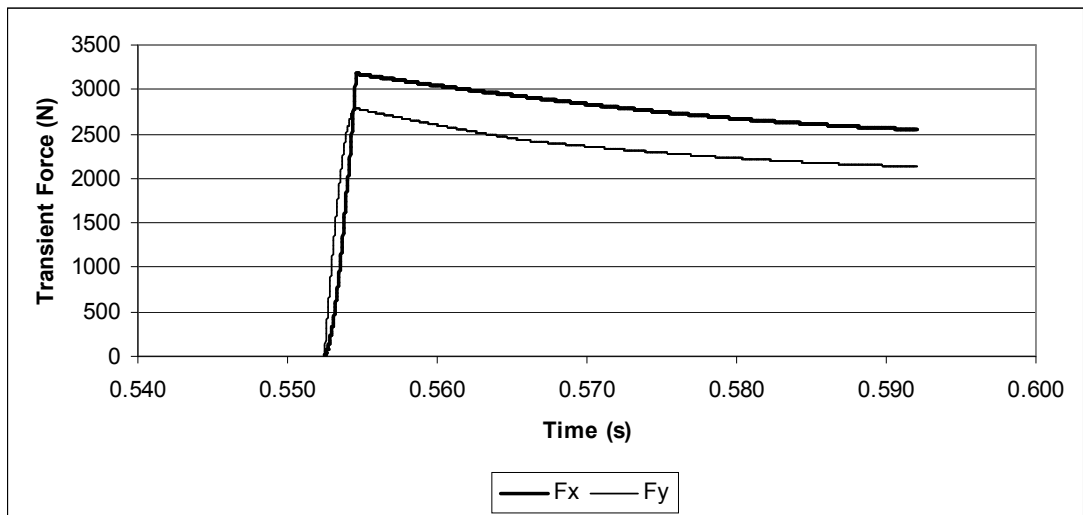


Figure 5.19 Transient force components for $L_{in} = 3.35$ m (11 ft) and $P_0 = 275.64$ kPa (40 psig).

Implementation of a 1-D solution technique by considering that the slug front is planar in the elbow and the vertical extension segment, and also accepting that the liquid slug is incompressible are the factors that prevents the consideration of the further deformation of the shape of the slug body during its motion. This fact can be thought to be a reason for the calculated transient forces to have a tendency towards an overestimation.

The plot for the normalized force values, F^* , vs. dispersion distances, D^* , is given in Figure 5.20. Here,

$$F^* = \frac{F_p}{F_m} \quad (5.1)$$

$$D^* = \frac{L_t}{L_{in}} \quad (5.2)$$

In (5.1) and (5.2);

F_p : experimentally obtained peak force at the elbow,

F_m : predicted force at the elbow with the numerical model,

L_t : travel distance of the slug.

Results for the normalized forces from 4 different studies are presented in Figure 5.20. These are Fenton's [26], Bozkuş's [2] and Baran's [27] results, and the results of the present study. Fenton's results are shown with vertical solid lines, and the vertical dash lines show Bozkuş's results. The small circles on the vertical dash lines symbolize the average values for each data group presented, and short horizontal dashes indicate extreme values. The extreme values for Baran's results are indicated with cross signs with also the mean values shown by solid squares. The mean values for the present study in which the F_m values were found from conservation of momentum principle applied on volume elements along the elbow are given by solid triangles and the extremes are shown by long, horizontal single dashes (results named as Kayhan-1). The mean values for the present study in which the F_m values were found from

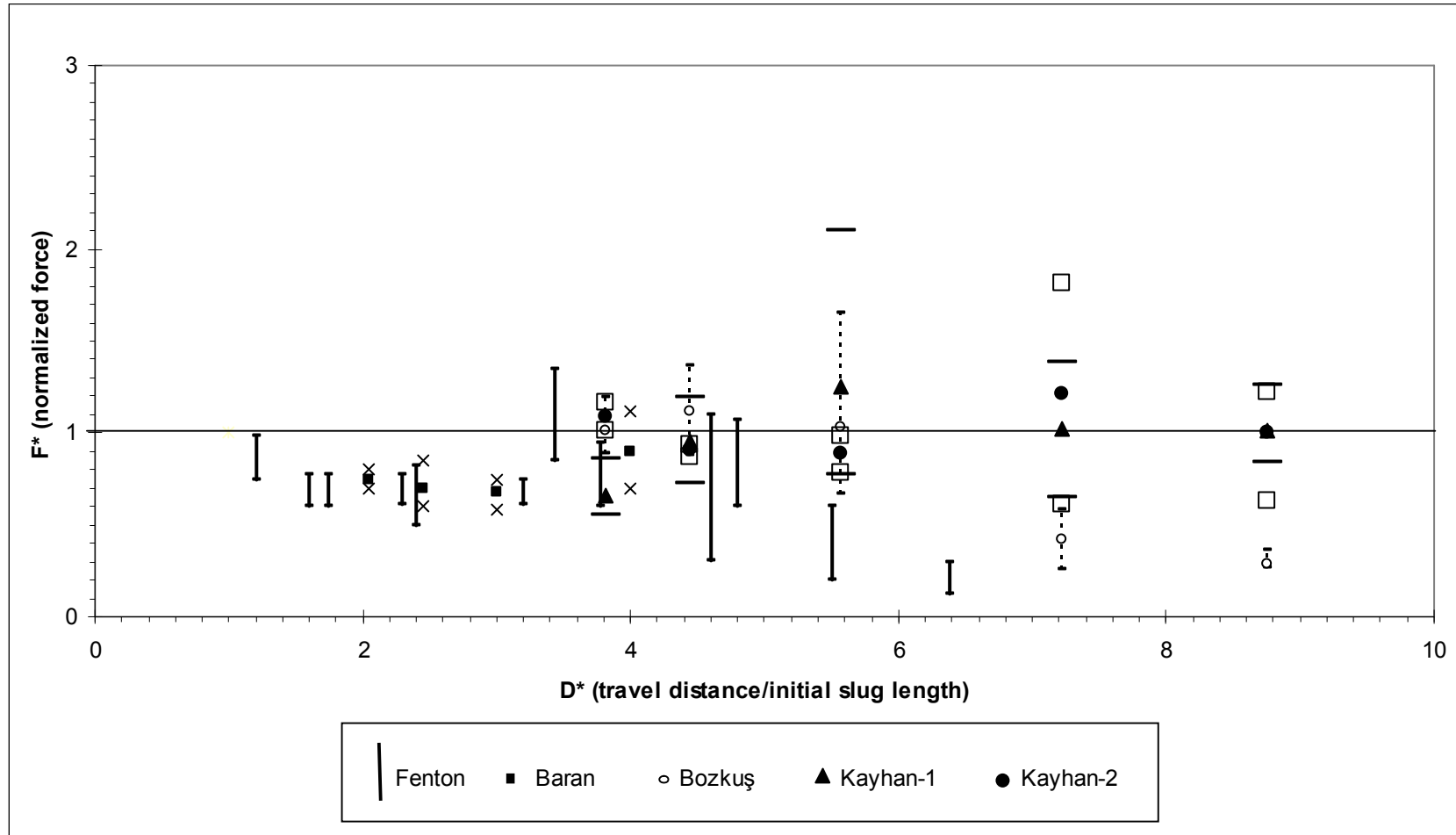


Figure 5.20 Values of F^* vs. D^* (Bozkuş's [2] 1st peaks were used for normalization).

$$F_m = p_{peak} A$$

are given by solid circles and the extremes are shown by hollow squares (results named as Kayhan-2).

The horizontal line at $F^* = 1$ in F^* vs. D^* plot in the current study indicates the values of F^* at which the experimentally obtained peak forces at the elbow are equal to the peak forces obtained from the numerical model.

The normalized forces, F^* , for the present study were obtained dividing Bozkuş's experimentally found peak forces, by the peak values of the numerically calculated horizontal transient forces of the present study.

In Figure 5.20, F^* vs. D^* values are presented in which the F^* values of Bozkuş, Kayhan-1 and Kayhan-2 were calculated; by using the values of the first pressure peaks in experimental pressure-time history plots of Bozkuş [2], for F_p . In this figure, the F^* values from the present study have the same data range as Bozkuş's data. From these two data set, it can be seen that the results from the present study of Kayhan-1 and Kayhan-2 are closer to unity with respect to Bozkuş's values for $D^* > 6$. For dispersion distance, D^* , values around 4; the normalized forces, F^* , from Kayhan-1 of the present study remain slightly below Fenton's and Baran's data. This can be explained by the fact that in Fenton's and Baran's numerical models, the mass loss from the liquid slug during the slug motion was neglected. It can also be said that the results from Kayhan-1 can be considered to be more correct than Kayhan-2 because in that the case of Kayhan-1, analytical transient force value is calculated by integration of forces over the whole volume of the elbow, rather than using a fixed point for peak pressure as in the case of Kayhan-2.

In Figure 5.21, F^* vs. D^* values were plotted in which the F^* values of Bozkuş, Kayhan-1 and Kayhan-2 were calculated; by using the values of the second pressure peaks in pressure-time history plots of Bozkuş [2], for F_p . The symbols for each data group here are the same as in the previous plot given by Figure 5.20. From 5.21, it can be deduced that F^* values of Bozkuş, Kayhan-1 and Kayhan-2 are in close agreement for $D^* > 4$. According to the plot in Figure 5.21; for $D^* < 4$,

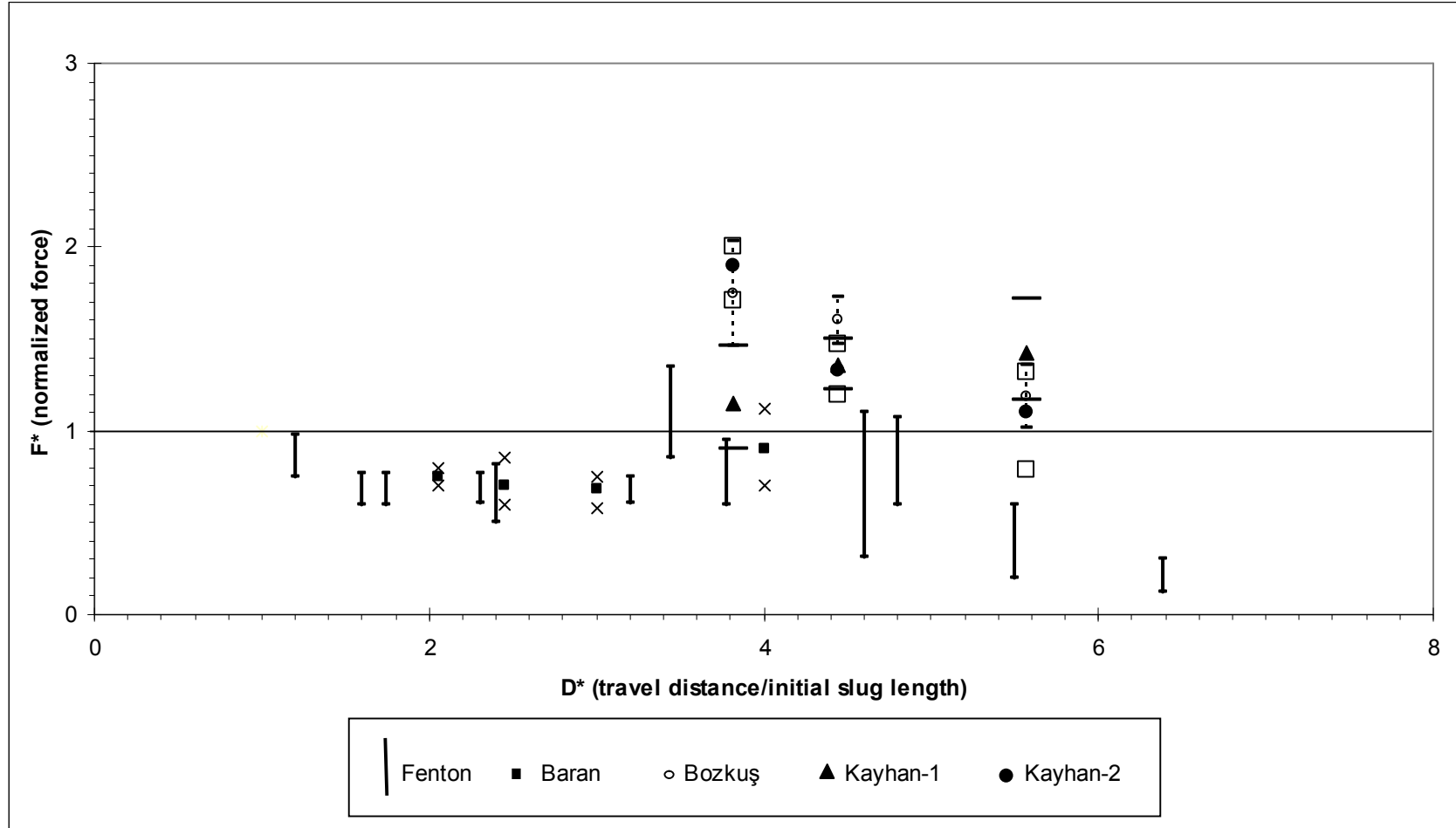


Figure 5.21 Values of F^* vs. D^* (Bozkuş's [2] 2nd peaks were used for normalization).

results from Kayhan-1 are smaller than Bozkuş's values as was also the case in Figure 5.20. Also, from Figure 5.21, it can be seen that the values from Bozkuş, Kayhan-1, and Kayhan-2 are higher than Fenton's [26] and Baran's [27] data which can be attributed to the fact that in Figure 5.21, F^* values were calculated with respect to the second pressure peaks in Bozkuş's experimental pressure-time history plots having higher values than the first peaks.

5.5 Impact Pressure Distribution at the Elbow

During the simulation of the liquid slug motion, the time dependent impact pressure distribution at the convex side of the elbow at projected locations C' (see Figure 4.9) from the axial s -curve of the elbow were calculated with the related expression given in Section 4.3.2.3 for every time step of the slug motion in the elbow and the vertical extension segment.

Some sample dynamic impact pressure distributions along the elbow are given from Figures 5.22 to 5.24 at different time, t , values; and for different initial slug lengths and initial tank pressures. The pressure distributions are given with respect to the node numbers, ip , along the s -curve. The total number of nodes along the elbow $NELBW$ here were determined with respect to the initial slug lengths. In these plots, the dynamic pressure values start with a decreasing pattern due to existence of friction and minor losses in the elbow. Then, the impact pressures start to increase as a result of the effect of the skewed shape of the axial velocity profile. This increase in pressure continues up to a point where the maximum shift of the velocity profile occurs. This point actually corresponds to the location for the occurrence of the maximum calibration angle, θ_{cmax} , of the calibration function, θ_c . After the point for the maximum value of the impact pressure distribution curve, the impact pressures start to decrease where the axial velocity profile is at a stage of attaining its symmetrical shape towards to downstream reaches of the elbow.

In impact pressure distribution plots given by Figures 5.22 to 5.24, it can be seen that there is a discontinuity prior to the point of maximum pressure in each plot. The discontinuous regions in the plots correspond to the unsmooth maximum point of the calibration function used in calibrating the axial velocity profile. At these points, the direction of change in shape of the axial velocity profile shows an abrupt

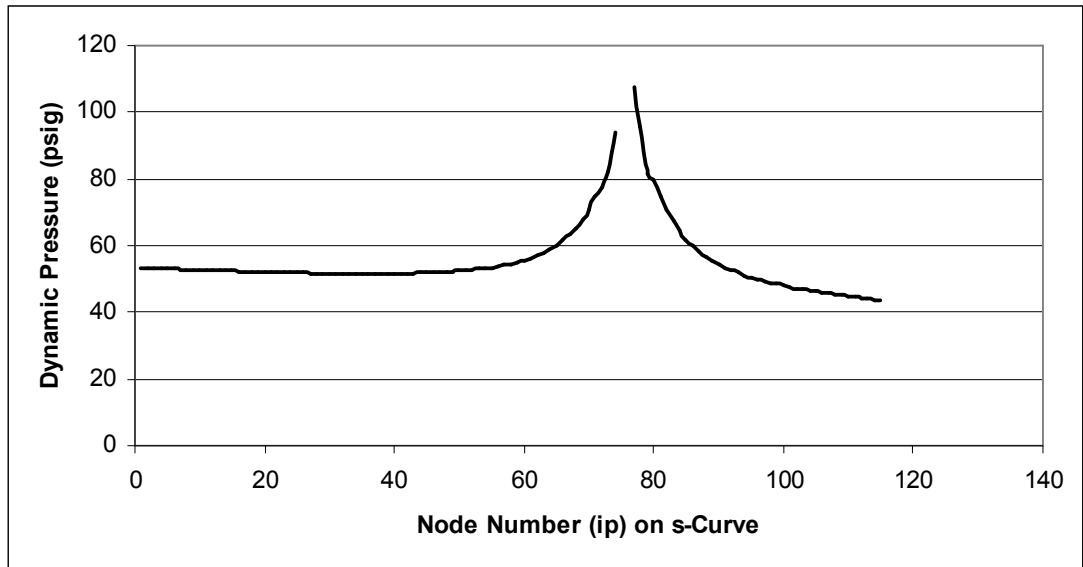


Figure 5.22 Dynamic pressure distribution for $L_{in} = 1.22$ m (4 ft),
 $P_0 = 137.82$ kPa (20 psi), $t = 0.539$ s and $NELBW = 115$.

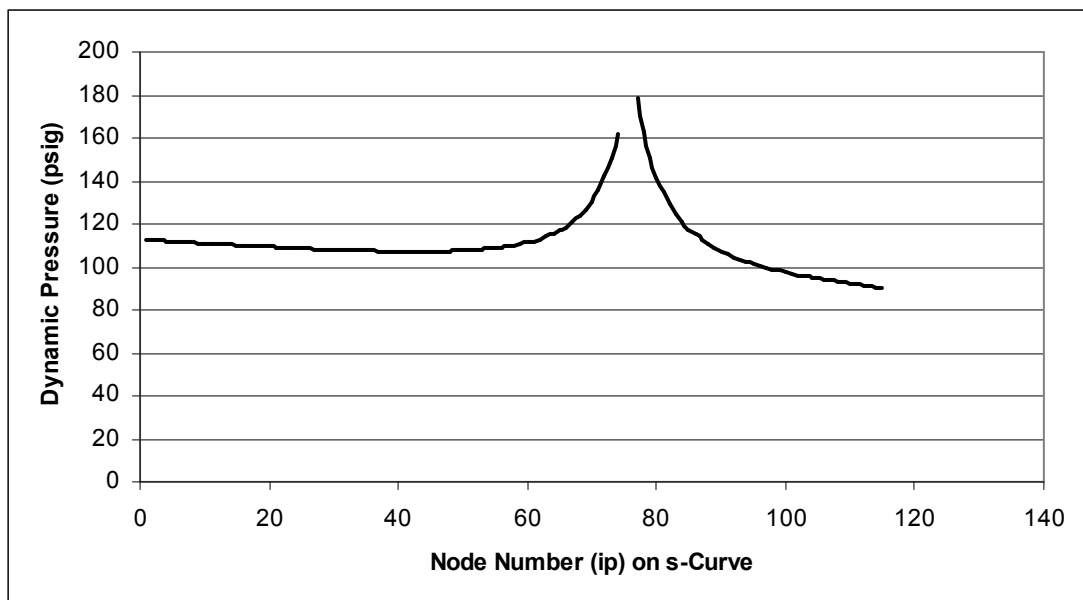


Figure 5.23 Dynamic pressure distribution for $L_{in} = 1.22$ m (4 ft),
 $P_0 = 275.64$ kPa (40 psi), $t = 0.375$ s and $NELBW = 115$.

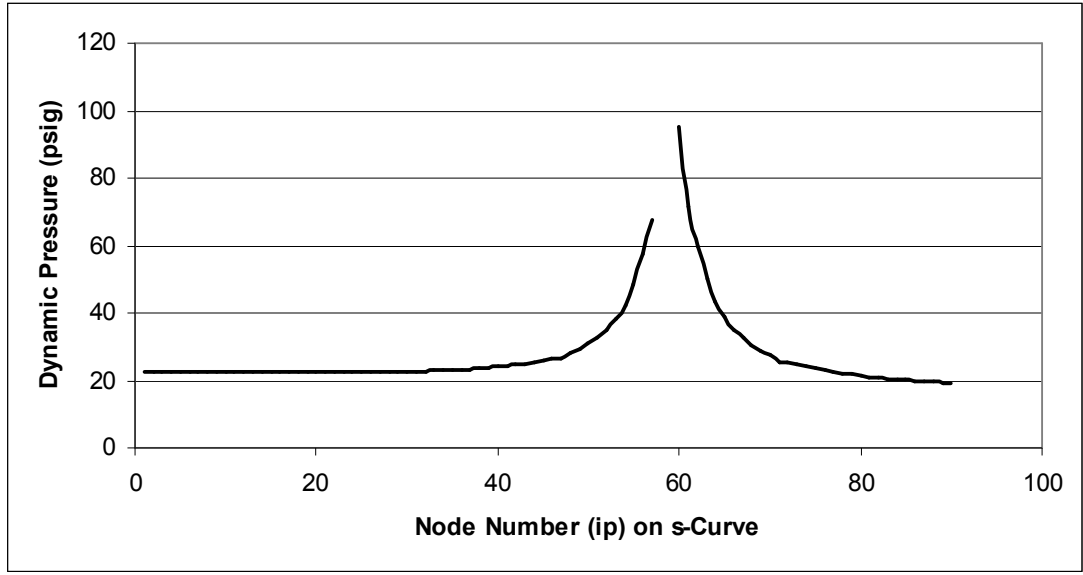


Figure 5.24 Dynamic pressure distribution for $L_{in} = 2.13$ m (7 ft),
 $P_0 = 68.91$ kPa (10 psi), $t = 0.942$ s and $NELBW = 90$.

variation and this abrupt change results in some fictitious calculated impact pressure values while evaluating the second derivatives in the differential equations. Therefore, the impact pressure values in those regions consisting of two nodal points were left and the resulting impact pressure distribution plots were formed as having discontinuous shapes.

Since it can be expected that the maximum impact pressure value occurs at the point along the s -curve, where $\theta_c = \theta_{cmax}$, the maximum value of the impact pressure was calculated by making an extrapolation from the downstream side of the discontinuous region using backward differences. θ_{cmax} value corresponds to the location of the nodal point just before the right end of the discontinuous region and it was possible to calculate the maximum impact pressure at this nodal point by extrapolating the impact pressures in the backward direction.

5.6 A Discussion on the Existence of Waterhammer Event

The validity of the assumption that waterhammer effects were neglected during the calculations for the slug in motion elbow and the vertical extension segment of the pipeline system was also checked in the present study. For this purpose, Bozkuş's [2] experimentally obtained peak pressures at the elbow were compared with Joukowsky pressure rise (Streeter and Wylie [33]) values for the fictitious case of a sudden valve closure at the elbow location. The Joukowsky pressure rise formula for the case of a shock wave travelling towards upstream is as follows:

$$\Delta P_{WH} = -\rho a \Delta U \quad (5.3)$$

In Equation (5.3);

ΔP_{WH} : pressure rise due to sudden valve closure,

a : wave speed,

ΔU : change in slug velocity.

By taking the final slug velocity as zero, Equation (5.3) can be written as

$$\Delta P_{WH} = -\rho a (0 - U_{pas}) \quad (5.4)$$

Here,

U_{pas} : slug passage velocity through the elbow.

The expression given by (5.4) can now be expressed as

$$\Delta P_{WH} = \rho a U_{pas} \quad (5.5)$$

The slug passage velocity through the elbow, U_{pas} , can be calculated with the equation

$$U_{pas} = \frac{L_{fin}}{\Delta t_{pas}} \quad (5.6)$$

In Equation (5.6),

Δt_{pas} : slug passage time through the elbow.

The L_{fin} values were taken from program KAYHAN as the slug length at the instant that the slug front face reaches the elbow. And the Δt_{pas} values were found from Bozkuş's experimentally obtained pressure-time history plots in Figures 5.2 to 5.13, by measuring the time period from the time of the occurrence of the first pressure peak up to the time that the pressure rise at the elbow falls to the initial tank pressure level.

The wave speed, a , in the PVC pipeline used in the current study was taken as 438 m/s as calculated by Bozkuş [2] with a spectral analysis. Also, the density of water, ρ , was taken as 500 kg/m³ as an approximation, by considering the reduction in the value of the liquid density due to air entrainment effect.

Then, the Joukowsky pressure rise values were calculated from Equation (5.5) and (5.6), and the results are presented in the last column of Table 5.1.

By comparing Bozkuş's [2] experimentally obtained peak pressures with Joukowsky pressure rise values in Table 5.1, it can be said the experimental peak pressures at the elbow are much lower than the values that would occur in the hypothetical case of sudden valve closure. Since the experimentally obtained peak pressures are much lower, it can be concluded that a waterhammer event does not take place during the impact of the liquid slug at the elbow probably due to rather smoothly curved shape of the elbow.

CHAPTER 6

CONCLUSIONS

6.1 Summary

In the present study, the transient force applied by the impact of an individual transient liquid slug on an elbow and on a vertical extension segment after the elbow, at the end of an initially voided horizontal line was solved numerically. The liquid slug was propelled in the pipeline system under the driving effect of pressurized air in a tank located at the upstream end of the pipeline.

The numerical calculations in the present study were made in two parts. In the first part of the calculations, the slug motion in the horizontal part of the pipeline was analyzed by using a previously written computer code BOZKUŞ-2 developed by Bozkuş [2]. As an improvement of this part of the calculations, the Swamee-Jain formula was used for finding the friction factor, and also a functional hold up coefficient concept was developed in the present study. Then, in the second stage of calculations, a 1-D numerical analysis of slug motion in the elbow and the vertical extension segment was made with the aid of an assumed and calibrated axial velocity profile function with 3-D shape, and along a curved line mesh. The shape of assumed axial velocity profile function was allowed to sway towards the convex side of the elbow along the curved line mesh with the aid of a calibration tool.

In the analysis of the elbow and the vertical extension segment, the impact pressure distribution at the convex side of the elbow was found by solving Reynolds Equations in 1-D. Also the horizontal and the vertical components of the transient forces acting on the elbow and the following vertical extension segment were found with the application of conservation of momentum principle over the selected volume elements along the curved line mesh and summing up the results for the

forces acting on each volume element.

The calculation of impact pressure distribution at the elbow and the transient forces acting on the elbow and the vertical extension segment were made for each time step of the slug motion in the elbow and the vertical extension segment.

During the impact pressure and transient force calculations, a correlation function was utilized for the determination of one of the unknown parameters of the calibration function used for the assumed velocity profile function with 3-D shape. To obtain the correlation function, the peak pressures obtained from the present study were correlated with Bozkuş's [2] experimentally obtained peak pressures. The correlation function obtained here is in the form of a function in terms of normalized initial slug length; and this correlation function is valid for all of data ranges of initial slug lengths and the initial tank pressures.

In the thesis, the obtained impact pressures and the transient forces at the elbow and the vertical extension segment were also compared with the results of the previous studies.

6.2 Concluding Remarks

Some comparisons of the peak pressures, pressure-time history plots and the transient forces from program KAYHAN of the present study were made with the results of some previous studies.

First of all, it can be said that the sinusoidal variation of the peak pressures at the elbow obtained from program KAYHAN of the present study was seen to provide a better approximation to Bozkuş's [2] experimentally obtained values than the values obtained from program BOZKUŞ-2 [2]. The advantage here brought by program KAYHAN can be attributed mainly to two different correlation functions used for obtaining the functional hold up coefficient, α , and for calculating the parameter θ_{cmax} of the calibration function for the assumed velocity profile in the present study.

Some differences were seen in the time values for the starting point of peak pressures in the pressure-time history plots from program KAYHAN and from Bozkuş's [2] experimental results. Since the time for the first peak can be considered as a very close value to the slug arrival time at the elbow, the differences in the time

values for the peak pressures were indicated to be related mainly with the horizontal pipe calculations performed by the improved version of the program BOZKUŞ-2 [2].

The waterhammer effects and air entrainment were neglected during the elbow and the vertical extension segment calculations of program KAYHAN in the present study, and this case was thought to be the reason for not seeing the wavy pattern in pressure-time history plots from program KAYHAN differing from Bozkuş's [2] experimental results.

The tail region of pressure-time history plots for 3.35 m (11 ft) slugs from program KAYHAN in the present study were seen to be in well agreement with Bozkuş's [2] experimental data. However, the tail regions from program KAYHAN in the case of 1.22 m, 1.52 m, 2.13 m and 2.74 m (4, 5, 7 and 9 ft) slugs remained above Bozkuş's experimental values. This case can be explained by neglecting the air entrainment effect in program KAYHAN of the present study.

The calculated horizontal component of the transient forces from program KAYHAN has come out to be greater than the vertical component of the transient forces, and this case can be stated to be due to the air pressure driving the slug acting in the horizontal direction from upstream.

The obtained normalized force, F^* , values from the present study were compared with Fenton's [22], Baran's [27] and Bozkuş's [2] data. From these comparisons, for D^* values around 4, it was seen that F^* values from Fenton's and Baran's study were slightly above the values from the present study. This case was attributed to the fact that in Fenton's and Baran's numerical model, the mass loss from the liquid slug during the slug motion was neglected. It was also seen that F^* values from the present study were closer to unity as compared to Bozkuş's values for $D^* > 6$.

It can be said that the well approximation of the peak pressures from the present study to the experimentally obtained pressure peaks from Bozkuş's data, program KAYHAN of the present study can be used in practice to predict the peak pressures at the elbow. In addition, due to F^* values obtained in the present study being close to unity, it can be suggested that a correct prediction of the transient forces at the elbow can be made with the formulation developed in the current study, at least within the domain of initial slug lengths and initial tank pressures used.

REFERENCES

- [1] Barhaghi, D. G. and Davidson, L. "Large Eddy Simulation of a Natural Convection Boundary Layer on a Vertical Cylinder." Department of Thermo and Fluid Dynamics. Chalmers University of Technology. 2003.
- [2] Bozkuş, Z. 1991. "The Hydrodynamics of an Individual Transient Liquid Slug in a Voided Line." Dissertation, Michigan State University.
- [3] Munson, B. R. and et.al. 1990. "Fundamentals of Fluid Mechanics". John Wiley & Sons, Inc. Singapore.
- [4] Zwillinger, D. 1957. "Handbook of Integration." Jones and Bartlett Publishers. Boston.
- [5] Ger, A. M. and Holley, E. R. "Turbulent Jets in Crossing Pipe Flow." University of Illinois. August, 1974.
- [6] Quarteroni, A., Vali, A. 1997. "Numerical Approximation of Partial Differential Equations." Springer Verlag. Berlin.
- [7] Kreyszig, E. 1993. "Advanced Engineering Mathematics." John Willey & Sons, Inc. Singapore.
- [8] Bird, R. B., Stewart, W. E. and Lightfoot, E. N. 1960. "Transport Phenomena." John Willey & Sons, Inc. New York.
- [9] Young, J. R. 1850. "The Elements of Analytical Geometry." E. H. Buttler & Co. Philadelphia.
- [10] Schlichting, H. 1960. "Boundary Layer Theory". Mc. Graw-Hill Book Company. New York.

- [11] Walski, T. M. 2003. "Advanced Water Distribution Modeling and Management." Haestad Methods, Inc. Waterbury.
- [12] Swamee, P. K., and Jain, A. K. "Explicit Equations for Pipe Flow Problems." *Journal of Hydraulic Engineering*, ASCE, 102(5), 657. 1976.
- [13] Prandtl, L. "The Mechanics of Viscous Fluids." *Aerodynamic Theory*, III. Vol. 142. 1935.
- [14] Prandtl, L. "Neuere Ergebnisse der Turbulenzforschung". *Z. VDI* 77. Vol. 105. 1933.
- [15] Davidson, P. A. 2005. "Turbulence." Oxford University Press, Inc. New York.
- [16] Mathews, J. H. 1987. "Numerical Methods." Prentice-Hall International, Inc. London.
- [17] Kim, J. H. "Water Hammer Prevention, Mitigation and Accommodations: A Perspective". *Transactions of the American Nuclear Society*. 55, 733-734. 1987.
- [18] Merilo, M.; Van Duyne, D. A.; Saffat, H. H. and Arastu, A. H. "Reducing the Frequency of Water Hammer in Nuclear Power Plants". In *Transient Thermal Hydraulics and Resulting Loads on Vessel and Piping Systems*. (eds. F. J. Moody, Y. W. Shin and J. Colton), PVP-Vol.190, pp 1-7. New York: ASME. 1990.
- [19] Wheeler, A. J. and Siegel, E. A. "Measurement of Forces in a Safety Valve Discharge Line". ASME Paper 82-WA/NE-8, New York: ASME.1982.
- [20] Bozkuş, Z. and Wiggert, D. C. "Liquid Slug Motion in a Voided Line". *Journal of Fluids and Structures*. Vol.11, pp.947-963.1997.
- [21] Smith, P. R. and Van Laan, T. J. 1987. "Piping and Pipe Support Systems." Mc.Graw-Hill.

- [22] Fenton, R. M. "The Forces at a Pipe Bend due to Clearing of Water Trapped Upstream". Master Thesis, Massachusetts Institute of Technology, October 1989.
- [23] Woo, H. and Papadakis, C. N. "Forces in Initially Empty Pipelines Subject to Rapid Filling". Boston, December 1987. Symposium on Fluid Transients in Fluid-Structure Interaction, ASME Winter Annual Meeting.
- [24] Neumann, A. and Griffith, P. "Forces on a Pipe Bend Resulting from Clearing a Pool of Liquid Upstream". Thermal-Hydraulics, and Structural Mechanics. ASME, 1992.
- [25] Hull, E. T., Enright, H. W., and Jackson R. K. "User's Guide for DVERK- A Subroutine for Solving Non-Stiff ODE's". TR No. 100, October 1976.
- [26] Fenton, R. M. and Griffith, P. "The Force at a Pipe Bend due to the Clearing of Water Trapped Upstream". In Transient Thermal Hydraulics and Resulting Loads on Vessel and Piping Systems, (eds. F. J. Moody, Y. W. Shin and J. Colton) PVP-Vol. 190, pp. 59-67. NewYork: ASME.1990.
- [27] Baran, Ö. U. "Experimental and Numerical Analysis of Transient Liquid Slug Motion in a Voided Line". M. Sc. Thesis. Department of Civil Engineering. Middle East Technical University. Ankara. Turkey. 1999.
- [28] Bozkuş, Z.; Baran, Ö. U.; Ger, M. "Experimental and Numerical Analysis of Transient Liquid Slug Motion in a Voided Line". Journal of Pressure Vessel Technology. Vol. 126. pp. 241-249. ASME. May, 2004.
- [30] Daugherty, R. L., Franzini, J. B., Finnemore, E. J. 1985. "Fluid Mechanics with Engineering Applications." McGraw-Hill.
- [31] Moody, F. J. 1989. "Introduction to Unsteady Thermofluid Mechanics." John Wiley & Sons. New York.
- [32] Chaudhry, M. H. 1979. "Applied Hydraulic Transients." Van Nostrand Reinhold Company. New York.

- [33] Streeter, V. L. and Wylie, E.B. 1982. "Fluid Transients." FEB. Press.
- [34] Mathieu, J. and Scott, J. 2000. "An Introduction to Turbulent Flow". Cambridge University Press. New York.
- [35] Jackson, R. K., Enright, H. W. and Hull, E. T. "Theoretical Criterion for Comparing Runge-Kutta Formulas." TR No. 101, January 1977.
- [36] Chen, C. J. and Jaw, S. Y. 1997. "Fundamentals of Turbulence Modeling." Taylor and Francis. New York.
- [37] Papadakis, C. N. and Hollingshead, D. "Transients in Empty Pipes Subject to Rapid Filling." Proceedings of the 1985 ASCE Hydraulics Division Specialty Conference on Hydraulics and Hydrology in the Small Computer Age. Lake Buena Vista, FL. August 12-17, 1985. pp. 1376-1381.
- [38] Laribi, B.; Wauters, P. and Aichouni, M. Experimental Study of Decay of Swirling Turbulent Pipe Flow and its Effect on Orifice Meter Performance. Proceedings of the FEDSM2001. 2001 ASME Fluids Engineering Conference May 29-June 1, 2001, New Orleans, USA.
- [39] Tannehill, J. C.; Anderson, D. A. and Pletcher, R. H. 1997 "Computational Fluid Mechanics and Heat Transfer." Taylor and Francis. Philadelphia.

APPENDICES

APPENDIX A

MATHEMATICAL DERIVATION OF THE EQUATIONS

A.1 Functional Hold up Coefficient Determination

To obtain a functional hold up coefficient; first of all, a formulation was made to get an expression for the average slug length that occurs during the travel of the slug. Then, the average slug length in this expression was replaced with the instantaneous slug length as an approximation. After that, by using this new expression and the results of the computer program BOZKUŞ-2 together with the experimental values for the peak pressures of Bozkuş [2], a set of hold up coefficient vs. the approximated instantaneous slug length values were tabulated. With these set of values, a correlation function was obtained at the end, which related the hold coefficient to the normalized travel distance of the slug with respect to the instantaneous slug length. This correlation function was used as the new functional hold up coefficient which allows the change of the value of the hold up coefficient with the slug length during the simulation of the slug motion along the horizontal part of the pipeline.

A.1.1 Formulation for the Average Slug Length

In this section, an expression for the average slug length in terms of the initial length of the slug and the corresponding hold up value is obtained.

For this purpose, the following differential expression derived by Bozkuş [2] was taken as the starting point for the formulation:

$$\frac{dL_s}{dt} = -\left(\frac{1}{\alpha} - 1\right)U_F \quad (\text{A.1})$$

In Equation (A.1),

U_F : slug front velocity,

α : hold up coefficient,

L_s : instantaneous slug length.

Equation (A.1) can also be written as

$$dL_s = -\left(\frac{1}{\alpha} - 1\right) U_F dt \quad (\text{A.2})$$

Integrating both sides of the differential expression in (A.2) from the time for beginning of slug motion to the instant of impact at the elbow, the expression becomes

$$\int_{L_{in}}^{L_{fin}} dL_s = \int_{t_{in}}^{t_{fin}} -\left(\frac{1}{\alpha} - 1\right) U_F dt \quad (\text{A.3})$$

In Equation (A.3), limits of the integration are as

L_{in} : initial slug length,

L_{fin} : final slug length of the horizontal pipe calculations,

t_{in} : initial time of slug motion,

t_{fin} : final time of slug motion.

After the integration, (A.3) becomes

$$L_{fin} - L_{in} = -\left(\frac{1}{\alpha} - 1\right) \int_{t_{in}}^{t_{fin}} U_F dt \quad (\text{A.4})$$

which can also be written as

$$L_{fin} - L_{in} = -\left(\frac{1}{\alpha} - 1\right) L_p \quad (\text{A.5})$$

where

L_p : length of the horizontal part of the pipeline.

Then, taking ΔL_s as the whole change in slug length during the travel of the slug from the pressurizer tank up to the elbow, (A.5) can be written as

$$\Delta L_s = -\left(\frac{1}{\alpha} - 1\right)L_p \quad (\text{A.6})$$

And the average length of the slug L_{ave} that occurs during the motion of the slug along the horizontal part of the pipeline can be expressed with a linear interpolation,

$$L_{ave} = L_{in} + \frac{\Delta L_s}{2} \quad (\text{A.7})$$

which can also be written by using (A.6) as

$$L_{ave} = L_{in} - \left(\frac{1}{\alpha} - 1\right)\frac{L_p}{2} \quad (\text{A.8})$$

With this expression, an average slug length can be calculated for a given initial slug length, L_{in} , and a given fixed value of hold up coefficient, α .

A.1.2 Correlation between the Hold up and the Instantaneous Slug Length

A correlation function between the hold up coefficient, α , and the normalized travel distance of the slug with respect to the instantaneous slug length was obtained by using the results of the computer program BOZKUŞ-2 coded by Bozkuş [2], and his experimental data as given in Figure A.1. The second column of Table A.1 was filled in according to the crossing point of the curves for the

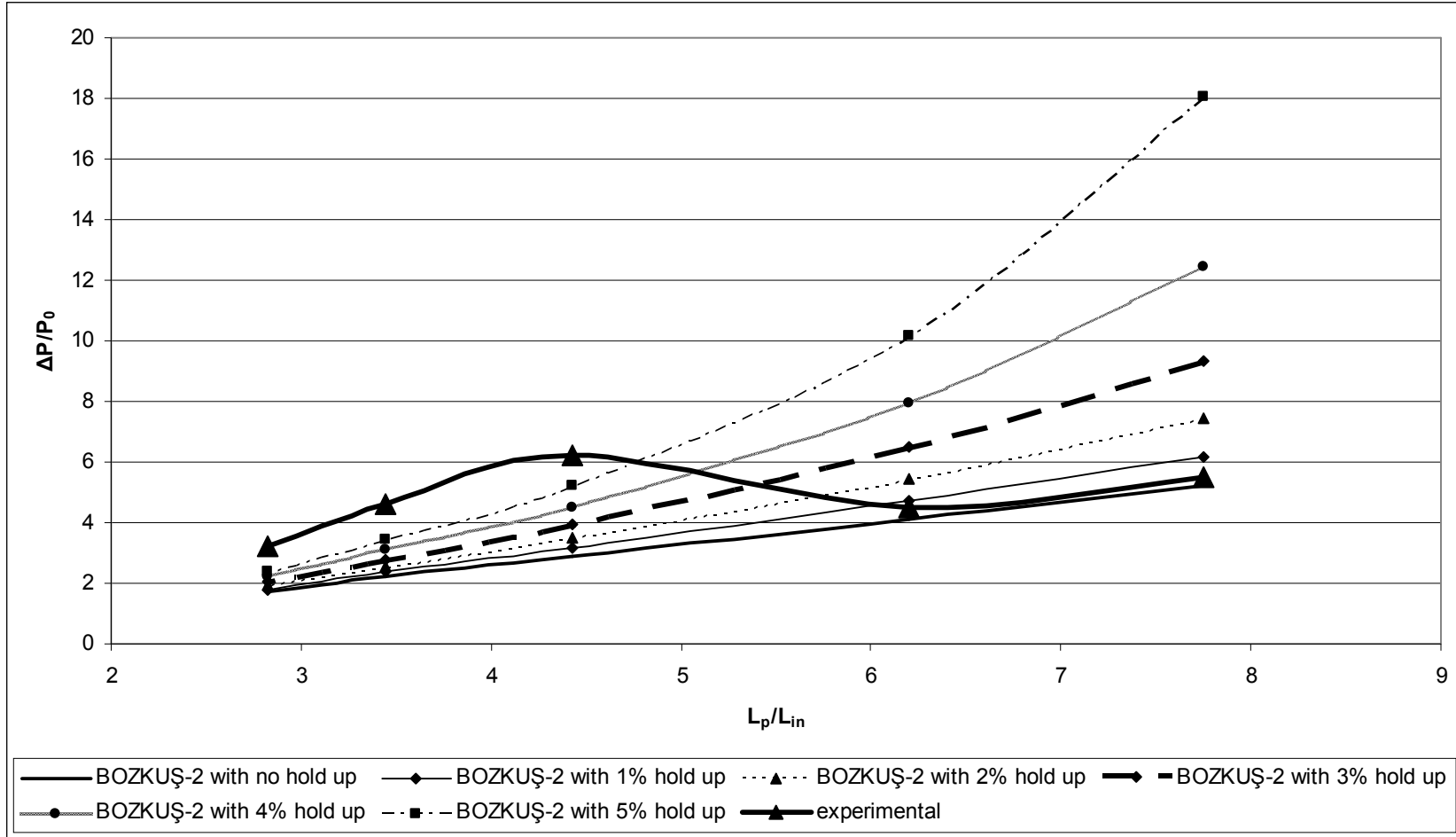


Figure A.1 Normalized peak pressures vs. L_p / L_{in} from program BOZKUŞ-2 and from the experimental data (Bozkuş [2]).

Table A.1 Calculation steps for L_p / L_{ave} ($L_p = 9.4488 \text{ m.}$).

Hold up Coefficient (α)	L_p/L_{in}	L_{in} (m)	L_{ave} (m) (Eq. A.8)	L_p/L_{ave}
1.00	6.8	1.3895	1.3895	6.8000
0.99	6.0	1.5748	1.5271	6.1875
0.98	5.7	1.6577	1.5613	6.0520
0.97	5.3	1.7828	1.6367	5.7732
0.96	5.1	1.8527	1.6559	5.7063
0.95	4.8	1.9685	1.7198	5.4940

normalized peak pressures from BOZKUŞ-2 and for the experimental results as shown in this figure. These crossing points actually give the optimum values of normalized travel distances of the slug with respect to the initial slug length, L_p / L_{in} , for the corresponding hold up coefficient values that Bozkuş [2] used in his study. By taking the length of the horizontal part of the pipeline as $L_p = 9.4488 \text{ m.}$ (or $L_p = 31 \text{ ft.}$), and using the equation given by (A.8), the remaining 3 columns of Table A.1 were also completed.

The travel distance values normalized with respect to the average slug length, L_p / L_{ave} , in Table A.1 were taken as an equivalent value to the travel distance values normalized with respect to the instantaneous slug length, L_p / L_s as an approximation. Then, the hold up coefficient, α , vs. the L_p / L_s values were plotted as given in Figure A.2.

By using the correlation function shown in Figure A.2, the following continuous function was obtained for the hold up, as given by Equation (3.54) in the main text.

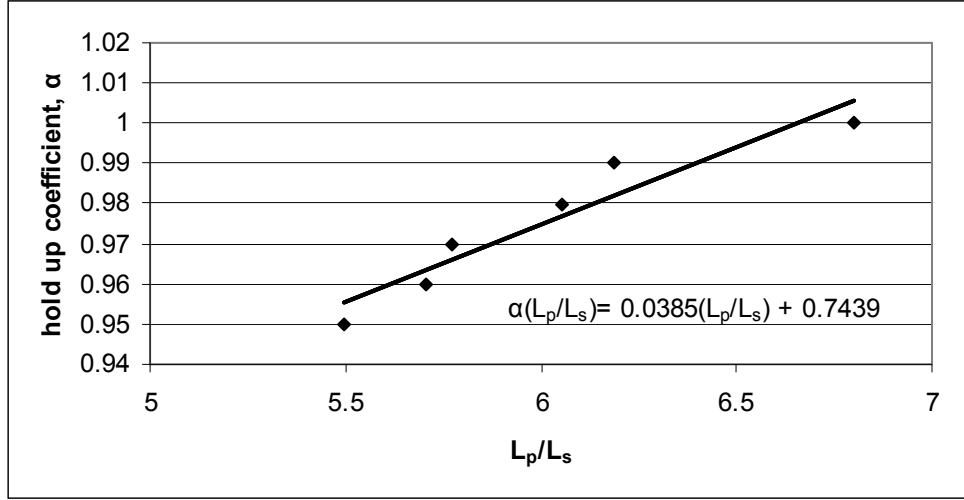


Figure A.2 Variation of hold up coefficient, α , as a function of L_p / L_s .

$$\alpha(L_p / L_s) = 0.0385(L_p / L_s) + 0.7439 \quad \text{if} \quad 5.4940 \leq L_p / L_s \leq 6.6519$$

and

$$\alpha(L_p / L_s) = 1. \quad \text{if} \quad 6.6519 < L_p / L_s$$

The boundaries of the function in (3.54) were arranged such that the maximum value of the function $\alpha(L_p / L_s)$ is 1. as a limiting condition brought by the definition of hold up.

A.2 Derivations for the Assumed Velocity Profile Function

In this section, the mathematical procedure for the derivation of assumed axial velocity profile function with 3-D shape in the elbow and the vertical extension segment of the pipeline are given. The procedures for the determination of the unknown parameters of the assumed velocity profile function are also presented.

A.2.1 Derivation of Bottom Cone Equation

To be able to obtain an equation for the assumed velocity profile function, two coordinate systems were combined as shown in Figure A.3, the upper coordinate

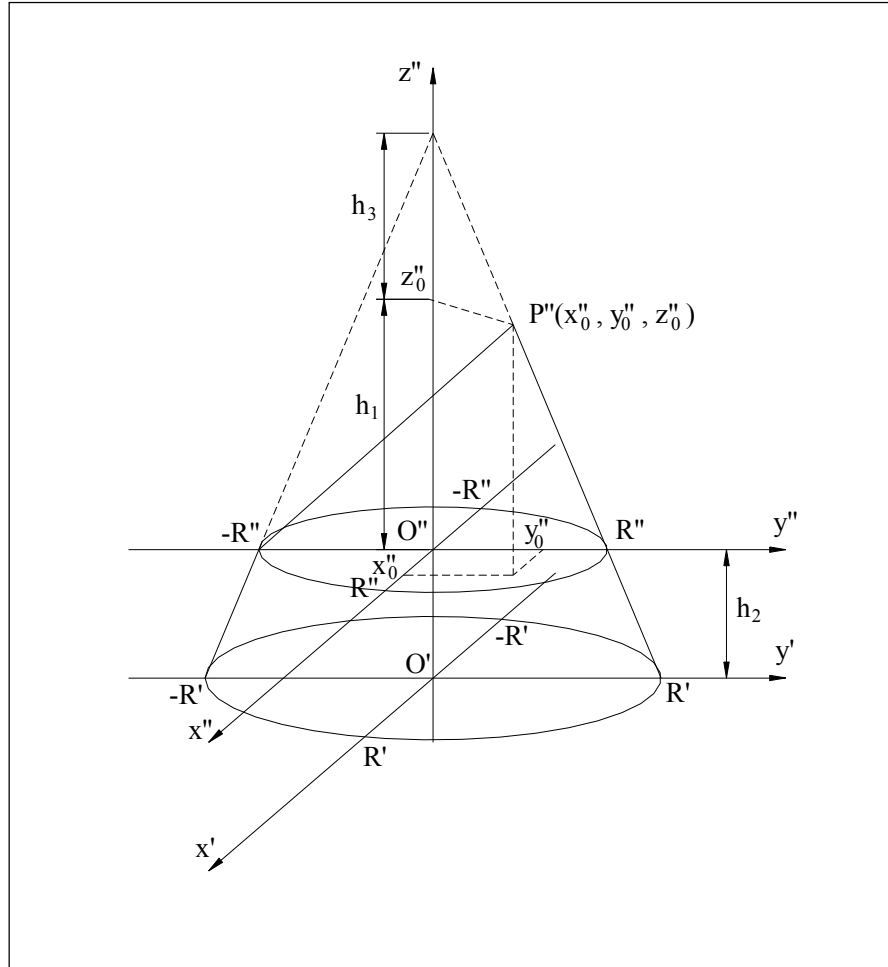


Figure A.3 Two coordinate systems combined together for the general oblique and symmetric cone equations.

system being for the oblique cone and the bottom one for the symmetric truncated cone.

The equation of the bottom symmetrical truncated cone can be obtained by using the general cone equation given in (4.1) with the parameters for this equation shown in Figure 4.2.

For the bottom cone equation, the parameters must be selected as follows according to Figures 4.2, A.3 and 4.4:

$x'_0 = 0$, $y'_0 = 0$ because for the symmetric cone, the projection of the apex point on the base circle falls on the origin.

z'_0 can be determined as

$$z'_0 = h_1 + h_2 + h_3 \quad (\text{A.9})$$

or

$$z'_0 = R \tan \theta_f \quad (\text{A.10})$$

and

$$R' = R \quad (\text{A.11})$$

Also by taking $z' = u_s$, where u_s is the assumed velocity profile function, the following equation was obtained:

$$R^2 \tan^2 \theta_f x'^2 + R^2 \tan^2 \theta_f y'^2 = R^2 (u_s - R \tan \theta_f)^2 \quad (\text{A.12})$$

or

$$\tan^2 \theta_f x'^2 + \tan^2 \theta_f y'^2 = (u_s - R \tan \theta_f)^2 \quad (\text{A.13})$$

u_s can be solved from (A.13) as

$$u_s = \left[R - (x'^2 + y'^2)^{\frac{1}{2}} \right] \tan \theta_f \quad (\text{A.14})$$

By substituting in (A.14);

$$x' = \xi \cos \eta \quad (\text{A.15})$$

and

$$y' = \xi \sin \eta \quad (\text{A.16})$$

where ξ is the radial distance and η is the angular coordinate over the pipe cross-section as shown in Figure 4.5, the following expression was obtained for u_s :

$$u_s = (R - \xi) \tan \theta_f$$

as expressed previously in (4.2)

Equation given by (4.2) is valid for the domain of the bottom cone which is defined by

$$y'_1 < \xi \leq R$$

according to the polar coordinate system given for the cross-sectional view of the elbow in Figure 4.5, and considering the placement pattern of the bottom cone in the cartesian coordinate system shown in Figure 4.4.

A.2.2 Derivation of Upper Cone Equation

For the derivation of the upper oblique cone equation, Equation (4.1) for the general case together with its parameters given in Figure 4.2 was considered again.

Equation (4.1) can be written for the upper oblique cone in Figure A.3 as

$$(x''_0 z'' - x'' z''_0)^2 + (y''_0 z'' - y'' z''_0)^2 = R''^2 (z'' - z''_0)^2 \quad (\text{A.17})$$

In the equation given by (A.17) the symbols are as,

x'' , y'' , z'' : coordinate axes of the upper coordinate system,

x''_0 , y''_0 , z''_0 : coordinates of the apex of the oblique cone with respect to the

upper coordinate system,

R'' : radius of the bottom circle of the oblique upper cone,

O'' : origin of the upper cartesian coordinate system

as given in Figure A.3.

A coordinate transformation between the upper and the lower coordinate system can be made in the following manner:

$$x' = x'' \quad (\text{A.18})$$

$$y' = y'' \quad (\text{A.19})$$

$$z' = z'' + h_2 \quad (\text{A.20})$$

Also according to Figure 4.4, with the values for the parameters: $x_0'' = 0$, $y_0'' = R_m$, $z_0'' = h_1$, $R'' = y_1'$; (A.17) can be written as

$$h_1^2 x'^2 + [R_m(z' - h_2) - h_1 y']^2 = y_1'^2 (z' - h_2 - h_1)^2 \quad (\text{A.21})$$

Using $z' = u_s$, (A.21) becomes

$$h_1^2 x'^2 + [R_m(u_s - h_2) - h_1 y']^2 = y_1'^2 (u_s - h_2 - h_1)^2 \quad (\text{A.22})$$

u_s can be solved from (A.22) as

$$u_s = \frac{1}{(y_1'^2 - R_m^2)} \left[y_1'^2 h_1 - R_m h_1 y' - R_m^2 h_2 + y_1'^2 h_2 \right. \\ \left. - \left(-2 y_1'^2 h_1^2 R_m y' - R_m^2 h_1^2 x'^2 + R_m^2 y_1'^2 h_1^2 + y_1'^2 h_1^2 x'^2 + y_1'^2 h_1^2 y'^2 \right)^{\frac{1}{2}} \right] \quad (\text{A.23})$$

The function given in (A.23) can be written in polar coordinates by using (A.15) and (A.16) as;

$$u_s = \frac{1}{(y_1'^2 - R_m^2)} \left[y_1'^2 h_1 - R_m h_1 \xi \sin \eta - R_m^2 h_2 + y_1'^2 h_2 - \left[-2 y_1'^2 h_1^2 R_m \xi \sin \eta - R_m^2 h_1^2 (\xi \cos \eta)^2 + R_m^2 y_1'^2 h_1^2 + y_1'^2 h_1^2 (\xi \cos \eta)^2 + y_1'^2 h_1^2 (\xi \sin \eta)^2 \right]^{\frac{1}{2}} \right]$$

which was previously given by (4.4).

The velocity profile function in (4.4) for the upper oblique cone part shown in Figure 4.4 is valid over that region of the pipe cross-section defined by

$$0 \leq \xi \leq y_1'$$

according to the polar coordinate system for the cross-section of the elbow given in Figure 4.5.

A.2.3 Calculation of Unknown Parameters

U_m values in (4.7) to (4.10) can be calculated in above equations from continuity principle that

$$Q = \int_A u_s dA \quad (\text{A.24})$$

where

A : cross-sectional area of the elbow, perpendicular to the flow direction

and

Q : discharge along the pipe.

Discharge Q in this study was taken constant along the pipe at any given time during the slug motion, due to continuity principle and the incompressible flow condition imposed. The value of Q in (A.24) is actually the volume under the velocity profile function over the domain of whole pipe cross-section. This volume can be calculated analytically as the addition of two volumes under the symmetric bottom cone, ∇_1 , and the oblique upper cone, ∇_2 , as seen in Figure 4.4:

$$Q = \nabla_1 + \nabla_2 \quad (\text{A.25})$$

or

$$Q = \left[\frac{1}{3} \pi R^2 (h_1 + h_2 + h_3) - \frac{1}{3} \pi y_1'^2 (h_1 + h_2) \right] + \frac{1}{3} \pi y_1'^2 h_1 \quad (\text{A.26})$$

, which can also be written as

$$Q = \frac{1}{3} \pi R^2 (h_1 + h_2 + h_3) - \frac{1}{3} \pi y_1'^2 h_1 - \frac{1}{3} \pi y_1'^2 h_3 + \frac{1}{3} \pi y_1'^2 h_1 \quad (\text{A.27})$$

Canceling second and third terms on the right-hand side,

$$Q = \frac{1}{3} \pi \left[R^2 (h_1 + h_2 + h_3) - y_1'^2 h_3 \right] \quad (\text{A.28})$$

Using

$$h_1 + h_2 + h_3 = R \tan \theta_f \quad (\text{A.29})$$

and

$$h_3 = R \tan \theta_f - U_m \quad (\text{A.30})$$

according to Figure 4.4, (A.28) can be written as

$$Q = \frac{1}{3} \pi \left[R^3 \tan \theta_f - y_1'^2 (R \tan \theta_f - U_m) \right] \quad (\text{A.31})$$

Substituting (4.8) in (A.31) and arranging,

$$\frac{(U_m - R \tan \theta_f)^3 (\tan \theta_c + \tan \theta_f)^2}{\tan^2 \theta_f (\tan \theta_c - \tan \theta_f)^2} + R^3 \tan \theta_f - \frac{3Q}{\pi} = 0 \quad (\text{A.32})$$

From (A.32), U_m can be solved as:

$$U_m = \left(\frac{\left(\frac{3Q}{\pi} - R^3 \tan \theta_f \right) \tan^2 \theta_f (\tan \theta_c - \tan \theta_f)^2}{(\tan \theta_c + \tan \theta_f)^2} \right)^{\frac{1}{3}} + R \tan \theta_f \quad (\text{A.33})$$

From (A.33); U_m , for any cross-section of the pipe and for any time step, can be solved for a given Q value at any instant in time, for an angle θ_f for the gradient of the velocity profile at the pipe wall, and a θ_c value for that cross-section which can be taken from the calibration function. The discharge, Q , here was calculated by using the expression

$$Q = U_{ave} A \quad (\text{A.34})$$

where

U_{ave} : average velocity of the slug along the pipe at any given time, t .

The average velocity U_{ave} here is to be calculated from a set of slug dynamics equations that are given in Section 4.3.3.

In order to get θ_f values, (i.e. the angle for the gradient of the velocity profile at the pipe wall) that occur during the motion of the slug through the elbow and the vertical extension segment; firstly, the Swamee-Jain formula (Walski [11]; Swamee and Jain [12]) together with an expression for the calculation of wall shear stress were utilized as given respectively in (3.14) and (3.13). The expressions for the Reynolds number and the wall shear stress can be rewritten as given below:

$$Re = \frac{\rho U_{ave} D}{\mu} \quad (\text{A.35})$$

$$\tau_0 = \frac{1}{8} f_f \rho U_{ave}^2 \quad (A.36)$$

The Swamee-Jain formula which is a functional representation of the Moody chart is valid for steady, fully developed and incompressible pipe flows (Munson [3], Walski [11]) and this formula was used for calculating the Darcy-Weishbach friction factor, f_f , here in this study, where the flow is actually unsteady and not fully developed, for simplification.

The Swamee-Jain formula given in Equation (3.14) is valid over a wide range of Reynolds numbers between

$$4 \times 10^3 \leq Re \leq 1 \times 10^8 \quad (A.37)$$

and for relative roughness, $\frac{\varepsilon}{D}$, having values between

$$1 \times 10^{-6} \leq \frac{\varepsilon}{D} \leq 1 \times 10^{-2} \quad (A.38)$$

Having calculated the wall friction, τ_0 , for a given average velocity over the pipe cross-section, U_{ave} , at any instant from Equations (A.35), (3.14) and (A.36); the gradient of the velocity profile at the pipe wall can be calculated by using the following equations given in Schlichting [10]:

$$\tau = \tau_0 \left(1 - \frac{y_w}{R} \right) \quad (A.39)$$

$$l = 0.4 y_w \quad (A.40)$$

$$\frac{du}{dy_w} = \frac{1}{l} \sqrt{\frac{\tau}{\rho}} \quad (A.41)$$

where

τ : shear stress value at y_w distance away from the wall of the circular pipe wall,

y_w : distance from the pipe wall,

l : mixing length,

$\frac{du}{dy_w}$: gradient of the velocity profile at point y_w .

In (A.39), (A.40) and (A.41), the distance y_w from the pipe wall can be expressed as

$$y_w = R - \xi \quad (\text{A.42})$$

where ξ is the radial distance of the selected point from the origin of the circular pipe cross-section.

Equation (A.40) is valid for very small distances of y_w from the pipe wall and in this study $y_w = R/250$ was taken to calculate gradient value $\frac{du}{dy_w}$ from (A.41). This value of the gradient calculated at a very small value of y_w distance away from the pipe wall was then accepted as equal to the gradient of the velocity profile at the pipe wall as an approximation.

Then, the angle for the gradient of the velocity profile at the pipe wall θ_f can be calculated as

$$\theta_f = \tan^{-1}\left(\frac{du}{dy_w}\right) \quad (\text{A.43})$$

with $\frac{du}{dy_w}$ evaluated at $y_w = R/250$ distance away from the pipe wall.

The same average θ_f value was utilized at all the points of the circumference of the pipe cross-section at the elbow and the vertical extension segment as it would

be for the case of a straight pipe, here as an approximation. The θ_f value was also taken as constant along the elbow and the vertical extension segment at any instant since the discharge was taken as the same along the pipeline at any given time due to incompressible flow assumption and continuity principle.

A.3. Derivations for the Pressure Distribution Equations

In this section, firstly, the procedures for the derivation of average pressure distribution equations along the axis of the vertical extension segment and of the elbow are given. Then, the derivation for the equation of impact pressure distribution at the convex side of the elbow is presented.

A.3.1 Derivation of Average Pressure Distribution Equation at the Vertical Extension Segment

For the derivation of the average pressure distribution equation at the vertical extension segment, the Reynolds Equation in y -direction given by (4.12) was taken.

The turbulent and the laminar friction terms in (4.12), which are the second and the third terms on the right-hand side of this Reynolds Equation, can be written in a combined form as in the following expression:

$$\rho \left[\frac{\partial V_y}{\partial t} + V_x \frac{\partial V_y}{\partial x} + V_y \frac{\partial V_y}{\partial y} + V_z \frac{\partial V_y}{\partial z} \right] = -\frac{\partial p}{\partial y} + \rho (\nu + \varepsilon_t) \nabla^2 V_y + \rho g_y \quad (\text{A.44})$$

In Equation (A.44), the symbols are as;

ν : kinematic viscosity of the liquid,

ε_t : turbulent eddy viscosity of the liquid,

and

∇ : divergence operator.

For the simplification of the differential expression given in Equation (A.44), a method utilized previously by Ger and Holley [5] was adopted in the present study. As a first step of the simplification of process, the friction term in the differential

equation given by Equation (A.44) was replaced by Darcy Weishbach friction formula (Munson [3]), and (A.44) was integrated over an infinitesimal volumetric pipe element shown in Figure 4.6. The integral equation is given with the expression in (A.45).

$$\begin{aligned} \int_{\Delta\forall} \rho \left[\frac{\partial V_y}{\partial t} + V_x \frac{\partial V_y}{\partial x} + V_y \frac{\partial V_y}{\partial y} + V_z \frac{\partial V_y}{\partial z} \right] d\forall = - \int_{\Delta\forall} \frac{\partial p}{\partial y} d\forall \\ - \int_{\Delta\forall} \rho \frac{f_f P_{wet} \bar{V}_y^2}{8A} d\forall + \int_{\Delta\forall} \rho g_y d\forall \end{aligned} \quad (A.45)$$

Here,

\bar{V}_y : average axial velocity in y -direction,

and

$\Delta\forall$: volume of the pipe element selected in the vertical extension segment.

Equation (A.45) can also be written as

$$\begin{aligned} \int_{\Delta\forall} \rho \left[\frac{\partial V_y}{\partial t} + V_x \frac{\partial V_y}{\partial x} + V_y \frac{\partial V_y}{\partial y} + V_z \frac{\partial V_y}{\partial z} \right] d\forall = - \int_{\Delta\forall} \frac{\partial p}{\partial y} d\forall \\ - \rho \frac{f_f P_{wet} \bar{V}_y^2 \Delta\forall}{8A} + \rho g_y \Delta\forall \end{aligned} \quad (A.46)$$

Now, this volume integral was converted to a combination of volume and surface integrals by applying Divergence Theorem of Gauss, and also using the continuity equation for the case of incompressible flow given in (A.47).

$$\frac{\partial V_x}{\partial x} + \frac{\partial V_y}{\partial y} + \frac{\partial V_z}{\partial z} = 0 \quad (A.47)$$

The combination of Gauss Theorem and Equation (A.47) yields the integral equation in (A.48) (Ger and Holley [5]; Quarteroni and Valli [6]).

$$\int_{\forall} \rho u_i \frac{\partial u_i}{\partial x_i} d\forall = \int_S \rho u_i n_i dS \quad (\text{A.48})$$

In this equation, u_i and x_i are the indicial velocities and coordinates for $i = 1, 2$ and 3 , and S is the surface area of the volumetric element.

Then, by using the expression in (A.48), the left-hand side of equation (A.46) can be rewritten in terms of surface integrals in the following manner;

$$\begin{aligned} \int_{\Delta\forall} \rho \frac{\partial V_y}{\partial t} d\forall + \int_{A_4} \rho V_x V_y dy dz + \int_{A_3} \rho V_y V_y dx dz + \int_{A_4} \rho V_z V_y dx dy = \\ - \int_{\Delta\forall} \frac{\partial p}{\partial y} d\forall - \rho \frac{f_f P_{wet} \bar{V}_y^2 \Delta\forall}{8A} + \rho g_y \Delta\forall \end{aligned} \quad (\text{A.49})$$

In Equation (A.49), A_3 and A_4 are the areas of the pipe cross-section and the pipe wall over the infinitesimal volumetric pipe element shown in Figure 4.6, respectively.

The summation of the second and the fourth terms on the left-hand side of Equation (A.49) is actually equal to the momentum flux through the pipe wall, and it is equal to zero due to no flow boundary condition at the wall. Eliminating these two terms, the expression becomes:

$$\int_{\Delta\forall} \rho \frac{\partial V_y}{\partial t} d\forall + \int_{A_3} \rho V_y^2 dx dz = - \int_{\Delta\forall} \frac{\partial p}{\partial y} d\forall - \rho \frac{f_f P_{wet} \bar{V}_y^2 \Delta\forall}{8A} + \rho g_y \Delta\forall \quad (\text{A.50})$$

where

$$d\forall = dx dy dz . \quad (\text{A.51})$$

Then, Equation (A.50) can be written as

$$\int_{\Delta y} \rho \frac{\partial V_y}{\partial t} d\forall + \int_{A_3} \rho V_y^2 dx dz = - \int_{A_3} p dx dz - \rho \frac{f_f P_{wet} \bar{V}_y^2 \Delta y}{8A} + \rho g_y \Delta y \quad (A.52)$$

or, considering also that the density of liquid, ρ , is constant,

$$\rho \int_{\Delta y} \frac{\partial V_y}{\partial t} d\forall + \rho \int_{A_3} V_y^2 dA_1 = - \int_{A_3} p dA_1 - \rho \frac{f_f P_{wet} \bar{V}_y^2 \Delta y}{8A} + \rho g_y \Delta y \quad (A.53)$$

Dividing both sides of the resulting equation by Δy , while Δy is approaching to 0 at the limit, the following equation is obtained:

$$\frac{\partial}{\partial y} \rho \int_{\Delta y} \frac{\partial V_y}{\partial t} d\forall + \frac{\partial}{\partial y} \rho \int_{A_3} V_y^2 dA_1 = - \frac{\partial}{\partial y} \int_{A_3} p dA_1 - \rho \frac{f_f P_{wet} \bar{V}_y^2 \Delta y}{8A \Delta y} + \frac{\rho g_y \Delta y}{\Delta y} \quad (A.54)$$

In (A.54), replacing A_3 with A , imposing the continuity condition that

$$Q = - \int_A V_y dA \quad (A.55)$$

and using the transformation equations

$$y = -s \quad (A.56)$$

$$V_y = -u_s \quad (A.57)$$

$$\bar{V}_y = -\bar{u}_s \quad (A.58)$$

$$g_y = -g \quad (A.59)$$

with the differentiated form of Equation (A.56);

$$dy = -ds \quad (\text{A.60})$$

on the s axis along the vertical extension segment, and also making some simplifications on Equation (A.54), the resulting equation becomes:

$$-\rho \frac{\partial Q}{\partial t} - \frac{\partial}{\partial s} \rho \int_A u_s^2 dA = \frac{\partial}{\partial s} \int_A p dA + \rho \frac{f_f P_{wet} \bar{u}_s^2}{8} - \rho g A \quad (\text{A.61})$$

In expression given by (A.61), Q is the discharge of the slug flow in s -direction at any section of pipe and at any instant during the slug motion. The discharge for the slug was taken as constant along the horizontal part of the pipeline, elbow and the vertical extension segment at any instant due to incompressible flow assumption for the liquid slug and the continuity principle.

Now, by using the equalities that

$$Q = \bar{u}_s A \quad (\text{A.62})$$

and

$$P = \frac{1}{A} \int_A p dA \quad (\text{A.63})$$

Equation (A.61) can also be written as

$$-\rho \frac{\partial \bar{u}_s}{\partial t} A - \frac{\partial}{\partial s} \rho \int_A u_s^2 dA = \frac{\partial P}{\partial s} A + \rho \frac{f_f P_{wet} \bar{u}_s^2}{8} - \rho g A \quad (\text{A.64})$$

Dividing both sides of Equation (A.64) by A and rearranging the terms, the expression below was obtained as given previously in (4.17):

$$\frac{\partial P}{\partial s} = -\rho \left[\left[\frac{\partial \bar{u}_s}{\partial t} \right]_{t=t_n} + \frac{1}{A} \frac{\partial}{\partial s} \int_A u_s^2 dA + \frac{f_f P_{wet} \bar{u}_s^2}{8A} - g \right]$$

The derivative expression in the first term in parenthesis on the right-hand side of Equation (4.17) was discretized by using first order backward finite differences as;

$$\left[\frac{\partial \bar{u}_s}{\partial t} \right]_{t=t_n} = \frac{(\bar{u}_s)^n - (\bar{u}_s)^{n-1}}{\Delta t_s}$$

as given previously in (4.18).

A.3.2 Derivation of Average Pressure Distribution Equation at the Elbow

The mathematical formulation for the derivation of average pressure distribution equation along the axis of the elbow is given in this section. To make formulations; firstly, the second and the third terms on the right-hand side of Equation (4.15) which stand respectively for the turbulent and the laminar frictional effects can be stated in a combined manner, also expressing the θ component of gravitational acceleration in terms of g according to Figure 4.5 with

$$g_\theta = -g \cos \theta , \quad (\text{A.65})$$

as:

$$\rho \left(\frac{\partial V_\theta}{\partial t} + V_r \frac{\partial V_\theta}{\partial r} + \frac{V_\theta}{r} \frac{\partial V_\theta}{\partial \theta} + \frac{V_r V_\theta}{r} + V_z \frac{\partial V_\theta}{\partial z} \right) = -\frac{1}{r} \frac{\partial p}{\partial \theta} + \rho(v + \varepsilon_t) \nabla^2 V_\theta - \rho g \cos \theta \quad (\text{A.66})$$

Taking the volume integral of both sides of (A.66) over an infinitesimal volumetric element selected in the elbow as shown in Figure 4.7, the following equation was obtained:

$$\begin{aligned}
& \int_{\Delta\forall} \rho \left(\frac{\partial V_\theta}{\partial t} + V_r \frac{\partial V_\theta}{\partial r} + \frac{V_\theta}{r} \frac{\partial V_\theta}{\partial \theta} + \frac{V_r V_\theta}{r} + V_z \frac{\partial V_\theta}{\partial z} \right) d\forall = - \int_{\Delta\forall} \frac{1}{r} \frac{\partial p}{\partial \theta} d\forall \\
& - \int_{\Delta\forall} \rho \frac{f_f P_{wet} \bar{V}_\theta^2}{8A} d\forall - \int_{\Delta\forall} \rho \frac{K_m \bar{V}_\theta^2}{2L_{elb}} d\forall - \int_{\Delta\forall} \rho g \cos \theta d\forall
\end{aligned} \tag{A.67}$$

In Equation (A.67);

$\Delta\forall$: volume of the element selected in the elbow,

\bar{V}_θ : average axial velocity in θ -direction,

The expression given by (A.67) can also be written as

$$\begin{aligned}
& \int_{\Delta\forall} \rho \left(\frac{\partial V_\theta}{\partial t} + V_r \frac{\partial V_\theta}{\partial r} + \frac{V_\theta}{r} \frac{\partial V_\theta}{\partial \theta} + \frac{V_r V_\theta}{r} + V_z \frac{\partial V_\theta}{\partial z} \right) d\forall = - \int_{\Delta\forall} \frac{1}{r} \frac{\partial p}{\partial \theta} d\forall \\
& - \rho \frac{f_f P_{wet} \bar{V}_\theta^2 \Delta\forall}{8A} - \rho \frac{K_m \bar{V}_\theta^2 \Delta\forall}{2L_{elb}} - \rho g \cos \theta \Delta\forall
\end{aligned} \tag{A.68}$$

To simplify the left-hand side of Equation (A.68), the following expression E can be taken as an appropriately chosen starting point, to obtain a similar integral expression as was used for the cartesian coordinate system given by Equation (A.48) in Section A.3.1.

$$E = \int_{\Delta\forall} \frac{1}{r^2} \frac{\partial(r^2 V_r V_\theta)}{\partial r} + \frac{1}{r} \frac{\partial(V_\theta V_\theta)}{\partial \theta} + \frac{\partial(V_\theta V_z)}{\partial z} d\forall \tag{A.69}$$

Taking the derivatives of multiplications, the expression in (A.69) becomes

$$E = \int_{\Delta\forall} \frac{2V_r V_\theta}{r} + V_r \frac{\partial V_\theta}{\partial r} + V_\theta \frac{\partial V_r}{\partial r} + \frac{V_\theta}{r} \frac{\partial V_\theta}{\partial \theta} + \frac{V_\theta}{r} \frac{\partial V_\theta}{\partial r} + V_\theta \frac{\partial V_z}{\partial z} + V_z \frac{\partial V_\theta}{\partial z} d\forall \tag{A.70}$$

Arranging the terms,

$$E = \int_{\Delta \forall} V_\theta \left(\frac{V_r}{r} + \frac{\partial V_r}{\partial r} + \frac{1}{r} \frac{\partial V_\theta}{\partial \theta} + \frac{\partial V_z}{\partial z} \right) + \frac{V_r V_\theta}{r} + V_r \frac{\partial V_\theta}{\partial r} + \frac{V_\theta}{r} \frac{\partial V_\theta}{\partial \theta} + V_z \frac{\partial V_\theta}{\partial z} d\forall \quad (A.71)$$

The expression in parenthesis in (A.71) is equal to zero due to continuity condition for incompressible flow. Then, (A.71) becomes

$$E = \int_{\Delta \forall} V_r \frac{\partial V_\theta}{\partial r} + \frac{V_\theta}{r} \frac{\partial V_\theta}{\partial \theta} + \frac{V_r V_\theta}{r} + V_z \frac{\partial V_\theta}{\partial z} d\forall \quad (A.72)$$

Now, (A.69) can also be rewritten here as;

$$E = \int_{\Delta \forall} \frac{V_r V_\theta}{r} + \frac{1}{r} \frac{\partial (r V_r V_\theta)}{\partial r} + \frac{1}{r} \frac{\partial (V_\theta V_\theta)}{\partial \theta} + \frac{\partial (V_\theta V_z)}{\partial z} d\forall \quad (A.73)$$

By using the divergence operator $\bar{\nabla}$ in cylindrical polar coordinates (Bird and et.al. [8]) given below

$$\bar{\nabla} = \bar{\delta}_r \frac{\partial}{\partial r} + \bar{\delta}_\theta \frac{\partial}{\partial \theta} + \bar{\delta}_z \frac{\partial}{\partial z} \quad (A.74)$$

(A.73) can be written as

$$E = \int_{\Delta \forall} \frac{V_r V_\theta}{r} + \bar{\nabla} \cdot (V_r V_\theta \bar{\delta}_r + V_\theta V_\theta \bar{\delta}_\theta + V_z V_\theta \bar{\delta}_z) d\forall. \quad (A.75)$$

Using the Gauss' Divergence Theorem (Kreyszig [7]) that

$$\int_{\forall} \bar{\nabla} \cdot \vec{F}_{vec} d\forall = \int_S \vec{F}_{vec} \cdot \vec{n} dS \quad (A.76)$$

and taking \vec{F}_{vec} here, as

$$\vec{F}_{vec} = V_r V_\theta \vec{\delta}_r + V_\theta V_\theta \vec{\delta}_\theta + V_z V_\theta \vec{\delta}_z \quad (\text{A.77})$$

with

$$d\forall = r dr d\theta dz \quad (\text{A.78})$$

Equation (A.75) becomes

$$E = \int_{\Delta\forall} \frac{V_r V_\theta}{r} d\forall + \int_{A_4} V_r V_\theta r d\theta dz + \int_{A_3} V_\theta V_\theta dr dz + \int_{A_4} V_z V_\theta r dr d\theta \quad (\text{A.79})$$

Combining Equations (A.72) and (A.79), the following equality was obtained:

$$\begin{aligned} \int_{\Delta\forall} V_r \frac{\partial V_\theta}{\partial r} + \frac{V_\theta}{r} \frac{\partial V_\theta}{\partial \theta} + \frac{V_r V_\theta}{r} + V_z \frac{\partial V_\theta}{\partial z} d\forall &= \int_{\Delta\forall} \frac{V_r V_\theta}{r} d\forall + \int_{A_4} V_r V_\theta r d\theta dz \\ &+ \int_{A_3} V_\theta V_\theta dr dz + \int_{A_4} V_z V_\theta r dr d\theta \end{aligned} \quad (\text{A.80})$$

over the selected infinitesimal volume element.

Now, using the equality given in (A.80), the left-hand side of Equation in (A.68) can be written by using three area integrals as follows:

$$\begin{aligned} \rho \left[\int_{\Delta\forall} \frac{\partial V_\theta}{\partial t} d\forall + \int_{\Delta\forall} \frac{V_r V_\theta}{r} d\forall + \int_{A_4} V_r V_\theta r d\theta dz + \int_{A_3} V_\theta V_\theta dr dz + \int_{A_4} V_z V_\theta r dr d\theta \right] = \\ - \int_{\Delta\forall} \frac{1}{r} \frac{\partial p}{\partial \theta} d\forall - \rho \frac{f_f P_{wet} \bar{V}_\theta^2 \Delta\forall}{8A} - \rho \frac{K_m \bar{V}_\theta^2 \Delta\forall}{2L_{elb}} - \rho g \cos \theta \Delta\forall \end{aligned} \quad (\text{A.81})$$

Introducing, according to Figure 4.5;

$$\beta = \frac{\pi}{2} - \theta \quad (\text{A.82})$$

$$u_\beta = -V_\theta \quad (\text{A.83})$$

, where u_β is the function type variable for the assumed and then calibrated axial velocity profile in the flow direction (in positive β -direction), and also using

$$d\beta = -d\theta \quad (\text{A.84})$$

obtained by differentiating both sides of Equation (A.82); Equation (A.81) becomes

$$\rho \left[- \int_{\Delta\forall} \frac{\partial u_\beta}{\partial t} d\forall - \int_{\Delta\forall} \frac{V_r u_\beta}{r} d\forall - \int_{A_4}^0 V_r u_\beta r d\beta dz - \int_{A_3} u_\beta^2 dr dz - \int_{A_4}^0 V_z u_\beta r dr d\beta \right] =$$

$$\int_{\Delta\forall} \frac{1}{r} \frac{\partial p}{\partial \beta} d\forall + \rho \frac{f_f P_{wet} \bar{u}_\beta^2 \Delta\forall}{8A} + \rho \frac{K_m \bar{u}_\beta^2 \Delta\forall}{2L_{elb}} - \rho g \sin \beta \Delta\forall \quad (\text{A.85})$$

Addition of the third and the fifth terms in parenthesis on the left-hand side of (A.85) is equal to the momentum flux through the pipe wall, and this momentum flux is equal to zero because of the no flow boundary condition at the pipe wall. Therefore, eliminating these two terms and using (A.78), Equation (A.85) can be written as;

$$\rho \left[- \int_{\Delta\forall} \frac{\partial u_\beta}{\partial t} r dr d\beta dz - \int_{\Delta\forall} \frac{V_r u_\beta}{r} r dr d\beta dz - \int_{A_3} u_\beta^2 dr dz \right] = \int_{\Delta\forall} \frac{1}{r} \frac{\partial p}{\partial \beta} r dr d\beta dz$$

$$+ \rho \frac{f_f P_{wet} \bar{u}_\beta^2 \Delta\forall}{8A} + \rho \frac{K_m \bar{u}_\beta^2 \Delta\forall}{2L_{elb}} - \rho g \sin \beta \Delta\forall \quad (\text{A.86})$$

With dA being written as in (A.87) below over the pipe cross-sectional area A as

$$dA = dr dz \quad (\text{A.87})$$

(A.86) can be expressed as:

$$\begin{aligned} \rho \left[- \int_{\Delta \forall} \frac{\partial u_\beta}{\partial t} r d\beta dA - \int_{\Delta \forall} V_r u_\beta d\beta dA - \int_A u_\beta^2 dA \right] &= \int_A p dA \\ + \rho \frac{f_f P_{wet} \bar{u}_\beta^2 \Delta \forall}{8A} + \rho \frac{K_m \bar{u}_\beta^2 \Delta \forall}{2L_{elb}} - \rho g \sin \beta \Delta \forall \end{aligned} \quad (\text{A.88})$$

Taking the integral average of the first term in parenthesis on the left-hand side of (A.88) over the infinitesimal volume element, and integrating the first term on the right-hand side the expression becomes

$$\begin{aligned} \rho \left[- R_0 \Delta \beta \left[\frac{\partial Q}{\partial t} \right]_{t=t_n} - \int_{\Delta \forall} V_r u_\beta d\beta dA - \int_A u_\beta^2 dA \right] &= P A + \rho \frac{f_f P_{wet} \bar{u}_\beta^2 \Delta \forall}{8A} \\ + \rho \frac{K_m \bar{u}_\beta^2 \Delta \forall}{2L_{elb}} - \rho g \sin \beta \Delta \forall \end{aligned} \quad (\text{A.89})$$

Here, the discharge Q was taken as constant at any time step t_n along that length of the s -curve remaining inside the liquid slug as the computational domain as a result of continuity principle together with the incompressible flow assumption, and therefore the derivative quantity $\frac{\partial Q}{\partial t}$ in Equation (A.89) at any time step t_n was also accepted as constant within the computational domain.

Replacing Q in Equation (A.89) with its equal as given below,

$$Q = \bar{u}_\beta A \quad (\text{A.90})$$

and multiplying both sides of (A.89) by $\frac{1}{A\Delta\beta}$ as $\lim \Delta\beta \rightarrow 0$, the following expression was obtained:

$$\begin{aligned} \rho \left[-R_0 \left[\frac{\partial \bar{u}_\beta}{\partial t} \right]_{t=t_n} - \frac{1}{A} \int_A V_r u_\beta dA - \frac{1}{A\Delta\beta} \int_A u_\beta^2 dA \right] &= \frac{\partial P}{\partial \beta} + \rho \frac{f_f P_{wet} \bar{u}_\beta^2 \Delta\forall}{8A^2 \Delta\beta} \\ + \rho \frac{K_m \bar{u}_\beta^2 \Delta\forall}{2L_{elb} A \Delta\beta} - \frac{\rho g \sin \beta \Delta\forall}{A \Delta\beta} \end{aligned} \quad (A.91)$$

By using that

$$\Delta\forall = R_0 \Delta\beta A \quad (A.92)$$

Equation (A.91) becomes

$$\begin{aligned} \rho \left[-R_0 \left[\frac{\partial \bar{u}_\beta}{\partial t} \right]_{t=t_n} - \frac{1}{A} \int_A V_r u_\beta dA - \frac{1}{A\Delta\beta} \int_A u_\beta^2 dA \right] &= \frac{\partial P}{\partial \beta} + \rho \frac{f_f P_{wet} \bar{u}_\beta^2 R_0}{8A} \\ + \rho \frac{K_m \bar{u}_\beta^2 R_0}{2L_{elb}} - \rho g R_0 \sin \beta \end{aligned} \quad (A.93)$$

To eliminate u_β from (A.93), the following continuity equation in cylindrical polar coordinates was used:

$$\frac{\partial V_r}{\partial r} + \frac{1}{r} \frac{\partial V_\theta}{\partial \theta} + \frac{V_r}{r} + \frac{\partial V_z}{\partial z} = 0 \quad (A.94)$$

By using (A.83) and (A.84), Equation (A.94) can be written as

$$\frac{\partial V_r}{\partial r} + \frac{1}{r} \frac{\partial u_\beta}{\partial \beta} + \frac{V_r}{r} + \frac{\partial V_z}{\partial z} = 0 \quad (A.95)$$

Equation (A.95) can be integrated over the pipe cross-section as below:

$$\int_A \frac{\partial V_r}{\partial r} + \frac{1}{r} \frac{\partial u_\beta}{\partial \beta} + \frac{V_r}{r} + \frac{\partial V_z}{\partial z} dA = 0 \quad (\text{A.96})$$

Rewriting (A.96) as,

$$\int_A \frac{\partial V_r}{\partial r} + \frac{1}{r} \frac{\partial u_\beta}{\partial \beta} + \frac{V_r}{r} dA + \int_A \frac{\partial V_z}{\partial z} dA = 0 \quad (\text{A.97})$$

the second integral is zero due to symmetry over the pipe cross-section. Then, it can be written that

$$\frac{\partial V_r}{\partial r} + \frac{1}{r} \frac{\partial u_\beta}{\partial \beta} + \frac{V_r}{r} = 0 \quad (\text{A.98})$$

or

$$r \frac{\partial V_r}{\partial r} + \frac{\partial u_\beta}{\partial \beta} + V_r = 0 \quad (\text{A.99})$$

which can also be written as

$$\frac{\partial(rV_r)}{\partial r} = -\frac{\partial u_\beta}{\partial \beta} \quad (\text{A.100})$$

Integrating both sides of (A.100) with respect to r , and solving for V_r ; Equation (A.101) was obtained.

$$V_r = -\frac{1}{r} \int_{R_0 - \sqrt{R^2 - z^2}}^r \frac{\partial u_\beta}{\partial \beta} dr \quad (\text{A.101})$$

The line integral in Equation in (A.101) is to be taken along a given line of constant z which is parallel to r -axis, starting from the pipe wall up to the point where the value of V_r is desired to be calculated, at a given cross-section of the pipe (Figure 4.5). The lower boundary of the integral here is always zero due to no slip condition at the pipe wall.

Then, Equation (A.93) can be written with u_β as the only velocity component, by using (A.101), as given below:

$$\rho \left[-R_0 \left[\frac{\partial \bar{u}_\beta}{\partial t} \right]_{t=t_n} + \frac{1}{A} \int_A \frac{1}{r} \left(\int_{R_0 - \sqrt{R^2 - z^2}}^r \frac{\partial u_\beta}{\partial \beta} dr \right) u_\beta dA - \frac{1}{A \partial \beta} \int_A u_\beta^2 dA \right] = \frac{\partial P}{\partial \beta} + \rho \frac{f_f P_{wet} \bar{u}_\beta^2 R_0}{8A} + \rho \frac{K_m \bar{u}_\beta^2 R_0}{2L_{elb}} - \rho g R_0 \sin \beta \quad (A.102)$$

Dividing both sides of (A.102) by R_0 ,

$$\rho \left[- \left[\frac{\partial \bar{u}_\beta}{\partial t} \right]_{t=t_n} + \frac{1}{R_0 A} \int_A \frac{1}{r} \left(\int_{R_0 - \sqrt{R^2 - z^2}}^r \frac{\partial u_\beta}{\partial \beta} dr \right) u_\beta dA - \frac{1}{R_0 A \partial \beta} \int_A u_\beta^2 dA \right] = \frac{\partial P}{R_0 \partial \beta} + \rho \frac{f_f P_{wet} \bar{u}_\beta^2}{8A} + \rho \frac{K_m \bar{u}_\beta^2}{2L_{elb}} - \rho g \sin \beta \quad (A.103)$$

and solving for $\frac{\partial P}{\partial s}$ from the equation above, with

$$s = R_0 \beta \quad (A.104)$$

and

$$ds = R_0 d\beta \quad (A.105)$$

the following expression was obtained as given in (4.19) previously:

$$\frac{\partial P}{\partial s} = -\rho \left[\left[\frac{\partial \bar{u}_\beta}{\partial t} \right]_{t=t_n} - \frac{1}{R_0 A} \int_A \frac{1}{r} \left(\int_{R_0 - \sqrt{R^2 - z^2}}^r \frac{\partial u_\beta}{\partial \beta} dr \right) u_\beta dA + \frac{1}{R_0 A} \frac{1}{\partial \beta} \int_A u_\beta^2 dA \right. \\ \left. + \frac{f_f P_{wet} \bar{u}_\beta^2}{8A} + \frac{K_m \bar{u}_\beta^2}{2L_{elb}} - g \sin \beta \right]$$

The first term in parenthesis on the right hand side of (4.19) was calculated with the finite difference expression given below, as expressed previously in (4.20):

$$\left[\frac{\partial \bar{u}_\beta}{\partial t} \right]_{t=t_n} = \frac{(\bar{u}_\beta)^n - (\bar{u}_\beta)^{n-1}}{\Delta t_s}$$

A.3.3 Derivation of the Equation for the Pressure at the Convex Side of the Elbow

The formula for the calculation of local pressure distribution at the convex side of the elbow was obtained by simplifying r -component of the Reynolds Equation given by (4.14).

It is indicated in Bird and et. al. [8] that in turbulent flows, the value of turbulent eddy viscosity is much higher than the molecular viscosity outside the viscous sublayer away from the pipe wall and; therefore, the third term on the right-hand side of Equation (4.14), which stands for the laminar friction effects was cancelled as an approximation. Then, the resulting equation becomes:

$$\rho \left(\frac{\partial V_r}{\partial t} + V_r \frac{\partial V_r}{\partial r} + \frac{V_\theta}{r} \frac{\partial V_r}{\partial \theta} - \frac{V_\theta^2}{r} + V_z \frac{\partial V_r}{\partial z} \right) = - \frac{\partial p}{\partial r} \\ - \rho \left[\frac{1}{r} \frac{\partial}{\partial r} (r \langle V_r V_r' \rangle) + \frac{1}{r} \frac{\partial}{\partial \theta} \langle V_r V_\theta' \rangle + \frac{\partial}{\partial z} \langle V_r V_z' \rangle - \frac{\langle V_\theta' V_\theta' \rangle}{r} \right] + \rho g_r \quad (A.106)$$

For the Reynolds Stresses in (A.106), the following expressions can be used as given in Mathieu and Scott [34]:

$$\langle V_r' V_r' \rangle = -\varepsilon_t \left(2 \frac{\partial V_r}{\partial r} \right) \quad (\text{A.107})$$

$$\langle V_r' V_\theta' \rangle = -\varepsilon_t \left(\frac{\partial V_r}{r \partial \theta} + \frac{\partial V_\theta}{\partial r} \right) \quad (\text{A.108})$$

$$\langle V_r' V_z' \rangle = -\varepsilon_t \left(\frac{\partial V_r}{\partial z} + \frac{\partial V_z}{\partial r} \right) \quad (\text{A.109})$$

Substituting (A.107), (A.108) and (A.109) into Equation (A.106), the Reynolds Equation becomes

$$\begin{aligned} & \rho \left(\frac{\partial V_r}{\partial t} + V_r \frac{\partial V_r}{\partial r} + \frac{V_\theta}{r} \frac{\partial V_r}{\partial \theta} - \frac{V_\theta^2}{r} + V_z \frac{\partial V_r}{\partial z} \right) = -\frac{\partial p}{\partial r} \\ & + \rho \left[\frac{1}{r} \frac{\partial}{\partial r} \left(r \varepsilon_t \frac{\partial V_r}{\partial r} \right) + \frac{1}{r^2} \frac{\partial}{\partial \theta} \left(\varepsilon_t \frac{\partial V_r}{\partial \theta} \right) + \frac{\partial}{\partial z} \left(\varepsilon_t \frac{\partial V_r}{\partial z} \right) - \varepsilon_t \frac{V_r}{r^2} - \frac{2}{r^2} \varepsilon_t \frac{\partial V_\theta}{\partial \theta} \right] + \rho g_r \end{aligned} \quad (\text{A.110})$$

as suggested by Barhaghi and Davidson [1].

By using (A.82), (A.83), (A.84) and Equation (A.111) below according to Figure 4.5,

$$g_r = -g \cos \beta \quad (\text{A.111})$$

Equation (A.110) becomes

$$\begin{aligned} & \rho \left(\frac{\partial V_r}{\partial t} + V_r \frac{\partial V_r}{\partial r} + \frac{u_\beta}{r} \frac{\partial V_r}{\partial \beta} - \frac{u_\beta^2}{r} + V_z \frac{\partial V_r}{\partial z} \right) = -\frac{\partial p}{\partial r} \\ & + \rho \left[\frac{1}{r} \frac{\partial}{\partial r} \left(r \varepsilon_t \frac{\partial V_r}{\partial r} \right) + \frac{1}{r^2} \frac{\partial}{\partial \beta} \left(\varepsilon_t \frac{\partial V_r}{\partial \beta} \right) + \frac{\partial}{\partial z} \left(\varepsilon_t \frac{\partial V_r}{\partial z} \right) - \varepsilon_t \frac{V_r}{r^2} - \frac{2}{r^2} \varepsilon_t \frac{\partial u_\beta}{\partial \beta} \right] \\ & - \rho g \cos \beta \end{aligned} \quad (\text{A.112})$$

Both sides of Equation (A.112) can be integrated over the volume element $\Delta \nabla_r$, also with some manipulation of the second term in parenthesis on the left-hand

side as:

$$\int_{\Delta \nabla_r} \rho \left(\frac{\partial V_r}{\partial t} + \frac{1}{2} \frac{\partial V_r^2}{\partial r} + \frac{u_\beta}{r} \frac{\partial V_r}{\partial \beta} - \frac{u_\beta^2}{r} + V_z \frac{\partial V_r}{\partial z} \right) d\nabla_r = RHS \quad , \quad (A.113)$$

where RHS is the integral of the right-hand side of Equation (A.112) with respect to ∇_r . In (A.113), the volume integral of the fifth term in parenthesis is equal to zero due to the symmetry of the volume element and of the assumed and calibrated axial velocity profile with respect to the vertical plane of $z = 0$ according to Figures 4.5, 4.8 and 4.4.

Equation (A.113) can now be differentiated back with respect to ∇_r remove the integral as

$$\begin{aligned} \rho \left(\frac{\partial V_r}{\partial t} + \frac{1}{2} \frac{\partial V_r^2}{\partial r} + \frac{u_\beta}{r} \frac{\partial V_r}{\partial \beta} - \frac{u_\beta^2}{r} \right) &= -\frac{\partial p}{\partial r} \\ + \rho \left[\frac{1}{r} \frac{\partial}{\partial r} \left(r \varepsilon_t \frac{\partial V_r}{\partial r} \right) + \frac{1}{r^2} \frac{\partial}{\partial \beta} \left(\varepsilon_t \frac{\partial V_r}{\partial \beta} \right) + \frac{\partial}{\partial z} \left(\varepsilon_t \frac{\partial V_r}{\partial z} \right) - \varepsilon_t \frac{V_r}{r^2} - \frac{2}{r^2} \varepsilon_t \frac{\partial u_\beta}{\partial \beta} \right] \\ - \rho g \cos \beta \end{aligned} \quad (A.114)$$

Since the impact pressures were intended to find at the convex side of the elbow at points along a curved line, where this part of the pipe wall and the vertical plane of $z = 0$ through the elbow centerline intersects, in the present study; the Equation given with (A.114) was utilized along the vertical radiuses of the cross-sections of the elbow shown in Figure 4.8. Therefore, using the expression for V_r given by (A.101) and taking $z = 0$ for the terms that do not contain a derivative with respect to z , the expression (A.115) was obtained as given below:

$$\begin{aligned}
& \rho \left[-\frac{1}{r} \frac{\partial}{\partial t} \int_{R_0-R}^r \frac{\partial u_\beta}{\partial \beta} dr + \frac{1}{2} \frac{\partial}{\partial r} \left(-\frac{1}{r} \int_{R_0-R}^r \frac{\partial u_\beta}{\partial \beta} dr \right)^2 + \frac{u_\beta}{r} \frac{\partial}{\partial \beta} \left(-\frac{1}{r} \int_{R_0-R}^r \frac{\partial u_\beta}{\partial \beta} dr \right) - \frac{u_\beta^2}{r} \right] = \\
& -\frac{\partial p}{\partial r} + \rho \left\{ \frac{1}{r} \frac{\partial}{\partial r} \left[r \varepsilon_t \frac{\partial}{\partial r} \left(-\frac{1}{r} \int_{R_0-R}^r \frac{\partial u_\beta}{\partial \beta} dr \right) \right] + \frac{1}{r^2} \frac{\partial}{\partial \beta} \left[\varepsilon_t \frac{\partial}{\partial \beta} \left(-\frac{1}{r} \int_{R_0-R}^r \frac{\partial u_\beta}{\partial \beta} dr \right) \right] \right. \\
& \left. + \frac{\partial}{\partial z} \left[\varepsilon_t \frac{\partial}{\partial z} \left(-\frac{1}{r} \int_{R_0-\sqrt{R^2-z^2}}^r \frac{\partial u_\beta}{\partial \beta} dr \right) \right] - \frac{\varepsilon_t}{r^2} \left(-\frac{1}{r} \int_{R_0-R}^r \frac{\partial u_\beta}{\partial \beta} dr \right) - \frac{2}{r^2} \varepsilon_t \frac{\partial u_\beta}{\partial \beta} \right\} - \rho g \cos \beta
\end{aligned} \tag{A.115}$$

Then, $\frac{\partial p}{\partial r}$ can be solved from the above equation as:

$$\begin{aligned}
\frac{\partial p}{\partial r} = & \rho \left\{ \frac{1}{r} \frac{\partial}{\partial t} \int_{R_0-R}^r \frac{\partial u_\beta}{\partial \beta} dr + \frac{1}{2} \frac{\partial}{\partial r} \left(\frac{1}{r} \int_{R_0-R}^r \frac{\partial u_\beta}{\partial \beta} dr \right)^2 + \frac{u_\beta}{r} \frac{\partial}{\partial \beta} \left(\frac{1}{r} \int_{R_0-R}^r \frac{\partial u_\beta}{\partial \beta} dr \right) + \frac{u_\beta^2}{r} \right. \\
& - \frac{1}{r} \frac{\partial}{\partial r} \left[r \varepsilon_t \frac{\partial}{\partial r} \left(\frac{1}{r} \int_{R_0-R}^r \frac{\partial u_\beta}{\partial \beta} dr \right) \right] - \frac{1}{r^2} \frac{\partial}{\partial \beta} \left[\varepsilon_t \frac{\partial}{\partial \beta} \left(\frac{1}{r} \int_{R_0-R}^r \frac{\partial u_\beta}{\partial \beta} dr \right) \right] \\
& \left. - \frac{\partial}{\partial z} \left[\varepsilon_t \frac{\partial}{\partial z} \left(\frac{1}{r} \int_{R_0-\sqrt{R^2-z^2}}^r \frac{\partial u_\beta}{\partial \beta} dr \right) \right] + \frac{\varepsilon_t}{r^3} \int_{R_0-R}^r \frac{\partial u_\beta}{\partial \beta} dr - \frac{2\varepsilon_t}{r^2} \frac{\partial u_\beta}{\partial \beta} \right\} - \rho g \cos \beta
\end{aligned} \tag{A.116}$$

The turbulent eddy viscosity, ε_t , in (A.116) was calculated by using Prandtl mixing-length theory with the formula

$$\varepsilon_t = l_m^2 \left| \frac{\partial V_{axial}}{\partial y_w} \right| \tag{A.117}$$

where

V_{axial} : axial velocity.

In Equation (A.117), the mixing length l_m is calculated from the expression

$$\frac{l_m}{R} = 0.14 - 0.08g_m^2 - 0.06g_m^4$$

given previously by (4.23), where

$$g_m = \left(1 - \frac{y_w}{R}\right) \quad (\text{A.118})$$

In the present study, the axial velocity in the elbow can be defined as,

$$V_{axial} = u_\beta \quad (\text{A.119})$$

Then, (A.117) can be expressed as follows:

$$\varepsilon_t = l_m^2 \left| \frac{\partial u_\beta}{\partial y_w} \right|$$

as stated previously in (4.24).

Also, using the expression for the distance from the pipe wall given by (A.42), Equation (A.118) becomes

$$g_m = \frac{\xi}{R}$$

as expressed previously by Equation (4.22)

The turbulent eddy viscosity, ε_t , can be calculated by using (4.22), (4.23) and (4.24) at any point in the elbow, given the radial distance from the pipe centerline, ξ , of that point.

A.4 Derivations for the Transient Force Calculations at the Elbow Part

In this section, the mathematical procedures for the derivation of horizontal and the vertical components of the transient forces acting on the elbow and the vertical extension segment of the pipeline are presented.

A.4.1 Derivations for the Horizontal Transient Force Distribution at the Elbow

For calculating the horizontal transient force distribution at the elbow, conservation of momentum equation given by (4.31) was applied over the sample control volume shown in Figure 4.11, and in the horizontal x -direction;

$$\frac{\partial}{\partial t} \int_{\Delta V} V_x \rho dV + \int_{CS} V_x \rho (\vec{V} \cdot \vec{n}) dA = \sum F_{xV} \quad (\text{A.120})$$

Here F_{xV} is force acting on the volumetric element in the horizontal x -direction.

Since the momentum flux through the pipe wall is zero due to no flow condition, Equation (A.120) can be written in terms of the surface integrals over the surfaces of the pipe cross-sectional areas S_u and S_d of the control volume shown in Figure 4.11, as

$$\frac{\partial}{\partial t} \int_{\Delta V} V_x \rho dV - \int_{S_u} V_{xu} \rho V_{\beta u} dA + \int_{S_d} V_{xd} \rho V_{\beta d} dA = -\Delta F_x + P_u \cos \beta_u A - P_d \cos \beta_d A \quad (\text{A.121})$$

In Equation (A.121);

V_{xu} : local velocity in x -direction at the upstream face of the control volume,

$V_{\beta u}$: local axial velocity at the upstream face of the control volume,

V_{xd} : local velocity in x -direction at the downstream face of the control volume,

$V_{\beta d}$: local axial velocity at the downstream face of the control volume.

In (A.121), the components of the axial forces acting on the control volume, which are the second and third terms on the right-hand side, were written according to Figure A.4.

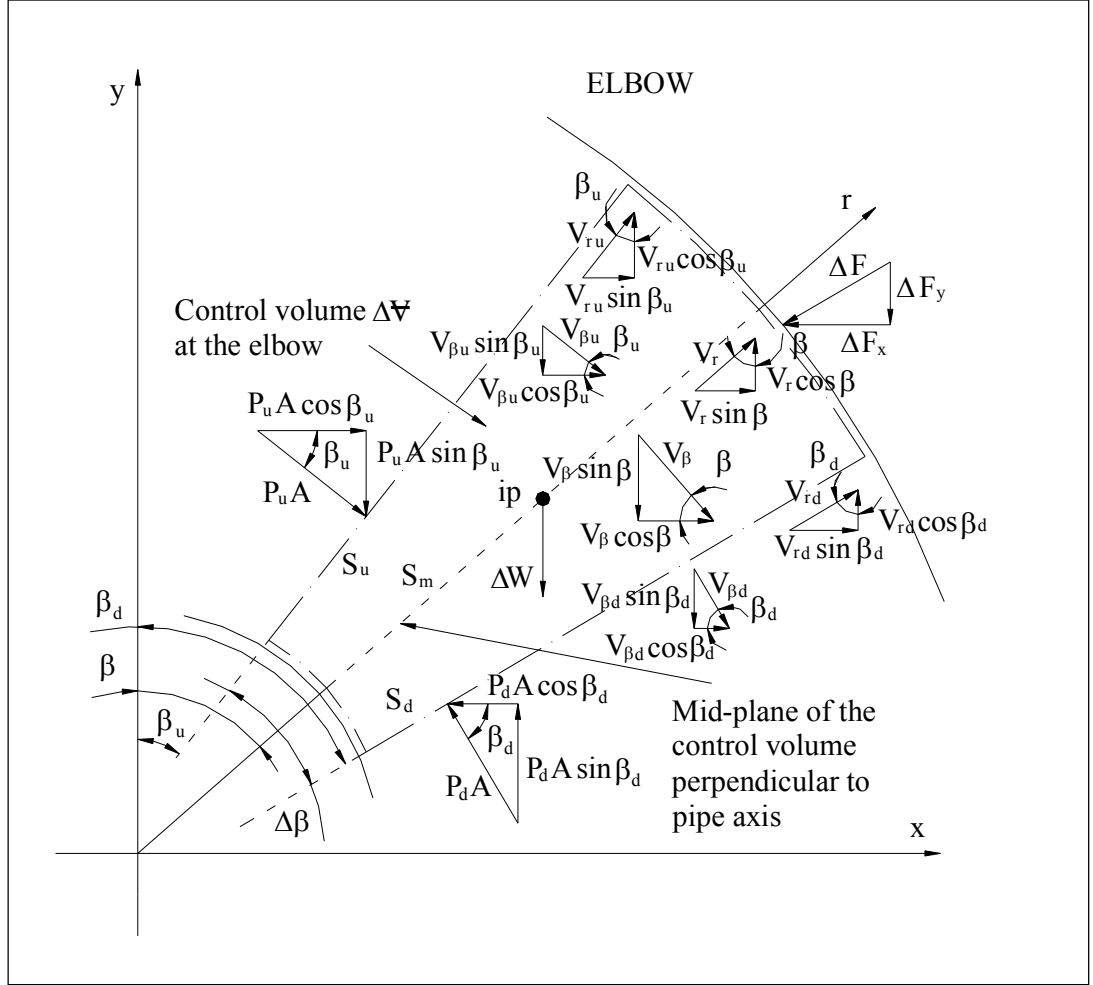


Figure A.4 Control volume at the elbow with the components of the forces and the velocities shown.

Also, from Figure A.4; V_x , V_{xu} and V_{xd} can be expressed as follows:

$$V_x = V_r \sin \beta + V_\beta \cos \beta \quad (\text{A.122})$$

$$V_{xu} = V_{ru} \sin \beta_u + V_{\beta u} \cos \beta_u \quad (\text{A.123})$$

$$V_{xd} = V_{rd} \sin \beta_d + V_{\beta d} \cos \beta_d \quad (\text{A.124})$$

In equations (A.122), (A.123) and (A.124) given above,

V_{ru} : local radial velocity at the upstream face of the control volume,

V_{rd} : local radial velocity at the downstream face of the control volume.

Substituting Equations (A.122), (A.123) and (A.124) into the expression given by (A.121), the following equation was obtained:

$$\begin{aligned} & \frac{\partial}{\partial t} \int_{\Delta \forall} (V_r \sin \beta + V_\beta \cos \beta) \rho d\forall - \int_{S_u} (V_{ru} \sin \beta_u + V_{\beta u} \cos \beta_u) \rho V_{\beta u} dA \\ & + \int_{S_d} (V_{rd} \sin \beta_d + V_{\beta d} \cos \beta_d) \rho V_{\beta d} dA = -\Delta F_x + P_u \cos \beta_u A - P_d \cos \beta_d A \quad (\text{A.125}) \end{aligned}$$

By using the expression given by (A.101) for the values of V_r , V_{ru} and V_{rd} ; and also substituting the value of the assumed and calibrated axial velocity profile function u_β for V_β as below

$$V_\beta = u_\beta \quad (\text{A.126})$$

the Equation (A.125) becomes

$$\begin{aligned} & \frac{\partial}{\partial t} \int_{\Delta \forall} \left[\left(-\frac{1}{r} \int_{R_0 - \sqrt{R^2 - z^2}}^r \frac{\partial u_\beta}{\partial \beta} dr \right) \sin \beta + u_\beta \cos \beta \right] \rho d\forall \\ & - \int_{S_u} \left[\left(-\frac{1}{r} \int_{R_0 - \sqrt{R^2 - z^2}}^r \frac{\partial u_{\beta u}}{\partial \beta} dr \right) \sin \beta_u + u_{\beta u} \cos \beta_u \right] \rho u_{\beta u} dA \\ & + \int_{S_d} \left[\left(-\frac{1}{r} \int_{R_0 - \sqrt{R^2 - z^2}}^r \frac{\partial u_{\beta d}}{\partial \beta} dr \right) \sin \beta_d + u_{\beta d} \cos \beta_d \right] \rho u_{\beta d} dA \\ & = -\Delta F_x + P_u \cos \beta_u A - P_d \cos \beta_d A \quad (\text{A.127}) \end{aligned}$$

The first term on the left-hand side of Equation (A.127) is a volume integral and it can be written as an area integral over the mid-plane of the volumetric element perpendicular to the pipe axis, shown in Figure A.4, by using

$$d\forall = R_0 \Delta\beta dA \quad (\text{A.128})$$

Also, solving for the horizontal reaction force, ΔF_x , from (A.127), the resulting equation becomes

$$\begin{aligned} \Delta F_x = & -\frac{\partial}{\partial t} \int_{S_m} \left[\left(-\frac{1}{r} \int_{R_0 - \sqrt{R^2 - z^2}}^r \frac{\partial u_\beta}{\partial \beta} dr \right) \sin \beta + u_\beta \cos \beta \right] \rho R_0 \Delta\beta dA \\ & + \int_{S_u} \left[\left(-\frac{1}{r} \int_{R_0 - \sqrt{R^2 - z^2}}^r \frac{\partial u_{\beta u}}{\partial \beta} dr \right) \sin \beta_u + u_{\beta u} \cos \beta_u \right] \rho u_{\beta u} dA \\ & - \int_{S_d} \left[\left(-\frac{1}{r} \int_{R_0 - \sqrt{R^2 - z^2}}^r \frac{\partial u_{\beta d}}{\partial \beta} dr \right) \sin \beta_d + u_{\beta d} \cos \beta_d \right] \rho u_{\beta d} dA \\ & + P_u \cos \beta_u A - P_d \cos \beta_d A \end{aligned} \quad (\text{A.129})$$

Equation (A.129) can also be written as

$$\begin{aligned} \Delta F_x = & \rho R_0 \Delta\beta \frac{\partial}{\partial t} \int_{S_m} \left[\left(\frac{1}{r} \int_{R_0 - \sqrt{R^2 - z^2}}^r \frac{\partial u_\beta}{\partial \beta} dr \right) \sin \beta - u_\beta \cos \beta \right] dA \\ & - \rho \int_{S_u} \left[\left(\frac{1}{r} \int_{R_0 - \sqrt{R^2 - z^2}}^r \frac{\partial u_{\beta u}}{\partial \beta} dr \right) \sin \beta_u - u_{\beta u} \cos \beta_u \right] u_{\beta u} dA \\ & + \rho \int_{S_d} \left[\left(\frac{1}{r} \int_{R_0 - \sqrt{R^2 - z^2}}^r \frac{\partial u_{\beta d}}{\partial \beta} dr \right) \sin \beta_d - u_{\beta d} \cos \beta_d \right] u_{\beta d} dA \\ & + P_u \cos \beta_u A - P_d \cos \beta_d A \end{aligned}$$

The above expression for the horizontal component of the transient force acting on the volume element in the elbow was previously stated by Equation (4.32).

A.4.2 Derivations for the Vertical Transient Force Distribution at the Elbow

To find the vertical transient forces acting on the volume elements at the elbow, Equation (4.31) was applied over a control volume selected at the elbow as shown in Figure 4.11, and was written in the direction of y -axis as given below:

$$\frac{\partial}{\partial t} \int_{\Delta V} V_y \rho dV + \int_{CS} V_y \rho (\vec{V} \cdot \vec{n}) dA = \sum F_{yV} \quad (\text{A.130})$$

In this equation;

F_{yV} : force acting on the volumetric element in y -direction.

Taking the momentum flux through the pipe wall as being zero, the surface integral term in (A.130) was written as two separate integral terms over the surfaces of the pipe cross-sectional areas S_u and S_d of the control volume depicted in Figure 4.11:

$$\begin{aligned} \frac{\partial}{\partial t} \int_{\Delta V} V_y \rho dV - \int_{S_u} V_{yu} \rho V_{\beta u} dA + \int_{S_d} V_{yd} \rho V_{\beta d} dA = \\ - \Delta F_y - P_u \sin \beta_u A + P_d \sin \beta_d A - \Delta W \end{aligned} \quad (\text{A.131})$$

Here,

V_{yu} and V_{yd} : local velocities in y -direction at respectively the upstream and the downstream faces of the control volume,

ΔW : weight of the control volume.

On the right-hand side of (A.131), the forces acting on the volume element were written according to Figure A.4.

From Figure A.4; V_y , V_{yu} and V_{yd} can be expressed as follows:

$$V_y = V_r \cos \beta - V_\beta \sin \beta \quad (\text{A.132})$$

$$V_{yu} = V_{ru} \cos \beta_u - V_{\beta u} \sin \beta_u \quad (\text{A.133})$$

$$V_{yd} = V_{rd} \cos \beta_d - V_{\beta d} \sin \beta_d \quad (\text{A.134})$$

Substituting (A.132), (A.133) and (A.134) into Equation (A.131);

$$\begin{aligned} & \frac{\partial}{\partial t} \int_{\Delta \forall} (V_r \cos \beta - V_\beta \sin \beta) \rho d\forall - \int_{S_u} (V_{ru} \cos \beta_u - V_{\beta u} \sin \beta_u) \rho V_{\beta u} dA \\ & + \int_{S_d} (V_{rd} \cos \beta_d - V_{\beta d} \sin \beta_d) \rho V_{\beta d} dA = \\ & - \Delta F_y - P_u \sin \beta_u A + P_d \sin \beta_d A - \Delta W \end{aligned} \quad (\text{A.135})$$

For the values of V_r , V_{ru} and V_{rd} in Equation (A.135); the expression for the radial velocity given by (A.101) can be used. Also, the assumed and calibrated axial velocity profile function, u_β , can be substituted for the value of V_β as stated in (A.126). Then, Equation (A.135) becomes

$$\begin{aligned} & \frac{\partial}{\partial t} \int_{\Delta \forall} \left[\left(-\frac{1}{r} \int_{R_0 - \sqrt{R^2 - z^2}}^r \frac{\partial u_\beta}{\partial \beta} dr \right) \cos \beta - u_\beta \sin \beta \right] \rho d\forall \\ & - \int_{S_u} \left[\left(-\frac{1}{r} \int_{R_0 - \sqrt{R^2 - z^2}}^r \frac{\partial u_{\beta u}}{\partial \beta} dr \right) \cos \beta_u - u_{\beta u} \sin \beta_u \right] \rho u_{\beta u} dA \\ & + \int_{S_d} \left[\left(-\frac{1}{r} \int_{R_0 - \sqrt{R^2 - z^2}}^r \frac{\partial u_{\beta d}}{\partial \beta} dr \right) \cos \beta_d - u_{\beta d} \sin \beta_d \right] \rho u_{\beta d} dA \\ & = -\Delta F_y - P_u \sin \beta_u A + P_d \sin \beta_d A - \Delta W \end{aligned} \quad (\text{A.136})$$

Using (A.128), Equation (A.136) becomes

$$\begin{aligned}
& -\frac{\partial}{\partial t} \int_{\Delta \forall} \left[\left(\frac{1}{r} \int_{R_0 - \sqrt{R^2 - z^2}}^r \frac{\partial u_{\beta}}{\partial \beta} dr \right) \cos \beta + u_{\beta} \sin \beta \right] \rho R_0 \Delta \beta dA \\
& + \int_{S_u} \left[\left(\frac{1}{r} \int_{R_0 - \sqrt{R^2 - z^2}}^r \frac{\partial u_{\beta u}}{\partial \beta} dr \right) \cos \beta_u + u_{\beta u} \sin \beta_u \right] \rho u_{\beta u} dA \\
& - \int_{S_d} \left[\left(\frac{1}{r} \int_{R_0 - \sqrt{R^2 - z^2}}^r \frac{\partial u_{\beta d}}{\partial \beta} dr \right) \cos \beta_d + u_{\beta d} \sin \beta_d \right] \rho u_{\beta d} dA \\
& = -\Delta F_y - P_u \sin \beta_u A + P_d \sin \beta_d A - \Delta W
\end{aligned} \tag{A.137}$$

ΔF_y can be solved from Equation (A.137) as

$$\begin{aligned}
\Delta F_y &= \frac{\partial}{\partial t} \int_{S_m} \left[\left(\frac{1}{r} \int_{R_0 - \sqrt{R^2 - z^2}}^r \frac{\partial u_{\beta}}{\partial \beta} dr \right) \cos \beta + u_{\beta} \sin \beta \right] \rho R_0 \Delta \beta dA \\
& - \int_{S_u} \left[\left(\frac{1}{r} \int_{R_0 - \sqrt{R^2 - z^2}}^r \frac{\partial u_{\beta u}}{\partial \beta} dr \right) \cos \beta_u + u_{\beta u} \sin \beta_u \right] \rho u_{\beta u} dA \\
& + \int_{S_d} \left[\left(\frac{1}{r} \int_{R_0 - \sqrt{R^2 - z^2}}^r \frac{\partial u_{\beta d}}{\partial \beta} dr \right) \cos \beta_d + u_{\beta d} \sin \beta_d \right] \rho u_{\beta d} dA \\
& - P_u \sin \beta_u A + P_d \sin \beta_d A - \Delta W
\end{aligned} \tag{A.138}$$

Substituting (A.139) below into Equation (A.138) and using (A.92),

$$\Delta W = \rho g \Delta \forall \tag{A.139}$$

the resulting expression becomes:

$$\begin{aligned}
\Delta F_y = & \rho R_0 \Delta \beta \frac{\partial}{\partial t} \int_{S_m} \left[\left(\frac{1}{r} \int_{R_0 - \sqrt{R^2 - z^2}}^r \frac{\partial u_\beta}{\partial \beta} dr \right) \cos \beta + u_\beta \sin \beta \right] dA \\
& - \rho \int_{S_u} \left[\left(\frac{1}{r} \int_{R_0 - \sqrt{R^2 - z^2}}^r \frac{\partial u_{\beta u}}{\partial \beta} dr \right) \cos \beta_u + u_{\beta u} \sin \beta_u \right] u_{\beta u} dA \\
& + \rho \int_{S_d} \left[\left(\frac{1}{r} \int_{R_0 - \sqrt{R^2 - z^2}}^r \frac{\partial u_{\beta d}}{\partial \beta} dr \right) \cos \beta_d + u_{\beta d} \sin \beta_d \right] u_{\beta d} dA \\
& - P_u \sin \beta_u A + P_d \sin \beta_d A - \rho g R_0 \Delta \beta A
\end{aligned}$$

The expression for the vertical component of the transient force acting on the volume element above was given previously in (4.35).

A.4.3 Derivations for the Horizontal Transient Force Distribution at the Vertical Extension Segment

The horizontal component of the transient force acting on the volume element in the vertical extension segment shown in Figure 4.13 was calculated by using the conservation of momentum principle in x -direction given by (A.120).

By writing the surface integral term in (A.120) as two integral terms over the areas of the pipe cross-section S_u and S_d of the selected control volume shown in Figure 4.13, the equation becomes

$$\frac{\partial}{\partial t} \int_{\Delta \forall} V_x \rho d\forall - \int_{S_u} V_{xu} \rho u_{su} dA + \int_{S_d} V_{xd} \rho u_{sd} dA = -\Delta F_x \quad (\text{A.140})$$

To find an expression for V_x in (A.140) in terms of the axial velocity profile function u_s , the incompressible continuity equation was used as given below.

$$\frac{\partial V_x}{\partial x} + \frac{\partial V_y}{\partial y} + \frac{\partial V_z}{\partial z} = 0 \quad (\text{A.141})$$

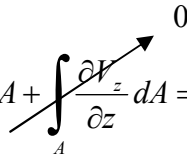
By using (A.56) and (A.57) for the values of y and V_y , the continuity equation in (A.141) becomes

$$\frac{\partial V_x}{\partial x} + \frac{\partial u_s}{\partial s} + \frac{\partial V_z}{\partial z} = 0 \quad (\text{A.142})$$

Equation (A.142) can be integrated over the pipe cross-section as

$$\int_A \frac{\partial V_x}{\partial x} + \frac{\partial u_s}{\partial s} + \frac{\partial V_z}{\partial z} dA = 0 \quad (\text{A.143})$$

or

$$\int_A \frac{\partial V_x}{\partial x} + \frac{\partial u_s}{\partial s} dA + \int_A \frac{\partial V_z}{\partial z} dA = 0 \quad (\text{A.144})$$


The second integral on the left-hand side of (A.144) is equal to zero because of the symmetric shape of the assumed axial velocity profile function and symmetry of the domain with respect to the plane of $z = 0$ according to Figure 4.5.

Then, (A.144) can be written as;

$$\int_A \frac{\partial V_x}{\partial x} + \frac{\partial u_s}{\partial s} dA = 0 \quad (\text{A.145})$$

or

$$\frac{\partial V_x}{\partial x} + \frac{\partial u_s}{\partial s} = 0 \quad (\text{A.146})$$

By writing the expression given in (A.146) as

$$\frac{\partial V_x}{\partial x} = -\frac{\partial u_s}{\partial s} \quad (\text{A.147})$$

and integrating both sides of the equation with respect to x ,

$$V_x = - \int_{R_0 - \sqrt{R^2 - z^2}}^x \frac{\partial u_s}{\partial s} dx \quad (\text{A.148})$$

For the calculation of the velocity V_x with the expression (A.148) at a given point on a cross-section of the vertical extension segment, the line integral in Equation (A.148) is to be taken at the given cross-section along a given line of constant z which is parallel to x -axis, starting from the pipe wall up to the given point at which the value of V_x is to be calculated (Figure 4.5 (b) and (d)).

Substituting the expression given by (A.148) into Equation (A.140), the following equation was obtained:

$$\begin{aligned} \frac{\partial}{\partial t} \int_{\Delta \forall} \left(- \int_{R_0 - \sqrt{R^2 - z^2}}^x \frac{\partial u_s}{\partial s} dx \right) \rho d\forall - \int_{S_u} \left(- \int_{R_0 - \sqrt{R^2 - z^2}}^x \frac{\partial u_{su}}{\partial s} dx \right) \rho u_{su} dA \\ + \int_{S_d} \left(- \int_{R_0 - \sqrt{R^2 - z^2}}^x \frac{\partial u_{sd}}{\partial s} dx \right) \rho u_{sd} dA = -\Delta F_x \end{aligned} \quad (\text{A.149})$$

The first integral on the left-hand side of Equation (A.149), which is a volume integral, can be transformed to an area integral written over the mid-plane of the cross-section of the volume element perpendicular to pipe axis by using

$$d\forall = \Delta s dA \quad (\text{A.150})$$

as given below:

$$\begin{aligned}
& -\frac{\partial}{\partial t} \int_{S_m} \left(\int_{R_0 - \sqrt{R^2 - z^2}}^x \frac{\partial u_s}{\partial s} dx \right) \rho \Delta s dA + \int_{S_u} \left(\int_{R_0 - \sqrt{R^2 - z^2}}^x \frac{\partial u_{su}}{\partial s} dx \right) \rho u_{su} dA \\
& - \int_{S_d} \left(\int_{R_0 - \sqrt{R^2 - z^2}}^x \frac{\partial u_{sd}}{\partial s} dx \right) \rho u_{sd} dA = -\Delta F_x
\end{aligned} \tag{A.151}$$

Here,

Δs : axial length of the volume element.

ΔF_x can be solved from (A.151) as;

$$\begin{aligned}
\Delta F_x &= \frac{\partial}{\partial t} \int_{S_m} \left(\int_{R_0 - \sqrt{R^2 - z^2}}^x \frac{\partial u_s}{\partial s} dx \right) \rho \Delta s dA - \int_{S_u} \left(\int_{R_0 - \sqrt{R^2 - z^2}}^x \frac{\partial u_{su}}{\partial s} dx \right) \rho u_{su} dA \\
&+ \int_{S_d} \left(\int_{R_0 - \sqrt{R^2 - z^2}}^x \frac{\partial u_{sd}}{\partial s} dx \right) \rho u_{sd} dA
\end{aligned}$$

The above expression was also given previously by Equation (4.36).

A.4.4 Derivations for the Vertical Transient Force Distribution at the Vertical Extension Segment

The vertical transient force distribution at the vertical extension segment of the pipeline was found by applying the conservation of momentum principle in y - direction given by (A.130) over the control volume shown in Figure 4.13.

Substituting in (A.130) the equivalent of V_y given by (A.57), the expression becomes

$$-\frac{\partial}{\partial t} \int_{\Delta V} u_s \rho dV - \int_{CS} u_s \rho (\vec{V} \cdot \vec{n}) dA = \sum F_{yV} \tag{A.152}$$

According to the control volume given in Figure 4.13, Equation (A.152) can be written as

$$-\frac{\partial}{\partial t} \int_{\Delta \forall} u_s \rho d\forall + \int_{S_u} u_{su}^2 \rho dA - \int_{S_d} u_{sd}^2 \rho dA = -\Delta F_y - P_u A + P_d A - \Delta W \quad (\text{A.153})$$

or by substituting the equal of $d\forall$ given by (A.150), the equation becomes

$$-\rho \Delta s \frac{\partial}{\partial t} \int_{S_m} u_s dA + \rho \int_{S_u} u_{su}^2 dA - \rho \int_{S_d} u_{sd}^2 dA = -\Delta F_y - P_u A + P_d A - \Delta W \quad (\text{A.154})$$

Also, using Equation (A.139), and (A.155) below;

$$\Delta \forall = \Delta s A \quad (\text{A.155})$$

the expression given by (A.154) can be written as

$$\begin{aligned} &-\rho \Delta s \frac{\partial}{\partial t} \int_{S_m} u_s dA + \rho \int_{S_u} u_{su}^2 dA - \rho \int_{S_d} u_{sd}^2 dA = \\ &-\Delta F_y - P_u A + P_d A - \rho g \Delta s A \end{aligned} \quad (\text{A.156})$$

By using (A.24), ΔF_y can be solved from Equation (A.156) as;

$$\Delta F_y = \rho \Delta s \frac{\partial Q}{\partial t} - \rho \int_{S_u} u_{su}^2 dA + \rho \int_{S_d} u_{sd}^2 dA - P_u A + P_d A - \rho g \Delta s A$$

The expression for ΔF_y above was given by previously in (4.37).

A.5 Derivations for Numerical Integration Formulas

In this section the mathematical procedures for the derivation of numerical area and line integrals developed in the present study are given.

A.5.1 Derivations for Double Integrals in Polar Coordinates

The transformation procedure for the evaluation of numerical area integrals from polar coordinates to the cartesian coordinates are given in this section.

The general form of the area integral to be taken is of the form

$$I_A = \int_A f(\xi, \eta) dA$$

or

$$I_A = \int_A f(\xi, \eta) r d\xi d\eta$$

which were also given previously by (4.40) and (4.41), respectively; according to the polar coordinate system for the pipe cross-section given in Figure 4.14.

For the transformation process; firstly, the integrant $f(\xi, \eta)$ can be integrated over a selected 9-point polar mesh element shown in Figure 4.15, as given below.

$$I_{A;m,n} = \int_{\eta_n - \frac{\Delta\eta}{2}}^{\eta_n + \frac{\Delta\eta}{2}} \int_{\xi_m - \frac{\Delta\xi}{2}}^{\xi_m + \frac{\Delta\xi}{2}} f(\xi, \eta) \xi d\xi d\eta \quad (\text{A.157})$$

Next, the variables of the polar coordinate system, ξ and η , can be written in terms of the cartesian coordinates s' and t' , respectively as

$$\xi = \xi_m + \frac{\Delta\xi}{2} s' \quad (\text{A.158})$$

$$\eta = \eta_n + \frac{\Delta\eta}{2}t' \quad (\text{A.159})$$

where

$$-1 \leq s' \leq 1 \quad (\text{A.160})$$

and

$$-1 \leq t' \leq 1 \quad (\text{A.161})$$

Here,

ξ_m, η_n : values of ξ and η at the center point of 9-point mesh element as in

Figure 4.15.

By differentiating (A.158) and (A.159), the differential expressions

$$d\xi = \frac{\Delta\xi}{2}ds' \quad (\text{A.162})$$

and

$$d\eta = \frac{\Delta\eta}{2}dt' \quad (\text{A.163})$$

are obtained for $d\xi$ and $d\eta$.

Then, by using Equations (A.158) to (A.163), the integral given by (A.157) can be written as

$$I_{A;m,n} = \frac{\Delta\xi \Delta\eta}{4} \int_{-1}^1 \int_{-1}^1 f(\xi, \eta) \left(\xi_m + \frac{\Delta\xi}{2}s' \right) ds' dt' \quad (\text{A.164})$$

By letting

$$g'(\xi, \eta) = f(\xi, \eta) \left(\xi_m + \frac{\Delta \xi}{2} s' \right),$$

which was given previously by (4.42), the expression in (A.164) becomes

$$I_{A;m,n} = \frac{\Delta \xi \Delta \eta}{4} \int_{-1}^1 \int_{-1}^1 g'(\xi, \eta) ds' dt' \quad (\text{A.165})$$

Now the integral $I_{A;m,n}$ has been put in a form of that which is in cartesian coordinates and can be integrated numerically by 2-D Gauss Quadrature Method for cartesian coordinate system, with the location of nodal points and the corresponding weighting coefficients for the Gauss Method being given in Figure 4.16 (Zwillinger, [4]).

To apply 2-D Gauss Quadrature formula for taking the integral in (A.165), the following discrete expression is utilized:

$$I_{A;m,n} = \frac{\Delta \xi \Delta \eta}{4} [w_1 (g'_1 + g'_3 + g'_7 + g'_9) + w_2 (g'_2 + g'_4 + g'_6 + g'_8) + w_3 g'_5],$$

which was previously stated by (4.43).

In Equation (4.43),

w_1 , w_2 and w_3 are the weighting coefficients as $w_1 = \frac{25}{81}$, $w_2 = \frac{40}{81}$, $w_3 = \frac{64}{81}$, and the parameters g'_i with the subscript i ranging from 1 to 9 stand for the values of the function given in (4.42) evaluated at the corresponding locations of the grid points shown in Figure 4.16.

A separate formulation is required to treat the center point of the circular domain over which the area integral given in (4.40) is taken. For this central part, mesh elements as given in Figure 4.17 were considered. Integration given by (4.40) over this triangular mesh element can be expressed as

$$I^c_{A;m,n} = \int_{\eta_n - \frac{\Delta\eta}{2}}^{\eta_n + \frac{\Delta\eta}{2}} \int_0^{\Delta\xi} f(\xi, \eta) \xi d\xi d\eta \quad (\text{A.166})$$

Then, a transformation from the polar variables ξ and η can be made, respectively to cartesian variables s' and t' , with the expressions given below.

$$\xi = \frac{\Delta\xi}{2} + \frac{\Delta\xi}{2} s' \quad (\text{A.167})$$

$$\eta = \eta_n + \frac{\Delta\eta}{2} t' \quad (\text{A.168})$$

with

$$-1 \leq s' \leq 1 \quad (\text{A.169})$$

and

$$-1 \leq t' \leq 1 \quad (\text{A.170})$$

Differentiating (A.167) and (A.168) the following equations are obtained

$$d\xi = \frac{\Delta\xi}{2} ds' \quad (\text{A.171})$$

$$d\eta = \frac{\Delta\eta}{2} dt' \quad (\text{A.172})$$

Then, by using (A.171) and (A.172), the equation in (A.166) can be written as

$$I^c_{A;m,n} = \frac{\Delta\xi \Delta\eta}{4} \int_{-1}^1 \int_{-1}^1 f(\xi, \eta) \left(\frac{\Delta\xi}{2} + \frac{\Delta\xi}{2} s' \right) ds' dt' \quad (\text{A.173})$$

And using

$$g'_c(\xi, \eta) = f(\xi, \eta) \left(\frac{\Delta \xi}{2} + \frac{\Delta \xi}{2} s' \right),$$

which was also stated in Equation (4.44), the expression in (A.173) becomes

$$I^c_{A;m,n} = \frac{\Delta \xi \Delta \eta}{4} \int_{-1}^1 \int_{-1}^1 g'_c(\xi, \eta) ds' dt' \quad (\text{A.174})$$

2-D Gauss Quadrature was applied on (A.174) to take the integral numerically which gave the following expression:

$$I^c_{A;m,n} = \frac{\Delta \xi \Delta \eta}{4} [w_1 (g'_{c1} + g'_{c3} + g'_{c7} + g'_{c9}) + w_2 (g'_{c2} + g'_{c4} + g'_{c6} + g'_{c8}) + w_3 g'_{c5}]$$

The above expression was also previously given in (4.45).

In Equation (4.45), parameter g'_{ci} with the subscript i ranging between values of 1 to 9 represents the values of the expression $g'_c(\xi, \eta)$ evaluated at the location of the nodal points depicted in Figure 4.16.

Now, by using the circular mesh taken over the pipe cross-section, which is shown in Figure 4.14, the area integral in (4.40) can be expressed numerically as

$$I_A = \sum_{n=1}^N \sum_{m=2}^M I_{A;m,n} + \sum_{n=1}^N I^c_{A;1,n},$$

which was also given previously by Equation (4.46).

A.5.2 Derivations for the Line Integrals

In this section, the mathematical procedures for the derivation of the formulas used in 1-D clustered mesh generation, and for the application of 3-Point Gauss

Quadrature Method are presented.

A.5.2.1 Derivations for 1-D Clustered Mesh Generation

For the generation of the clustered line mesh; firstly, the following condition that

$$\sum_{q=1}^{M_L} \Delta r_q = D \quad (\text{A.175})$$

was imposed.

Equation (A.175) indicates that the addition of the lengths of the generated mesh elements in the whole clustered line mesh is equal to the length of the diameter of the circular cross-section of the elbow since the clustered line mesh is generated along the diameter.

The expression in (A.175) can also be written as

$$\Delta r_1 + \Delta r_2 + \Delta r_3 + \dots + \Delta r_{M_L} = D. \quad (\text{A.176})$$

To have clustered mesh elements increase in size with increasing nodal number, q , values; a mesh ratio of the following form was utilized.

$$\Delta r_{q+1} = c_r \Delta r_q \quad (\text{A.177})$$

with

$$c_r > 1. \quad (\text{A.178})$$

Then, Equation (A.176) can be written as

$$\Delta r_1 + c_r \Delta r_1 + c_r^2 \Delta r_1 + \dots + c_r^{M_L-1} \Delta r_1 = D \quad (\text{A.179})$$

or

$$\Delta r_1 \left(1 + c_r + c_r^2 + \dots + c_r^{M_L-1} \right) = D \quad (\text{A.180})$$

The expression given in (A.180) can also be written after some algebra, as

$$\Delta r_1 \left(\frac{c_r^{M_L} - 1}{c_r - 1} \right) = D \quad (\text{A.181})$$

From here, Δr_1 can be solved as

$$\Delta r_1 = \frac{D(c_r - 1)}{c_r^{M_L} - 1} \quad (\text{A.182})$$

Using the relation given in (A.177), Δr_q can be expressed as

$$\Delta r_q = \Delta r_1 c_r^{q-1} \quad (\text{A.183})$$

and substituting for Δr_1 in Equation (A.183), the expression given by (A.182); the size of all the mesh elements in the clustered mesh can be calculated with formula

$$\Delta r_q = \frac{D(c_r - 1)}{c_r^{M_L} - 1} c_r^{q-1}$$

as given previously in (4.47).

A.5.2.2 Derivations for 3-Point Gauss Quadrature Method

The application of 3-Point Gauss Quadrature for the evaluation of line integrals in the present study are given in this section.

The line integral given previously in (4.48) as stated below

$$I_L = \int_{A'}^{K'} h'(\xi, \eta) dr$$

evaluated over any Gauss element shown in Figure 4.19 can be expressed as

$$I_{L,q} = \int_{r_q - \frac{\Delta r_q}{2}}^{r_q + \frac{\Delta r_q}{2}} h'(\xi, \eta) dr \quad (\text{A.184})$$

where

r_q : radial location of the center point Gauss element over the clustered mesh, with respect to the cylindrical coordinate system.

To apply the three point Gauss Quadrature the following transformation can be made as

$$r = r_q + \frac{\Delta r_q}{2} a' \quad (\text{A.185})$$

where

$$-1 \leq a' \leq 1. \quad (\text{A.186})$$

In above equations, a' is the coordinate axis used as the transformation parameter.

By differentiating (A.185), the relation that

$$dr = \frac{\Delta r_q}{2} da' \quad (\text{A.187})$$

is obtained.

Then, by using the differential relation in (A.187), the expression for the line integral given by Equation (A.184) can be rewritten as

$$I_{L,q} = \frac{\Delta r_q}{2} \int_{-1}^1 h'(\xi, \eta) da' . \quad (\text{A.188})$$

The ξ and η values here can be calculated with expressions

$$\xi = \sqrt{z^2 + (r - R_0)^2}$$

and

$$\eta = \tan^{-1} \left(\frac{R_0 - r}{z} \right)$$

while evaluating the line integral, which were derived from geometry depicted in Figure 4.18, and given previously by Equations (4.49) and (4.50), respectively.

Using 3-point Gauss Quadrature, the line integral given in (A.188) over any Gauss element can be expressed as

$$I_{L,q} = \frac{\Delta r_q}{2} (w_1 h'_1 + w_2 h'_2 + w_3 h'_3) ,$$

where the weighting coefficients are $w_1 = \frac{5}{9}$, $w_2 = \frac{8}{9}$; and h'_1 , h'_2 and h'_3 are the values of the integrand function $h'(\xi, \eta)$ in Equation (4.48), as evaluated at the locations for the nodal points of the Gauss element shown in Figure 4.19.

Finally, according to the above formulation, the original line integral given in (4.48) becomes

$$I_L = \sum_{q=1}^{Q_K} I_{L,q} ,$$

given previously in (4.52). The summation in (4.52) is to be taken over the elements of the 1-D clustered line mesh between the points A' and K' as given in Figure 4.18.

A.6 Derivations for the Calibration Function

In this section, the mathematical derivations for the calibration function θ_c is given, which was used for the variation of the skewed 3-D shape of the assumed axial velocity profile along the s -curve, in the elbow and the vertical extension segment of the pipeline.

For the case that $0 \leq s < s_{max}$, by using the equation of a straight line, it can be written according to Figure 4.20 that:

$$\theta_c - \theta_{cmax} = m_{\theta c1} (s - s_{max}) \quad (\text{A.189})$$

And θ_c can be solved by substituting (4.53) for $m_{\theta c1}$, in Equation (A.189) as

$$\theta_c = \theta_{cmax} + \frac{\theta_{cmax}}{s_{max} + 75D} (s - s_{max}) \quad \text{if} \quad 0 \leq s < s_{max} ,$$

which was given previously in Equation (4.55).

For the case that $s_{max} \leq s \leq s_{ext}$, the straight line equation can be written as

$$\theta_c - \theta_{cmax} = m_{\theta c2} (s - s_{max}) \quad (\text{A.190})$$

Substituting Equation (4.54) for $m_{\theta c2}$, into the expression given by (A.190), θ_c can be solved as

$$\theta_c = \theta_{cmax} - \frac{\theta_{cmax}}{s_{elb} + 75D - s_{max}} (s - s_{max}) \quad \text{if} \quad s_{max} \leq s \leq s_{ext} ,$$

which was also expressed in Equation (4.56).

APPENDIX B

CORRELATION FUNCTION FOR THE MAXIMUM CALIBRATION ANGLE

To obtain a correlation function for the maximum calibration angle, $\theta_{c\max}$, of the assumed axial velocity profile function with 3-D shape, a total number of 120 runs were made with the computer program KAYHAN-nc in the present study. The program KAYHAN-nc is actually the same computer code as program KAYHAN except that the correlation function for $\theta_{c\max}$ itself, which will be obtained here is not included in KAYHAN-nc. Therefore, program KAYHAN-nc calculates the corresponding impact pressures at the elbow and finds the transient forces, for different arbitrarily given $\theta_{c\max}$ values and for different initial slug lengths and initial tank pressures. The calculated peak pressure values from program KAYHAN-nc were then, correlated with Bozkuş's [2] experimental data for getting a correlation function for $\theta_{c\max}$ in terms of the normalized slug travel distance L_p / L_{in} .

The peak pressures obtained from KAYHAN-nc for different maximum calibration angle, $\theta_{c\max}$, values and for different initial slug lengths and initial tank pressures are given in Table B.1. Bozkuş's [2] experimental data for the peak pressures are also given in this table.

By normalizing the peak pressures from program KAYHAN-nc given in Table B.1 with respect to initial tank pressures, the graphs presented in Figures B.1 to B.6 were plotted. In Figures B.1 to B.6, the normalized peak pressures from program KAYHAN-nc and from Bozkuş's [2] experimental data are given together.

Table B.1. Peak pressures used for correlating $\theta_{c\max}$ (all in psig).

Initial Slug Length	Initial Tank Pressure	KAYHAN-nc						Bozkuş's Experiment	
		$\theta_{c\max}$						1 st peak	2 nd peak
		89.60°	89.70°	89.75°	89.77°	89.80°	89.82°		
1.22 m (4 ft)	68.91 kPa (10 psi)	30.08	38.13	48.11	54.86	70.97	86.25	49±14	-
	137.82 kPa (20 psi)	58.14	68.99	81.80	85.58	109.67	129.77	137±62	-
	206.73 kPa (30 psi)	85.28	97.90	112.70	122.40	144.91	162.83	142±31	-
	275.64 kPa (40 psi)	112.87	127.11	143.51	154.28	179.09	205.63	217±119	-
1.52 m (5 ft)	68.91 kPa (10 psi)	25.26	33.83	42.86	48.91	63.18	74.47	28±6	-
	137.82 kPa (20 psi)	51.37	61.32	72.90	71.21	99.38	114.69	131±48	-
	206.73 kPa (30 psi)	75.10	86.68	100.05	108.73	128.65	139.39	-	-
	275.64 kPa (40 psi)	100.03	113.09	127.98	137.68	159.72	183.01	-	-
2.13 m (7 ft)	68.91 kPa (10 psi)	28.09	35.77	45.08	51.34	66.19	79.45	96±17	79±9
	137.82 kPa (20 psi)	55.71	65.79	77.36	84.88	97.13	123.49	135±35	151±18
	206.73 kPa (30 psi)	82.24	94.05	107.59	116.32	136.20	157.14	139±27	222±41
	275.64 kPa (40 psi)	109.64	123.05	138.15	147.90	170.08	193.30	173±32	264±31
2.74 m (9 ft)	68.91 kPa (10 psi)	28.47	35.97	45.11	51.23	65.69	79.28	56±11	71±6
	137.82 kPa (20 psi)	57.06	67.06	78.45	85.82	92.61	124.43	78±16	131±5
	206.73 kPa (30 psi)	84.77	96.56	109.98	118.60	138.18	158.71	-	-
	275.64 kPa (40 psi)	113.82	127.30	142.42	152.13	174.24	197.32	-	-
3.35 m (11 ft)	68.91 kPa (10 psi)	26.70	34.35	43.08	48.91	62.63	75.19	38±4	65±7
	137.82 kPa (20 psi)	55.12	64.70	75.48	82.39	88.50	115.40	63±14	124±8
	206.73 kPa (30 psi)	82.27	93.61	106.40	114.54	132.91	152.01	104±42	171±12
	275.64 kPa (40 psi)	110.97	123.97	138.42	147.65	168.50	190.09	126±40	207±16

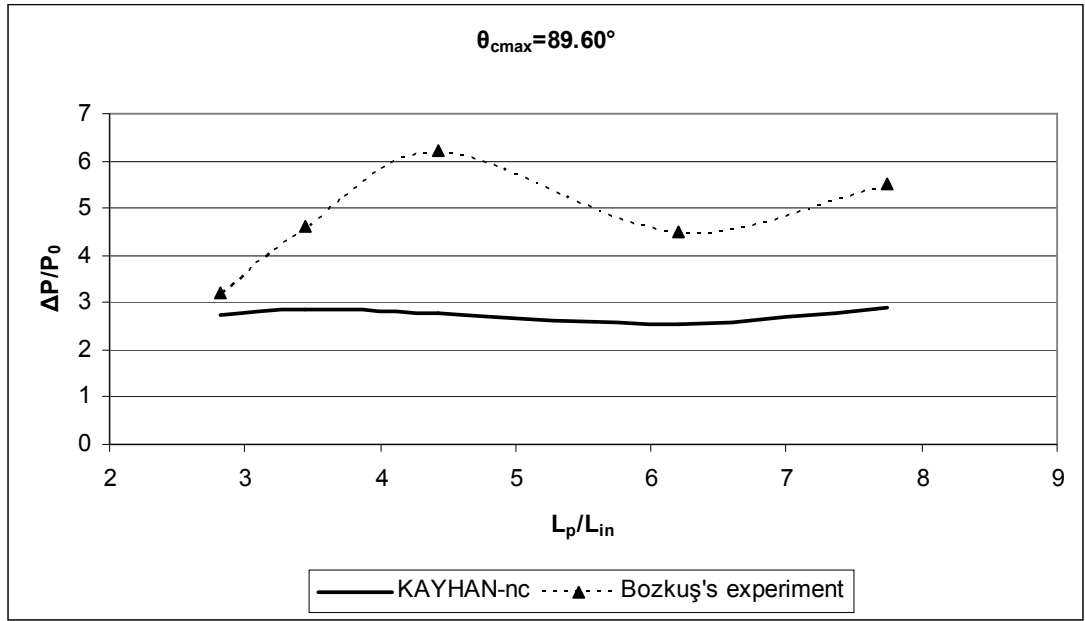


Figure B.1 Normalized peak pressures at the elbow for $\theta_{cmax} = 89.60^\circ$.

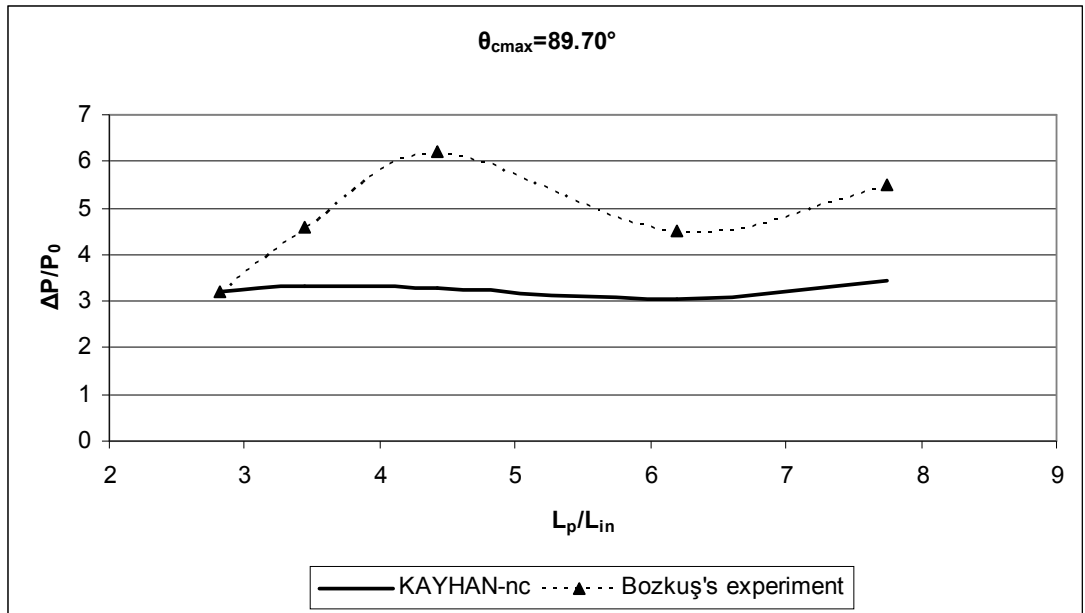


Figure B.2 Normalized peak pressures at the elbow for $\theta_{cmax} = 89.70^\circ$.

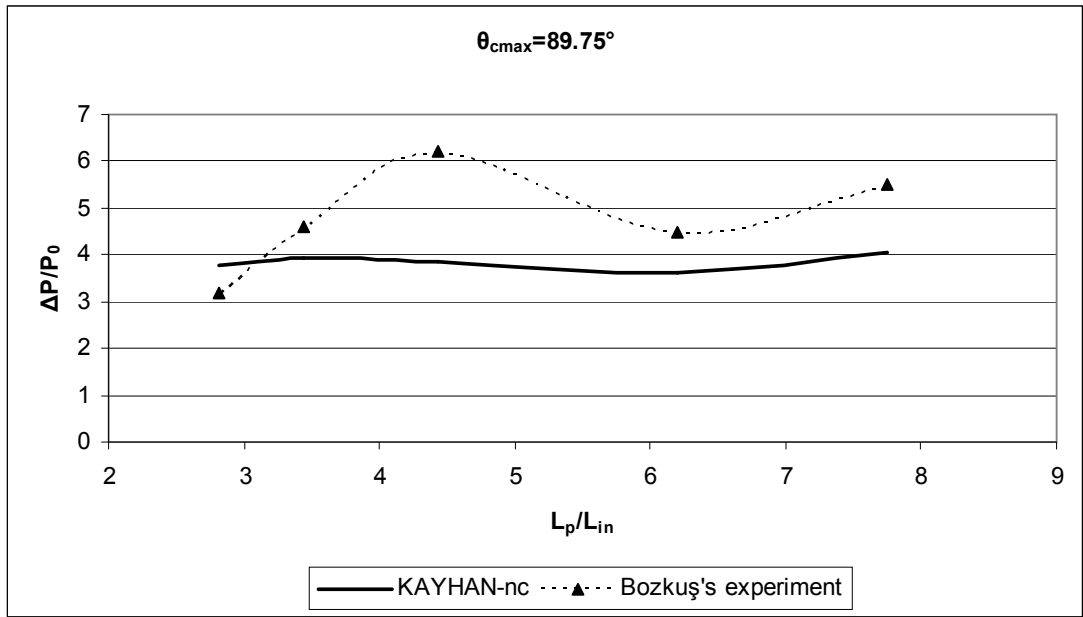


Figure B.3 Normalized peak pressures at the elbow for $\theta_{cmax} = 89.75^\circ$.

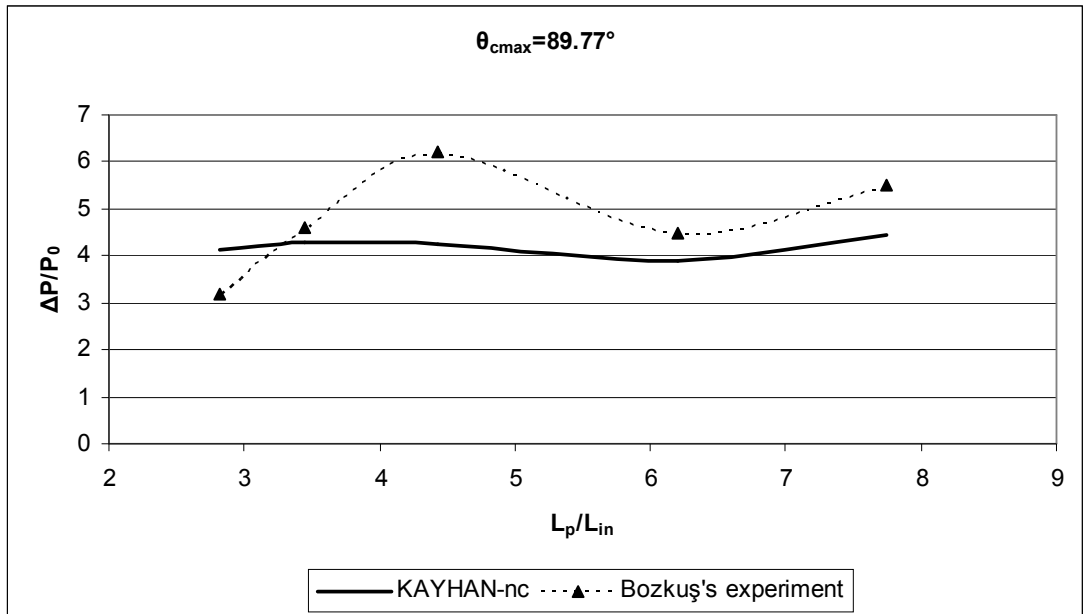


Figure B.4 Normalized peak pressures at the elbow for $\theta_{cmax} = 89.77^\circ$.

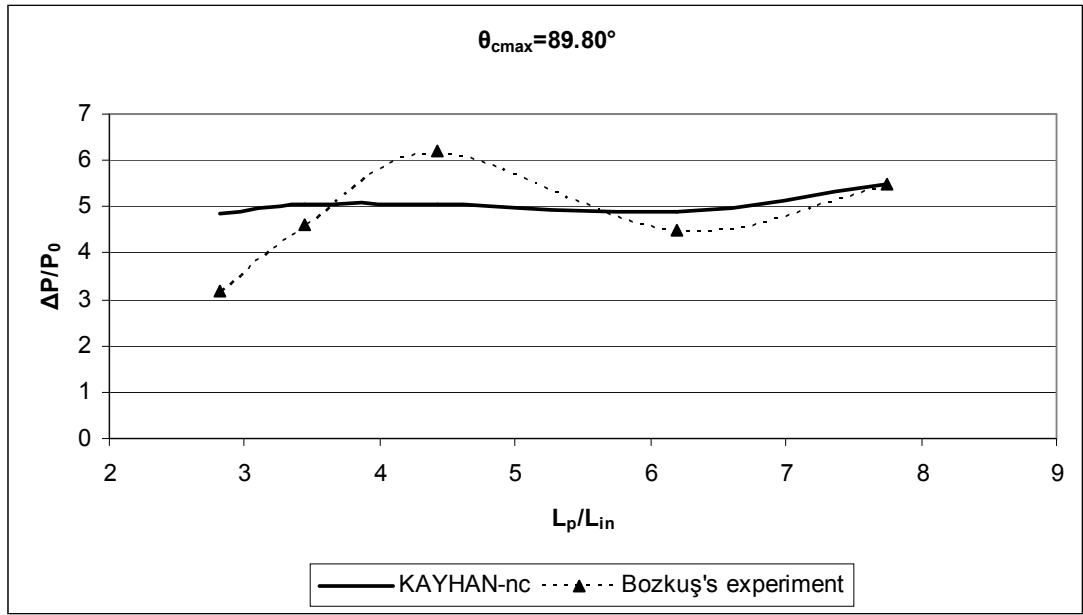


Figure B.5 Normalized peak pressures at the elbow for $\theta_{cmax} = 89.80^\circ$.

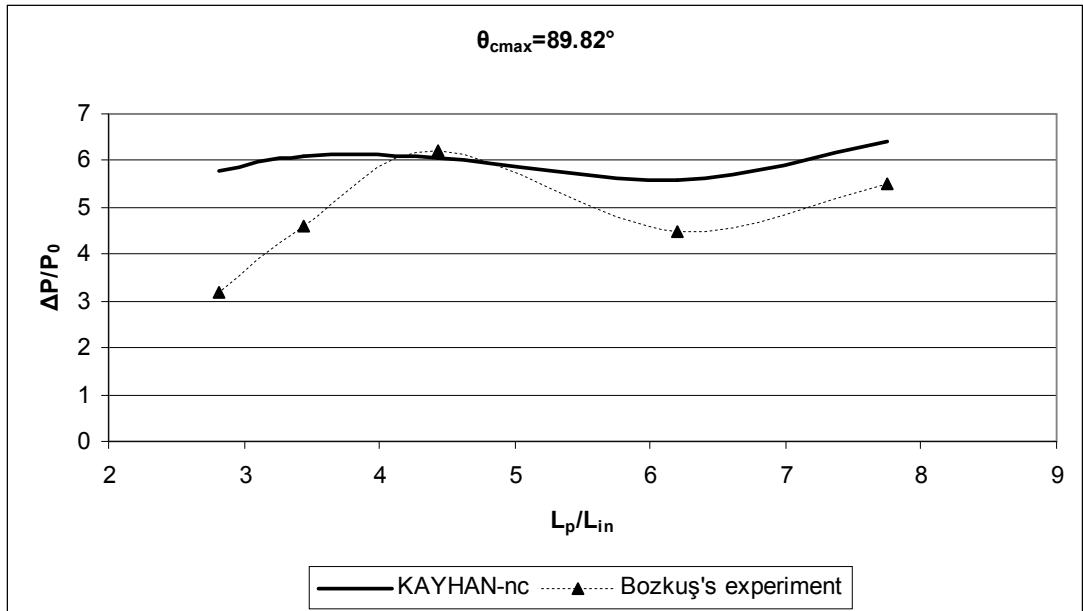


Figure B.6 Normalized peak pressures at the elbow for $\theta_{cmax} = 89.82^\circ$.

Then, the maximum calibration angle $\theta_{c\max}$ values vs. the normalized slug travel distances L_p / L_{in} , at the cross points of the curves for the peak pressures from program KAYHAN-nc and Bozkuş's [2] experimental data given in Figures B.1 to B.6 were tabulated in Table B.2.

Table B.2 $\theta_{c\max}$ values vs. L_p / L_{in} used for correlation procedure.

$\theta_{c\max}$	L_p/L_{in}
89.60°	2.6
89.70°	2.8
89.75°	3.1
89.77°	3.2
89.80°	3.6
89.80°	5.7
89.80°	7.7
89.82°	4.2
89.82°	4.8

Using the values given in Table B.2, a correlation function was obtained for $\theta_{c\max}$ in terms of the normalized slug travel distance L_p / L_{in} as depicted in Figure B.7.

This function for $\theta_{c\max}$ can be expressed as

$$\theta_{c\max} = 0.0124(L_p / L_{in})^3 - 0.2072(L_p / L_{in})^2 + 1.1001(L_p / L_{in}) + 87.951 \quad (B.1)$$

The correlation function for $\theta_{c\max}$ given by Equation (B.1) is valid for all the data range of initial slug lengths and the initial tank pressures used in the analysis. This function was used in program KAYHAN for calculating the unknown parameter $\theta_{c\max}$ of the calibration function θ_c of the assumed axial velocity profile function with 3-D shape, given in Section 4.6.

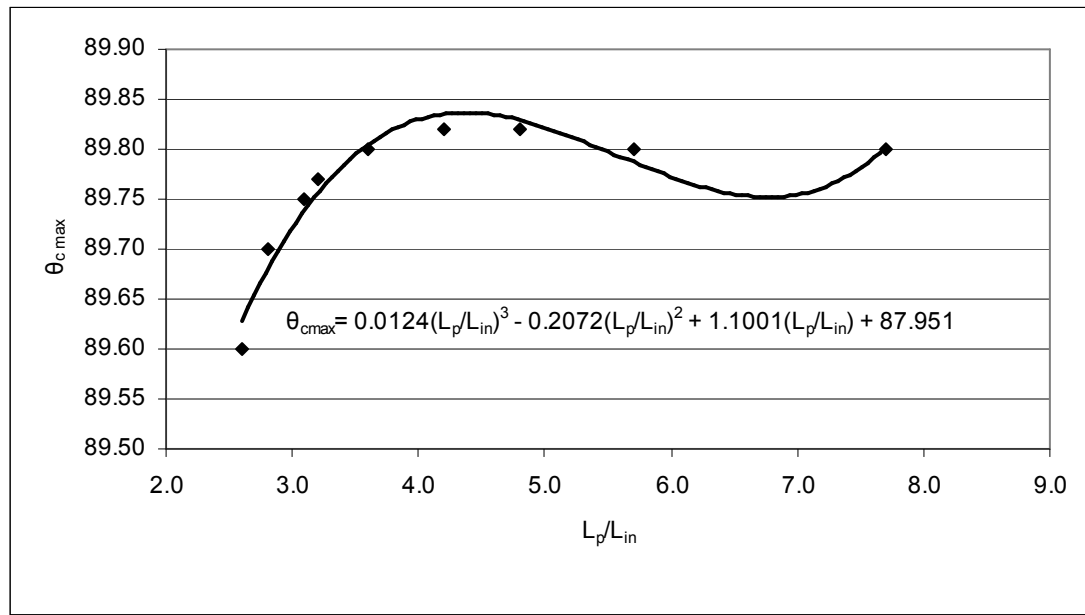


Figure B.7 Correlation function for $\theta_{c \max}$ vs. L_p / L_{in} .

APPENDIX C

COMPUTER PROGRAMS

C.1 Explanations for the Functions of the Computer Programs

BOZKUŞ-1: This program is composed of two parts. In the first part, the program simulates the motion of a liquid slug which is moving along a horizontal pipeline under the pushing effect of high pressure gas from an upstream pressurizer. The mass loss from the liquid slug due to interaction of liquid slug with the pipe wall during the slug motion is considered with the aid of a calibration parameter. The time dependent decrease in the value of the pressure of the gas supplied by the pressurizer that occurs during the slug motion is also taken into account in the program. For the gas region upstream the slug, no gas dynamics effects are considered in this program, so the timely decreasing gas pressure value from the pressurizer is taken directly as equal to the gas pressure at the upstream face of the slug without any waterhammer effects, during the slug motion. The boundary conditions for the slug dynamics equations that govern the motion of the slug are composed of the driving gas pressure at the upstream face of the slug and the atmospheric pressure at the downstream slug face. With these boundary conditions for the pressure values, slug moves along the horizontal pipeline from zero initial velocity, to a final impact speed at the time the front face of the slug reaches the elbow located at the end of the horizontal pipe. The solution for the slug dynamics equations is made with Runge-Kutta-Verner 5th and 6th order method by using a subroutine with the name DVERK developed by Hull and et. al. [25]. At the time the front face of the slug reaches the entrance section of the elbow, an impact pressure value is calculated by using a formula derived for the calculation of forcing function at the elbow.

When the front face of the slug reaches the elbow, a second part of the

program starts. In this part, the event that the slug exits from the elbow to the atmosphere is simulated to get the forcing function acting on the elbow during that exiting period of the slug. No mass loss from the slug is considered to occur in this part of the program. For the flow in the gas region upstream the slug, again no gas dynamics effects are considered as in the case of the first part of the program. Pressure boundary conditions for the slug dynamics equations are also the same as in the first part except that the location for the downstream boundary condition of the slug is fixed at the elbow with zero atmospheric pressure value there. The tank pressure and slug velocity values at the end of the first part of the program are used as initial values at the beginning of the second part of the simulation. Also, different from the previous part of the program, a new set of slug dynamics equations that considers no mass loss from the slug is utilized here in the second part. These set of equations are again solved with Runge-Kutta-Verner 5th and 6th order method as in the previous case. The impact pressure value at the elbow is calculated at each time step, and the simulation is stopped when the slug length remaining in the horizontal part of the pipeline becomes less than 0.05 m., which is a previously defined value (Bozkuş, [2]).

BOZKUŞ-2: This program simulates the motion of a liquid slug that is moving along a horizontal pipeline under the effect of a driving high pressure gas from an upstream pressurizer. The mass loss from the liquid slug is considered with a calibration parameter as in the case of the program BOZKUŞ-1. The decrease in the pressure of the gas supplied by the pressurizer with time during the slug motion is also taken into account. For the gas region upstream the slug, gas dynamics effects are considered in this program, and thus, the pressure variations due to waterhammer effects between the pressurizer and the upstream face of the slug are taken into account during the slug motion. Parameters for the fluid flow in the gas region are solved with method of characteristics. Upstream boundary conditions for the solution in this region consists of the value of the pressure at the pressurizer tank which decreases with time, and the downstream boundary conditions are determined by the kinematics of the liquid slug which is moving along the horizontal pipeline. The motion of the liquid slug is governed by a set of slug dynamics equations. For the

boundary conditions of the slug dynamics equations, gas pressure value at the upstream face of the liquid slug and zero atmospheric pressure at the downstream face of the slug are utilized. The initial slug velocity is taken as zero and the liquid slug accelerates from zero initial velocity to a final impact speed at the elbow during the simulation. When the front face of the slug reaches the elbow, the peak pressure at the elbow is calculated with a formula developed to calculate the forcing function at the elbow, and the simulation is stopped (Bozkuş, [2]).

KAYHAN: In this program, the simulation for the motion of a liquid slug along a horizontal pipeline and then, along a following 90° elbow and a vertical extension part, is performed. The liquid slug moves with the driving effect of a high pressure gas from an upstream pressurizer. For the part of the simulation along the horizontal part of the pipeline, the computer code BOZKUŞ-2 developed by Bozkuş [2], which takes into account the gas dynamics effects, is utilized. The slug length, slug velocity and the value for the magnitude of the gas pressure driving the liquid slug, from program BOZKUŞ-2 at the instant the slug front face reaches the entrance section of the elbow, is used as the initial conditions for the elbow and vertical extension part calculations of program KAYHAN.

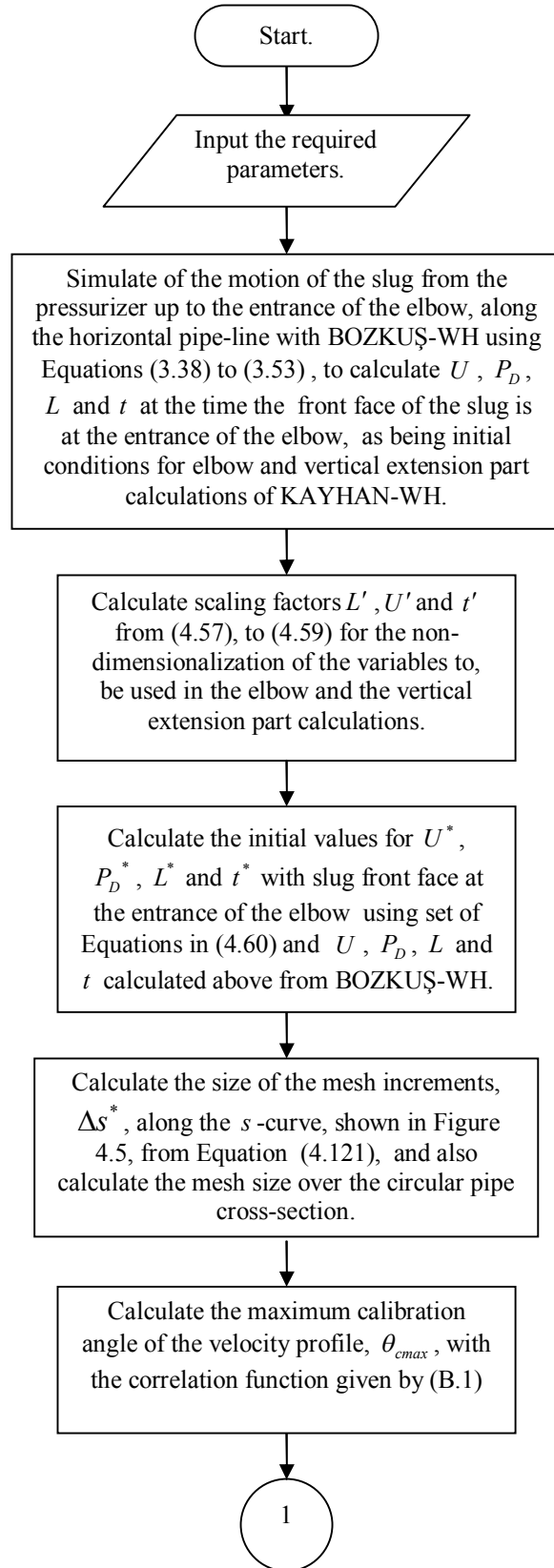
In program KAYHAN, a modification was made on program BOZKUŞ-2 such that during the simulation along the horizontal part of the pipeline, the calibration parameter that accounts for the mass loss from the slug is calculated with a correlation function which was determined by using experimental data for the peak pressures in Bozkuş's study [2]. This correlation function which determines the mass loss from the liquid slug is expressed in terms of the normalized travel distance of the slug with respect to the initial slug length. Another change that was made on program BOZKUŞ-2 is the use of Swamee-Jain formula (Walski [11]; and Swamee-Jain [12]) to calculate the friction factor for the flow of gas and the liquid slug, instead of using fixed value.

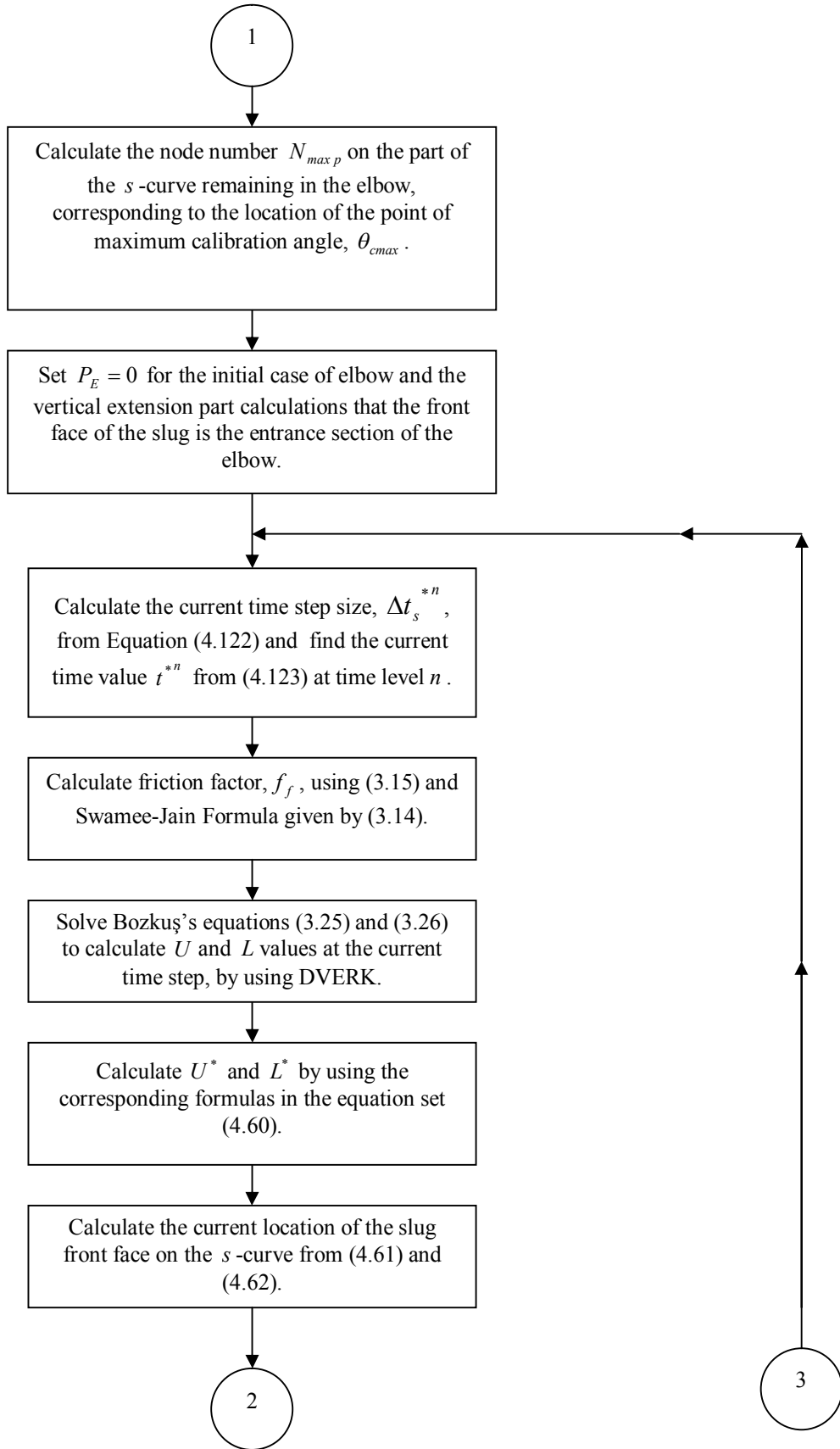
In the elbow and the vertical extension part calculations of program KAYHAN, the incompressible cylindrical polar Reynolds Equations are solved over the elbow, and incompressible 1-D cartesian Reynolds Equation is solved along the axis of the vertical extension part (Figure 4.5). The solution domain for the Reynolds

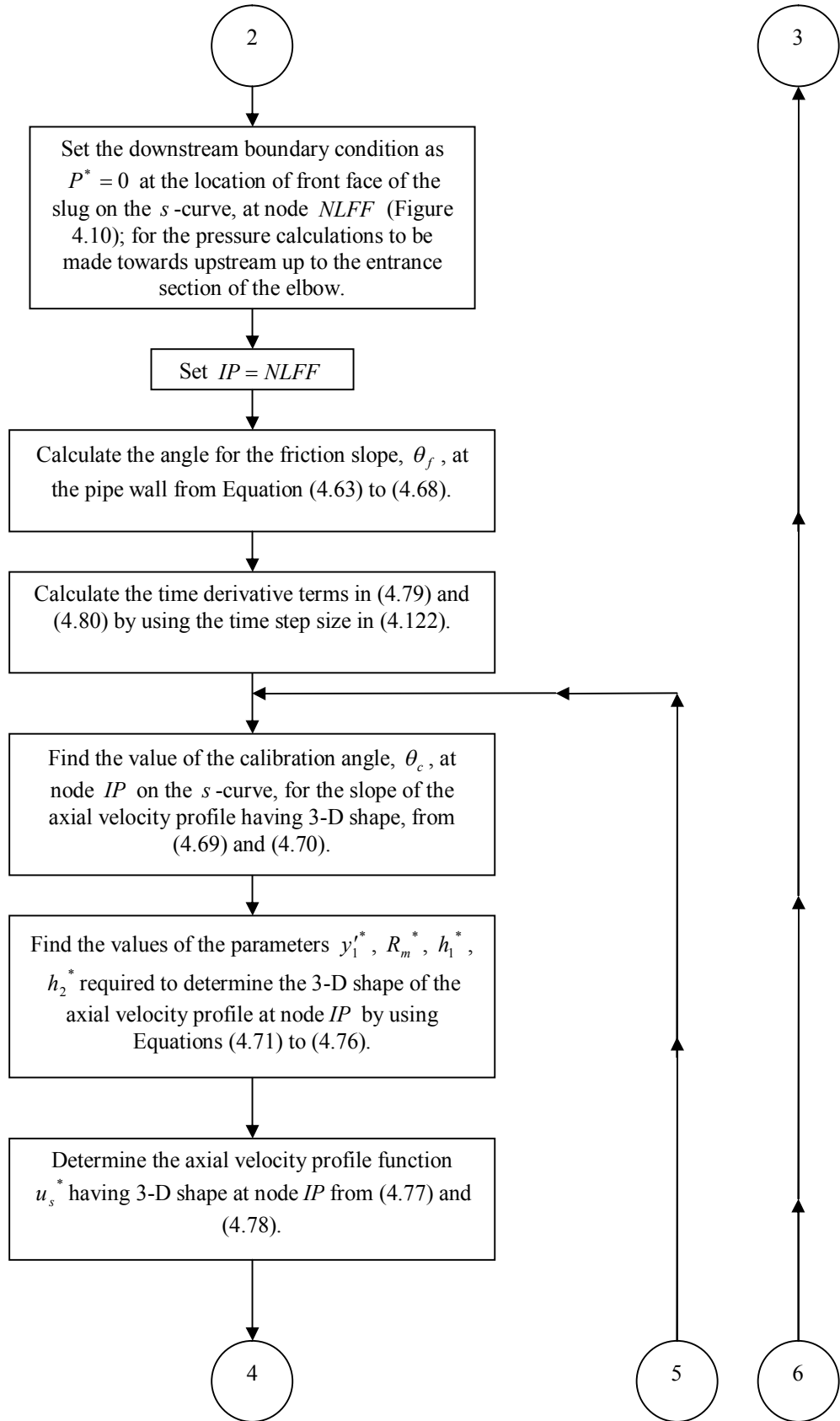
Equations is taken as the region between the entrance section of the elbow and location of the front face of the liquid slug if the slug front face is at a stage of advancing in the elbow or the vertical extension part, and the domain is selected as the whole region within the elbow and the vertical extension part if the slug front has exited to the atmosphere from the end section of the vertical extension part. For the solution of the average pressure values in the elbow and the vertical extension part, the downstream boundary condition is taken as zero atmospheric pressure at the slug front face location or at the cross-section at the exit of the vertical extension part, and the average pressure values are solved towards upstream up to the entrance section of the elbow shown in Figure 4.10 with backward differences and using a subroutine DVERK, developed by Hull and et. al. [25], which is an ordinary-differential-equation-solver that uses Runge-Kutta-Verner 5th and 6th order method. The solution for the average pressure distribution along the elbow and the vertical extension part is made at every time step, and the location of the front face of the slug needed as downstream boundary condition for this procedure is calculated at the beginning of each time step by using the kinematics of the liquid slug. The slug kinematics is determined at the beginning of each time step by solving the slug velocity from Bozkuş's [2] slug dynamics equations as applied on that part of the slug remaining in the horizontal part of the pipeline. While calculating the velocity from these equations, the retarding average pressure value at the entrance section of the elbow is also considered in program KAYHAN. During the elbow part calculations, after the calculation of the average pressure at a cross-section, the cylindrical polar Reynolds Equation written in the direction of radius of curvature of the elbow is solved with DVERK along a line mesh starting from the center point of the elbow cross-section up to the top point of that cross-section on the convex side of the elbow, to find the local impact pressures at these top points (Figure 4.8). Here, the starting local pressure value as the boundary condition at the center point of the cross-section is taken as equal to the average pressure at the same cross-section of the elbow as an assumption. The horizontal and vertical components of the transient forces acting on the center points of the volume elements along the axes of the elbow and the vertical extension part are also found by using the calculated average pressure values at the upstream and downstream faces of the volume elements and with the application of

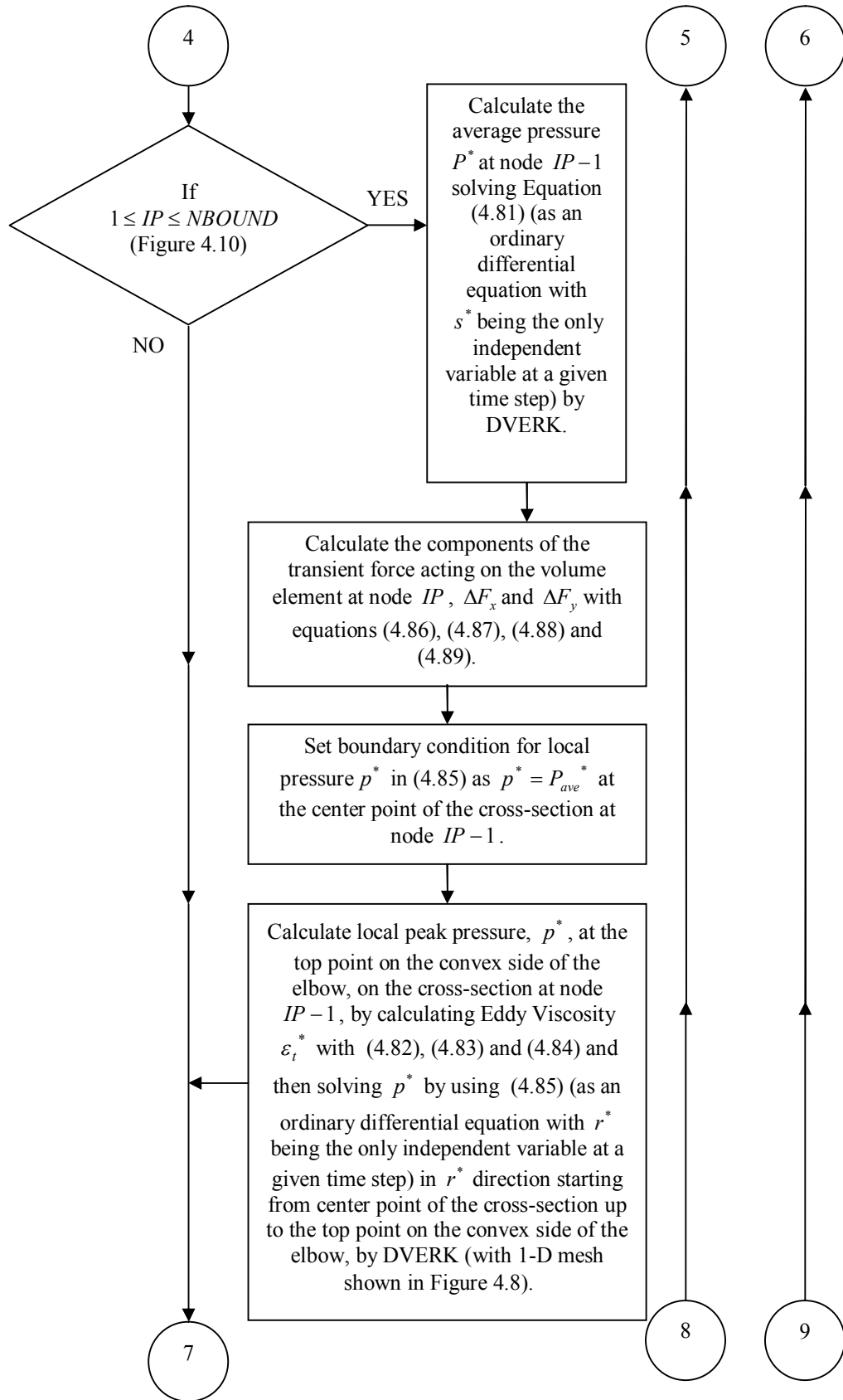
conservation of momentum principle on these volume elements. In this way, a set of values for the impact pressure distribution along the elbow and another set of transient force values acting on the volume elements along the elbow and the vertical extension part were obtained for each time step of the calculations. The discharge through the pipe was taken as constant at any time step all along the horizontal pipe, elbow and the vertical extension parts due to incompressible flow assumption made for the liquid slug. However, the variation of the shape of the velocity profile along the elbow and the vertical extension parts are taken into consideration. During the solution of the Reynolds Equations, an axial velocity profile function is assumed for the flow of the liquid slug in the elbow and the vertical extension part, and the variation of 3-D shape of this axial velocity profile along the elbow and the vertical extension part is calibrated with the aid of a calibration function. Parameters of the calibration function is determined based on a set of experimental data for the peak pressures at the elbow, given in Bozkuş's [2] study. When the upstream face of the slug, which is advancing in the horizontal part of the pipeline comes to very close locations before the entrance section of the elbow, the simulation is stopped to leave the calculations with unstable oscillations that would arise due to slug's being unstable under the effect of driving and retarding forces reaching very close values

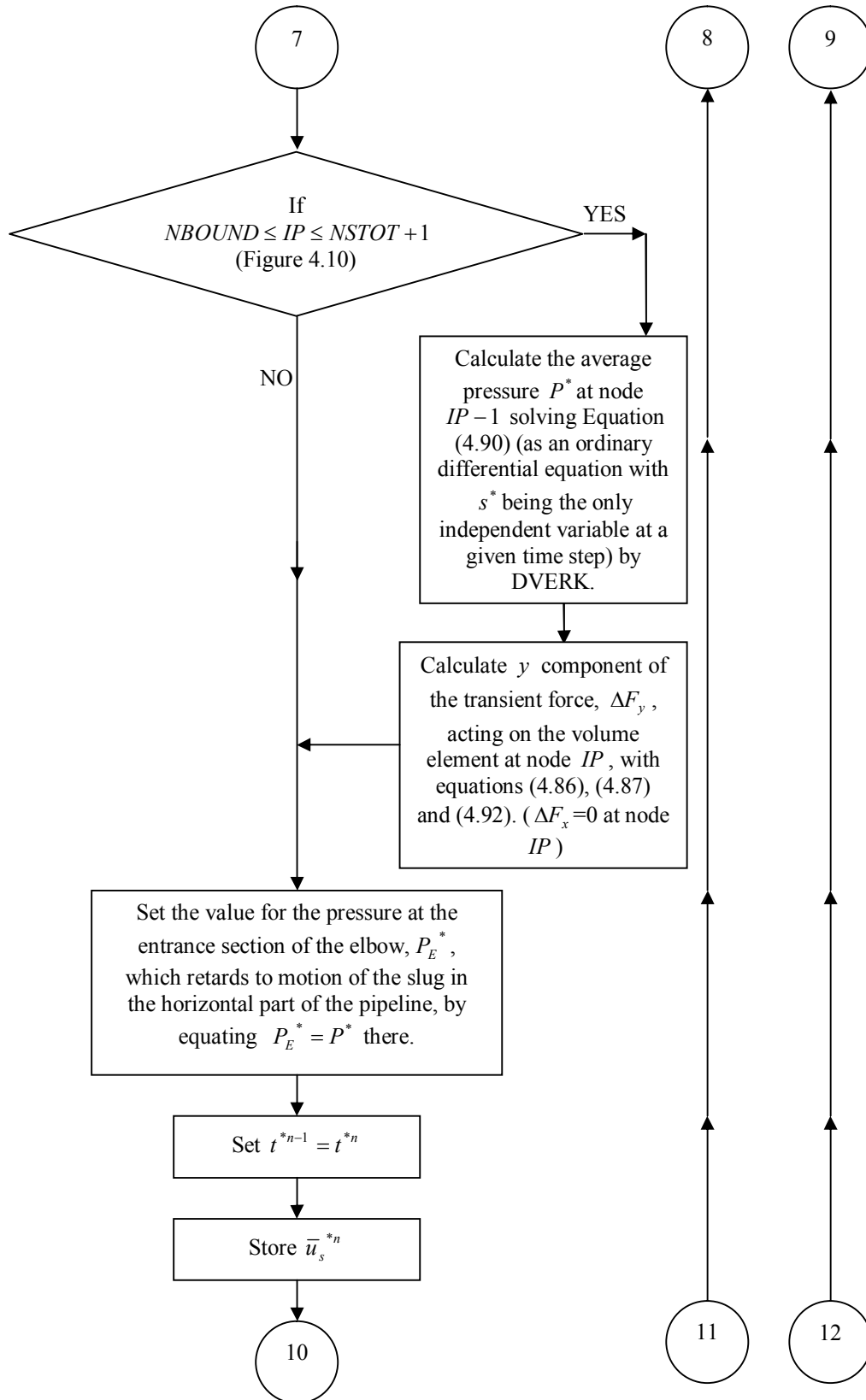
C.2 Flow-Chart for the Computer Code KAYHAN

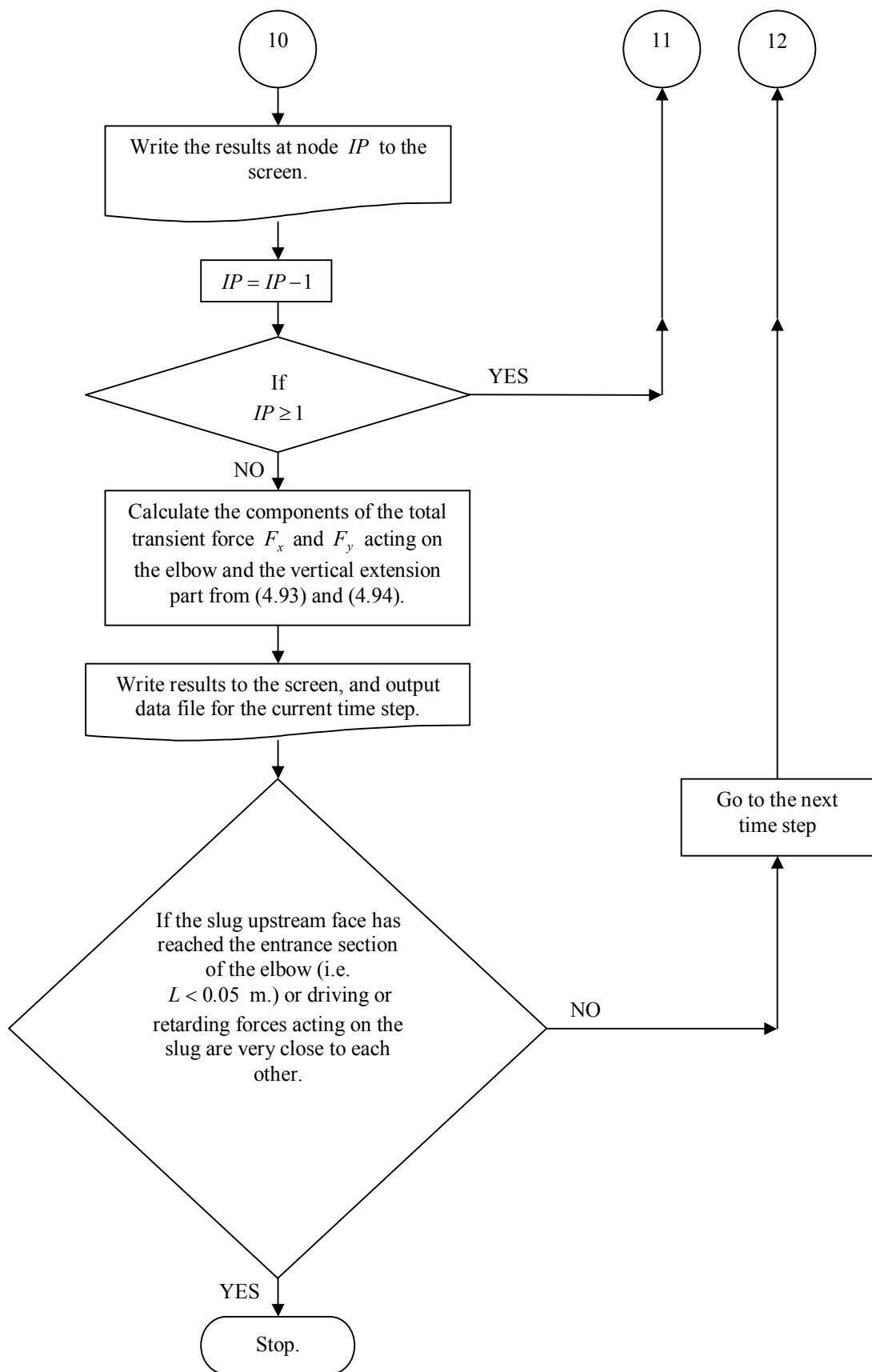












C.3 Computer Code KAYHAN in FORTRAN Language

```

C      KAYHAN.F
C      CCCCCCCCCCCCCCCCCCCCCCCCCC      PROGRAM DESCRIPTION      CCCCCCCCCCCCCCCCCCCCCC
C
C      This program simulates the experimental model used to
C      investigate the hydro-dynamics of a liquid slug motion. The
C      experimental model consists of an air tank and water storage tank
C      at the upstream. Attached to the air tank is a 31 ft long, 2"
C      diameter, transparent, horizontal pipe. At the downstream section of
C      an elbow is attached to the piping, a dynamic pressure transducer
C      located on this elbow is used to measure the pressures during
C      the impact of the liquid slug on the elbow. A certain length of a liquid
C      slug is generated at the upstream section by filling a segment of
C      the pipe by gravity through a hose connected to the water storage tank.
C      The U/S end of the segment now filled with water can be pressurized
C      by simply pressurizing the air tank to which the segment is connected.
C      The only mechanism keeping the liquid slug in place is a quick opening
C      ball valve located at the D/S end of the segment. The motion is started
C      by quickly opening this ball valve. The liquid slug then moves into
C      the initially empty pipe. During the impact around the elbow, the dynamic
C      pressure is recorded.
C
C      It is the objective of this program to simulate numerically the above
C      described phenomenon with an acceptable accuracy by taking into
C      account the gas dynamics behind the slug. The program employs the
C      method of characteristics for the gas dynamics using the U/S air tank as
C      the upstream boundary and treating the slug hydro-dynamics as the moving
C      downstream boundary condition. The static pressure variation in the
C      U/S air tank is measured initially by a differential pressure transducer,
C      this data will be put in the program as part of the U/S boundary
C      conditions. The theory behind the program assumes that the ideal gas law
C      holds in the system. Isothermal gas law is assumed during the entire
C      motion. The fact that slug loses some mass during its motion in the
C      pipe due to frictional effects, is considered by using a coefficient
C      called void ratio coeff. in the slug hydro-dynamics equations.
C
C      The program will compute air velocity, air pressure, air density
C      slug velocity, slug length, slug position, and time at which those
C      variables are computed.
C
C      At the time slug impacts the elbow, the peak pressure caused by the
C      momentum change will be computed from the velocity, density of the
C      slug. (i.e.  $(\rho) \cdot u^2$ )
C
C      Written by Zafer Bozkus, in May-June 1990.
C      CCCCCCCCCCCCCCCCCCCCCCCCCCCCCCCCCCCCCCCCCCCCCCCCCCCCCCCCCCCCCC
C
C      THE PRESSURE DISTRIBUTION CALCULATIONS AT THE ELBOW ARE MADE AS AN
C      INITIAL VALUE PROBLEM USING THE IMSL LIBRARY SUBROUTINE WITH THE
C      NAME DVERK, IT IS A DIFFERENTIAL EQUATION SOLVER - RUNGE KUTTA -
C      VERNER FIFTH AND SIXTH ORDER METHOD.
C      HERE IS HOW TO COMPILE THE SOURCE FILE FOR THIS PROGRAM ON VAX/VMS
C      USING THE OLD VERSION OF THE IMSL LIBRARY.
C
C      FOR FILENAME                                (NO EXTENSION!)
C      LINK FILENAME, LOCAL:[IMSL.V92]IMSL/LIB      (NO EXTENSION!)
C      RUN FILENAME                                (NO EXTENSION!)
C
C      LAST MODIFIED ON April 5, 1990 (CORRECTED MOMENTUM EQUATION)
C      LAST MODIFIED ON JUNE 26, 1990 (ELBOW MODELING ADDED)
C      (NO HOLDUP AT THE ELBOW CONSIDERED)
C
C-----
C      ON November 15, 2007 A NUMERICAL ANALYSIS PART WAS ADDED FOR THE
C      DETERMINATION OF THE PRESSURE DISTRIBUTION AT THE ELBOW AND AT THE
C      EXTENSION PART DOWNSTREAM THE ELBOW, BY BÜLENT ABBAS KAYHAN.
C-----
C      ON May 24, 2008 PRESSURE DISTRIBUTION CALCULATIONS AT THE ELBOW
C      AND THE VERTICAL EXTENSION PART WERE DEVELOPED BY USING A
C      CYLINDRICAL COORDINATE SYSTEM FOR THE ELBOW PART, 2-D GAUSS
C      QUADRATURE FOR NUMERICAL INTEGRATION, AND A CORRELATION FUNCTION
C      FOR THE HOLD UP COEFFICIENT, BY BÜLENT ABBAS KAYHAN.

```



```

REAL*8 PAVE(1),PCNVX(1),PAVEST(1),PCVXST(1)
REAL*8 QPRETS,QPTSST
REAL*8 EPSLN,UAVEI
REAL*8 TI1,PAVE1
REAL*8 SAV,SALR,SAPR,SAPT,SAPRG,SAPTG
REAL*8 XOUT(N3),Y1OUT(0:N3),Y2OUT(N3),SSOUT(N3),PDOUT(N3,N4)
REAL*8 DFXOUT(N3,N4),DFYOUT(N3,N4)
REAL*8 FXOUT(N4),FYOUT(N4)
REAL*8 CLSTRT
REAL*8 DSCST1,DBETA1
REAL*8 PAVNST,PAVUST,PAVMST,PAVDST,PAVPST
REAL*8 SCNST,SCUST,SCMST,SCDST,SCPST
REAL*8 FXST,FYST,FX,FY
REAL*8 SCSTCP
REAL*8 SNMST,PNMST,PNM1ST,PNM2ST,PPEAST
COMMON/ COEFFS/ C1, C2, C3
COMMON/ CONST/PB,RO,PAVE,MU
CHARACTER CC*15
EXTERNAL UST,DBUST,TRARLN,UP2ST,PDS1ST,PDS2ST,PCTFST
COMMON /PRM1S1/ R,TC,TF,QST,PI
COMMON /PRM2S2/ RMST,UMST,LPR,UPR,TPR
COMMON /PRM3S3/ DKSIST,DETA
COMMON /PRM4S4/ R0,DBETA,DSCST
COMMON /PRM5S5/ MR,MC,ML
COMMON /PRM6S6/ EMELRT
COMMON /PRM7S7/ TCMAX,SCMAX,SCELB
COMMON /PRM8S8/ BSL,BSU,NB
COMMON /PRM9S9/ QPTSST,TIST
COMMON /PRM10S10/ EPSLN,D,F
COMMON /PRM11S11/ DRCLST
COMMON /PRM12S12/ DSCST1,DBETA1
COMMON /PRM13S13/ UM1ST,UM2ST,RM1ST,RM2ST,TC1,TC2
COMMON /PRM14S14/ PAVUST,PAVDST
COMMON /PRM15S15/ SCUST,SCMST,SCDST
COMMON /PRM16S16/ ACRSS
COMMON /PRM17S17/ SCSTCP
COMMON /TERMS2/ C4,C6,C7,C8
COMMON /TERMS3/ C9,C10,C11,C12
COMMON /TERMS4/ DRDIST,MLD
COMMON /TERMS6/ BETA,G
COMMON /W/ C15
COMMON /DBDVR/ IP,IPD
EXTERNAL FCN2
C-----
C
C ----- ENTER INPUT DATA -----
C
C-----
      WRITE(*,33)
33  FORMAT(' PLEASE ENTER NAME OF INPUT FILE:',$)
      READ(5,'(A)') FINP
      OPEN(UNIT=1,FILE=FINP,FORM='FORMATTED',STATUS='OLD')
      READ(1,271) N
271  FORMAT(/,I10)
      WRITE(*,66)
66  FORMAT(' ENTER NAME OF TANK PRESSURE DATA FILE:',$)
      READ(*,'(A)') FDAT
      OPEN(UNIT=3,FILE=FDAT,FORM='FORMATTED',STATUS='OLD')
      DO 6 M=1, N
      READ(3,*) T(M), PL(M)
6  CONTINUE
      PRES=PL(1)
      PRI=PRES
      WRITE(*,67)
67  FORMAT(' ENTER THE NAME OF THE PEAK PRESSURE TIME HISTORY OUTPUT D
*ATA FILE:',$)
      READ(*,'(A)') FDAT2
      OPEN(UNIT=7,FILE=FDAT2,FORM='FORMATTED',STATUS='NEW')
      WRITE(*,68)
68  FORMAT(' ENTER THE NAME OF THE TIME HISTORIES OUTPUT DATA FILE FOR
* Fx AND Fy:',$)
      READ(*,'(A)') FDAT3
      OPEN(UNIT=8,FILE=FDAT3,FORM='FORMATTED',STATUS='NEW')
C-----

```

```

READ(1,273) EPSLN,D
READ(1,273) DA,DW
READ(1,273) MUA,MUW
READ(1,274) PLL
READ(1,274) TEMP
READ(1,274) PO
READ(1,273) VF,XI
READ(1,274) LSS
READ(1,274) R0
READ(1,274) G
READ(1,274) LEXTSN
READ(1,274) KM
READ(1,274) PAVE(1)
READ(1,275) MR
READ(1,274) MRT
READ(1,275) ML
READ(1,274) CLSTRT
READ(1,275) MLPRSS
READ(1,275) NSLUG
READ(1,274) SCMAX
272 FORMAT(/,F16.7,F16.7,F16.7)
273 FORMAT(/,F16.7,F16.7)
274 FORMAT(/,F16.7)
275 FORMAT(/,I10)
CLOSE(UNIT=1)
WRITE(*,35) EPSLN,D,DA,DW,MUA,MUW,PLL,TEMP,PO,VF,XI,LSS,PRES,N
WRITE(*,36) R0,G,LEXTSN,KM,PAVE(1),MR,MRT,ML,NSLUG,SCMAX
35 FORMAT(/,4X,' EPSLN=',F12.8,2X,' D=',F7.4,2X,' DA=',F8.2,2X,' DW='
+,F8.2,/,4X,' MUA=',F10.8,2X,' MUW=',F10.8,2X,' PLL=',F7.3,2X,
+' TEMP=',F5.1,/,4X,' PO=',F10.1,2X,' VF=',F7.4,2X,' XI=',F6.2,2X,
+' LSS=',F7.3,/,4X,' PRES=',F10.4,2X,' N=',I7/)
36 FORMAT(4X,' R0=',F7.4,2X,' G=',F6.4,2X,' LEXTSN=',F8.4,2X,' KM=',
+F6.2,2X,/,4X,' Boundary value for PAVE(1)=',F14.4,/,4X,' MR=',I6,
+2X,' MRT=',F6.2,2X,' ML=',I6,2X,' NSLUG=',I5,2X,' SCMAX=',F7.3)
C-----
WRITE(*,98)
98 FORMAT(' PLEASE ENTER NAME FOR SCREEN OUTPUT DATA FILE:',$)
READ(*,'(A)') FPLOT
OPEN(UNIT=2,FILE=FPLOT,FORM='FORMATTED',STATUS='NEW')
C-----
WRITE(2,35) EPSLN,D,DA,DW,MUA,MUW,PLL,TEMP,PO,VF,XI,LSS,PRES,N
WRITE(2,36) R0,G,LEXTSN,KM,PAVE(1),MR,MRT,ML,NSLUG,SCMAX
C-----
WRITE(*,93)
93 FORMAT(' WOULD YOU LIKE TO CREATE A DIMENSIONLESS PARAMETER FILE F
+OR THE HORIZONTAL',/,' PART OF THE PIPE LINE ? TYPE (Y) ES OR (N)
+O:',$)
READ(*,'(A)') ANSW
C-----
IF(ANSW(1:1).EQ.'Y'.OR.ANSW(1:1).EQ.'y') THEN
    SAYI=1.
    WRITE(*,94)
94 FORMAT (' Enter Name for Dimensionless Output File:',$)
    READ(*,'(A)') FDIM
    OPEN(UNIT=4,FILE=FDIM,FORM='FORMATTED',STATUS='NEW')
    ENDIF
C-----
C-----
DO 7 I = 1, N
C converting the U/S gage pressure in psi to abs. pressure in pascals)
    PL(I) = ((PL(I)/14.7) + 1.)*PO !Equation (3) U/S
C setting the U/S boundary position equal to zero.
    XL(I) = 0.
7 CONTINUE
C-----
C-----COMPUTATION COEFFICIENTS-----
C-----
TABS=TEMP+273
CWS = SQRT(287.0*TABS) !Equation (5)
C-----
PP = 2*PLL + XI !computation of stopping criterion value
EP = PLL+ LSS !computation of slug location
ELLOC=EP
C-----

```

```

        WRITE(*,34) TABS,CWS,PP,EP
        WRITE(2,34) TABS,CWS,PP,EP
34      FORMAT(/,4X,' TABS=',F7.2,2X,' CWS=',F11.5,2X,' PP=',F9.4,2X,
        *'EP=',F9.4,/)
C-----
C-----
C-----
C-----BOUNDARY CONDITIONS-----
C-- The initial conditions or known values at the earlier time
C-- steps have the subscript, S.
C-- The unknowns at U/S boundary have the subscript, L.
C-- The unknowns at D/S boundary have the subscript, R.
C-----
C
999    IF (PLL/LSS.LE.6.6519) THEN
        VF1=0.0385*(PLL/LSS)+0.7439
    ELSE
        VF1=1.
    ENDIF
C    ABOVE EQUATION IS A CORRELATION FUNCTION USED FOR VOID COEFFICIENT
C    CALCULATION
        RTO=2*(1-VF1)/VF1
        AA = 0.5*RTO
C-----
C setting the initial conditions
        XS(0) = XI
        LS(0) = LSS
        VS(0) = 0.
        TS(0) = 0.
        PS(0) = PL(1)
        ALPHA = 0.
        DT1 = 0.
        DAS(0)=PL(1)/CWS**2
        COUNT=0.
C-----
C
C-----
        WRITE(*,108)
        WRITE(2,108)
108    FORMAT(/,1X,'TR(sec.)',1X,'PR(psi)',1X,'VR(m/s)',1X,'LR(m)',2X,
        +'LOC(m)',1X,'MOM(psi)',1X,'TL(sec)',1X,'PL(psi)',1X,'VL(m/s)',
        +1X,'dP/dx')
C-----
        IF (SAYI.EQ.1.0) THEN
            WRITE(4,777)
777    FORMAT(' TSTAR      PSTAR      LSTAR      XSTAR      VSTAR')
        ENDIF
C-----
C
        VL(0)=0.
C----- ACTUAL COMPUTATIONS -----
        DO 20 I=0,N
            J=I+1
            K=J+1
C
            IF (PLL/LS(I).LE.6.6519) THEN
                VF=0.0385*(PLL/LS(I))+0.7439
            ELSE
                VF=1.
            ENDIF
            RTO=2*(1-VF)/VF
C-----
            IF (VL(J-1).NE.0.) THEN
                CALL FCAL(ABS(VL(J-1)),DA,MUA,EPSLN,D,FA)
            ELSE
                FA=0.
            ENDIF
            FDA = FA/(2*D)
C-----
C    ABOVE EQUATION IS A CORRELATION FUNCTION USED FOR VOID COEFFICIENT
C    CALCULATION
C-----UPSTREAM BOUNDARY COMPUTATIONS-----
C
        TL(J) = TS(I) + (XL(J)-XS(I))/(VS(I)-CWS)      !Equation (2) U/S

```

```

      DT = TL(J) - TS(I)                                !Equation (6) U/S
C-----
      ALPHA = TL(J)
      CALL LINEAR(T,PL,N,ALPHA,S)
      PT(J)=S
C      PL(J) = S
      DAL(J) = S/CWS**2                                !Equation (4) U/S
C-----
      R= (CWS*DAS(I)*(FDA*VS(I)*DT+1.0))
      VL(J)=(S-PS(I)+CWS*DAS(I)*VS(I))/R                !Equation (1) U/S
C
C----- DOWNSTREAM BOUNDARY COMPUTATIONS-----
C
C-----
      IF (VS(I).NE.0.) THEN
        CALL FCAL(VS(I),DA,MUA,EPSLN,D,FA)
      ELSE
        FA=0.
      ENDIF
      IF (VS(I).NE.0.) THEN
        CALL FCAL(VS(I),DW,MUW,EPSLN,D,FW)
      ELSE
        FW=0.
      ENDIF
      FDW = FW/(2*D)
      FDA = FA/(2*D)
C-----
C.....Following Equation is equation (8) D/S.....
      XR(K) = ((VS(I)*DT+XS(I))* (VL(J)+CWS) -XL(J)*VS(I)) / ((VL(J)+
      *CWS)-VS(I))
      DT1 = (XR(K) - XL(J)) / (VL(J)+CWS)                !Equation (2) D/S
      TR(K) = TL(J) + DT1                                !Equation (2) D/S
      DT2 = TR(K) - TS(I)                                !Equation (4) D/S
      LR(K) = LS(I)-0.5*RTO*VS(I)*DT2                    !Equation (5) D/S
      A = (FDA*VL(J)*DT1 + 1)*DAL(J)*CWS
      B = 1+(FDW - RTO/LS(I))*VS(I)*DT2
      PR(K) = S+DAL(J)*CWS*VL(J) -
      2(A/B)*((1./DW)*((PS(I)-PO)/LS(I))*DT2 + VS(I))    !Equation (1) D/S
      VR(K) = ((1./DW)*((PS(I)-PO)/LS(I))*DT2 + VS(I))/B !Equation (6) D/S
C----- PRINTING DATA FOR PLOTS-----
      MOM(K)=(DW*VR(K)**2)/6891.1565                    !RHO*V**2 Term in psi.
      LOC(K)=XR(K)+LR(K)-XI                              !Front Loc. from U/S elbow
C-----
C--- Computation of slug arrival time and peak pressure at the elbow, using
C--- interpolation.
      IF(COUNT.EQ.0.AND.LOC(K).GE.EP) THEN
        SAT = TR(K-1) + ((TR(K)-TR(K-1))*(EP-LOC(K-1)))/(LOC(K)-LOC(K-1))
        SAV = VR(K-1) + ((VR(K)-VR(K-1))*(EP-LOC(K-1)))/(LOC(K)-LOC(K-1))
        PPE = MOM(K-1)+((MOM(K)-MOM(K-1))*(EP-LOC(K-1)))/(LOC(K)-LOC(K-1))
        SALR = LR(K-1) + ((LR(K)-LR(K-1))*(EP-LOC(K-1)))/(LOC(K)-LOC(K-1))
        SAPR = PR(K-1) + ((PR(K)-PR(K-1))*(EP-LOC(K-1)))/(LOC(K)-LOC(K-1))
        SAPT = PT(J-1) + ((PT(J)-PT(J-1))*(EP-LOC(K-1)))/(LOC(K)-LOC(K-1))
        COUNT=1
      ENDIF
C-----
      PSK=(PR(K)-PO)/6891.1565                          !Gage press. behind slug
      PSJ=(S-PO)/6891.1565                              !Gage press.in the tank
C-----
      PX=(PSJ-PSK)/TR(K)
C-----
      WRITE(*,109)TR(K),PSK,VR(K),LR(K),LOC(K),MOM(K),TL(J),PSJ,VL(J),PX
      WRITE(2,109)TR(K),PSK,VR(K),LR(K),LOC(K),MOM(K),TL(J),PSJ,VL(J),PX
109  FORMAT(1X,F7.5,2X,F6.3,1X,F7.3,1X,F6.4,1X,F6.3,1X,F7.2,2X,
      2F8.6,2X,F6.3,1X,F6.3,1X,F7.5)
C-----
C-----
C----- COMPUTE THE SCALED PARAMETERS TO BE USED LATER.
      IF (I.EQ.0) THEN
        CALL FCAL(VR(K),DW,MUW,EPSLN,D,FW)
        LO= (2*D/FW)*(1-AA)                             !Length Scaling Parameter
        VO = SQRT((PRES*6891.1565)/DW)                  !Velocity Scaling Parameter
        TO = LO/VO                                       !Time Scaling Parameter
      ENDIF
C----- COMPUTE AND PRINT DIMENSIONLESS PARAMETERS

```

```

C-----
      IF(SAYI.EQ.1.0) THEN
        VSTAR = VR(K)/VO           !Scaled Slug Velocity
        PSTAR = PSK/PRES           !Scaled Driving Pressure
        LSTAR = LR(K)/LO           !Scaled Slug Length
        TSTAR = TR(K)/TO           !Scaled Time
        XSTAR = LOC(K)/LO           !Scaled Slug Position
        WRITE(4,110) TSTAR, PSTAR, LSTAR, XSTAR, VSTAR
110    FORMAT(F10.6,2X,F10.7,2X,F10.7,2X,F10.5,2X,F10.5)
        ENDIF

C-----
C-----
C      STOPPING CRITERIA
C      WHEN INPUT DATA TIME RANGE WAS PASSED/OR THE SLUG PASSED THE
C      ELBOW BY PLL AND/OR SLUG LENGTH REDUCES TO ZERO.
      IF(TR(K).GT.(0.98*T(N)).OR.XR(K).GE.PP.OR.LR(K).LE.0.10) THEN
888    WRITE(*,106)
C      WRITE(3,106)
106    FORMAT( ' SLUG LENGTH HAS APPROACHED ZERO! ',/,
+           ' OR SLUG TRAVELLED THE SPECIFIED DISTANCE! ',/,
+           ' OR INPUT DATA TIME RANGE WAS PASSED!!!' )
        WRITE(*,111) SAT,PPE,EP
        WRITE(2,111) SAT,PPE,EP
111    FORMAT( ' Slug arrived at the elbow at ',1X,F7.5,1X,'sec.',/,
+           ' peak pressure due to momentum was ',F8.2,1X,'psig',/,
+           ' Elbow location is ',1X,F6.3,1X,'meters',///)
        GO TO 200
      ELSE
        CONTINUE
      ENDIF

C
C  SLUG Subscript Adjustments
      TS(I+1) = TR(K)
      VS(I+1) = VR(K)
      PS(I+1) = PR(K)
      XS(I+1) = XR(K)
      LS(I+1) = LR(K)
      DAS(I+1) = PR(K)/CWS**2

C
20    CONTINUE
C
C---Compute scaled arrival time, peak pressure,and elbow location
C
C-----
200    IF(SAYI.EQ.1.0) THEN
      SAT=SAT/TO
      PPE = PPE/PRES
      EP = EP/LO
      WRITE(4,112) SAT,PPE,EP
      WRITE(4,113) TO,VO,LO,PRES
      WRITE(*,112) SAT,PPE,EP
      WRITE(*,113) TO,VO,LO,PRES
      ENDIF

C-----
112    FORMAT( //' Scaled Arr. Time at the elbow is ',1X,F9.5,/,
+           ' Scaled Peak Pres. at the elbow is ',F8.4,/,
+           ' Scaled Elbow Location is ',1X,F6.3,/)

C-----
113    FORMAT( ' Scaling parameter for time was T =',2X,F7.5,1X,'sec.',/,
+           ' Scaling parameter for vel. was V =',2X,F10.2,1X,'m/s',/,
+           ' Scaling parameter for length was L =',2X,F10.7,1X,'m',/,
+           ' Scaling parameter for pressure was Pi =', F7.3,1X,'psig')

C-----
      Y1OUT(0)=SAV

C-----
C-----CALCULATIONS FOR THE ELBOW-----
C-----
      N2=N
199    CONTINUE
      WRITE(*,202)
202    FORMAT(1X,'Initializations for the arrays are being made...')
      DO 201 II=1,N3
      DO 201 JI=1,N4
        PDOUT(II,JI)=0.

```

```

        DFXOUT(II,JI)=0.
        DFYOUT(II,JI)=0.
201    CONTINUE
        WRITE(*,203)
203    FORMAT(1X,'Initializations for the arrays were completed.',///)
        DO 198 I = 1, N2
C      converting th U/S abs. pressure in pascals to gage pressure in pascals
        PL(I) = PL(I)-PO
198    CONTINUE
        MU=MUW
        RO=DW
        PI=4.*ATAN(1.)
        R=D/2.
        QPRETS=Y1OUT(0)*PI*R**2
        PWET=2*PI*R
        ACRSS=PI*R**2
        LELBW=1/4.*2*PI*RO
C      Derived Lengths
        LSLIMP=SALR
        DSC=LSLIMP/NSLUG
        TIIN=DSC/SAV
        WRITE(*,232) 'Space increment along the s-curve, DSC (m.) :',DSC
        WRITE(2,232) 'Space increment along the s-curve, DSC (m.) :',DSC
232    FORMAT(1X,A45,F12.8)
        TPR=TIIN
        LPR=2*LELBW/KM
        UPR=LPR/TPR
        QPTSST=QPRETS/(UPR*LPR**2)
C      For the elements of the computational mesh at any cross-
C      section of the pipe:
C      MR= number of mesh elements radial direction; MC= number of mesh
C      elements in the circumferential direction.
        MC=MR*MRT
        MSHSZ=MR*MC
        WRITE(*,230) "Mesh size over the pipe cross-section: MR x MC=",MR,
        *"  x",MC
        WRITE(2,230) "Mesh size over the pipe cross-section: MR x MC=",MR,
        *"  x",MC
230    FORMAT(/,1X,A47,I5,A3,I5)
        DKSI=R/MR
        DKSIST=DKSI/LPR
        DELTA=2*PI/MC
C-----
        WRITE(*,233) "Maximum mesh size for the line integrals at any cros
        *s-section: ML=",ML
        WRITE(2,233) "Maximum mesh size for the line integrals at any cros
        *s-section: ML=",ML
233    FORMAT(1X,A66,I5,A3,I5)
C-----
C-----
C      For the nodal points of the computational mesh along the
C      elbow:
C      The starting node at the upstream end of the elbow is NODE 1.
        EMELRT=1./100
C      EMERLT: End Mesh Element Lentgth Ratio
        NELBW=LELBW/DSC+1
        DSLAS1=LELBW-(NELBW-1)*DSC
        DSLST1=DSLAS1/LPR
C      The criteria here in this IF statement above was also used
C      for the starting node (NSTOT) of the backward calculational
C      procedure along the curve s.
        IF (DSLST1.LE.DSC*EMELRT) THEN
            NELBW=NELBW-1
            DSLST1=0.
        ENDIF
        NEXTSN=LEXTSN/DSC+1
        DSLAST=LEXTSN-(NEXTSN-1)*DSC
C      The criteria here in this IF statement above was also used
C      for the starting node (NSTOT) of the backward calculational
C      procedure along the curve s.
        IF (DSLAST.LE.DSC*EMELRT) THEN
            NEXTSN=NEXTSN-1
            DSLAST=0.
        ENDIF

```

```

DSCST=DSC/LPR
DSCNST=DSLST/LPR
NSTOT=NELBW+NEXTSN
LTOT=LELBW+LEXTSN
LTOTST=LTOT/LPR
SCEXT=LTOT
SCENT=0.
DBETA=DSC/R0
DBELST=DSLST1/R0
NLBF=0
NLFF=0
WRITE(*,262) NELBW
WRITE(2,262) NELBW
262 FORMAT(1X,'Total number of volume elements along the elbow: NELBW=
* ',I5)
WRITE(*,261) NSTOT
WRITE(2,261) NSTOT
261 FORMAT(1X,'Total number of volume elements along the total s-curve
*: NSTOT=',I5)
WRITE(*,270) MLPRSS
WRITE(2,270) MLPRSS
270 FORMAT(1X,'Mesh size along the pipe radius for local pressure calc
* ulation at the ',/,1X,'pipe wall: MLPRSS=',I5,/)
C      Clustering of the line mesh for the line integral.
CALL MCLSTR(R,ML,CLSTRT,DRCLST)
C-----
C      An initial calculation for the value of the friction angle TF.
UAVEI=SAV
IF (UAVEI.NE.0.) THEN
CALL TFCAL(UAVEI)
ELSE
F=0.
ENDIF
C-----
TCLMAX=TF*180/PI
TCDMAX=0.0124*(PLL/LSS)**3-0.2072*(PLL/LSS)**2+1.1001*(PLL/LSS)
*+87.951
WRITE(*,269) TCDMAX
WRITE(2,269) TCDMAX
269 FORMAT(1X,'Maximum calibration angle of the velocity profile in de
* grees that occurs along ',/, " the s-curve: TCDMAX=",F9.5,/)
IF (TCDMAX.GT.TCLMAX) THEN
WRITE(*,281) TCLMAX
WRITE(2,281) TCLMAX
281 FORMAT(1X,'The calculated maximum calibration angle TCDMAX is grea
* ter than ',F9.4,/, ' degree, which is the maximum allowable value.')
WRITE(*,282)
WRITE(2,282)
282 FORMAT(/,1X,'Program failed to continue...')
STOP
ENDIF
SCELB=LELBW
TCMAX=TCDMAX/180*PI
C-----
C      The nodal point on the elbow axis, for which the maximum
C      pressure at the convex side of the elbow occurs, is calculated
C      here.
NMAXP=INT((SCMAX/LPR-DSCST/2.)/DSCST+0.5+0.5)+1
WRITE(7,13) 'NMAXP=',NMAXP
13 FORMAT(1X,A6,I5,/)
WRITE(7,12) 'Time(s)', 'Peak Pressure(psi)'
12 FORMAT(4X,A7,12X,A18)
C-----
WRITE(8,17) 'Time(s)', 'Fx (N)', 'Fy (N)'
17 FORMAT(4X,A7,8X,A6,8X,A6)
C-----
WRITE(*,15) 'Output for the Pressure Distribution at each Time Ste
*p: '
15 FORMAT(/,1X,A55)
WRITE(2,14)
14 FORMAT(/,1X,'T (sec.)',3X,'VF (m/s)',3X,'LSS (m)'
*,2X,'Tank (psi)',5X,'Rise ',3X,'Scaled Rise'/)
C-----
J=0

```

```

      FROLST=0.
      XEND=SAT
      XPRES=XEND
      Y(1)=SAV
      Y(2)=SALR
      SAPRG=SAPR-PO
      SAPTG=SAPT-PO
C-----
      DO 16 I = K, N2
C-----
      TI=DSC/Y(1)
      UAVE=Y(1)
      IF (UAVE.NE.0.) THEN
      CALL TFCAL(UAVE)
      ELSE
      F=0.
      ENDIF
      FXST=0.
      FYST=0.
      C1 = (F/(2*D))
C-----
C      SET INITIAL FLAGS
C-----
      NW = 3
      N = 2
      X =XEND
      TOL = 0.0001
      IND=1
      XEND = XEND+TI
C-----
      J=J+1
      ALPHA=XEND
      CALL LINEAR(T,PL,N2,ALPHA,S)
      PB=S-(SAPTG-SAPRG)
C      Above substruction for tank pressure was made for the head loss
C      along the part of the pipeline filled with air. PB here is the
C      driving gage presure applied by the air at the upstream side of
C      the slug.
      SS = PB/6891.1565
C-----
      CALL DVERK(N,FCN2,X,Y,XEND,TOL,IND,C,NW,W)
      MP(I) = RO*Y(1)**2
      PSI = MP(I)/6891.1565
      PPE = PSI/PRI
C-----
      XOUT(J)=X
      Y1OUT(J)=Y(1)
      Y2OUT(J)=Y(2)
      SSOUT(J)=SS
      WRITE(*,21) 'For T=',XOUT(J),'sec:'
21      FORMAT(1X,A6,F8.5,1X,A4)
      WRITE(*,22) 'VF=',Y1OUT(J),'m/s','LSS=',Y2OUT(J),'m','Driving Pr.=
*','SSOUT(J)','psi'
22      FORMAT(1X,A3,F9.4,1X,A3,2X,A,F6.3,1X,A1,2X,A12,F8.4,1X,A3)
      WRITE(*,18) 'NODE','PRESSURE RISE (psi)','deltaFx (N)',
*'deltaFy (N)'
18      FORMAT(1X,A4,3X,A19,10X,A11,6X,A11)
C-----
C      Parameters for the subroutine DVERK defined again
      NW=1
      N=1
      SCST=0.
      TOL=0.0001
      IND=1
C-----
      UAVE=Y1OUT(J)
      UAVEST=UAVE/UPR
      Q=UAVE*PI*R**2
      QST=Q/(UPR*LPR**2)
      TIST=TI/TPR
C-----
C      Calculating the boundary values at the exit of the vertical
C      extension part.
      PAVE(1)=0.

```



```

PAVEST(1)=PAVE(1)/(RO*UPR**2)
PAVMST=0.
C-----
FROLST=FROLST+UAVEST*TIST
IF (FROLST.LT.DSCST/2.) THEN
NLFF=0
ELSE IF (FROLST.GE.DSCST/2. .AND.FROLST.LE.LELBW/LPR+DSCST/2.
*.AND.DBELST.LE.EMELRT*DBETA) THEN
NLFF=1+INT((FROLST-DSCST/2.)/DSCST)
ELSE IF (FROLST.GE.DSCST/2. .AND.FROLST.LT.LELBW/LPR-DSLST1.
*.AND.DBELST.GT.EMELRT*DBETA) THEN
NLFF=1+INT(FROLST/DSCST)
ELSE IF (FROLST.GE.LELBW/LPR-DSLST1.AND.FROLST.LT.LELBW/LPR-
*.DSLST1/2. .AND.DBELST.GT.EMELRT*DBETA) THEN
NLFF=1+INT((FROLST-DSLST1/2.)/DSCST)
ELSEIF (FROLST.GE.LELBW/LPR-DSLST1/2. .AND.FROLST.LT.LELBW/
*.LPR .AND. DBELST.GT.EMELRT*DBETA) THEN
NLFF=NELBW
ELSE IF (FROLST.GE.LELBW/LPR.AND.FROLST.LT.LTOT/LPR-DSCST/2.
*.AND.DSCLST.LT.DSCST*EMELRT) THEN
NLFF=NELBW+INT((FROLST-LELBW/LPR)/DSCST)
ELSE IF (FROLST.GE.LELBW/LPR.AND.FROLST.LT.LTOT/LPR-DSCLST/2.
*.AND.DSCLST.GT.DSCST*EMELRT) THEN
NLFF=NELBW+INT((FROLST-LELBW/LPR)/DSCST)
ELSE IF (FROLST.GE.LTOT/LPR-DSCST/2. .AND.FROLST.LT.LTOT/LPR
*.AND.DBELST.LT.EMELRT*DBETA) THEN
NLFF=NSTOT
ELSE IF (FROLST.GE.LTOT/LPR-DSCLST/2. .AND.FROLST.LT.LTOT/LPR
*.AND.DBELST.GT.EMELRT*DBETA) THEN
NLFF=NSTOT
ELSE IF (FROLST.GE.LTOT/LPR) THEN
NLFF=NSTOT+1
ENDIF
DTUAST=(Y1OUT(J)/UPR-Y1OUT(J-1)/UPR)/TIST
C4=-DTUAST
C9=C4
C      Calculations for average pressure are being made by using
C      backward differences at point IP-1 (at coordinate SCEND on
C      curve s).
C      Calculations for deltaFx and deltaFy are being made at point
C      IP using control volume approach.
DO 220 IP=NLFF,NLBF+1,-1
IND=1
IF (IP.LE.NELBW) THEN
C-----
IF ((IP.LT.NELBW.OR.DBELST.LE.EMELRT*DBETA) .AND.IP.EQ.NLBF+1) THEN
SCST=(IP-1)*DSCST+DSCST/2.
SCEDST=(IP-1)*DSCST
DSCST1=DSCST/2.
DBETA1=DSCST1*LPR/RO
CALL UMSTCL(SCST)
IF (IP.EQ.NLFF) CALL INCRAR(SCST,UP2ST,MOMFL2)
CALL UMSTCL(SCEDST)
CALL INCRAR(SCEDST,UP2ST,MOMFL1)
C6=-LPR**3/(RO*ACRSS)*(MOMFL2-MOMFL1)/DBETA1
C7=-LPR*(F*PWET/(8*ACRSS))*UAVEST**2-UAVEST**2
BETA=DBETA*(IP-1)+DBETA/2.
C8=LPR*G/UPR**2*SIN(BETA)
C      SCEND MUST BE SMALLER THAN SC BECAUSE THE COMPUTATION
C      IS BEING MADE BACKWARDS HERE, ALONG THE 1-D MESH, WITH
C      SUBROUTINE DVERK.
CALL DVERK(N,PDS1ST,SCST,PAVEST,SCEDST,TOL,IND,C,NW,W)
IF (IP.LE.NSTOT.AND.IP.LT.NLFF) THEN
SCUST=(IP-1)*DSCST
SCMST=(IP-1)*DSCST+DSCST/2.
SCDST=(IP-1)*DSCST+DSCST
SCPST=(IP-1)*DSCST+DSCST+DSCST/2.
PAVUST=PAVEST(1)
CALL PINTER(PAVDST,SCDST,PAVMST,PAVPST,SCMST,SCPST)
CALL DFELBW(DFXST,DFYST)
ENDIF
C-----
ELSE IF (IP.LT.NELBW) THEN
SCST=(IP-1)*DSCST+DSCST/2.

```

```

SCEDST=(IP-2)*DSCST+DSCST/2.
DSCST1=DSCST
DBETA1=DSCST1*LPR/R0
CALL UMSTCL(SCST)
IF (IP.EQ.NLFF) CALL INCRAR(SCST,UP2ST,MOMFL2)
CALL UMSTCL(SCEDST)
CALL INCRAR(SCEDST,UP2ST,MOMFL1)
C6=-LPR**3/(R0*ACRSS)*(MOMFL2-MOMFL1)/DBETA1
C7=-LPR*(F*PWET/(8*ACRSS))*UAVEST**2-UAVEST**2
BETA=DBETA*(IP-1)+DBETA/2.
C8=LPR*G/UPR**2*SIN(BETA)
CALL DVERK(N,PDS1ST,SCST,PAVEST,SCEDST,TOL,IND,C,NW,W)
IF (IP.LE.NSTOT.AND.IP.LT.NLFF) THEN
SCNST=(IP-2)*DSCST+DSCST/2.
SCUST=(IP-2)*DSCST+DSCST/2.+DSCST/2.
SCMST=(IP-1)*DSCST+DSCST/2.
SCDST=(IP-1)*DSCST+DSCST/2.+DSCST/2.
SCPST=(IP-1)*DSCST+DSCST/2.+DSCST/2.+DSCST/2.
IF (IP.EQ.NELBW-1.AND.DBELST.GT.EMELRT*DBETA) SCPST=(IP-1)*DSCST+
*DSCST/2.+DSCST/2.+DSLST1/2.
PAVNST=PAVEST(1)
CALL PINTER(PAVUST,SCUST,PAVNST,PAVMST,SCNST,SCMST)
CALL PINTER(PAVDST,SCDST,PAVMST,PAVPST,SCMST,SCPST)
CALL DFELBW(DFXST,DFYST)
ENDIF
C-----
ELSE IF (IP.EQ.NELBW.AND.DBELST.LE.EMELRT*DBETA.AND.IP.GT.1) THEN
SCST=(IP-2)*DSCST+DSCST/2.+DSCST/2.+DSCST/2.
SCEDST=(IP-2)*DSCST+DSCST/2.
DSCST1=DSCST
DBETA1=DSCST1*LPR/R0
CALL UMSTCL(SCST)
IF (IP.EQ.NLFF) CALL INCRAR(SCST,UP2ST,MOMFL2)
CALL UMSTCL(SCEDST)
CALL INCRAR(SCEDST,UP2ST,MOMFL1)
C6=-LPR**3/(R0*ACRSS)*(MOMFL2-MOMFL1)/DBETA1
C7=-LPR*(F*PWET/(8*ACRSS))*UAVEST**2-UAVEST**2
BETA=DBETA*(IP-2)+DBETA/2.+DBETA/2.+DBETA/2.
C8=LPR*G/UPR**2*SIN(BETA)
CALL DVERK(N,PDS1ST,SCST,PAVEST,SCEDST,TOL,IND,C,NW,W)
IF (IP.LE.NSTOT.AND.IP.LT.NLFF) THEN
SCNST=(IP-2)*DSCST+DSCST/2.
SCUST=(IP-2)*DSCST+DSCST/2.+DSCST/2.
SCMST=(IP-2)*DSCST+DSCST/2.+DSCST/2.+DSCST/2.
SCDST=(IP-1)*DSCST+DSCST/2.+DSCST/2.
SCPST=(IP-1)*DSCST+DSCST/2.+DSCST/2.+DSCST/2.
PAVNST=PAVEST(1)
CALL PINTER(PAVUST,SCUST,PAVNST,PAVMST,SCNST,SCMST)
CALL PINTER(PAVDST,SCDST,PAVMST,PAVPST,SCMST,SCPST)
CALL DFELBW(DFXST,DFYST)
ENDIF
C-----
ELSE IF (IP.EQ.NELBW.AND.DBELST.GT.EMELRT*DBETA.AND.IP.GT.1) THEN
SCST=(IP-2)*DSCST+DSCST/2.+DSCST/2.+DSLST1/2.
SCEDST=(IP-2)*DSCST+DSCST/2.
DSCST1=DSCST/2.+DSLST1/2.
DBETA1=DSCST1*LPR/R0
CALL UMSTCL(SCST)
IF (IP.EQ.NLFF) CALL INCRAR(SCST,UP2ST,MOMFL2)
CALL UMSTCL(SCEDST)
CALL INCRAR(SCEDST,UP2ST,MOMFL1)
C6=-LPR**3/(R0*ACRSS)*(MOMFL2-MOMFL1)/DBETA1
C7=-LPR*(F*PWET/(8*ACRSS))*UAVEST**2-UAVEST**2
BETA=DBETA*(IP-2)+DBETA/2.+DBETA/2.+DBELST/2.
C8=LPR*G/UPR**2*SIN(BETA)
CALL DVERK(N,PDS1ST,SCST,PAVEST,SCEDST,TOL,IND,C,NW,W)
IF (IP.LE.NSTOT.AND.IP.LT.NLFF) THEN
SCNST=(IP-2)*DSCST+DSCST/2.
SCUST=(IP-2)*DSCST+DSCST/2.+DSCST/2.
SCMST=(IP-2)*DSCST+DSCST/2.+DSCST/2.+DSLST1/2.
SCDST=(IP-2)*DSCST+DSCST/2.+DSCST/2.+DSLST1
SCPST=(IP-2)*DSCST+DSCST/2.+DSCST/2.+DSLST1+DSCST/2.
PAVNST=PAVEST(1)
CALL PINTER(PAVUST,SCUST,PAVNST,PAVMST,SCNST,SCMST)

```

```

CALL PINTER(PAVDST,SCDST,PAVMST,PAVPST,SCMST,SCPST)
CALL DFELBW(DFXST,DFYST)
ENDIF
ENDIF
C-----
      ELSE IF (IP.EQ.NELBW+1 .AND.DBELST.LE.EMELRT*DBETA.AND.NLFF.NE.
*NELBW+1) THEN
C      Here, the average pressure value at the last node of the
C      of the elbow is calculated.
C      (Point NELBW+1 corresponds to the connection boundary of the
C      elbow and the vertical extension part as a special case here.)
      SCST=LELBW/LPR
      SCEDST=LELBW/LPR-DSCST/2.
      DSCST1=DSCST/2.
      DBETA1=DSCST1*LPR/R0
      CALL UMSTCL(SCST)
      IF (IP.EQ.NLFF) CALL INCRAR(SCST,UP2ST,MOMFL2)
      CALL UMSTCL(SCEDST)
      CALL INCRAR(SCEDST,UP2ST,MOMFL1)
      C6=-LPR**3/(R0*ACRSS)*(MOMFL2-MOMFL1)/DBETA1
      C7=-LPR*(F*PWET/(8*ACRSS))*UAVEST**2-UAVEST**2
      BETA=DBETA*(IP-1)
      C8=LPR*G/UPR**2*SIN(BETA)
      PAVUST=PAVEST(1)
      CALL DVERK(N,PDS1ST,SCST,PAVEST,SCEDST,TOL,IND,C,NW,W)
      IF (IP.LE.NSTOT.AND.IP.LT.NLFF) THEN
        SCUST=LELBW/LPR
        SCMST=LELBW/LPR+DSCST/2.
        SCDST=LELBW/LPR+DSCST
        SCPST=LELBW/LPR+DSCST+DSCST/2.
        CALL PINTER(PAVDST,SCDST,PAVMST,PAVPST,SCMST,SCPST)
        CALL DFEXTN(DFXST,DFYST)
      ENDIF
C-----
      ELSE IF (IP.EQ.NELBW+1 .AND.DBELST.GE.EMELRT*DBETA.AND.NLFF.NE.
*NELBW+1) THEN
C      Here, the average pressure value at the last node of the
C      of the elbow is calculated.
      SCST=LELBW/LPR
      SCEDST=LELBW/LPR-DSLST1/2.
      DSCST1=DSLST1/2.
      DBETA1=DSCST1*LPR/R0
      CALL UMSTCL(SCST)
      IF (IP.EQ.NLFF) CALL INCRAR(SCST,UP2ST,MOMFL2)
      CALL UMSTCL(SCEDST)
      CALL INCRAR(SCEDST,UP2ST,MOMFL1)
      C6=-LPR**3/(R0*ACRSS)*(MOMFL2-MOMFL1)/DBETA1
      C7=-LPR*(F*PWET/(8*ACRSS))*UAVEST**2-UAVEST**2
      BETA=DBETA*(IP-3)+DBETA/2.+DBETA/2.+DBELST
      C8=LPR*G/UPR**2*SIN(BETA)
      PAVUST=PAVEST(1)
      CALL DVERK(N,PDS1ST,SCST,PAVEST,SCEDST,TOL,IND,C,NW,W)
      IF (IP.LE.NSTOT.AND.IP.LT.NLFF) THEN
        SCUST=LELBW/LPR
        SCMST=LELBW/LPR+DSCST/2.
        SCDST=LELBW/LPR+DSCST
        SCPST=LELBW/LPR+DSCST+DSCST/2.
        CALL PINTER(PAVDST,SCDST,PAVMST,PAVPST,SCMST,SCPST)
        CALL DFEXTN(DFXST,DFYST)
      ENDIF
C-----
      ELSE IF (IP.EQ.NELBW+1 .AND.DBELST.LE.EMELRT*DBETA.AND.NLFF.EQ.
*NELBW+1) THEN
      SCST=LELBW/LPR+DSCST/2.
      SCEDST=LELBW/LPR
      DSCST1=DSCST/2.
      DBETA1=DSCST1*LPR/R0
      CALL UMSTCL(SCST)
      IF (IP.EQ.NLFF) CALL INCRAR(SCST,UP2ST,MOMFL2)
      CALL UMSTCL(SCEDST)
      CALL INCRAR(SCEDST,UP2ST,MOMFL1)
      C10=-LPR**2/ACRSS*(MOMFL2-MOMFL1)/DSCST1
      C11=-F*PWET/(8*ACRSS)*LPR*UAVEST**2
      C12=G*LPR/UPR**2

```

```

CALL DVERK(N,PDS2ST,SCST,PAVEST,SCEDST,TOL,IND,C,NW,W)
CONTINUE
IND=1
PAV1ST=PAVEST(1)
MOMFL2=MOMFL1
SCST=LELBW/LPR
SCEDST=LELBW/LPR-DSCST/2.
DSCST1=DSCST/2.
DBETA1=DSCST1*LPR/R0
CALL UMSTCL(SCST)
IF (IP.EQ.NLFF) CALL INCRAR(SCST,UP2ST,MOMFL2)
CALL UMSTCL(SCEDST)
CALL INCRAR(SCEDST,UP2ST,MOMFL1)
C6=-LPR**3/(R0*ACRSS)*(MOMFL2-MOMFL1)/DBETA1
C7=-LPR*(F*PWET/(8*ACRSS))*UAVEST**2-UAVEST**2
BETA=DBETA*(IP-1)
C8=LPR*G/UPR**2*SIN(BETA)
CALL DVERK(N,PDS1ST,SCST,PAVEST,SCEDST,TOL,IND,C,NW,W)
PBOUST=PAVEST(1)
PAVEST(1)=PAV1ST
C-----
ELSE IF (IP.EQ.NELBW+1 .AND.DBELST.GE.EMELRT*DBETA.AND.NLFF.EQ.
*NELBW+1) THEN
SCST=LELBW/LPR+DSCST/2.
SCEDST=LELBW/LPR
DSCST1=DSCST/2.
DBETA1=DSCST1*LPR/R0
CALL UMSTCL(SCST)
IF (IP.EQ.NLFF) CALL INCRAR(SCST,UP2ST,MOMFL2)
CALL UMSTCL(SCEDST)
CALL INCRAR(SCEDST,UP2ST,MOMFL1)
C10=-LPR**2/ACRSS*(MOMFL2-MOMFL1)/DSCST1
C11=-F*PWET/(8*ACRSS)*LPR*UAVEST**2
C12=G*LPR/UPR**2
CALL DVERK(N,PDS2ST,SCST,PAVEST,SCEDST,TOL,IND,C,NW,W)
CONTINUE
IND=1
PAV1ST=PAVEST(1)
MOMFL2=MOMFL1
SCST=LELBW/LPR
SCEDST=LELBW/LPR-DSLST1/2.
DSCST1=DSLST1/2.
DBETA1=DSCST1*LPR/R0
CALL UMSTCL(SCST)
IF (IP.EQ.NLFF) CALL INCRAR(SCST,UP2ST,MOMFL2)
CALL UMSTCL(SCEDST)
CALL INCRAR(SCEDST,UP2ST,MOMFL1)
C6=-LPR**3/(R0*ACRSS)*(MOMFL2-MOMFL1)/DBETA1
C7=-LPR*(F*PWET/(8*ACRSS))*UAVEST**2-UAVEST**2
BETA=DBETA*(IP-3)+DBETA/2.+DBELST
C8=LPR*G/UPR**2*SIN(BETA)
CALL DVERK(N,PDS1ST,SCST,PAVEST,SCEDST,TOL,IND,C,NW,W)
PBOUST=PAVEST(1)
PAVEST(1)=PAV1ST
C-----
ELSE IF (IP.GT.NELBW.AND.IP.EQ.NELBW+2) THEN
SCST=LELBW/LPR+(IP-NELBW-1)*DSCST+DSCST/2.
SCEDST=LELBW/LPR+(IP-NELBW-2)*DSCST+DSCST/2.
DSCST1=DSCST
DBETA1=DSCST1*LPR/R0
CALL UMSTCL(SCST)
IF (IP.EQ.NLFF) CALL INCRAR(SCST,UP2ST,MOMFL2)
CALL UMSTCL(SCEDST)
CALL INCRAR(SCEDST,UP2ST,MOMFL1)
C10=-LPR**2/ACRSS*(MOMFL2-MOMFL1)/DSCST1
C11=-F*PWET/(8*ACRSS)*LPR*UAVEST**2
C12=G*LPR/UPR**2
CALL DVERK(N,PDS2ST,SCST,PAVEST,SCEDST,TOL,IND,C,NW,W)
IF (IP.LE.NSTOT.AND.IP.LT.NLFF) THEN
SCNST=LELBW/LPR+DSCST/2.
SCUST=LELBW/LPR+DSCST
SCMST=LELBW/LPR+DSCST+DSCST/2.
SCDST=LELBW/LPR+DSCST+DSCST
SCPST=LELBW/LPR+DSCST+DSCST+DSCST/2.

```

```

PAVNST=PAVEST(1)
CALL PINTER(PAVUST, SCUST, PAVNST, PAVMST, SCNST, SCMST)
CALL PINTER(PAVDST, SCDST, PAVMST, PAVPST, SCMST, SCPST)
CALL DFEXTN(DFXST, DFYST)
ENDIF
CONTINUE
IND=1
PAV1ST=PAVEST(1)
MOMFL2=MOMFL1
C      Calculating the pressure value at the connection point of the
C      elbow and the vertical extension part.
SCST=LELBW/LPR+DSCST/2.
SCEDST=LELBW/LPR
DSCST1=DSCST/2.
DBETA1=DSCST1*LPR/R0
CALL UMSTCL(SCST)
IF (IP.EQ.NLFF) CALL INCRAR(SCST,UP2ST,MOMFL2)
CALL UMSTCL(SCEDST)
CALL INCRAR(SCEDST,UP2ST,MOMFL1)
C10=-LPR**2/ACRSS*(MOMFL2-MOMFL1)/DSCST1
C11=-F*PWET/(8*ACRSS)*LPR*UAVEST**2
C12=G*LPR/UPR**2
CALL DVERK(N,PDS2ST,SCST,PAVEST,SCEDST,TOL,IND,C,NW,W)
PBOUST=PAVEST(1)
PAVEST(1)=PAV1ST
C-----
ELSE IF (IP.LT.NSTOT.AND.IP.GT.NELBW+2) THEN
SCST=LELBW/LPR+(IP-NELBW-1)*DSCST+DSCST/2.
SCEDST=LELBW/LPR+(IP-NELBW-2)*DSCST+DSCST/2.
DSCST1=DSCST
DBETA1=DSCST1*LPR/R0
CALL UMSTCL(SCST)
IF (IP.EQ.NLFF) CALL INCRAR(SCST,UP2ST,MOMFL2)
CALL UMSTCL(SCEDST)
CALL INCRAR(SCEDST,UP2ST,MOMFL1)
C10=-LPR**2/ACRSS*(MOMFL2-MOMFL1)/DSCST1
C11=-F*PWET/(8*ACRSS)*LPR*UAVEST**2
C12=G*LPR/UPR**2
CALL DVERK(N,PDS2ST,SCST,PAVEST,SCEDST,TOL,IND,C,NW,W)
IF (IP.LE.NSTOT.AND.IP.LT.NLFF) THEN
SCNST=LELBW/LPR+(IP-NELBW-2)*DSCST+DSCST/2.
SCUST=LELBW/LPR+(IP-NELBW-2)*DSCST+DSCST/2.+DSCST/2.
SCMST=LELBW/LPR+(IP-NELBW-1)*DSCST+DSCST/2.
SCDST=LELBW/LPR+(IP-NELBW-1)*DSCST+DSCST/2.+DSCST/2.
SCPST=LELBW/LPR+(IP-NELBW-1)*DSCST+DSCST/2.+DSCST/2.+DSCST/2.
PAVNST=PAVEST(1)
CALL PINTER(PAVUST, SCUST, PAVNST, PAVMST, SCNST, SCMST)
CALL PINTER(PAVDST, SCDST, PAVMST, PAVPST, SCMST, SCPST)
CALL DFEXTN(DFXST, DFYST)
ENDIF
C-----
ELSE IF (IP.EQ.NSTOT.AND.DSCLST.LE.DSCST*EMELRT.AND.IP.GT.NELBW+1)
*THEN
SCST=LELBW/LPR+(IP-NELBW-1)*DSCST+DSCST/2.
SCEDST=LELBW/LPR+(IP-NELBW-2)*DSCST+DSCST/2.
DSCST1=DSCST
DBETA1=DSCST1*LPR/R0
CALL UMSTCL(SCST)
IF (IP.EQ.NLFF) CALL INCRAR(SCST,UP2ST,MOMFL2)
CALL UMSTCL(SCEDST)
CALL INCRAR(SCEDST,UP2ST,MOMFL1)
C10=-LPR**2/ACRSS*(MOMFL2-MOMFL1)/DSCST1
C11=-F*PWET/(8*ACRSS)*LPR*UAVEST**2
C12=G*LPR/UPR**2
CALL DVERK(N,PDS2ST,SCST,PAVEST,SCEDST,TOL,IND,C,NW,W)
IF (IP.LE.NSTOT.AND.IP.LT.NLFF) THEN
SCNST=LELBW/LPR+(IP-NELBW-2)*DSCST+DSCST/2.
SCUST=LELBW/LPR+(IP-NELBW-2)*DSCST+DSCST/2.+DSCST/2.
SCMST=LELBW/LPR+(IP-NELBW-1)*DSCST+DSCST/2.
SCDST=LELBW/LPR+(IP-NELBW-1)*DSCST+DSCST/2.+DSCST/2.
PAVNST=PAVEST(1)
CALL PINTER(PAVUST, SCUST, PAVNST, PAVMST, SCNST, SCMST)
PAVDST=0.
CALL DFEXTN(DFXST, DFYST)

```

```

      ENDIF
C-----
      ELSE IF (IP.EQ.NSTOT.AND.DSCLST.GT.DSCST*EMELRT.AND.IP.GT.NELBW+1)
*THEN
      SCST=LLEBW/LPR+(IP-NELBW-2)*DSCST+DSCST/2.+DSCST/2.+DSCLST/2.
      SCEDST=LLEBW/LPR+(IP-NELBW-2)*DSCST+DSCST/2.
      DSCST1=DSCST/2.+DSCLST/2.
      DBETA1=DSCST1*LPR/R0
      CALL UMSTCL(SCST)
      IF (IP.EQ.NLFF) CALL INCRAR(SCST,UP2ST,MOMFL2)
      CALL UMSTCL(SCEDST)
      CALL INCRAR(SCEDST,UP2ST,MOMFL1)
      C10=-LPR**2/ACRSS*(MOMFL2-MOMFL1)/DSCST1
      C11=-F*PWET/(8*ACRSS)*LPR*UAVEST**2
      C12=G*LPR/UPR**2
      CALL DVERK(N,PDS2ST,SCST,PAVEST,SCEDST,TOL,IND,C,NW,W)
      IF (IP.LE.NSTOT.AND.IP.LT.NLFF) THEN
      SCNST=LLEBW/LPR+(IP-NELBW-2)*DSCST+DSCST/2.
      SCUST=LLEBW/LPR+(IP-NELBW-2)*DSCST+DSCST/2.+DSCST/2.
      SCMST=LLEBW/LPR+(IP-NELBW-1)*DSCST+DSCLST/2.
      SCDST=LLEBW/LPR+(IP-NELBW-1)*DSCST+DSCLST/2.+DSCLST/2.
      PAVNST=PAVEST(1)
      CALL PINTER(PAVUST,SCUST,PAVNST,PAVMST,SCNST,SCMST)
      PAVDST=0.
      CALL DFEXTN(DFXST,DFYST)
      ENDIF
C-----
      ELSE IF (IP.EQ.NSTOT+1 .AND.DSCLST.LE.DSCST*EMELRT.AND.IP.GT.
*NELBW+1) THEN
      SCST=LTOT/LPR
      SCEDST=LTOT/LPR-DSCST/2.
      DSCST1=DSCST/2.
      DBETA1=DSCST1*LPR/R0
      CALL UMSTCL(SCST)
      IF (IP.EQ.NLFF) CALL INCRAR(SCST,UP2ST,MOMFL2)
      CALL UMSTCL(SCEDST)
      CALL INCRAR(SCEDST,UP2ST,MOMFL1)
      C10=-LPR**2/ACRSS*(MOMFL2-MOMFL1)/DSCST1
      C11=-F*PWET/(8*ACRSS)*LPR*UAVEST**2
      C12=G*LPR/UPR**2
      CALL DVERK(N,PDS2ST,SCST,PAVEST,SCEDST,TOL,IND,C,NW,W)
C-----
      ELSE IF (IP.EQ.NSTOT+1 .AND.DSCLST.GT.DSCST*EMELRT.AND.IP.GT.
*NELBW+1) THEN
      SCST=LTOT/LPR
      SCEDST=LTOT/LPR-DSCLST/2.
      DSCST1=DSCST/2.
      DBETA1=DSCST1*LPR/R0
      CALL UMSTCL(SCST)
      IF (IP.EQ.NLFF) CALL INCRAR(SCST,UP2ST,MOMFL2)
      CALL UMSTCL(SCEDST)
      CALL INCRAR(SCEDST,UP2ST,MOMFL1)
      C10=-LPR**2/ACRSS*(MOMFL2-MOMFL1)/DSCST1
      C11=-F*PWET/(8*ACRSS)*LPR*UAVEST**2
      C12=G*LPR/UPR**2
      CALL DVERK(N,PDS2ST,SCST,PAVEST,SCEDST,TOL,IND,C,NW,W)
      ENDIF
C-----
      MOMFL2=MOMFL1
      IF (IP.EQ.1) PAVE(1)=PAVEST(1)*RO*UPR**2
      IF (IP.LE.NELBW+1.AND.IP.GE.1) THEN
      IF (IP.GT.1) THEN
      DSCST1=DSCST
      DBETA1=DSCST1*LPR/R0
C      SCST values are recalculated here because above application of
C      the subroutine DVERK changes the value of this variable.
      SCST=DSCST/2.+DSCST*(IP-1)
      CALL UMSTCL(SCST-DSCST1)
      UM2ST=UMST
      RM2ST=RMST
      TC2=TC
      CALL UMSTCL(SCST)
      UM1ST=UMST
      RM1ST=RMST

```

```

TC1=TC
IF (IP.EQ.NELBW.AND.IP.GE.2 .AND.DBELST.GE.EMELRT*DBETA) THEN
DSCST1=DSLST1/2.+DSCST/2.
DBETA1=DSCST1*LPR/R0
SCST=DSCST/2.+DSCST*(IP-2)+DSCST/2.+DSLST1/2.
CALL UMSTCL(SCST-DSCST1)
UM2ST=UMST
RM2ST=RMST
TC2=TC
CALL UMSTCL(SCST)
UM1ST=UMST
RM1ST=RMST
TC1=TC
ENDIF
PAVE(1)=PAVEST(1)*RO*UPR**2
PCVXST(1)=PAVEST(1)
MLD=MLPRSS-1
DRDIST=(R/LPR)/MLD
DO 40 IPD=1,MLD
RDIST=R0/LPR+DRDIST*(IPD-1)
RDEDST=RDIST+DRDIST
SCSTCP=SCEDST
IND=1
CALL DVERK(N,PCTFST,RDIST,PCVXST,RDEDST,TOL,IND,C,NW,W)
40 CONTINUE
PCNVX(1)=PCVXST(1)*RO*UPR**2
PDOUT(J,IP-1)=PCNVX(1)
ENDIF
IF (IP.LT.NLFF.AND.IP.NE.NSTOT+1) THEN
DFXOUT(J,IP)=DFXST*RO*UPR**2*LPR**2
DFYOUT(J,IP)=DFYST*RO*UPR**2*LPR**2
FXST=FXST+DFXST
FYST=FYST+DFYST
ENDIF
IF (IP.NE.NELBW+1) THEN
IF (IP.EQ.NMAXP-1 .OR.IP. EQ.NMAXP-2) THEN
WRITE(*,249) IP,PDOUT(J,IP)/6891.1565,'cnvx. (ind.)',
*DFXOUT(J,IP),DFYOUT(J,IP)
GOTO 44
ENDIF
WRITE(*,250) IP,PDOUT(J,IP)/6891.1565,'cnvx.',
*DFXOUT(J,IP),DFYOUT(J,IP)
ELSE IF (IP.EQ.NELBW+1) THEN
IF (IP.EQ.NMAXP-1 .OR.IP. EQ.NMAXP-2) THEN
WRITE(*,249) IP,PDOUT(J,IP)/6891.1565,'cnvx. (ind.)',
*DFXOUT(J,IP),DFYOUT(J,IP)
GOTO 44
ENDIF
WRITE(*,251) IP,PDOUT(J,IP)/6891.1565,'avg.',
*DFXOUT(J,IP),DFYOUT(J,IP)
ENDIF
44 CONTINUE
IF (IP.EQ.1) THEN
FX=FXST*RO*UPR**2*LPR**2
FY=FYST*RO*UPR**2*LPR**2
WRITE(*,43) FX,FY
43 FORMAT(32X,'FX=',F9.2,1X,'N',3X,'FY=',F9.2,1X,'N')
FXOUT(J)=FX
FYOUT(J)=FY
ENDIF
IF (IP-1 .EQ.NMAXP.AND.IP+1 .LT.NLFF) THEN
SNMST=SCEDST
PNMST=PDOUT(J,IP-1)/(RO*UPR**2)
PNM1ST=PDOUT(J,IP)/(RO*UPR**2)
PNM2ST=PDOUT(J,IP+1)/(RO*UPR**2)
CALL PEAKCL(SNMST,DSCST,PNMST,PNM1ST,PNM2ST,SCMAX,PPEAST)
PPEAK=PPEAST*RO*UPR**2
WRITE(7,41) X,PPEAK/6891.1565
41 FORMAT(1X,F10.5,5X,F12.2)
ENDIF
ELSE IF (IP.GT.NELBW.AND.IP.GE.2) THEN
IF (IP.LT.NLFF.AND.IP.NE.NSTOT+1) THEN
DFXOUT(J,IP)=DFXST*RO*UPR**2*LPR**2
DFYOUT(J,IP)=DFYST*RO*UPR**2*LPR**2

```

```

        FXST=FXST+DFXST
        FYST=FYST+DFYST
    ENDIF
    PAVE(1)=PAVEST(1)*RO*UPR**2
    PDOUT(J,IP-1)=PAVE(1)
    IF (IP.LT.NSTOT+1) THEN
        WRITE(*,251) IP,PDOUT(J,IP)/6891.1565,'avg.',
*DFXOUT(J,IP),DFYOUT(J,IP)
    ENDIF
    IF (IP-1.EQ.NMAXP) WRITE(7,42) X,PDOUT(J,IP-1)/6891.1565
42    FORMAT(1X,F10.5,5X,F12.2)
    ENDIF
249    FORMAT(1X,I5,3X,F8.2,1X,A12,2X,F12.2,5X,F12.2)
250    FORMAT(1X,I5,3X,F8.2,1X,A5,9X,F12.2,5X,F12.2)
251    FORMAT(1X,I5,3X,F8.2,1X,A4,10X,F12.2,5X,F12.2)
    PAVPST=PAVMST
    PAVMST=PAVEST(1)
    IF (IP.EQ.NELBW+2 .OR. (IP.EQ.NELBW+1 .AND.NLFF.EQ.NELBW+1))
*PAVEST(1)=PBOUST
220    CONTINUE
    QPTSST=QST
    WRITE(*,*) " "
C-----
C-----
    ITSTP=J
    IF (ITSTP.EQ.1) THEN
        WRITE(2,296) 'Output for the Pressure Distribution at each Time St
*ep:'
296    FORMAT(1X,A55)
    ENDIF
    WRITE(2,291) 'For T=',XOUT(ITSTP),'sec:'
291    FORMAT(1X,A6,F8.5,1X,A4)
    WRITE(2,292) 'VF=',Y1OUT(ITSTP),'m/s','LSS=',Y2OUT(ITSTP),'m',
*'Driving Pr.=',SSOUT(ITSTP),'psi'
292    FORMAT(1X,A3,F9.4,1X,A3,2X,A4,F6.3,1X,A1,2X,A12,F8.4,1X,A3)
    WRITE(2,294) 'NODE','PRESSURE RISE (psi)','deltaFx (N)',
*'deltaFy (N)'
294    FORMAT(1X,A4,3X,A19,10X,A11,6X,A11)
    DO 300 INPTS=NLBF,NSTOT
        IF (INPTS.LE.NELBW) THEN
            IF (INPTS.EQ.NMAXP-1 .OR.INPTS.EQ.NMAXP-2. AND.INPTS.NE.0) THEN
                WRITE(2,249) INPTS,PDOUT(ITSTP,INPTS)/6891.1565,'cnvx. (ind.)',
*DFXOUT(ITSTP,INPTS),DFYOUT(ITSTP,INPTS)
                GOTO 308
            ENDIF
            IF (INPTS.NE.0) WRITE(2,250) INPTS,PDOUT(ITSTP,INPTS)/6891.1565,'c
*nvx.',DFXOUT(ITSTP,INPTS),DFYOUT(ITSTP,INPTS)
308    CONTINUE
            ELSE IF (INPTS.GT.NELBW) THEN
                WRITE(2,251) INPTS,PDOUT(ITSTP,INPTS)/6891.1565,'avg.',
*DFXOUT(ITSTP,INPTS),DFYOUT(ITSTP,INPTS)
            ENDIF
            IF (INPTS.EQ.NSTOT) THEN
                WRITE(2,299) FXOUT(ITSTP),FYOUT(ITSTP)
299    FORMAT(32X,'FX=',F9.2,1X,'N',3X,'FY=',F9.2,1X,'N')
                WRITE(8,306) XOUT(ITSTP),FXOUT(ITSTP),FYOUT(ITSTP)
306    FORMAT(1X,F10.5,5X,F9.2,5X,F9.2)
            ENDIF
300    CONTINUE
            WRITE(2,*) ' '
307    CONTINUE
C-----
C        Here a ratio Rs, expressing the stability of the slug, is used
C        in the criteria to stop the simulation.
        Y1ST=Y(1)/UPR
        Y2ST=Y(2)/LPR
        PBST=PB/(RO*UPR**2)
        RS=ABS((-F*Y2ST*LPR*ACRSS*Y1ST**2/(2*D)+
*PBST*ACRSS-PAVEST(1)*ACRSS)/(PBST*ACRSS))
C-----
        IF (RS.LT.0.15 .AND.NLFF.GT.NELBW) THEN
            WRITE(*,303)
            WRITE(2,303)
303    FORMAT (//,1X," Now the driving and the retarding forces ac

```



```

*ting on the slug",/,1X," has become very close to each other and s
*imulation stopped",/,1X," to leave calculations with unstable osci
*llations!",/)
      GO TO 19
      ELSE IF (Y(2).LE.0.05) THEN
        WRITE(*,11)
        WRITE(2,11)
11      FORMAT(1X,' THE SLUG HAS EXITED HORIZONTAL PIPE!')
      GO TO 19
      ENDIF
16    CONTINUE
C-----
C-----
C-----
19    CONTINUE
      WRITE(*,310)
310    FORMAT(/,1X,' Hope this was a pleasant simulation for you!')
      WRITE(2,305)
305    FORMAT(/,1X,' This is the end of output data file.')
      CLOSE(UNIT=2)
      CLOSE(UNIT=7)
      CLOSE(UNIT=8)
      STOP
      END
C-----
      SUBROUTINE FCN2(N,X,Y,YPRIME)
      INTEGER N
      REAL*8 Y(N),YPRIME(N),X,C1,C2,C3,PB,RO,PAVE(1),MU
      COMMON/ COEFFS/ C1, C2, C3
      COMMON/ CONST/PB,RO,PAVE,MU
      YPRIME(1) = -C1*Y(1)**2 + PB/(RO*Y(2))-PAVE(1)/(RO*Y(2))
      YPRIME(2) = -Y(1)
      RETURN
      END
C-----
C-----SUBROUTINE LINEAR-----
C-----
C GIVEN ARRAYS T AND PL, EACH LENGTH N, AND GIVEN A VALUE T, THIS
C ROUTINE RETURNS A VALUE PL, BY LINEAR INTERPOLATION.
C
C   N:      AN INTEGER FOR THE DIMENSION OF ARRAYS;
C   T(I):   N-DIMENSIONAL INDEPENDENT VARIABLE ARRAY;
C   PL(I):  N-DIMENSIONAL DEPENDENT VARIABLE ARRAY;
C   ALPHA:  A T VALUE AT WHICH VALUE OF PL IS DESIRED.
C
C-----
C-----
      SUBROUTINE LINEAR(T,PL,N,ALPHA,S)
      IMPLICIT REAL*8 (A-H,O-Z)
      DIMENSION T(10010),PL(10010)
      REAL*8 H,ALPHA,S
      CALL LOCATE(T,N,ALPHA,J)
      H=T(J+1)-T(J)
      S=PL(J)+(ALPHA-T(J))*(PL(J+1)-PL(J))/H
C      WRITE(3,1)J,ALPHA,S
C      WRITE(*,1)J,ALPHA,S
1      FORMAT(2X,'INTEGER=',I4,5X,'ALPHA=',2X,F9.7,3X,'PRES. IS =',F10.0)
      RETURN
      END
C
      SUBROUTINE LOCATE(T,N,ALPHA,J)
C Given an array T of length N, and given a value ALPHA, returns a value J
C such that ALPHA is between T(J) and T(J+1). T must be monotonic, either
C increasing or decreasing. J=0 or J=N is returned to indicate that ALPHA
C is out of range.
      IMPLICIT REAL*8 (A-H,O-Z)
      DIMENSION T(10010)
      REAL*8 ALPHA
      JL=0                                !Initialize lower
      JU=N+1                              !and upper limits
10     IF((JU-JL).GT.1)THEN                !if we are not yet done,
          JM=(JU+JL)/2                    !compute a midpoint,
C
          IF((T(N).GT.T(1)).EQV.(ALPHA.GT.T(JM)))THEN

```

```

C          JL =JM          !and replace either the lower limit
          ELSE
          JU = JM          !or the upper limit, as appropriate.
          ENDIF
GO TO 10          !Repeat until
ENDIF          !the test condition 10 is satisfied
J=JL          !Then set the output
RETURN          !and return.
END

SUBROUTINE BISECT(X,XL,XU,NB,IER,F)
C      This subroutine is given in Antia,2002. Numerical Methods for
C      Scientists and Engineers. Birkhauser, Verlag.
      IMPLICIT REAL*8 (A-H,O-Z)

      IF(NB.LE.0) THEN
          IER=401
          RETURN
      ENDIF

      FL=F(XL)
      FU=F(XU)
      IER=-1
C      If the function value is zero at either point then quit
      IF(FL.EQ.0.0) THEN
          X=XL
          RETURN
      ELSE IF(FU.EQ.0.0) THEN
          X=XU
          RETURN
      ENDIF

      IF(FL.GT.0.0.EQV.FU.GT.0.0) THEN
C      If the function has the same sign at both end points then quit
          IER=421
          RETURN
      ENDIF

C      Loop for bisection
      DO 1000 K=1,NB
          X=(XL+XU)/2.
          FX=F(X)
C      If function is zero then quit
          IF(FX.EQ.0.0) RETURN
          IF(FX.GT.0.0.EQV.FU.GT.0.0) THEN
              XU=X
              FU=FX
          ELSE
              XL=X
              FL=FX
          ENDIF
1000 CONTINUE

C      linear interpolation between XL and XU
      X=(XL*FU-XU*FL)/(FU-FL)
      IER=0
      END

      SUBROUTINE FCAL(UAVE1,RO1,MU1,EPSLN1,D1,F1)
      IMPLICIT REAL*8 (A-H,O-Z)
      REAL*8 UAVE1,RO1,MU1,EPSLN1,D1,RE1,F1
      RE1=RO1*UAVE1*D1/MU1
      F1=1.325/(LOG(EPSLN1/(3.7*D1)+5.74/RE1**0.9))**2
      RETURN
      END

      SUBROUTINE TFCAL(UAVE)
      IMPLICIT REAL*8 (A-H,O-Z)
      REAL*8 EPSLN,D
      REAL*8 PB,RO,PAVEST,MU
      REAL*8 R,TC,TF,QST,PI
      REAL*8 UAVE,F,RE
      REAL*8 YW,TAU,TAU0,LMX,FRSLP

```

```

COMMON /PRMTS1/ R,TC,TF,QST,PI
COMMON /PRMTS14/ EPSLN,D,F
COMMON/ CONST/PB,RO,PAVEST,MU
RE=RO*UAVE*D/MU
F=1.325/(LOG(EPSLN/(3.7*D)+5.74/RE**0.9))**2
TAU0=1/8.*F*RO*UAVE**2
C      The ratio of 1/250. below was selected such that the distance
C      YW=R*(1/250.) is very close to the pipe wall.
      YW=R/250.
      TAU=TAU0*(1.-YW/R)
      LMX=0.4*YW
      FRSLP=1./LMX*(TAU/RO)**.5
      TF=ATAN(FRSLP)
      RETURN
      END

SUBROUTINE UMSTCL(SCST)
IMPLICIT REAL*8 (A-H,O-Z)
REAL*8 R,TC,TF,QST,PI,RMST,UMST,LPR,UPR,TPR,SCST
COMMON /PRMTS1/ R,TC,TF,QST,PI
COMMON /PRMTS2/ RMST,UMST,LPR,UPR,TPR
COMMON /TERMS4/ DRDIST,MLD
CALL TCCAL(SCST)
UMST=-1/UPR*(-((3*QST*UPR*LPR**2/PI)-R**3*TAN(TF))*TAN(TF)**2*(
*TAN(TC)-TAN(TF))**2/(TAN(TC)+TAN(TF))**2))*((1./3)+R/UPR*TAN(TF)
RMST=R/LPR-UMST/(TPR*TAN(TF))
RETURN
END

FUNCTION UST(KSIST,SCST,ETA)
C      This subprogram calculates UST at a cross-section of the elbow
C      or the extension part, where angle BETA or location on the
C      S-curve, S, is constant.
IMPLICIT REAL*8 (A-H,O-Z)
REAL*8 R,TC,TF,QST,PI,RMST,UMST,LPR,UPR,TPR,KSIST,SCST,ETA
REAL*8 Y1ST,H1ST,Y2ST,H2ST
COMMON /PRMTS1/ R,TC,TF,QST,PI
COMMON /PRMTS2/ RMST,UMST,LPR,UPR,TPR
CALL TCCAL(SCST)
Y1ST=1./LPR*(UMST*UPR-R*TAN(TF))*(TAN(TC)+TAN(TF))/(TAN(TF)*(TAN
*(TC)-TAN(TF)))
H1ST=(UMST*UPR-R*TAN(TF))/(TAN(TC)-TAN(TF))*2*TAN(TC)/LPR
Y2ST=(2*R*TAN(TC)*TAN(TF)-UMST*UPR*(TAN(TC)+TAN(TF)))/(TAN(TF)*(
*TAN(TC)-TAN(TF))*LPR)
H2ST=Y2ST*TAN(TF)
IF (KSIST.LT.Y1ST) THEN
UST=TPR/(Y1ST**2-RMST**2)*(Y1ST**2*H1ST+Y1ST**2*H2ST-
*RMST**2*H2ST-RMST*H1ST*KSIST*SIN(ETA)-
*(-2.*Y1ST**2*H1ST**2*RMST*KSIST*SIN(ETA)+
*RMST**2*Y1ST**2*H1ST**2-
*(RMST**2*H1ST**2-Y1ST**2*H1ST**2)*COS(ETA)**2*KSIST**2+
*Y1ST**2*H1ST**2*SIN(ETA)**2*KSIST**2))*0.5)
ELSE IF (KSIST.GE.Y1ST) THEN
UST=LPR/UPR*(R/LPR-KSIST)*TAN(TF)
ENDIF
END

FUNCTION UP2ST(KSIST,SCST,ETA)
C      This subprogram calculates U**2 at a cross-section of the elbow
C      or the extension part, where angle BETA or location on the
C      S-curve, S, is constant.
IMPLICIT REAL*8 (A-H,O-Z)
REAL*8 R,TC,TF,QST,PI,RMST,UMST,LPR,UPR,TPR,KSIST,SCST,ETA
REAL*8 Y1ST,H1ST,Y2ST,H2ST
COMMON /PRMTS1/ R,TC,TF,QST,PI
COMMON /PRMTS2/ RMST,UMST,LPR,UPR,TPR
CALL TCCAL(SCST)
Y1ST=1./LPR*(UMST*UPR-R*TAN(TF))*(TAN(TC)+TAN(TF))/(TAN(TF)*(TAN
*(TC)-TAN(TF)))
H1ST=(UMST*UPR-R*TAN(TF))/(TAN(TC)-TAN(TF))*2*TAN(TC)/LPR
Y2ST=(2*R*TAN(TC)*TAN(TF)-UMST*UPR*(TAN(TC)+TAN(TF)))/(TAN(TF)*(
*TAN(TC)-TAN(TF))*LPR)
H2ST=Y2ST*TAN(TF)
IF (KSIST.LT.Y1ST) THEN

```

```

    UST=TPR/(Y1ST**2-RMST**2)*(Y1ST**2*H1ST+Y1ST**2*H2ST-
    *RMST**2*H2ST-RMST*H1ST*KSIST*SIN(ETA)-
    *(-2.*Y1ST**2*H1ST**2*RMST*KSIST*SIN(ETA)+
    *RMST**2*Y1ST**2*H1ST**2-
    *(RMST**2*H1ST**2-Y1ST**2*H1ST**2)*COS(ETA)**2*KSIST**2+
    *Y1ST**2*H1ST**2*SIN(ETA)**2*KSIST**2)**.5)
    ELSE IF (KSIST.GE.Y1ST) THEN
        UST=LPR/UPR*(R/LPR-KSIST)*TAN(TF)
    ENDIF
    UP2ST=UST**2
END

SUBROUTINE TCCAL(SCST)
    IMPLICIT REAL*8(A-H,O-Z)
    REAL*8 R,TC,TF,QST,PI
    REAL*8 RMST,UMST,LPR,UPR,TPR
    REAL*8 TCMAX,SCMAX,SCELB
    COMMON /PRMTS1/ R,TC,TF,QST,PI
    COMMON /PRMTS2/ RMST,UMST,LPR,UPR,TPR
    COMMON /PRMTS7/ TCMAX,SCMAX,SCELB
    COMMON /PRMTS14/ EPSLN,D,F
    IF (SCST.LT.SCMAX/LPR) THEN
        TC=TCMAX+TCMAX/(SCMAX+75*D)*(SCST*LPR-SCMAX)
    ELSE IF (SCST.GE.SCMAX/LPR) THEN
        TC=TCMAX-TCMAX/(SCELB+75*D-SCMAX)*(SCST*LPR-SCMAX)
    ENDIF
    RETURN
END

SUBROUTINE INCRAR(SCST, FNCTN, INTEG)
    IMPLICIT REAL*8(A-H,O-Z)
    INTEGER MR,MC,ML,ICRAR,JCRAR
    REAL*8 R,TC,TF,QST,PI,RMST,UMST,LPR,UPR,TPR,DKSIST,DETA
    REAL*8 R0,DBETA,DSCST
    REAL*8 KSIST,SCST,ETA,KSISTM,ETAN,INTEG,INTEG1,INTEG2
    REAL*8 W1,W2,W3,SPRC,TPRC
    REAL*8 G1PR,G2PR,G3PR,G4PR,G5PR,G6PR,G7PR,G8PR,G9PR
    COMMON /PRMTS1/ R,TC,TF,QST,PI
    COMMON /PRMTS2/ RMST,UMST,LPR,UPR,TPR
    COMMON /PRMTS3/ DKSIST,DETA
    COMMON /PRMTS4/ R0,DBETA,DSCST
    COMMON /PRMTS5/ MR,MC,ML
    INTEG1=0.
    INTEG2=0.
    W1=25./81
    W2=40./81
    W3=64./81
    SPRC=(3./5)**.5
    TPRC=(3./5)**.5
    DO 10 ICRAR=2,MR
        KSISTM=DKSIST/2+DKSIST*(ICRAR-1)
    DO 10 JCRAR=1,MC
        ETAN=DETA/2+DETA*(JCRAR-1)
        KSIST=KSISTM+DKSIST/2*SPRC
        ETA=ETAN+DETA/2*TPRC
        G1PR=FNCTN(KSIST,SCST,ETA)*KSIST
        KSIST=KSISTM
        ETA=ETAN+DETA/2*TPRC
        G2PR=FNCTN(KSIST,SCST,ETA)*KSIST
        KSIST=KSISTM-DKSIST/2*SPRC
        ETA=ETAN+DETA/2*TPRC
        G3PR=FNCTN(KSIST,SCST,ETA)*KSIST
        KSIST=KSISTM+DKSIST/2*SPRC
        ETA=ETAN
        G4PR=FNCTN(KSIST,SCST,ETA)*KSIST
        KSIST=KSISTM
        ETA=ETAN
        G5PR=FNCTN(KSIST,SCST,ETA)*KSIST
        KSIST=KSISTM-DKSIST/2*SPRC
        ETA=ETAN
        G6PR=FNCTN(KSIST,SCST,ETA)*KSIST
        KSIST=KSISTM+DKSIST/2*SPRC
        ETA=ETAN-DETA/2*TPRC
        G7PR=FNCTN(KSIST,SCST,ETA)*KSIST

```

```

KSIST=KSISTM
ETA=ETAN-DETA/2*TPRC
G8PR=FNCTN (KSIST, SCST, ETA) *KSIST
KSIST=KSISTM-DKSIST/2*SPRC
ETA=ETAN-DETA/2*TPRC
G9PR=FNCTN (KSIST, SCST, ETA) *KSIST
INTEG1=INTEG1+ (DKSIST*DETA/4) * (W1* (G1PR+G3PR+G7PR+G9PR) +W2* (G2PR+
*G4PR+G6PR+G8PR) +W3*G5PR)
10 CONTINUE
C For the central point of the circular domain
KSISTM=DKSIST/2
DO 20 JCRAR=1,MC
ETA=DETA/2+DETA* (JCRAR-1)
KSIST=KSISTM+DKSIST/2*SPRC
ETA=ETAN+DETA/2*TPRC
G1PR=FNCTN (KSIST, SCST, ETA) *KSIST
KSIST=KSISTM
ETA=ETAN+DETA/2*TPRC
G2PR=FNCTN (KSIST, SCST, ETA) *KSIST
KSIST=KSISTM-DKSIST/2*SPRC
ETA=ETAN+DETA/2*TPRC
G3PR=FNCTN (KSIST, SCST, ETA) *KSIST
KSIST=KSISTM+DKSIST/2*SPRC
ETA=ETAN
G4PR=FNCTN (KSIST, SCST, ETA) *KSIST
KSIST=KSISTM
ETA=ETAN
G5PR=FNCTN (KSIST, SCST, ETA) *KSIST
KSIST=KSISTM-DKSIST/2*SPRC
ETA=ETAN
G6PR=FNCTN (KSIST, SCST, ETA) *KSIST
KSIST=KSISTM+DKSIST/2*SPRC
ETA=ETAN-DETA/2*TPRC
G7PR=FNCTN (KSIST, SCST, ETA) *KSIST
KSIST=KSISTM
ETA=ETAN-DETA/2*TPRC
G8PR=FNCTN (KSIST, SCST, ETA) *KSIST
KSIST=KSISTM-DKSIST/2*SPRC
ETA=ETAN-DETA/2*TPRC
G9PR=FNCTN (KSIST, SCST, ETA) *KSIST
INTEG2=INTEG2+ (DKSIST*DETA/4) * (W1* (G1PR+G3PR+G7PR+G9PR) +W2* (G2PR+
*G4PR+G6PR+G8PR) +W3*G5PR)
20 CONTINUE
INTEG=INTEG1+INTEG2
END

FUNCTION DBUST (KSIST, SCST, ETA)
IMPLICIT REAL*8 (A-H, O-Z)
REAL*8 R, TC, TF, QST, PI, RMST, UMST, LPR, UPR, TPR, R0, DBETA, DSCST
REAL*8 KSIST, SCST, ETA
REAL*8 DSCST1, DBETA1
REAL*8 UM1ST, UM2ST, RM1ST, RM2ST, TC1, TC2
COMMON /PRMTS1/ R, TC, TF, QST, PI
COMMON /PRMTS2/ RMST, UMST, LPR, UPR, TPR
COMMON /PRMTS4/ R0, DBETA, DSCST
COMMON /PRMTS16/ DSCST1, DBETA1
COMMON /PRMTS17/ UM1ST, UM2ST, RM1ST, RM2ST, TC1, TC2
UMST=UM1ST
RMST=RM1ST
TC=TC1
UST1=UST (KSIST, SCST+DSCST1, ETA)
UMST=UM2ST
RMST=RM2ST
TC=TC2
UST2=UST (KSIST, SCST, ETA)
DBUST= (UST1-UST2) /DBETA1
RETURN
END

SUBROUTINE INTLIN (KSIST, SCST, ETA, FNCTNL, INTEGL)
C This subprogram takes an integral along a straight line between
C given boundaries by using 3-point Gauss Quadrature.
IMPLICIT REAL*8 (A-H, O-Z)
INTEGER MR, MC, ML, MLNEW, IML

```

```

REAL*8 R,TC,TF,QST,PI,RMST,UMST,LPR,UPR,TPR,DKSIST,DETA
REAL*8 R0,DBETA,DSCST,EMELRT,DRST,RST
REAL*8 H1PRST,H2PRST,H3PRST
REAL*8 W1,W2,APRC,RSTR,ZST,RSTL
REAL*8 KSIST,ETA,INTEGL
REAL*8 DRCLST(2000)
REAL*8 SPLGST,DRSTP
COMMON /PRM1S1/ R,TC,TF,QST,PI
COMMON /PRM1S2/ RMST,UMST,LPR,UPR,TPR
COMMON /PRM1S3/ DKSIST,DETA
COMMON /PRM1S4/ R0,DBETA,DSCST
COMMON /PRM1S5/ MR,MC,ML
COMMON /PRM1S6/ EMELRT
COMMON /PRM1S15/ DRCLST
INTEGL=0.
W1=5./9
W2=8./9
APRC=(3./5)**.5
RSTR=R0/LPR+KSIST*SIN(ETA)
ZST=-KSIST*COS(ETA)
RSTL=R0/LPR-(R**2/LPR**2-ZST**2)**.5
SPLGST=0.
IML=0
30 SPLGST=SPLGST+DRCLST(IML+1)
IF (SPLGST.LE.RSTR-RSTL) THEN
IML=IML+1
GOTO 30
ENDIF
MLNEW=IML
SPLGST=SPLGST-DRCLST(MLNEW+1)
DO 10 ILINT=1,MLNEW
C -----
IF (ILINT.EQ.1) THEN
RST=RSTL+DRCLST(ILINT)/2
DRST=DRCLST(ILINT)
ELSE
RST=RST+DRCLST(ILINT-1)/2+DRCLST(ILINT)/2
DRST=DRCLST(ILINT)
ENDIF
C -----
20 KSIST=(ZST**2+(RST-DRST/2*APRC-R0/LPR)**2)**.5
CALL ETAC(ZST,RST-DRST/2*APRC,ETA)
H1PRST=FNCTNL(KSIST,SCST,ETA)
C -----
KSIST=(ZST**2+(RST-R0/LPR)**2)**.5
CALL ETAC(ZST,RST,ETA)
H2PRST=FNCTNL(KSIST,SCST,ETA)
C -----
KSIST=(ZST**2+(RST+DRST/2*APRC-R0/LPR)**2)**.5
CALL ETAC(ZST,RST+DRST/2*APRC,ETA)
H3PRST=FNCTNL(KSIST,SCST,ETA)
C -----
INTEGL=INTEGL+(DRST/2)*(W1*H1PRST+W2*H2PRST+W1*H3PRST)
IF ((RSTR-RSTL)-SPLGST)/DRST.GT.EMELRT .AND. ILINT.EQ.MLNEW)
*THEN
DRSTP=DRST
DRST=(RSTR-RSTL)-SPLGST
RST=RST+DRSTP/2+DRST/2
MLNEW=MLNEW+1
GOTO 20
ENDIF
10 CONTINUE
RETURN
END

SUBROUTINE MCLSTR(R,ML,CLSTRT,DRCLST)
IMPLICIT REAL*8 (A-H,O-Z)
REAL*8 R,CLSTRT,DRCL(2000),DRCLST(2000)
INTEGER N4,ML
REAL*8 RMST,UMST,LPR,UPR,TPR
COMMON /PRM1S2/ RMST,UMST,LPR,UPR,TPR
DO 10 I=1,ML+2
DRCL(I)=2*R*(CLSTRT-1)/(CLSTRT**ML-1)*CLSTRT**(I-1)
10 DRCLST(I)=DRCL(I)/LPR

```

```

RETURN
END

SUBROUTINE PDS1ST(N,SCST,Y,YPRIME)
IMPLICIT REAL*8 (A-H,O-Z)
REAL*8 Y(N),YPRIME(N),SCST,C4,C6,C7,C8
INTEGER N
COMMON/ TERMS2/ C4,C6,C7,C8
YPRIME(1)=C4+C6+C7+C8
RETURN
END

SUBROUTINE PDS2ST(N,SCST,Y,YPRIME)
IMPLICIT REAL*8 (A-H,O-Z)
REAL*8 Y(N),YPRIME(N),SCST,C9,C10,C11,C12
INTEGER N
COMMON/ TERMS3/ C9,C10,C11,C12
YPRIME(1)=C9+C10+C11+C12
RETURN
END

SUBROUTINE PCTFST(N,RDIST,Y,YPRIME)
IMPLICIT REAL*8 (A-H,O-Z)
REAL*8 Y(N),YPRIME(N),SCEDST,C13,C14,C15,C17,C18,C19,C20,C21
REAL*8 YPR1,YPR2,YPR3,YPR4,YPR5,YPR6,YPR7,YPR8,YPR9,YPR10
REAL*8 KSIST,KSISTM,ETA,RDIST,RDISTM,SCSTL,ETAN,ZST,ZSTK,DZST
REAL*8 RMST,UMST,LPR,UPR,TPR,RO,MU,SCMAX,AS,BS,HS,BETA
REAL*8 R,TC,TF,QST,PI
REAL*8 Q1ST,QPTSST
REAL*8 PAVE(1)
REAL*8 EPSTST,E11,E12,E21,E22,E31,E32
REAL*8 UM1ST,UM2ST,RM1ST,RM2ST,TC1,TC2
INTEGER N,NUM
EXTERNAL DBUST,ust
COMMON /PRMTS1/ R,TC,TF,QST,PI
COMMON /PRMTS2/ RMST,UMST,LPR,UPR,TPR
COMMON /PRMTS4/ R0,DBETA,DSCST
COMMON /PRMTS7/ TCMAX,SCMAX,SCELB
COMMON /PRMTS13/ QPTSST,TIST
COMMON /PRMTS16/ DSCST1,DBETA1
COMMON /PRMTS17/ UM1ST,UM2ST,RM1ST,RM2ST,TC1,TC2
COMMON /PRMTS21/ SCEDST
COMMON /TERMS4/ DRDIST,MLD
COMMON/ CONST/PB,RO,PAVE,MU
COMMON /TERMS6/ BETA,G
COMMON /W/ C15
COMMON /DBDVR/ IP,IPD
DZST=DRDIST
ZST=0.
ZSTK=ZST
RDISTM=RDIST
KSISTM=(ZSTK**2+(RDISTM-R0/LPR)**2)**.5
CALL ETAC(ZSTK,RDISTM,ETAN)
SCSTL=SCEDST
CALL UMSTCL(SCSTL)
UM2ST=UMST
RM2ST=RMST
TC2=TC
CALL UMSTCL(SCSTL+DSCST1)
UM1ST=UMST
RM1ST=RMST
TC1=TC
CALL INTLIN(KSISTM,SCSTL,ETAN,DBUST,C13)
Q1ST=QST
QST=QPTSST
KSISTM=(ZSTK**2+(RDISTM-R0/LPR)**2)**.5
CALL ETAC(ZSTK,RDISTM,ETAN)
SCSTL=SCEDST
CALL UMSTCL(SCSTL)
UM2ST=UMST
RM2ST=RMST
TC2=TC
CALL UMSTCL(SCSTL+DSCST1)
UM1ST=UMST

```

```

RM1ST=RMST
TC1=TC
CALL INTLIN(KSISTM, SCSTL, ETAN, DBUST, C14)
QST=Q1ST
ZSTK=ZST
RDISTM=RDIST+DRDIST
KSISTM=(ZSTK**2+(RDISTM-R0/LPR)**2)**.5
CALL ETAC(ZSTK, RDISTM, ETAN)
SCSTL=SCEDST
CALL UMSTCL(SCSTL)
UM2ST=UMST
RM2ST=RMST
TC2=TC
CALL UMSTCL(SCSTL+DSCST1)
UM1ST=UMST
RM1ST=RMST
TC1=TC
CALL INTLIN(KSISTM, SCSTL, ETAN, DBUST, C15)
ZSTK=ZST
RDISTM=RDIST
KSISTM=(ZSTK**2+(RDISTM-R0/LPR)**2)**.5
CALL ETAC(ZSTK, RDISTM, ETAN)
SCSTL=SCEDST+DSCST1
CALL UMSTCL(SCSTL)
UM2ST=UMST
RM2ST=RMST
TC2=TC
CALL UMSTCL(SCSTL+DSCST1)
UM1ST=UMST
RM1ST=RMST
TC1=TC
CALL INTLIN(KSISTM, SCSTL, ETAN, DBUST, C16)
ZSTK=ZST
RDISTM=RDIST
KSISTM=(ZSTK**2+(RDISTM-R0/LPR)**2)**.5
CALL ETAC(ZSTK, RDISTM, ETAN)
SCSTL=SCEDST
CALL UMSTCL(SCSTL)
C21=UST(KSISTM, SCSTL, ETAN)
C-----
C      Calculation of the terms in the differential ordinary
C      differential equation to be used for the calculation of the
C      impact pressure at the outer-most point at the convex side of the
C      elbow.
      YPR1=1./RDIST*(C13-C14)/TIST
C-----
      YPR2=1./2*(1/(RDIST+DRDIST)*C15)**2-(1/RDIST*C13)**2)/DRDIST
C-----
      YPR3=C21/RDIST**2*(C16-C13)/DBETA1
C-----
      YPR4=C21**2/RDIST
C-----
      ZSTK=ZST
      RDISTM=RDIST
      KSISTM=(ZSTK**2+(RDISTM-R0/LPR)**2)**.5
      CALL ETAC(ZSTK, RDISTM, ETAN)
      SCSTL=SCEDST
      CALL UMSTCL(SCSTL)
      CALL EDDY(KSISTM, SCSTL, ETAN, EPSTST)
      YPR8=EPSTST/RDIST**3*C13
C-----
      ZSTK=ZST
      RDISTM=RDIST
      KSISTM=(ZSTK**2+(RDISTM-R0/LPR)**2)**.5
      CALL ETAC(ZSTK, RDISTM, ETAN)
      SCSTL=SCEDST
      CALL UMSTCL(SCSTL)
      CALL EDDY(KSISTM, SCSTL, ETAN, EPSTST)
      YPR9=2*EPSTST/RDIST**2*(C16-C13)/DBETA1
C-----
      YPR10=LPR/UPR**2*G*COS(BETA-DBETA1)
C-----
C-----
      YPRIME(1)=YPR1+YPR2+YPR3+YPR4+YPR8-YPR9+YPR10

```



```

RETURN
END

SUBROUTINE ETAC(ZST,RCST,ETA)
IMPLICIT REAL*8 (A-H,O-Z)
COMMON /PRMTS1/ R,TC,TF,QST,PI
COMMON /PRMTS2/ RMST,UM,LPR,UPR,TPR
COMMON /PRMTS4/ R0,DBETA,DSCST
REAL*8 ZST,RCST,ETA
REAL*8 R,TC,TF,QST,PI,RMST,UMST,LPR,UPR,TPR,R0,DBETA,DSCST
IF (ZST.EQ.0. .AND. RCST-R0/LPR.EQ.0) THEN
ETA=PI/2
ELSE IF (ZST.EQ.0. .AND. RCST-R0/LPR.GT.0) THEN
ETA=PI/2.
ELSE IF (ZST.EQ.0. .AND. RCST-R0/LPR.LT.0) THEN
ETA=3*PI/2.
ELSE
ETA=ATAN((R0/LPR-RCST)/ZST)
IF (RCST-R0/LPR.LT.0. .AND. ZST.LT.0.) THEN
ETA=ETA+2*PI
ELSE
IF (ZST.GT.0.) ETA=ETA+PI
ENDIF
ENDIF
RETURN
END

SUBROUTINE PEAKCL(SNMST,DSCST,PNMST,PNM1ST,PNM2ST,SCMAX,PPEAST)
IMPLICIT REAL*8 (A-H,O-Z)
REAL*8 SNMST,DSCST,PNMST,PNM1ST,PNM2ST,SCMAX,PPEAST
REAL*8 RMST,UM,LPR,UPR,TPR
COMMON /PRMTS2/ RMST,UM,LPR,UPR,TPR
C      Finite difference method with second order forward differences
C      were used here.
PPEAST=PNMST+(-3*PNMST+4*PNM1ST-PNM2ST)/(2*DSCST)*(SCMAX/LPR
*-SNMST)
RETURN
END

SUBROUTINE PINTER(PST,SCST,P1ST,P2ST,SC1ST,SC2ST)
IMPLICIT REAL*8 (A-H,O-Z)
REAL*8 PST,SCST,P1ST,P2ST,SC1ST,SC2ST
C      This subroutine is used for calculating the average presssure
C      values at the intermediary faces of the volume elements, along the
C      elbow and the vertical extension part.
PST=P2ST+(P2ST-P1ST)/(SC2ST-SC1ST)*(SCST-SC2ST)
RETURN
END

SUBROUTINE DFELBW(DFXST,DFYST)
IMPLICIT REAL*8 (A-H,O-Z)
REAL*8 DFXST,DFYST,LPR,R0,DBETAV,QST,QPTSST,TIST
REAL*8 BETAU,BETAM,BETAD,IBUST,IBDST,PAVUST,PAVDST,ACRSS
REAL*8 PAVNST,PAVMST,PAVPST
REAL*8 SCUST,SCDST,SCNST,SCMST,SCPST
EXTERNAL UP2ST
COMMON /PRMTS1/ R,TC,TF,QST,PI
COMMON /PRMTS2/ RMST,UMST,LPR,UPR,TPR
COMMON /PRMTS4/ R0,DBETA,DSCST
COMMON /TERMS6/ BETA,G
COMMON /PRMTS13/ QPTSST,TIST
COMMON /PRMTS18/ PAVUST,PAVDST
COMMON /PRMTS19/ SCUST,SCMST,SCDST
COMMON /PRMTS20/ ACRSS
BETAU=SCUST*LPR/R0
BETAM=SCMST*LPR/R0
BETAD=SCDST*LPR/R0
DBETAV=BETAD-BETAU
CALL UMSTCL(SCUST)
CALL INCRAR(SCUST,UP2ST,IBUST)
CALL UMSTCL(SCDST)
CALL INCRAR(SCDST,UP2ST,IBDST)
DFXST=-1./LPR*R0*DBETAV*COS(BETAM)*(QST-QPTSST)/TIST+
*COS(BETAU)*IBUST-COS(BETAD)*IBDST+

```

```

*1./LPR**2*PAVUST*COS(BETAU)*ACRSS-
*1./LPR**2*PAVDST*COS(BETAD)*ACRSS
  DFYST=1./LPR*R0*DBETAV*SIN(BETAM)*(QST-QPTSST)/TIST-
*SIN(BETAU)*IBUST+SIN(BETAD)*IBDST-
*1./LPR**2*PAVUST*SIN(BETAU)*ACRSS+
*1./LPR**2*PAVDST*SIN(BETAD)*ACRSS-
*G*R0*DBETAV*ACRSS/(LPR**2*UPR**2)
  RETURN
  END

SUBROUTINE DFEXTN(DFXST,DFYST)
  IMPLICIT REAL*8(A-H,O-Z)
  REAL*8 DFYST,LPR,R0,DSCVST,QST,QPTSST,TIST
  REAL*8 ISUST,ISDST,PAVUST,PAVDST,ACRSS
  REAL*8 PAVNST,PAVMST,PAVPST
  REAL*8 SCUST,SCDST,SCNST,SCMST,SCPST
  EXTERNAL UP2ST
  COMMON /PRMTS1/ R,TC,TF,QST,PI
  COMMON /PRMTS2/ RMST,UMST,LPR,UPR,TPR
  COMMON /PRMTS4/ R0,DBETA,DSCST
  COMMON /TERMS6/ BETA,G
  COMMON /PRMTS13/ QPTSST,TIST
  COMMON /PRMTS18/ PAVUST,PAVDST
  COMMON /PRMTS19/ SCUST,SCMST,SCDST
  COMMON /PRMTS20/ ACRSS
  DSCVST=SCDST-SCUST
  CALL UMSTCL(SCUST)
  CALL INCRAR(SCUST,UP2ST,ISUST)
  CALL UMSTCL(SCDST)
  CALL INCRAR(SCDST,UP2ST,ISDST)
  DFXST=0.
  DFYST=DSCVST*(QST-QPTSST)/TIST-
  *ISUST+ISDST-
*1./LPR**2*PAVUST*ACRSS+
*1./LPR**2*PAVDST*ACRSS-
*G*R0*DSCVST*ACRSS/(LPR**2*UPR**2)
  RETURN
  END

SUBROUTINE EDDY(KSIST,SCST,ETA,EPSTST)
C      This subroutine calculates Eddy Viscosity at any point in the
C      elbow by using Mixing Length Theory given in Chen, C. J. and Yaw
C      S. Y. 1997. Fundamentals of Turbulence Modeling. Taylor and
C      Francis Ltd. New York.
  IMPLICIT REAL*8(A-H,O-Z)
  REAL*8 KSIST,SCST,ETA,EPSTST,GM,LPR,R,LMST,DKSXST
  COMMON /PRMTS1/ R,TC,TF,QST,PI
  COMMON /PRMTS2/ RMST,UMST,LPR,UPR,TPR
  COMMON /TERMS4/ DKSXST,MLD
  GM=KSIST*LPR/R
  LMST=R/LPR*(0.14-0.08*GM**2-0.06*GM**4)
  EPSTST=LMST**2*ABS((UST(KSIST+DKSXST,SCST,ETA)-UST(KSIST,SCST,
  *ETA))/DKSXST)
  RETURN
  END

      subroutine dverk (n, fcn, x, y, xend, tol, ind, c, nw, w)
      integer n, ind, nw, k
      double precision x, y(n), xend, tol, c(24), w(nw,9), temp
C
C*****
C
C note added 11/14/85.
C
C if you discover any errors in this subroutine, please contact
C
C      kenneth r. jackson
C      department of computer science
C      university of toronto
C      toronto, ontario,
C      canada m5s 1a4
C
C      phone: 416-978-7075
C
C

```

```

c      electronic mail:
c      uucp: {cornell,decvax,ihnp4,linus,uw-beaver}!utcsri!krj
c      csnet: krj@toronto
c      arpa: krj.toronto@csnet-relay
c      bitnet: krj%toronto@csnet-relay.arpa
c
c dverk is written in fortran 66.
c
c the constants dwarf and rreb -- c(10) and c(11), respectively -- are
c set for a vax in double precision. they should be reset, as
c described below, if this program is run on another machine.
c
c the c array is declared in this subroutine to have one element only,
c although more elements are referenced in this subroutine. this
c causes some compilers to issue warning messages. there is, though,
c no error provided c is declared sufficiently large in the calling
c program, as described below.
c
c the following external statement for fcn was added to avoid a
c warning message from the unix f77 compiler. the original dverk
c comments and code follow it.
c
c*****
c
c      external fcn
c
c*****
c
c      purpose - this is a runge-kutta subroutine based on verner's
c fifth and sixth order pair of formulas for finding approximations to
c the solution of a system of first order ordinary differential
c equations with initial conditions. it attempts to keep the global
c error proportional to a tolerance specified by the user. (the
c proportionality depends on the kind of error control that is used,
c as well as the differential equation and the range of integration.)
c
c      various options are available to the user, including different
c kinds of error control, restrictions on step sizes, and interrupts
c which permit the user to examine the state of the calculation (and
c perhaps make modifications) during intermediate stages.
c
c      the program is efficient for non-stiff systems. however, a good
c variable-order-adams method will probably be more efficient if the
c function evaluations are very costly. such a method would also be
c more suitable if one wanted to obtain a large number of intermediate
c solution values by interpolation, as might be the case for example
c with graphical output.
c
c
c                        hull-enright-jackson  1/10/76
c
c*****
c
c      use - the user must specify each of the following
c
c      n      number of equations
c
c      fcn      name of subroutine for evaluating functions - the subroutine
c                itself must also be provided by the user - it should be of
c                the following form
c                subroutine fcn(n, x, y, yprime)
c                integer n
c                double precision x, y(n), yprime(n)
c                *** etc ***
c                and it should evaluate yprime, given n, x and y
c
c      x      independent variable - initial value supplied by user
c
c      y      dependent variable - initial values of components y(1), y(2),
c                ..., y(n) supplied by user
c
c      xend    value of x to which integration is to be carried out - it may
c                be less than the initial value of x
c
c      tol     tolerance - the subroutine attempts to control a norm of the

```

```

c      local error in such a way that the global error is *
c      proportional to tol. in some problems there will be enough *
c      damping of errors, as well as some cancellation, so that *
c      the global error will be less than tol. alternatively, the *
c      control can be viewed as attempting to provide a *
c      calculated value of y at xend which is the exact solution *
c      to the problem  $y' = f(x,y) + e(x)$  where the norm of  $e(x)$  *
c      is proportional to tol. (the norm is a max norm with *
c      weights that depend on the error control strategy chosen *
c      by the user. the default weight for the k-th component is *
c       $1/\max(1, \text{abs}(y(k)))$ , which therefore provides a mixture of *
c      absolute and relative error control.) *
c      *
c      ind indicator - on initial entry ind must be set equal to either *
c      1 or 2. if the user does not wish to use any options, he *
c      should set ind to 1 - all that remains for the user to do *
c      then is to declare c and w, and to specify nw. the user *
c      may also select various options on initial entry by *
c      setting ind = 2 and initializing the first 9 components of *
c      c as described in the next section. he may also re-enter *
c      the subroutine with ind = 3 as mentioned again below. in *
c      any event, the subroutine returns with ind equal to *
c      3 after a normal return *
c      4, 5, or 6 after an interrupt (see options c(8), c(9)) *
c      -1, -2, or -3 after an error condition (see below) *
c      *
c      c communications vector - the dimension must be greater than or *
c      equal to 24, unless option c(1) = 4 or 5 is used, in which *
c      case the dimension must be greater than or equal to n+30 *
c      *
c      nw first dimension of workspace w - must be greater than or *
c      equal to n *
c      *
c      w workspace matrix - first dimension must be nw and second must *
c      be greater than or equal to 9 *
c      *
c      the subroutine will normally return with ind = 3, having *
c      replaced the initial values of x and y with, respectively, the value *
c      of xend and an approximation to y at xend. the subroutine can be *
c      called repeatedly with new values of xend without having to change *
c      any other argument. however, changes in tol, or any of the options *
c      described below, may also be made on such a re-entry if desired. *
c      *
c      three error returns are also possible, in which case x and y *
c      will be the most recently accepted values - *
c      with ind = -3 the subroutine was unable to satisfy the error *
c      requirement with a particular step-size that is less than or *
c      equal to hmin, which may mean that tol is too small *
c      with ind = -2 the value of hmin is greater than hmax, which *
c      probably means that the requested tol (which is used in the *
c      calculation of hmin) is too small *
c      with ind = -1 the allowed maximum number of fcn evaluations has *
c      been exceeded, but this can only occur if option c(7), as *
c      described in the next section, has been used *
c      *
c      there are several circumstances that will cause the calculations *
c      to be terminated, along with output of information that will help *
c      the user determine the cause of the trouble. these circumstances *
c      involve entry with illegal or inconsistent values of the arguments, *
c      such as attempting a normal re-entry without first changing the *
c      value of xend, or attempting to re-enter with ind less than zero. *
c      *
c      *****
c      *
c      options - if the subroutine is entered with ind = 1, the first 9 *
c      components of the communications vector are initialized to zero, and *
c      the subroutine uses only default values for each option. if the *
c      subroutine is entered with ind = 2, the user must specify each of *
c      these 9 components - normally he would first set them all to zero, *
c      and then make non-zero those that correspond to the particular *
c      options he wishes to select. in any event, options may be changed on *
c      re-entry to the subroutine - but if the user changes any of the *
c      options, or tol, in the course of a calculation he should be careful *
c      about how such changes affect the subroutine - it may be better to *

```

```

c restart with ind = 1 or 2. (components 10 to 24 of c are used by the *
c program - the information is available to the user, but should not *
c normally be changed by him.) *
c *
c c(1) error control indicator - the norm of the local error is the *
c max norm of the weighted error estimate vector, the *
c weights being determined according to the value of c(1) - *
c if c(1)=1 the weights are 1 (absolute error control) *
c if c(1)=2 the weights are 1/abs(y(k)) (relative error *
c control) *
c if c(1)=3 the weights are 1/max(abs(c(2)),abs(y(k))) *
c (relative error control, unless abs(y(k)) is less *
c than the floor value, abs(c(2)) ) *
c if c(1)=4 the weights are 1/max(abs(c(k+30)),abs(y(k))) *
c (here individual floor values are used) *
c if c(1)=5 the weights are 1/abs(c(k+30)) *
c for all other values of c(1), including c(1) = 0, the *
c default values of the weights are taken to be *
c 1/max(1,abs(y(k))), as mentioned earlier *
c (in the two cases c(1) = 4 or 5 the user must declare the *
c dimension of c to be at least n+30 and must initialize the *
c components c(31), c(32), ..., c(n+30).) *
c *
c c(2) floor value - used when the indicator c(1) has the value 3 *
c *
c c(3) hmin specification - if not zero, the subroutine chooses hmin *
c to be abs(c(3)) - otherwise it uses the default value *
c 10*max(dwarf,rreb*max(weighted norm y/tol,abs(x))), *
c where dwarf is a very small positive machine number and *
c rreb is the relative roundoff error bound *
c *
c c(4) hstart specification - if not zero, the subroutine will use *
c an initial hmag equal to abs(c(4)), except of course for *
c the restrictions imposed by hmin and hmax - otherwise it *
c uses the default value of hmax*(tol)**(1/6) *
c *
c c(5) scale specification - this is intended to be a measure of the *
c scale of the problem - larger values of scale tend to make *
c the method more reliable, first by possibly restricting *
c hmax (as described below) and second, by tightening the *
c acceptance requirement - if c(5) is zero, a default value *
c of 1 is used. for linear homogeneous problems with *
c constant coefficients, an appropriate value for scale is a *
c norm of the associated matrix. for other problems, an *
c approximation to an average value of a norm of the *
c jacobian along the trajectory may be appropriate *
c *
c c(6) hmax specification - four cases are possible *
c if c(6).ne.0 and c(5).ne.0, hmax is taken to be *
c min(abs(c(6)),2/abs(c(5))) *
c if c(6).ne.0 and c(5).eq.0, hmax is taken to be abs(c(6)) *
c if c(6).eq.0 and c(5).ne.0, hmax is taken to be *
c 2/abs(c(5)) *
c if c(6).eq.0 and c(5).eq.0, hmax is given a default value *
c of 2 *
c *
c c(7) maximum number of function evaluations - if not zero, an *
c error return with ind = -1 will be caused when the number *
c of function evaluations exceeds abs(c(7)) *
c *
c c(8) interrupt number 1 - if not zero, the subroutine will *
c interrupt the calculations after it has chosen its *
c preliminary value of hmag, and just before choosing htrial *
c and xtrial in preparation for taking a step (htrial may *
c differ from hmag in sign, and may require adjustment if *
c xend is near) - the subroutine returns with ind = 4, and *
c will resume calculation at the point of interruption if *
c re-entered with ind = 4 *
c *
c c(9) interrupt number 2 - if not zero, the subroutine will *
c interrupt the calculations immediately after it has *
c decided whether or not to accept the result of the most *
c recent trial step, with ind = 5 if it plans to accept, or *
c ind = 6 if it plans to reject - y(*) is the previously *

```

```

c          accepted result, while w(*,9) is the newly computed trial *
c          value, and w(*,2) is the unweighted error estimate vector. *
c          the subroutine will resume calculations at the point of *
c          interruption on re-entry with ind = 5 or 6. (the user may *
c          change ind in this case if he wishes, for example to force *
c          acceptance of a step that would otherwise be rejected, or *
c          vice versa. he can also restart with ind = 1 or 2.) *
c          *
c*****
c          summary of the components of the communications vector *
c          *
c          prescribed at the option      determined by the program *
c          of the user *
c          *
c          c(10) rreb(rel roundoff err bnd) *
c          c(1) error control indicator  c(11) dwarf (very small mach no) *
c          c(2) floor value              c(12) weighted norm y *
c          c(3) hmin specification        c(13) hmin *
c          c(4) hstart specification     c(14) hmag *
c          c(5) scale specification      c(15) scale *
c          c(6) hmax specification        c(16) hmax *
c          c(7) max no of fcn evals      c(17) xtrial *
c          c(8) interrupt no 1           c(18) htrial *
c          c(9) interrupt no 2           c(19) est *
c          *
c          c(20) previous xend *
c          c(21) flag for xend *
c          c(22) no of successful steps *
c          c(23) no of successive failures *
c          c(24) no of fcn evals *
c          *
c          if c(1) = 4 or 5, c(31), c(32), ... c(n+30) are floor values *
c          *
c*****
c          an overview of the program *
c          *
c          begin initialization, parameter checking, interrupt re-entries *
c          .....abort if ind out of range 1 to 6 *
c          . cases - initial entry, normal re-entry, interrupt re-entries *
c          . case 1 - initial entry (ind .eq. 1 or 2) *
c          v.....abort if n.gt.nw or tol.le.0 *
c          . if initial entry without options (ind .eq. 1) *
c          . set c(1) to c(9) equal to zero *
c          . else initial entry with options (ind .eq. 2) *
c          . make c(1) to c(9) non-negative *
c          . make floor values non-negative if they are to be used *
c          . end if *
c          . initialize rreb, dwarf, prev xend, flag, counts *
c          . case 2 - normal re-entry (ind .eq. 3) *
c          .....abort if xend reached, and either x changed or xend not *
c          . re-initialize flag *
c          . case 3 - re-entry following an interrupt (ind .eq. 4 to 6) *
c          v transfer control to the appropriate re-entry point..... *
c          . end cases *
c          . end initialization, etc. *
c          *
c          . loop through the following 4 stages, once for each trial step *
c          . stage 1 - prepare *
c          *****error return (with ind=-1) if no of fcn evals too great *
c          . calc slope (adding 1 to no of fcn evals) if ind .ne. 6 *
c          . calc hmin, scale, hmax *
c          *****error return (with ind=-2) if hmin .gt. hmax *
c          . calc preliminary hmag *
c          *****interrupt no 1 (with ind=4) if requested.....re-entry.v *
c          . calc hmag, xtrial and htrial *
c          . end stage 1 *
c          v stage 2 - calc ytrial (adding 7 to no of fcn evals) *
c          . stage 3 - calc the error estimate *
c          . stage 4 - make decisions *
c          . set ind=5 if step acceptable, else set ind=6 *
c          *****interrupt no 2 if requested.....re-entry.v *
c          . if step accepted (ind .eq. 5) *
c          . update x, y from xtrial, ytrial *

```

```

c .          add 1 to no of successful steps *
c .          set no of successive failures to zero *
c*****return(with ind=3, xend saved, flag set) if x .eq. xend *
c .          else step not accepted (ind .eq. 6) *
c .          add 1 to no of successive failures *
c*****error return (with ind=-3) if hmag .le. hmin *
c .          end if *
c .          end stage 4 *
c .          end loop *
c . *
c begin abort action *
c   output appropriate message about stopping the calculations, *
c   along with values of ind, n, nw, tol, hmin, hmax, x, xend, *
c   previous xend, no of successful steps, no of successive *
c   failures, no of fcn evals, and the components of y *
c   stop *
c end abort action *
c *
c*****
c
c   *****
c   * begin initialization, parameter checking, interrupt re-entries *
c   *****
c
c   .....abort if ind out of range 1 to 6
c       if (ind.lt.1 .or. ind.gt.6) go to 500
c
c   cases - initial entry, normal re-entry, interrupt re-entries
c       go to (5, 5, 45, 1111, 2222, 2222), ind
c       case 1 - initial entry (ind .eq. 1 or 2)
c   .....abort if n.gt.nw or tol.le.0
c       5   if (n.gt.nw .or. tol.le.0.d0) go to 500
c           if (ind.eq. 2) go to 15
c           initial entry without options (ind .eq. 1)
c           set c(1) to c(9) equal to 0
c           do 10 k = 1, 9
c               c(k) = 0.d0
c       10   continue
c           go to 35
c       15   continue
c           initial entry with options (ind .eq. 2)
c           make c(1) to c(9) non-negative
c           do 20 k = 1, 9
c               c(k) = dabs(c(k))
c       20   continue
c           make floor values non-negative if they are to be used
c           if (c(1).ne.4.d0 .and. c(1).ne.5.d0) go to 30
c           do 25 k = 1, n
c               c(k+30) = dabs(c(k+30))
c       25   continue
c       30   continue
c       35   continue
c           initialize rreb, dwarf, prev xend, flag, counts
c           c(10) = 2.d0**(-56)
c           c(11) = 1.d-35
c           set previous xend initially to initial value of x
c           c(20) = x
c           do 40 k = 21, 24
c               c(k) = 0.d0
c       40   continue
c           go to 50
c       case 2 - normal re-entry (ind .eq. 3)
c   .....abort if xend reached, and either x changed or xend not
c       45   if (c(21).ne.0.d0 .and.
c           +   (x.ne.c(20) .or. xend.eq.c(20))) go to 500
c           re-initialize flag
c           c(21) = 0.d0
c           go to 50
c       case 3 - re-entry following an interrupt (ind .eq. 4 to 6)
c           transfer control to the appropriate re-entry point.....
c           this has already been handled by the computed go to
c           .
c       end cases *
c       50   continue
c

```

```

c      end initialization, etc.
c
c      *****
c      * loop through the following 4 stages, once for each trial step *
c      * until the occurrence of one of the following *
c      * (a) the normal return (with ind .eq. 3) on reaching xend in *
c      * stage 4 *
c      * (b) an error return (with ind .lt. 0) in stage 1 or stage 4 *
c      * (c) an interrupt return (with ind .eq. 4, 5 or 6), if *
c      * requested, in stage 1 or stage 4 *
c      *****
c
99999 continue
c
c      *****
c      * stage 1 - prepare - do calculations of hmin, hmax, etc., *
c      * and some parameter checking, and end up with suitable *
c      * values of hmag, xtrial and htrial in preparation for taking *
c      * an integration step. *
c      *****
c
c*****error return (with ind=-1) if no of fcn evals too great
      if (c(7).eq.0.d0 .or. c(24).lt.c(7)) go to 100
      ind = -1
      return
100      continue
c
c      calculate slope (adding 1 to no of fcn evals) if ind .ne. 6
      if (ind .eq. 6) go to 105
      call fcn(n, x, y, w(1,1))
      c(24) = c(24) + 1.d0
105      continue
c
c      calculate hmin - use default unless value prescribed
      c(13) = c(3)
      if (c(3) .ne. 0.d0) go to 165
      calculate default value of hmin
      first calculate weighted norm y - c(12) - as specified
      by the error control indicator c(1)
      temp = 0.d0
      if (c(1) .ne. 1.d0) go to 115
      absolute error control - weights are 1
      do 110 k = 1, n
          temp = dmax1(temp, dabs(y(k)))
110      continue
      c(12) = temp
      go to 160
115      if (c(1) .ne. 2.d0) go to 120
      relative error control - weights are 1/dabs(y(k)) so
      weighted norm y is 1
      c(12) = 1.d0
      go to 160
120      if (c(1) .ne. 3.d0) go to 130
      weights are 1/max(c(2),abs(y(k)))
      do 125 k = 1, n
          temp = dmax1(temp, dabs(y(k))/c(2))
125      continue
      c(12) = dmin1(temp, 1.d0)
      go to 160
130      if (c(1) .ne. 4.d0) go to 140
      weights are 1/max(c(k+30),abs(y(k)))
      do 135 k = 1, n
          temp = dmax1(temp, dabs(y(k))/c(k+30))
135      continue
      c(12) = dmin1(temp, 1.d0)
      go to 160
140      if (c(1) .ne. 5.d0) go to 150
      weights are 1/c(k+30)
      do 145 k = 1, n
          temp = dmax1(temp, dabs(y(k))/c(k+30))
145      continue
      c(12) = temp
      go to 160
150      continue

```



```

c          default case - weights are 1/max(1,abs(y(k)))
c          do 155 k = 1, n
c              temp = dmax1(temp, dabs(y(k)))
155          continue
c              c(12) = dmin1(temp, 1.d0)
160          continue
c              c(13) = 10.d0*dmax1(c(11),c(10)*dmax1(c(12)/tol,dabs(x)))
165          continue
c
c          calculate scale - use default unless value prescribed
c          c(15) = c(5)
c          if (c(5) .eq. 0.d0) c(15) = 1.d0
c
c          calculate hmax - consider 4 cases
c          case 1 both hmax and scale prescribed
c              if (c(6) .ne. 0.d0 .and. c(5) .ne. 0.d0)
c                  + c(16) = dmin1(c(6), 2.d0/c(5))
c          case 2 - hmax prescribed, but scale not
c              if (c(6) .ne. 0.d0 .and. c(5) .eq. 0.d0) c(16) = c(6)
c          case 3 - hmax not prescribed, but scale is
c              if (c(6) .eq. 0.d0 .and. c(5) .ne. 0.d0) c(16) = 2.d0/c(5)
c          case 4 - neither hmax nor scale is provided
c              if (c(6) .eq. 0.d0 .and. c(5) .eq. 0.d0) c(16) = 2.d0
c
c          *****error return (with ind=-2) if hmin .gt. hmax
c          if (c(13) .le. c(16)) go to 170
c              ind = -2
c              return
170          continue
c
c          calculate preliminary hmag - consider 3 cases
c          if (ind .gt. 2) go to 175
c          case 1 - initial entry - use prescribed value of hstart, if
c          any, else default
c              c(14) = c(4)
c              if (c(4) .eq. 0.d0) c(14) = c(16)*tol**(1./6.)
c              go to 185
175          if (c(23) .gt. 1.d0) go to 180
c          case 2 - after a successful step, or at most one failure,
c          use min(2, .9*(tol/est)**(1/6))*hmag, but avoid possible
c          overflow. then avoid reduction by more than half.
c              temp = 2.d0*c(14)
c              if (tol .lt. (2.d0/.9d0)**6*c(19))
c                  + temp = .9d0*(tol/c(19))**(1./6.)*c(14)
c              c(14) = dmax1(temp, .5d0*c(14))
c              go to 185
180          continue
c          case 3 - after two or more successive failures
c              c(14) = .5d0*c(14)
185          continue
c
c          check against hmax
c          c(14) = dmin1(c(14), c(16))
c
c          check against hmin
c          c(14) = dmax1(c(14), c(13))
c
c          *****interrupt no 1 (with ind=4) if requested
c          if (c(8) .eq. 0.d0) go to 1111
c              ind = 4
c              return
c          resume here on re-entry with ind .eq. 4 .....re-entry..
1111          continue
c
c          calculate hmag, xtrial - depending on preliminary hmag, xend
c          if (c(14) .ge. dabs(xend - x)) go to 190
c          do not step more than half way to xend
c              c(14) = dmin1(c(14), .5d0*dabs(xend - x))
c              c(17) = x + dsign(c(14), xend - x)
c              go to 195
190          continue
c          hit xend exactly
c              c(14) = dabs(xend - x)
c              c(17) = xend

```

```

195      continue
c
c      calculate htrial
c      c(18) = c(17) - x
c
c      end stage 1
c
c      *****
c      * stage 2 - calculate ytrial (adding 7 to no of fcn evals). *
c      * w(*,2), ... w(*,8) hold intermediate results needed in *
c      * stage 3. w(*,9) is temporary storage until finally it holds *
c      * ytrial.
c      *****
c
c      temp = c(18)/1398169080000.d0
c
c      do 200 k = 1, n
c          w(k,9) = y(k) + temp*w(k,1)*233028180000.d0
200      continue
c      call fcn(n, x + c(18)/6.d0, w(1,9), w(1,2))
c
c      do 205 k = 1, n
c          w(k,9) = y(k) + temp*( w(k,1)*74569017600.d0
+                               + w(k,2)*298276070400.d0 )
205      continue
c      call fcn(n, x + c(18)*(4.d0/15.d0), w(1,9), w(1,3))
c
c      do 210 k = 1, n
c          w(k,9) = y(k) + temp*( w(k,1)*1165140900000.d0
+                               - w(k,2)*3728450880000.d0
+                               + w(k,3)*3495422700000.d0 )
210      continue
c      call fcn(n, x + c(18)*(2.d0/3.d0), w(1,9), w(1,4))
c
c      do 215 k = 1, n
c          w(k,9) = y(k) + temp*( - w(k,1)*3604654659375.d0
+                               + w(k,2)*12816549900000.d0
+                               - w(k,3)*9284716546875.d0
+                               + w(k,4)*1237962206250.d0 )
215      continue
c      call fcn(n, x + c(18)*(5.d0/6.d0), w(1,9), w(1,5))
c
c      do 220 k = 1, n
c          w(k,9) = y(k) + temp*( w(k,1)*3355605792000.d0
+                               - w(k,2)*11185352640000.d0
+                               + w(k,3)*9172628850000.d0
+                               - w(k,4)*427218330000.d0
+                               + w(k,5)*482505408000.d0 )
220      continue
c      call fcn(n, x + c(18), w(1,9), w(1,6))
c
c      do 225 k = 1, n
c          w(k,9) = y(k) + temp*( - w(k,1)*770204740536.d0
+                               + w(k,2)*2311639545600.d0
+                               - w(k,3)*1322092233000.d0
+                               - w(k,4)*453006781920.d0
+                               + w(k,5)*326875481856.d0 )
225      continue
c      call fcn(n, x + c(18)/15.d0, w(1,9), w(1,7))
c
c      do 230 k = 1, n
c          w(k,9) = y(k) + temp*( w(k,1)*2845924389000.d0
+                               - w(k,2)*9754668000000.d0
+                               + w(k,3)*7897110375000.d0
+                               - w(k,4)*192082660000.d0
+                               + w(k,5)*400298976000.d0
+                               + w(k,7)*201586000000.d0 )
230      continue
c      call fcn(n, x + c(18), w(1,9), w(1,8))
c
c      calculate ytrial, the extrapolated approximation and store
c      in w(*,9)
c      do 235 k = 1, n
c          w(k,9) = y(k) + temp*( w(k,1)*104862681000.d0

```

```

+           + w(k,3)*545186250000.d0
+           + w(k,4)*446637345000.d0
+           + w(k,5)*188806464000.d0
+           + w(k,7)*15076875000.d0
+           + w(k,8)*97599465000.d0   )
235      continue
c
c      add 7 to the no of fcn evals
c      c(24) = c(24) + 7.d0
c
c      end stage 2
c
c      *****
c      * stage 3 - calculate the error estimate est. first calculate *
c      * the unweighted absolute error estimate vector (per unit *
c      * step) for the unextrapolated approximation and store it in *
c      * w(*,2). then calculate the weighted max norm of w(*,2) as *
c      * specified by the error control indicator c(1). finally, *
c      * modify this result to produce est, the error estimate (per *
c      * unit step) for the extrapolated approximation ytrial. *
c      *****
c
c      calculate the unweighted absolute error estimate vector
c      do 300 k = 1, n
c          w(k,2) = (   w(k,1)*8738556750.d0
+                   + w(k,3)*9735468750.d0
+                   - w(k,4)*9709507500.d0
+                   + w(k,5)*8582112000.d0
+                   + w(k,6)*95329710000.d0
+                   - w(k,7)*15076875000.d0
+                   - w(k,8)*97599465000.d0)/1398169080000.d0
300      continue
c
c      calculate the weighted max norm of w(*,2) as specified by
c      the error control indicator c(1)
c      temp = 0.d0
c      if (c(1) .ne. 1.d0) go to 310
c      absolute error control
c      do 305 k = 1, n
c          temp = dmax1(temp,dabs(w(k,2)))
305      continue
c      go to 360
310      if (c(1) .ne. 2.d0) go to 320
c      relative error control
c      do 315 k = 1, n
c          temp = dmax1(temp, dabs(w(k,2)/y(k)))
315      continue
c      go to 360
320      if (c(1) .ne. 3.d0) go to 330
c      weights are 1/max(c(2),abs(y(k)))
c      do 325 k = 1, n
c          temp = dmax1(temp, dabs(w(k,2))
+                   / dmax1(c(2), dabs(y(k))) )
325      continue
c      go to 360
330      if (c(1) .ne. 4.d0) go to 340
c      weights are 1/max(c(k+30),abs(y(k)))
c      do 335 k = 1, n
c          temp = dmax1(temp, dabs(w(k,2))
+                   / dmax1(c(k+30), dabs(y(k))) )
335      continue
c      go to 360
340      if (c(1) .ne. 5.d0) go to 350
c      weights are 1/c(k+30)
c      do 345 k = 1, n
c          temp = dmax1(temp, dabs(w(k,2)/c(k+30)))
345      continue
c      go to 360
350      continue
c      default case - weights are 1/max(1,abs(y(k)))
c      do 355 k = 1, n
c          temp = dmax1(temp, dabs(w(k,2))
+                   / dmax1(1.d0, dabs(y(k))) )
355      continue

```

```

360      continue
c
c      calculate est - (the weighted max norm of w(*,2))*hmag*scale
c      - est is intended to be a measure of the error per unit
c      step in ytrial
c      c(19) = temp*c(14)*c(15)
c
c      end stage 3
c
c      *****
c      * stage 4 - make decisions. *
c      *****
c
c      set ind=5 if step acceptable, else set ind=6
c      ind = 5
c      if (c(19) .gt. tol) ind = 6
c
c      *****interrupt no 2 if requested
c      if (c(9) .eq. 0.d0) go to 2222
c      return
c      resume here on re-entry with ind .eq. 5 or 6 ...re-entry..
2222      continue
c
c      if (ind .eq. 6) go to 410
c      step accepted (ind .eq. 5), so update x, y from xtrial,
c      ytrial, add 1 to the no of successful steps, and set
c      the no of successive failures to zero
c      x = c(17)
c      do 400 k = 1, n
c      y(k) = w(k,9)
400      continue
c      c(22) = c(22) + 1.d0
c      c(23) = 0.d0
c      *****return(with ind=3, xend saved, flag set) if x .eq. xend
c      if (x .ne. xend) go to 405
c      ind = 3
c      c(20) = xend
c      c(21) = 1.d0
c      return
405      continue
c      go to 420
410      continue
c      step not accepted (ind .eq. 6), so add 1 to the no of
c      successive failures
c      c(23) = c(23) + 1.d0
c      *****error return (with ind=-3) if hmag .le. hmin
c      if (c(14) .gt. c(13)) go to 415
c      ind = -3
c      return
415      continue
420      continue
c
c      end stage 4
c
c      go to 99999
c      end loop
c
c      begin abort action
500      continue
c
c      write(6,505) ind, tol, x, n, c(13), xend, nw, c(16), c(20),
c      + c(22), c(23), c(24), (y(k), k = 1, n)
505      format( /// 1h0, 58hcomputation stopped in dverk with the followin
c      +g values -
c      + / 1h0, 5hind =, i4, 5x, 6htol =, 1pd13.6, 5x, 11hx =,
c      + 1pd22.15
c      + / 1h , 5hn =, i4, 5x, 6hhmin =, 1pd13.6, 5x, 11hxend =,
c      + 1pd22.15
c      + / 1h , 5hnw =, i4, 5x, 6hhmax =, 1pd13.6, 5x, 11hprev xend =,
c      + 1pd22.15
c      + / 1h0, 14x, 27hno of successful steps =, 0pf8.0
c      + / 1h , 14x, 27hno of successive failures =, 0pf8.0
c      + / 1h , 14x, 27hno of function evals =, 0pf8.0
c      + / 1h0, 23hthe components of y are

```

```
      + // (1h , 1p5d24.15) )
c
      stop
c
c end abort action
c
      end
```

CURRICULUM VITAE

PERSONAL INFORMATION

Surname, Name: Kayhan, Bülent Abbas
Nationality: Turkish (TC)
Date and Place of Birth: 18 August 1974, Ankara
Marital Status: Single
Phone: +90 312 240 92 65
email: bulentkayhan@hotmail.com

EDUCATION

Degree	Institution	Year of Graduation
MS	Kırıkkale University Civil Engineering	2001
BS	METU Civil Engineering	1997
High School	Bahçelievler Deneme Lisesi, Ankara	1991

WORK EXPERIENCE

Year	Place	Enrollment
1997-1998	TABAR Mühendislik	Civil Engineer
1995 August	PROKON Ltd.	Student
1994 July	OYAK İnşaat	Student

FOREIGN LANGUAGES

Good command of English